國立臺灣大學工學院土木工程學系

博士論文

Department of Civil Engineering
College of Engineering
National Taiwan University

Doctoral Dissertation

從力學特性與微觀組構看 EICP 改良砂土成效

Mechanical Enhancement of Sand through Enzyme-Induced Carbonate Precipitation: Experimental Insights and Microstructural Analysis

若艾瑪

Amali Gitanjali Rayappan Kennedy

指導教授：葛宇甯 博士

Advisor: Louis Ge, Ph.D.

中華民國 113 年 9 月

September, 2024

doi:10.6342/NTU202404421

ACKNOWLEDGEMENTS

It is a great pleasure to acknowledge the roles of every individual who was an instrument in completing my PhD research.

First, I would like to express my gratitude to Dr. Louis Ge, who encouraged me to pursue the research despite all my shortcomings and always enlightened me on the way to completion. I truly enjoyed the research work and being a part of his research team, which made me evolve as a researcher. Dr. Louis Ge's intellectual guidance, innovative ideas, and stoic patience are greatly appreciated. My heartfelt thanks for believing in me and helping in all the circumstances. This work would not materialize without the financial support of Dr. Louis Ge.

I am greatly indebted to my colleagues (Dr. Yu Syuan Jho, Dr. Fu Hsuan Yeh, and Dr. Chris Chu) and the entire research group for their timely advice, encouragement, and companionship. Thanks to Mr. Kuo and Mr. Chou for helping me conduct my laboratory experiments. I would also like to thank my friends Dr. Kalpana Shankwar, Mr. Suyash Kishor Wagh, and Ms. Ashwini Kumar for their support throughout my PhD.

Special thanks to my husband, Mr. Geoffrey Dominic, for his continuous support and understanding. Finally, I would like to express my heartfelt thanks to my loving family members, father and mother, Mrs. and Mr. Rayappan Kennedy, my loving in-laws, Mrs. and Mr. Dominic, and my beloved sister, Ms. Bibiana Kennedy, for their patience and understanding. Without all your mental support, it's impossible for me to be here.

doi:10.6342/NTU202404421

DEDICATION

This thesis is dedicated to Our Lady of Health Velankanni for her continuous support. In all the times she motivated me and made me believe in myself. Thanks for providing me with good health and a proper mental state to complete my project.

doi:10.6342/NTU202404421

摘要

近年來，酶誘導碳酸鹽沉澱（EICP）作為一種仿生工程技術，受到土木工程界的廣泛關注。透過 EICP 進行的生物膠結可通過堵塞空隙和利用碳酸鈣將土壤顆粒粘結來增加土壤的強度、剛度和抗液化性。該方法涉及使用脲酶與尿素和氯化鈣相結合以誘導碳酸鈣沉澱。EICP 處理的有效性受化學成分濃度和脲酶影響。初步研究旨在確定尿素、氯化鈣與脲酶的最佳濃度及EICP處理樣品的抗滲深度。透過Falcon試管試驗，尿素濃度範圍為 0.25M 至 1M，比例分別為（CaCl2：尿素）1:1、1:1.2、1:1.5 和 1:1.75，脲酶濃度分別為1 g/l、3 g/l、5 g/l 和 6g/l。研究使用 Falcon 試管測試顯示，當尿素濃度為 1 M，氯化鈣濃度為 0.67 M，脲酶濃度為 3 g/l 時，獲得了較為高的碳酸鈣和沉澱率。本研究採用了由 1M 尿素、0.67M 氯化鈣二水合物和 3g/l 脲酶組成的最佳第一階段 EICP 膠結溶液配方。隨後，對四種不同組合進行了落錐試驗，測量了不同養護時間（3 天和 7 天）下單次處理週期（N-1）和第 7 天的兩次處理週期（N-2）中的滲透深度。值得注意的是，兩次處理週期（N-2）中的滲透深度明顯低於第 3 天和第 7 天的數值。進行落錐試驗後，通過酸消化法測量碳酸鈣沉澱量以分析樣品的均勻性。酸消化試驗結果表明，較低濃度的尿素和氯化鈣產生的樣品更為均勻，而較高濃度則導致樣品頂部碳酸鈣含量增加，底部碳酸鈣含量減少。這種差異歸因於脲酶與膠結溶液的快速反應，使樣品底部不透水。隨後，使用已確定的最佳 EICP 配方來研究實驗測試前樣品中碳酸鈣沉澱的均勻分佈。在排水和不排水條件下，研究了三軸試樣中碳酸鈣的分佈。結果顯示，在不排水條件下進行的 EICP 處理獲得了更為均勻的碳酸鈣沉澱。EICP 溶液滯留在紙模中，從而有助於產生更均勻的

doi:10.6342/NTU202404421

沉澱。該研究的目的是通過在兩種不同的脲酶條件下進行單調固結排水三軸試驗和不排水循環三軸試驗，來評估EICP處理砂的力學行為。對純砂和EICP處理砂進行了7天和14天養護下的單調三軸試驗，分別在50、100和200 kPa的圍壓下進行。EICP膠結顯著提高了單次處理週期內的偏應力、膨脹性和剪切強度參數。在所有養護期間，EICP 處理砂均顯示出明顯的有效內聚力。生物膠結的增加提高了峰值和殘餘狀態下的有效內聚力，而有效摩擦角則保持不變。研究還對純砂和 EICP 處理樣品在 7 天養護下100 kPa圍壓的抗液化循環反應進行了研究。循環抗液化性通過減少壓縮應變和延長達到液化的週期數而得到改善。為進一步理解碳酸鈣沉澱引起的微觀結構變化，進行了顯微結構分析，包括場發射掃描電子顯微鏡（FE-SEM）分析、能量色散光譜（EDS）元素映射和X射線衍射（XRD）研究，其樣本來自Falcon試管試驗的純砂和EICP處理樣品。FE-SEM和EDS分析結果顯示，EICP處理增強了顆粒間接觸和顆粒與方解石沉澱的接觸強度。XRD 結果則確認通過 EICP 處理形成的晶體主要由方解石組成。最後，三軸試驗後的酸消化顯示在飽和、固結和剪切過程中，處理樣品的碳酸鈣損失量較小。由於本研究討論了單次處理週期，更多的處理週期和較高的膠結濃度可以使樣品在飽和和剪切過程中更加耐受。

關鍵詞：酶誘導方解石沈澱法 (EICP)、獵鷹管試驗、落錐試驗、液化、酸消化、排水三軸測試和微觀分析

doi:10.6342/NTU202404421

ABSTRACT

In recent years, Enzyme-induced carbonate precipitation (EICP) has emerged as a bio-inspired and innovative technique that has captured the attention of geotechnical engineers specializing in soil stabilization. Bio-cementation via EICP increases the strength, stiffness, and soil liquefaction resistance by clogging the voids and binding the soil particles with calcium carbonate. This method involves the utilization of urease enzymes combined with urea and calcium chloride to induce calcium carbonate precipitation. The effectiveness of the EICP treatment is influenced by the concentration of the chemical components and the urease enzyme. The preliminary research aimed to identify the optimal concentrations of urea and calcium chloride with the urease enzyme and penetration depth resistance in EICP-treated specimens. Falcon tube tests were conducted with urea concentration (0.25M to 1M) in various ratios ($CaCl_2$: Urea) – 1:1, 1:1.2, 1:1.5, and 1:1.75 with different proportions of urease enzymes (1 g/l, 3 g/l, 5 g/l, and 6g/l). The research employed falcon tube tests, revealing that a combination of 1 M urea, 0.67 M $CaCl_2$, and 3 g/l urease enzyme resulted in a higher $CaCO_3$ and precipitation ratio. This study adopted an optimal formulation of a one-phase EICP cementation solution consisting of 1M Urea, 0.67M Calcium chloride dihydrate, and 3g/l urease enzyme. Subsequent fall cone tests were conducted on four different combinations, measuring penetration depth at various curing times (3 and 7 days) in a single treatment cycle (N-1) and two treatment cycles (N-2) on day 7. Notably, the penetration depth at two treatment cycles (N-2) significantly decreased compared to values observed on days 3 and 7. Following the fall cone tests, specimen uniformity was analyzed by assessing $CaCO_3$ precipitation using the acid digestion. The acid digestion test results indicated that lower concentrations of urea and calcium chloride yielded more uniform specimens. In contrast,

doi:10.6342/NTU202404421

higher concentrations led to non-uniform specimens with elevated $CaCO_3$ at the top and reduced $CaCO_3$ at the bottom. This disparity was attributed to the rapid reactivity of the urease enzyme with the cementation solution, rendering the bottom portion of the specimen impermeable. The identified optimal EICP formulation was then employed to investigate the uniform distribution of calcium carbonate precipitation in the prepared specimens before subjecting them to experimental testing. The distribution of calcium carbonate in the triaxial specimen was studied in both drained and undrained conditions. The EICP treatment under undrained conditions obtained a more uniform calcium carbonate precipitation. The EICP solution gets retained in the paper mold, which helps produce a more uniform precipitation. The objective of the study involves assessing the mechanical behavior of the EICP-treated sand by performing monotonic consolidated drained triaxial and undrained cyclic triaxial tests in two different urease enzymes. The monotonic triaxial tests on pure sand and EICP-treated sand with 3,7 and 14 curing days were carried out at 50, 100, and 200 kPa confining pressures, respectively. Bio-cementation through EICP significantly enhanced the deviatoric stress, dilatancy, and shear strength parameters in one treatment cycle. A noticeable effective cohesion was observed for EICP-treated sand for all curing durations. The increase in bio-cementation increased the effective cohesion at both peak and residual state while the effective friction angle remained constant. The cyclic response under an effective confining pressure of 100 kPa in the pure sand and EICP-treated specimen was studied in 7 days of curing time. The cyclic resistance to liquefaction improved by reducing compression strain and prolonged cycles to attain liquefaction. Microscopic analyses were performed to comprehend further the microstructural transformations resulting from calcium carbonate precipitation. These include field-emission scanning electron microscopy (FE-SEM)

doi:10.6342/NTU202404421

analysis, Energy Dispersive Spectroscopy (EDS) elemental mapping, and X-ray Diffraction (XRD) studies on calcium carbonate precipitate from falcon tube test, pure sand, and EICP-treated sample. The FE-SEM and EDS analysis revealed augmented strength particle-to-particle contact and particle-to-calcite precipitation due to EICP treatment. Notably, XRD results confirm that the crystals formed through EICP treatment primarily comprise calcite. Finally, acid digestion after the triaxial test revealed a minor amount of loss of $CaCO_3$ in the treated specimen during the saturation, consolidation, and shearing process. As the study discussed the one cycle of treatment, multiple treatment cycles with higher cementation makes the specimen resistant under saturation and shearing process.

Keywords: Enzyme-Induced Calcite Precipitation methods (EICP), Falcon Tube test, Fall cone test, Liquefaction, Acid Digestion, Drained Triaxial Testing, and microscopic analysis

doi:10.6342/NTU202404421

TABLE OF CONTENTS

ACKNOWLEDGEMENTS ..... **ii**

DEDICATION ..... **iii**

摘要 ..... **iv**

ABSTRACT ..... **vi**

LIST OF FIGURES ..... **xiv**

LIST OF TABLES ..... **xxi**

Chapter 1 INTRODUCTION **1**

1.1 Motivation 1

1.2 Bio-cementation Techniques 3

1.3 Applications of EICP treatment 7

1.4 Advantages of EICP 8

1.5 Limitations of EICP 9

1.6 Field Applications in EICP Treatment 10

1.7 Cost Applications 12

1.8 Scope of Study 13

1.9 Novelty of the Study 15

1.10 Organization 16

Chapter 2 LITERATURE REVIEW **17**

doi:10.6342/NTU202404421

2.1 Introduction 17

2.2 Urea Hydrolysis in EICP treatment 18

2.3 Factors influencing the formation of $CaCO_3$ precipitation 19

2.3.1 Electrical conductivity (EC) and pH 19

2.3.2 Temperature 24

2.3.3 Cementation Solution Concentration 26

2.4 Prior Studies 30

2.5 Bio-cementation Techniques using EICP with additives 31

2.6 Compressive Strength Tests 36

2.6.1 Single-phase Treatment Cycle 36

2.6.2 Multiple-phase Treatment Cycles 39

2.7 Static Triaxial Studies 41

2.8 Dynamic Response Studies 44

2.8.1 MICP Treatment 44

2.8.2 EICP Treatment 48

Chapter 3 EXPERIMENTAL PROGRAM 52

3.1 Materials 52

3.1.1 Sand 52

3.1.2 Characteristics of Urease Enzyme and Reagents 53

3.1.3 Paper Mould 55

doi:10.6342/NTU202404421

3.1.4 Magnetic stirrer 55
3.1.5 Whatman Ashless Filter Papers 56
3.1.6 Hydrochloric Acid 58
3.1.7 Falcon Tubes 58
3.1.8 Monitoring of Urease activity in solution 60
3.1.9 Microscopic Examination 62
3.2 Specimen Preparation 65
3.2.1 Fall Cone Test 65
3.2.2 Triaxial Testing 67
3.3 Laboratory Tests 69
3.3.1 Falcon Tube Test 69
3.3.2 Fall Cone Test 71
3.3.3 Consolidated Drained Triaxial Testing 71
3.3.4 Undrained Cyclic Triaxial Testing 72
3.4 Acid Digestion 73
3.4.1 Determination of Calcium Carbonate Content (CCC) 73
3.4.2 Assessment of Uniformity in Triaxial Specimen 74
Chapter 4 RESULTS AND DISCUSSIONS 81
4.1 Falcon Tube Test Results from Sigma Urease 81
4.1.1 0.25 M Urea Concentration 81

doi:10.6342/NTU202404421

4.1.2 0.5 M Urea Concentration 82
4.1.3 0.61 M Urea Concentration 83
4.1.4 1 M Urea Concentration 84
4.2 Fall Cone Test from Sigma Urease 87
4.2.1 Variation of Penetration Depth at One Treatment Cycle 87
4.2.2 Variation of Penetration Depth at Two Treatment Cycles 89
4.2.3 Analysis of Acid Digestion Outcomes from Fall Cone Testing 92
4.2.4 Analysis of Acid Digestion of Triaxial Specimen 95
4.3 Monitoring of Electrical Conductivity (EC) mS/cm and pH 96
4.3.1 Sigma Urease 96
4.3.2 CDH Urease 100
4.4 Isotropic Consolidated Drained (CID) Triaxial Tests 101
4.4.1 Stress-Strain Behavior 101
4.4.2 Peak and Residual Strength Parameters 107
4.4.3 Volumetric Behavior 112
4.5 Study of Liquefaction Resistance 115
4.5.1 Cyclic Triaxial Testing and Discussion with CDH-Treated Specimen 115
4.5.2 Cyclic Triaxial Testing and Discussion with Sigma-Treated Specimen 123
4.6 Microscopic Examination 129
4.6.1 Field Emission – Scanning Electron Microscopy (FE-SEM) analysis 129

doi:10.6342/NTU202404421

4.6.2 Energy Dispersive Spectroscopy (EDS) Examination 140

4.6.3 X-ray Diffraction (XRD) analysis 144

4.7 Acid Digestion for Triaxial Specimens 147

Chapter 5 CONCLUSIONS 152

RECOMMENDATIONS 156

REFERENCES 158

doi:10.6342/NTU202404421

LIST OF FIGURES

Figure 1: Earthquake Induced Liquefaction 2

Figure 2: Mechanisms of Microbial-Induced Calcite Precipitation (MICP) and Enzyme-Induced Calcite Precipitation (EICP) in the $CaCO_3$ precipitation. 7

Figure 3: Flow Chart of Research Framework 15

Figure 4: Soil Stabilization using Enzyme-Induced Calcite Precipitation (EICP) 18

Figure 5: Temporal relations of EC and pH when subjected to the effect of NH_4Cl addition: (A) EC and (B) pH (Hu et al. 2021) 20

Figure 6: Variations of (a) concentration of Ca2+ with different initial pHs (b) pH on urease activity (Xie et al. 2023). 22

Figure 7: Variations of solution EC with time ((a) urease enzyme;(b) bacteria solution) Variations of solution pH with time ((c) urease enzyme;(d) bacteria solution) (Jiang et al. 2016). 24

Figure 8: Influence of (a) temperature (b) Variations of concentration of Ca^{2+} at different temperatures (Xie et al. 2023). 25

Figure 9: Effect of temperature on enzymatic $CaCO_3$ production: ( )22 ◦C, ( ) 50 ◦C; (Nemati and Voordouw 2003). 26

Figure 10: Results of test-tube experiments ((a) changes in pH with time and (b) relation between initial Ca and consumed Ca concentrations) (Yasuhara et al. 2012) 27

Figure 11: Correlation between urease concentration and $CaCO_3$ precipitation ratio (Neupane et al. 2013). 28

Figure 12: Test-tube experiments. Relation between urea-$CaCl_2$ concentration and $CaCO_3$ precipitation ratio (Carmona et al. 2016) 29

doi:10.6342/NTU202404421

Figure 13: PR plotted against (a) urea–calcium chloride concentration, [S0]; (b) enzyme concentration, [E0] (g/l) (Ahenkorah et al. 2021b). 30
Figure 14: Timeline of research developments in EICP technique 35
Figure 15: Timeline of research developments for the dynamic behavior of EICP and MICP treatments in cyclic triaxial testing. 51
Figure 16: Grain Size Distribution Curve 53
Figure 17: Types of Urease used in the study (a) Sigma Aldrich urease with 5 U/mg (b) CDH urease 54
Figure 18: Chemical Reagents used 54
Figure 19: Paper mold 55
Figure 20: EICP solution 56
Figure 21: Filter papers used 57
Figure 22: Falcon Tubes 59
Figure 23: Electrical Conductivity (EC) meter 60
Figure 24: pH meter 61
Figure 25: (a) Sample collected in Carbon Paper (b) Process of Sputtering 63
Figure 26: Field Emission- Scanning Electron Microscopy (FE-SEM) Hitachi S-4800 coupled with Energy Dispersive Spectroscopy (EDS) 63
Figure 27: (a) Sample collected in the holder (b) X-ray Diffraction (XRD) Bruker D8 Venture 64
Figure 28: Fall cone test (a) EICP Solution (b) One-phase EICP treatment (drained) soil columns (c) Curing of treated samples (d) Testing 66

doi:10.6342/NTU202404421

Figure 29: (a) Pouring of EICP treatment solution (percolation method) (b) EICP-treated specimen (Curing) (c) EICP-treated specimen on Monotonic Triaxial plate (d) EICP-treated specimen on Cyclic Triaxial plate (e) Monotonic Triaxial Setup (f) Cyclic Triaxial Setup 69

Figure 30: Falcon Tube test procedure (a) Light milky patches at the initial point of EICP reactions (b) Deposits of $CaCO_3$ after 24 hours (c, d) $CaCO_3$ filtration (e) Dried $CaCO_3$... 71

Figure 31: Acid Digestion (a) EICP-treated specimen (b) Sand samples before acid digestion (c) Effervescence in the sand..... 74

Figure 32: Sigma-treated specimen preparation under drained conditions 76

Figure 33: CDH-treated specimen preparation under undrained conditions 77

Figure 34: Acid digestion of Sigma-treated specimen at drained and undrained conditions at 3 days of curing 78

Figure 35: Uniformity study of CDH-treated specimen (a) CDH-treated specimen (b) Specimen cut in five parts (c) Samples taken for acid digestion (d) Effervescence from acid digestion..... 79

Figure 36: Acid digestion of CDH-treated specimen at 7 days of curing. 79

Figure 37: Falcon Tube test results of 0.25 M Urea Concentration 82

Figure 38: Falcon Tube test results of 0.5 M Urea Concentration 83

Figure 39: Falcon Tube test results of 0.61 M Urea Concentration 84

Figure 40: Falcon Tube test results of 1 M Urea Concentration 86

Figure 41: Fall cone test result at 3-days of curing 88

Figure 42: Fall cone test result at 7 days of curing..... 89

Figure 43: Fall cone test result at 7 days of curing at two treatment cycles..... 91

Figure 44: Schematic illustration at two cycles of bio-cementation 91

doi:10.6342/NTU202404421

Figure 45: Acid Digestion results at 3 days of curing 93
Figure 46: Acid Digestion results at 7 days of curing 94
Figure 47: Acid Digestion results at 7 days of curing in two treatment cycles 95
Figure 48: Triaxial acid digestion results in four combinations 96
Figure 49: Electrical conductivity and pH Versus Time in EICP solution (Sigma Urease). 99
Figure 50: EICP solution (a) After the addition of urease (b) deposition of $CaCO_3$ at the bottom (c) end of the test 99
Figure 51: Electrical conductivity and pH Versus Time in EICP solution (CDH Urease) 100
Figure 52: EICP solution (a) After the addition of urease (b and c) end of the test 100
Figure 53: Results of Drained Triaxial test (CDH Urease)- Stress-Strain Behavior at 50 kPa, 100 kPa, and 200 kPa effective confining pressure (a) Pure sand (PS) (b) CDH-treated specimen at 3 days curing (c) CDH-treated specimen at 7 days curing (d) CDH-treated specimen at 14 days curing 102
Figure 54: Summary of CD triaxial test in untreated and CDH-treated specimens - Stress ratio (Deviatoric stress (q)/ Mean effective stress (p')) versus axial strain (%) 104
Figure 55: Summary of Drained Triaxial test (Sigma Urease) – Stress-Strain Behavior of pure sand and Sigma-treated specimen at 7 days of curing under 50 kPa, 100 kPa and 200 kPa effective confining pressure 104
Figure 56: Summary of CD triaxial test in untreated and Sigma-treated specimens - Stress ratio (Deviatoric stress (q)/ Mean effective stress (p')) versus axial strain (%) 106
Figure 57: Mohr-Coulomb failure envelopes for untreated and CDH-treated sand (a) Pure Sand – Peak Strength (b) Pure Sand – Residual Strength (c) CDH Day 3 – Peak Strength (d)

doi:10.6342/NTU202404421

CDH Day 3 – Residual Strength (e) CDH 7 – Peak Strength (f) CDH Day 7 – Residual Strength (g) CDH Day 14 – Peak Strength (h) CDH Day 14 – Residual Strength. 107
Figure 58: Mohr-Coulomb failure envelope for pure sand and Sigma-treated specimen (a) Pure Sand – Peak Strength (b) Pure Sand - Residual Strength (c) Sigma Day 7 – Peak Strength (d) Sigma Day 7 – Residual Strength 110
Figure 59: Results of Drained Triaxial test – Volumetric Strain Behavior at 50 kPa, 100 kPa, and 200 kPa effective confining pressure (a) Pure sand (PS) (b) CDH-treated specimen at 3 days curing (c) CDH-treated specimen at 7 days curing (d) CDH-treated specimen at 14 days curing 113
Figure 60: Summary of Drained Triaxial test – Volumetric Strain Behavior of Pure sand and Sigma-treated specimen at 7 days of curing under 50 kPa, 100 kPa, and 200 kPa effective confining pressure 115
Figure 61: Relationships of axial strain, excess pore water pressure ratio, and number of load cycles 118
Figure 62: Cyclic stress-strain curves and stress paths 120
Figure 63: Liquefaction resistance curves for pure sand and treated sand at an effective confining pressure of 100 kPa 122
Figure 64: (a and b) Strain development at pure sand and Sigma-treated specimen in CSR 0.3 and 0.25 (c and d) Pore pressure development at pure sand and Sigma-treated specimen in CSR 0.3 and 0.25 126
Figure 65: (a and c) Stress-Strain development at pure sand and Sigma-treated specimen in CSR 0.3 and 0.25 (b and d) Cyclic Deformation characteristics at pure sand and Sigma-treated specimen in CSR 0.3 and 0.25 129

doi:10.6342/NTU202404421

Figure 66: Particle to Particle Contact Precipitation (a) pure sand (b-d) Sigma-treated.... 131
Figure 67: Particle to Particle Contact Precipitation (a) pure sand (b-f) CDH-treated 132
Figure 68: Particle to Calcite Precipitation (a-b) Pure sand (c-d) Sigma-treated samples. 133
Figure 69: Particle to Calcite Precipitation (a-b) Pure sand (c-d) CDH-treated samples... 134
Figure 70: Microscopic analysis of Calcium Carbonate precipitate. (a and b) FE-SEM (c) EDS - Elemental mapping 135
Figure 71: (a) FE-SEM image of Calcium carbonate precipitate (b) 18 selected crystals . 137
Figure 72: Histogram plot of the calcium carbonate crystal highlighted in figure 71a 138
Figure 73: 3D imaging of $CaCO_3$ precipitate (7.5k magnification) 139
Figure 74: 3D imaging of $CaCO_3$ precipitate (2.5k magnification) 139
Figure 75: Texture of Pure Sand..... 140
Figure 76: EDS mapping in Pure Sand..... 141
Figure 77: EDS mapping of CDH-treated samples (a-f) 7 days of curing 142
Figure 78: EDS mapping of CDH-treated samples (a-c) 14 days of curing..... 143
Figure 79: EDS mapping of Sigma-treated samples (a-i) 7 days of curing..... 144
Figure 80: XRD results of (a) pure sand, (b) CDH-treated soil at 7 days of curing, (c) CDH-treated soil at 14 days of curing..... 145
Figure 81: XRD results of (a) Calcite, (b) Pure Sand, (c) Sigma-treated soil at 7 days of curing 147
Figure 82: Acid Digestion Test results after static triaxial test (a) CDH-treated specimen at 3 days of curing (b) CDH-treated specimen at 7 days of curing (c) CDH-treated specimen at 14 days of curing 148

doi:10.6342/NTU202404421

Figure 83: Acid Digestion Test results after static triaxial test (a) Sigma-treated specimen at 7 days of curing 149

Figure 84: Schematic representation of flush off of weak $CaCO_3$ precipitate (Liu et al. 2019b). 150

Figure 85: Variation of shear wave velocity during shearing 151

doi:10.6342/NTU202404421

LIST OF TABLES

Table 1: Cost Analysis 13

Table 2: Grouting Scheme 46

Table 3: Properties of filter papers 57

Table 4: Properties of Falcon Tube 59

Table 5: Summary of Different Combinations of EICP Technique 66

Table 6: Test Scheme in Cyclic Triaxial (CDH-Treated Specimen) 116

Table 7: Test Scheme in Cyclic Triaxial (Sigma-Treated Specimen) 123

doi:10.6342/NTU202404421

Chapter 1 INTRODUCTION

1.1 Motivation

Taiwan's geographical location is situated between two tectonic plates: The Eurasian plate and the Philippine Sea plate. In the eastern half of Taiwan, the Philippine Sea plate moves beneath the Eurasian plate. Along the Manila Trench in southern Taiwan, the South China Sea of the Eurasian plate is subducted eastward beneath the Philippine Sea plate. This geodynamic configuration results in a high level of seismic activity in the region. Earthquake-induced liquefaction is a critical factor to consider, as it has the potential to devastate engineering structures and result in significant financial loss and human casualties (Loh *et al.* 2019; Yuan *et al.* 2004). Cyclic liquefaction is the most common type of liquefaction observed in significant cases. It occurs due to the dissipation of pore water pressure resulting from repeated cycles of earthquake loading or other ground motions. During cyclic loading, loosely packed sand grains attempt to move closer, achieving a denser state. However, the water trapped in the pores hinders the soil particles from interlocking, increasing the accumulated pore water pressure. When the pore water pressure equals the total stress, causing the effective stress of the soil to become nil, cyclic liquefaction onset occurs (Tuttle *et al.* 2019). Figure 1 illustrates the aftermath of the earthquake-induced soil liquefaction. Therefore, it is vital to improve the loosely packed sand grains with proper interlocking densely packed structures, reduce permeability, and improve the strength and stiffness of the soil.

doi:10.6342/NTU202404421

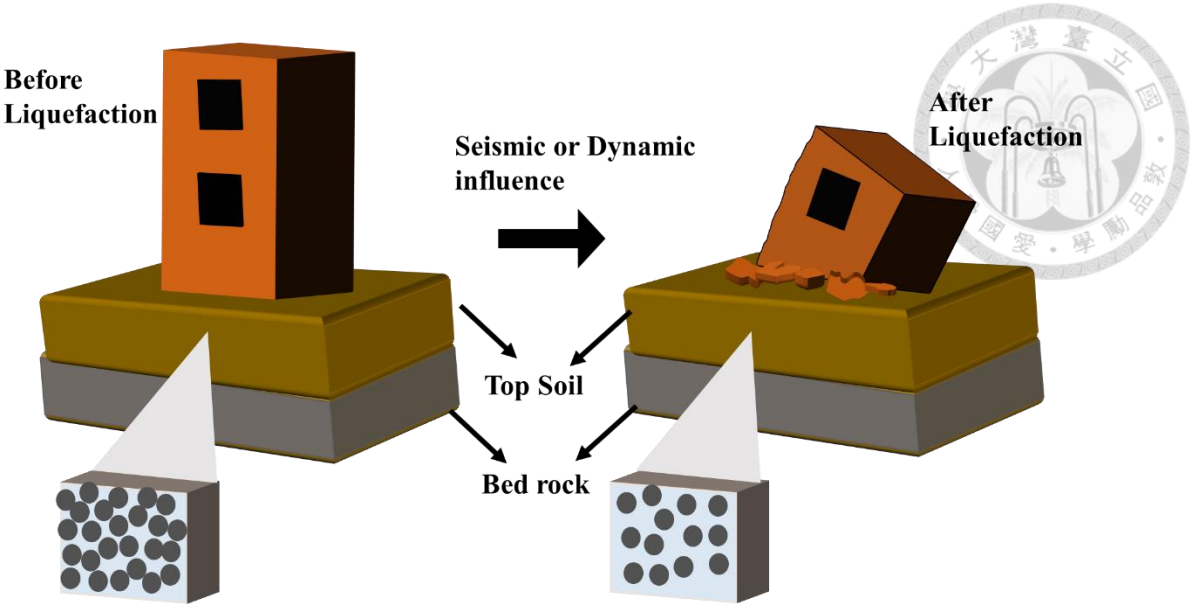

Figure 1: Earthquake Induced Liquefaction

The population growth and the industrial revolution have led to hasty construction activity. A significant challenge is inadequate land with good ground conditions for the construction of civil engineering projects. The need for favorable site conditions for construction activity highlights the importance of soil stabilization. Soil stabilization is performed on the sub-soil, which is unsuitable for construction purposes and is of different types like mechanical, chemical, and biological modifications of soil engineering. The mechanical soil stabilization process involves altering the engineering soil properties by increasing the dry density of the soil and increasing the shear strength parameters for soil improvement. This stabilization consists of compaction and densification. Mechanical stabilization releases tremendous energy through rollers, rammers, vibration techniques, and blasting. Compaction in the soil causes rearrangement and interlocking of particles, and densification involves expulsing air from soil voids without much change in moisture content. The mixing of chemicals and by-products in the soil performs chemical stabilization. This stabilization modifies the interactions between water and soil through chemical

doi:10.6342/NTU202404421

reactions to make the soil favorable for the engineering target. Chemical stabilization has attracted greater attention due to its effectiveness in soil improvement by calcite precipitation methods. Soil stabilization is intended to enhance the shear strength, reduce permeability and compressibility, and improve the durability and plasticity of ground conditions. Soil strength can be enhanced through soil stabilizations, and the soil's resistance to softening by water can be increased by bonding the soil particles together or waterproofing them (Sherwood 1993).

1.2 Bio-cementation Techniques

Recently, bio-inspired techniques have drawn the attention of many geotechnical researchers. In this stabilization, one such method is the Calcite-Induced Precipitation Method (CIPM), which has become a superior technique for improving the shearing strength of the soil. Bio-cementation is an emerging trend in soil improvement methods. Calcium carbonate ($CaCO_3$) is primarily used in this method to adhere soil particles together to increase shear resistance (Terzis *et al.* 2019) and fill in the pores to reduce the permeability of the soil. The precipitated calcite binds the soil particles and increases the particle-to-particle contact. This increases the particle roughness on the surface of the soil. Due to interlocking or particle-particle contact and roughness of the soil surface, the shear strength of the soil, stiffness, and dilatancy improved. There are mainly two approaches for $CaCO_3$ production via urea hydrolysis: a) Microbial–induced carbonate precipitation (MICP) with urease-producing bacteria and b) Enzyme-induced carbonate precipitation (EICP) using free urease enzymes. Irrespective of whether it's EICP or MICP treatment, the outcome is calcium carbonate precipitation. Calcium carbonate precipitates dissolve very slowly on a geological time scale. This dissolution can occur either through continuous flushing by buffered acidic groundwater

doi:10.6342/NTU202404421

or due to acidification processes within the pores (Paassen *et al.* 2010). The process of EICP and MICP treatment is shown in Figure 2.

MICP is a bio-geochemical process that induces calcium carbonate to precipitate in the soil matrix. The induced calcite precipitation binds the sand grains together at the particle-particle contact, increasing the soil's strength and stiffness (Mortensen 2011). MICP method uses urease-producing aerobic bacteria like *Bacillus Pasteurii* (Li *et al.* 2020), *Bacillus Megtarium,* and other anaerobic bacteria like *Pseudomonas denitrificans*. There are various processes to develop MICP, including bacterial ureolysis, sulfate reduction, and denitrification. Various processes develop when urease is deduced from ureolytic bacteria, and the hydrolysis of urea is catalyzed into ammonia (NH_3) and carbon dioxide (CO_2) in aerobic conditions. In anaerobic conditions, bacteria utilize nitrogen for growth in a process similar to MICP. Nitrate is reduced to nitrogen gas, while organic carbon is oxidized to inorganic carbon or bicarbonate, which then reacts with calcium ions to produce calcium carbonate precipitates. This process, called Microbial Induced Desaturation and Precipitation (MIDP), differs from MICP in that it does not result in the release of ammonia gas. When the MICP solution is injected into the soil, the bacteria and cementation solutions may lead to clogging in the injection point. This may also affect the groundwater flow path by increasing the pore pressure in the soil. The retaining permeability is a significant factor in MICP, limiting its use for deeper depths (Rajasekar *et al.* 2021; Tobler *et al.* 2012). The transport of bacteria and their activity are limited in fine-grained soils (Paassen *et al.* 2010). The release of ammonium chloride as a byproduct of EICP/MICP treatments is undesirable, making it crucial to minimize its release. Meanwhile, the other methods in MICP, such as denitrification, release nil ammonium (NH_4) in the eco-friendly process (Gao *et al.* 2022).

doi:10.6342/NTU202404421

Only a limited number of studies have explored the application of MICP treatment in field conditions, making it challenging to predict the achievable treatment depth. The growth of the microorganism could degrade with the depth due to reduction in soil organic matter, nutrient availability and oxygen limitation (Gomez *et al.* 2018). Given these limitations in field applications, denitrification is a viable alternative to MICP treatment. However, one key challenge of MIDP is its slower reaction rate, which leads to lower calcium carbonate precipitation compared to MICP (Gao *et al.* 2022). Zeng *et al.* (2022) conducted a field experiment to evaluate the feasibility of MIDP for stabilizing silty soil. Indigenous nitrate-reducing bacteria were used to generate nitrogen gas, while calcium nitrate and calcium acetate promoted calcium carbonate precipitation. Each test plot had one extraction well surrounded by six injection wells, all installed with PVC pipes at a depth of 5 meters. Several sensors were placed to monitor electrical conductivity, volumetric water content, and the chemical composition of extracted groundwater samples, providing insight into the MIDP process. The treatment solution's distribution and calcium carbonate precipitation were notably influenced by preferential flow through the more permeable soil layers.

According to literature reviews, surface percolation techniques have generally been applied to sand columns ranging from 1 to 2 meters in depth. Cheng *et al.* (2014) conducted a study on soil stabilization using MICP treatment in both fine and coarse sand through surface percolation. The experiment involved a 2-meter sand column, with 12 alternating layers of bacterial and cementation solution in fine sand, and 6 layers in coarse sand. The results showed that due to clogging issues in fine sand, the cementation depth was limited to less than 1 meter. In contrast, the coarse sand column achieved full cementation up to the maximum height of 2 meters. Paassen *et al.* (2010) performed a large-scale experiment of

doi:10.6342/NTU202404421

$100m^3$ (8m x 5.6m x 2.5m) in the evaluating the feasibility of bio-grouting using MICP for ground improvement. In the test area, three injection wells were installed for the MICP treatment solution, while extraction wells on the opposite side were used to collect any excess solution. To prevent sand erosion during the injection process, geotextile was placed over the extraction wells to facilitate the horizontal transport of the treatment solution.

EICP is an innovative and bio-inspired technique for ground improvement and liquefaction resistance. The EICP treatment solution involves a mixture of cementation solutions (urea ($CO(NH_2)_2$) and calcium chloride ($CaCl_2$)) along with urease enzyme. EICP is a straightforward process. EICP is a low-carbon emission, sustainable, ecologically friendly field application technique.

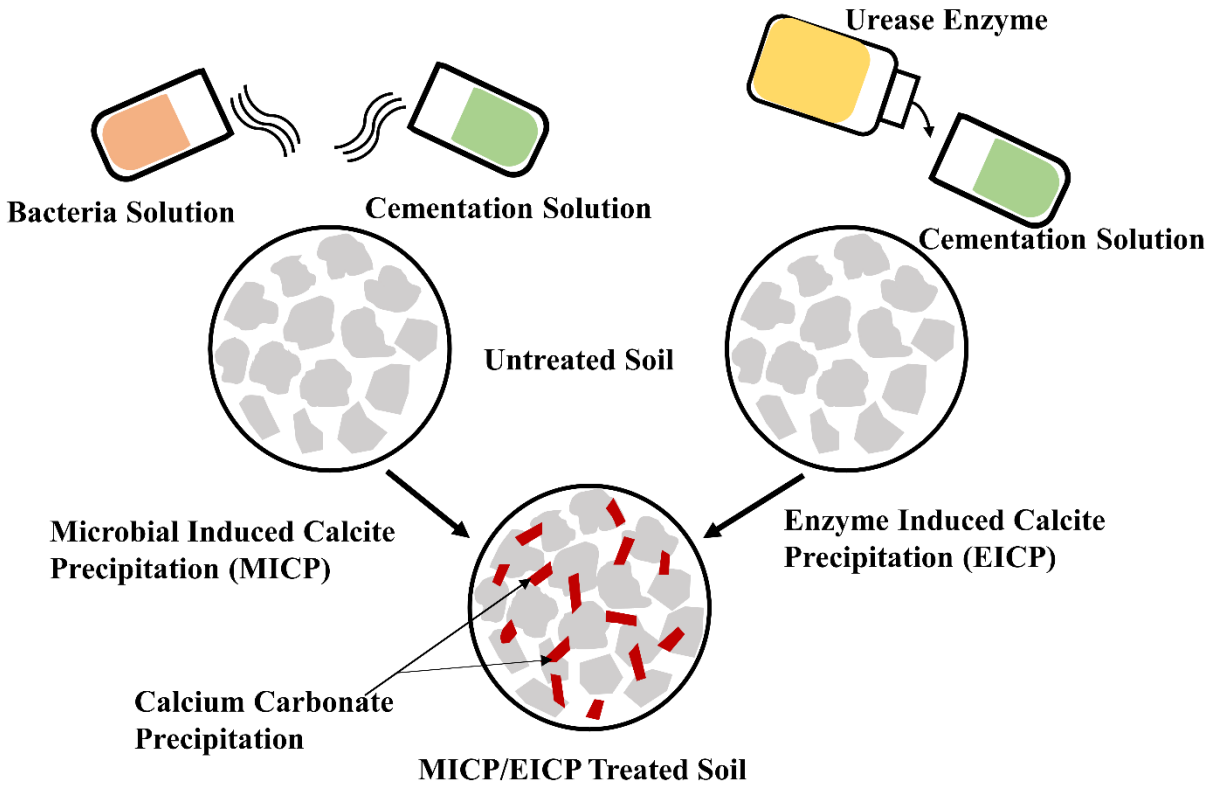

doi:10.6342/NTU202404421

Figure 2: Mechanisms of Microbial-Induced Calcite Precipitation (MICP) and Enzyme-Induced Calcite Precipitation (EICP) in the $CaCO_3$ precipitation.

Figure 2 illustrates the mechanisms of Microbial-Induced Calcite Precipitation (MICP) and Enzyme-Induced Calcite Precipitation (EICP) for calcium carbonate precipitation. In MICP treatment, urease-producing bacteria facilitate the hydrolysis of urea, resulting in the formation of carbonate and ammonium ions. The carbonate ions then react with calcium ions to produce calcium carbonate. In contrast, EICP treatment employs urease enzymes instead of bacteria to catalyze the urea hydrolysis process, relying on the same chemical reactions as MICP. Both EICP and MICP ultimately yield calcium carbonate as the end product, contributing to soil improvement.

1.3 Applications of EICP treatment

Enzyme-induced calcite precipitation (EICP) has a broader range of applications in the soil improvement compared to Microbial induced calcite precipitations (MICP) due to smaller size of urease enzyme, water solubility and viscosity of the EICP solutions. The precipitated calcium carbonate acts as a binder, fills pore spaces, and makes the soil particles rougher, increasing their strength, stiffness, and dilatancy. The bio-cemented soil behavior depends upon the type of ureases (Almajed *et al.* 2018), relative density (Xiao *et al.* 2019a), particle shape (Xiao *et al.* 2019d), and particle size distribution (Nafisi *et al.* 2020). Enzyme-induced carbonate precipitation has a wide range of potential applications in geotechnical engineering. Bio-cementation via EICP ameliorates the ground improvement (Gao *et al.* 2018; Kavazanjian *et al.* 2015; Meng *et al.* 2021b; Putra *et al.* 2020), liquefaction resistance (Huang *et al.* 2017; Xiao *et al.* 2018a), slope protection (He *et al.* 2022a; Liu *et al.* 2020;

doi:10.6342/NTU202404421

Yuan *et al*. 2020), seepage control, remediation from heavy metal contamination and erosion mitigation (Meng *et al.* 2021a).

1.4 Advantages of EICP

EICP is a candid procedure that uses free urease enzymes for calcite precipitation. EICP lacks nucleation sites (Yuan *et al*. 2020), unlike MICP. This method has advantages over the commonly used MICP process as it does not involve issues related to bio-safety. The free urease enzyme in EICP has a size of 12nm per subunit (Blakeley *et al*. 1984) and is soluble in water. The viscosity of the urease enzyme is the same as that of water, so it is easier to penetrate the small pore spaces, and thereby, it is instrumental in fine-grained soil. Therefore, EICP can be used both in coarse and fine-grained soil; consequently, it has no hindrance in its application due to its size. (Almajed *et al*. 2021a; Saif *et al*. 2022). MICP via bacteria typically have cell diameters ranging from 0.5 to 3μm and can vary in shape, including round, spiral, and rod-like forms. However, they cannot enter pore throat sizes smaller than 0.4μm (Mitchell *et al*. 2005) unlike EICP.

Using free urease enzymes could also reduce long-term environmental impacts due to a reduction in enzymatic activity and functionality over time (Marzadori *et al*. 1998; Pettit *et al*. 1976). For short-term engineering goals, ephemeral urease activity would be more appropriate, since after the enzyme has degraded, there will be no potential biological consequences. Even though the free urease enzyme is expected to degrade quickly, the sorbed urease can persist without losing any function or being degraded by proteolysis for a longer period of time (Pettit *et al*. 1976). The use of free urease enzyme is much easier than the use of ureolytic microbes because there is no need to cultivate or stimulate the bacteria. Because the microbes in MICP settle in the soil, specific environmental protocols could be required

doi:10.6342/NTU202404421

to ensure a safe and eco-friendly environment. The use of microbes in MICP requires favorable conditions for growth and technical expertise in handling the bacterial solution and controlling the technique in ground conditions (Yasuhara *et al.* 2012). Therefore, it is necessary to provide storage for bacterial strains, increasing the cost.

1.5 Limitations of EICP

Both EICP and MICP treatments induce calcium carbonate precipitation in highly alkaline conditions. However, a by-product of these processes is the release of ammonium chloride, a toxic and undesirable salt that accumulates in the soil post-treatment. This ammonium chloride, along with other harmful salts, can cause corrosion and potentially contaminate groundwater (Saif *et al.* 2022). Therefore, it is crucial to flush out the deposited ammonium chloride by rinsing or draining the soil with water to mitigate these risks. Several researchers have investigated this issue and proposed various solutions. One promising approach is electro-kinetic assistance with EICP/MICP treatment, which has shown potential in reducing the release of ammonium ions (Keykha *et al.* 2017). A commonly adopted method for removing ammonium ions from bio-cemented soil is rinsing, as demonstrated by Lee *et al.* (2019). Yu *et al.* (2021) proposed a technique using microbial induced struvite precipitation. In this treatment, ammonia or ammonium ions from the ureolysis reactions gets converted to struvite (magnesium ammonium phosphate) Its molecular formula is $NH_4MgPO_4.6H_2O$ or $MgNH_4PO_4(H_2O)_6$. Gowthaman *et al.* (2023) employed enzyme-induced calcium phosphate precipitation (EICPP), using calcium phosphate as a calcium source, which effectively limited the release of harmful by-products from the treatment.

Calcium chloride is a primary chemical component in EICP and MICP treatments for calcium carbonate precipitation. However, the release of chloride ions or their combination

doi:10.6342/NTU202404421

with ammonium can lead to corrosion of metals, damage to underground pipes, and groundwater contamination (Fouladi *et al.* 2023). These issues can result in increased costs associated with repairing substructures. To mitigate chloride ion release, it is essential to consider alternative calcium sources. Calcium acetate ($Ca(CH_3COO)_2$) is a viable substitute, which has been shown to reduce ammonia emissions by 54.2% (Xiang *et al.* 2022).

A significant challenge in adopting the EICP technique is its dependency on a commercially produced form of urease enzyme, primarily manufactured on a small scale for medical purposes. However, even a few grams of the pure urease enzyme are used for field applications, especially considering the substantial quantities required for large-scale field applications. To mitigate the cost of enzyme production, strategies like production for economical purposes and shifting from medical grade to industrial-grade production, and exploring urease enzymes derived from plant derivatives (such as soybeans, jack beans, and watermelon seeds), as well as microorganisms like bacteria, fungi, and yeast have been suggested (Javadi *et al.* 2018). Encouraging mass production of urease enzymes could also contribute to lowering their cost.

One of the significant areas for improvement in using urease enzymes is that the high purity and activity of urease enzymes available for commercial purposes are expensive at market rates. Lower activity and purity of urease enzyme leads to less and slower calcite precipitation, which results in a massive cost for the urease enzyme. Hence, it is essential to reduce the cost of urease enzyme for field applications.

1.6 Field Applications in EICP Treatment

In field applications the efficiency of the EICP treatment depends upon the adsorption and retention reaction of sand. Adopting one phase EICP treatment (urease and cementation

doi:10.6342/NTU202404421

solution) could lead to rapid formation of calcium carbonate at the injection point causing lesser penetration of EICP solution in the ground. This could lead to uneven distribution of calcium carbonate. To achieve uniform distribution, few researchers have come up with a technique of using one-phase low pH (Cui *et al.* 2020) and one-phase low temperature methods (Xiao *et al.* 2022). Generally pressurized injection of EICP treatment solution were performed to the desired level of treatment (Martin *et al.* 2024). This technique provide control over the flow rate of injection and hydraulic gradients but this technique could be complex when adopted for a large scale field application. This technique can be performed in the saturated soils so adopting this technique for deeper soil could be challenging. However, pressurized injection of EICP treatment for larger scale could increase the cost and complexity of the project (Zhang *et al.* 2023).

Hence few researchers came up with an idea of gravimetric injection or surface percolation where bacteria/urease solution and cementation sprayed on the top of the soil surface. The infiltration of the treatment solution is driven by gravity and capillary forces thereby enabling the treatment to be performed in all kinds of saturation. Gravimetric injection can be more cost effective compared to pressurized injection. However still more field research required for finding the range of depth where EICP treatment can be performed. Martin *et al.* (2024) conducted field scale study of biocemented soil column in a dry poorly graded sand using EICP and Tube-a-manchette (TAM) permeation grouting. The test was conducted in a test pit of 3.8m long. The biocemented soil column was installed using TAM and slide seal peaker (injection of EICP solution). The study was also conducted with 0.3-0.9m of overburden pressure above the cementation zone. For a better horizontal transport, geosynthetic circular aprons were used to prevent the vertical migration of the treatment

doi:10.6342/NTU202404421

solution from the injection ports. This study confirms that EICP technique can be adopted in field application using the conventional grouting system.

For consistent application of EICP treatment in a test area, various monitoring techniques can be employed, such as moisture sensors, pH measurements, electrical conductivity, downhole seismic testing, and cone penetration testing (CPT). The effectiveness of urease activity can be evaluated by measuring calcium carbonate precipitation, as well as monitoring the concentrations of reaction by-products, such as carbonate and ammonia, over time. The research considered overburden depths ranging from 5 to 20 meters below the ground surface. Since there is limited research on field-scale studies at such depths, further work is needed to explore deeper applications, particularly considering overburden pressure. The lack of research on EICP treatment at greater depths presents challenges, particularly in achieving uniform calcium carbonate distribution. However, the higher urease activity (5U/mg from Sigma Aldrich) used in this study, when injected at a high rate, could promote more uniform distribution of the solution, preventing rapid or uneven calcium carbonate precipitation (Hamdan *et al.* 2016).

1.7 Cost Applications

The urease enzyme used in this study was also sourced from Jack beans. Research indicates that crude urease can be a more cost-effective option for large-scale field applications (Tirkolaei *et al.* 2020). However, extracting these enzymes requires some technical expertise, and further research is necessary to enable large-scale urease production. For a rough estimate of material costs in a small-scale test, a $1m^3$ sandbox was used to assess the one-phase EICP treatment in soil. Table 1 outlines the costs of EICP treatment with its

doi:10.6342/NTU202404421

chemical components, excluding labor and miscellaneous expenses. These rates are based on Taiwan's 2023 market prices and may vary slightly by time and region.

Table 1: Cost Analysis

S.No	Chemical Constituents	Quantity ($1m^3$ of soil)	Cost (USD)
1	Urease enzyme – Jack bean (CDH)	3 kg	12000
2	Urease enzyme – Jack bean (Sigma)	3 kg	84377
3	Urea	60 kg	3440
4	Calcium Chloride dihydrate	100 kg	1400
		Total	16,840 (CDH Urease) 89217 (Sigma Urease)

1.8 Scope of Study

Extensive research has been studied on the compressive strength of the EICP-treated soil in one-phase, double-phase, and multiple-phase and premix of urease solution and cementation solution; meager studies have been carried out in the monotonic loading and cyclic loading test in EICP treatment. Often, geotechnical engineering challenges occur due to low to modern confining pressures. It is significant to learn about the influence of the mechanical behavior of EICP-treated soil under high confining pressure, which unravels the insight into the ground conditions like offshore piling, deep pile foundations, tunnels, and high earth dams (Marri *et al.* 2012). There are numerous methods for the increase of bio-cementation. Much research has focused on the compressive strength of the EICP-treated sand. Based on

doi:10.6342/NTU202404421

prior studies, a small amount of research has focused on the shear strength properties and liquefaction resistance in the EICP treatment.

In this study, free urease enzymes were added to the cementation solution, and the surface percolation method was used in the soil application. The jack bean urease used in this work was not found to be toxic (Follmer *et al.* 2001). This research work has made new efforts to study the influence of bio-cementation via EICP under different confining pressures. The mechanical behavior of the EICP-treated sand is greatly influenced by cementation and confining pressures (Feng *et al.* 2016; Simatupang *et al.* 2019). From the knowledge of the literature papers, samples prepared by percolation showed better particle cementation than those prepared by mixing EICP solution with sand. Hence, all specimens in this study were made using a one-phase method of mixing urease enzyme, urea, and calcium chloride in the pore volume solution to percolate in the triaxial sample mold and left for the respective curing time. A series of conventional drained compression triaxial tests were conducted to evaluate how different confining pressures affect the stress–strain–volume change behavior of specimens undergoing EICP treatment. The following Figure 3 shows the research framework carried in the study.

doi:10.6342/NTU202404421

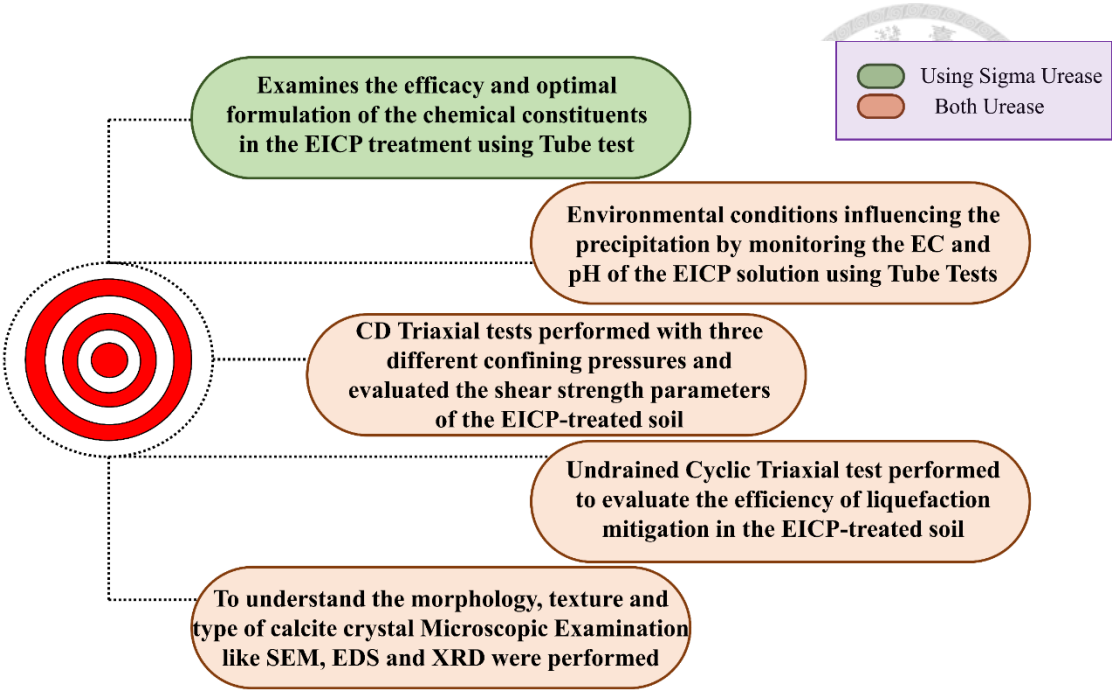

Figure 3: Flow Chart of Research Framework

1.9 Novelty of the Study

Extensive literature papers on EICP have focused more on the compressive strength test, treatment methods, and different types of urease enzymes but needed more research in studying monotonic and cyclic loading in the EICP-treated soil. This research focused on examining the uniform distribution of calcium carbonate in EICP-treated specimens, analyzing the mechanical behavior through consolidated triaxial compression test results, and evaluating liquefaction resistance based on cyclic triaxial test results.

- The EICP treatment solution, with a urea to $CaCl_2$ ratio of 1.5 (comprising 1 M urea and 0.67 M $CaCl_2$) and 3 g/L of urease enzyme, achieved the highest precipitation ratio and was subsequently used for soil treatment.
- The percolation method was employed for the EICP treatment, and the EICP-treated triaxial specimens, prepared under undrained conditions, showed uniform calcium carbonate distribution in poorly graded silica sand at room temperature.

doi:10.6342/NTU202404421

- Bio-cementation positively influenced the increase in effective cohesion over time, leading to improvements in both peak and residual strength.
- The preferential deposition of calcium carbonate in silica sand during EICP treatment enhanced shear strength and cyclic resistance through improved particle-to-particle contact and particle-to-calcite bonding.
- Calcite, the most stable form of calcium carbonate crystal, was identified as the primary product of the EICP treatment.

1.10 Organization

This dissertation is organized in the following chapters:

- Chapter 1 outlines the motivation for the research, provides background on EICP and MICP treatments, and briefly discusses their applications, benefits, limitations, and cost analysis, with a focus on EICP treatment.
- Chapter 2 presents a timeline study of EICP treatment, examining compressive strength, and static and dynamic triaxial tests using various treatment methods.
- Chapter 3 details the specifications of the experimental materials, the preparation of specimens, and the testing procedures applied to EICP-treated soil samples.
- Chapter 4 presents the results and discussion of the laboratory tests, evaluating the mechanical behavior of EICP-treated soils, and concludes with mineralogical analyses of the treated samples.
- Chapter 5 summarizes the research findings and provides conclusions drawn from the study.

doi:10.6342/NTU202404421

Chapter 2 LITERATURE REVIEW

2.1 Introduction

Soil plays a vital role in the infrastructural developments in developing countries or historic cities, which have geographic constraints in expanding the location. This creates intense engineering problems for the demand of human needs, which emphasizes the need to improve the ground sustainability for construction activities. Additionally, it leads to developing sustainable ground improvement techniques like EICP. Most ground improvement techniques using mechanical energy or binders like cement or lime could enhance the strength and stiffness of the ground. However, using these techniques could negatively influence the method by the increase in carbon dioxide emission, energy consumption, and leaching in lime-treated soil over a longer period. Over the past 15 years, several researchers have worked to induce calcite precipitation in the soil using bacteria and urease enzymes. Many researchers were performed in the last decade using MICP technique, but only a few sources are available on the EICP technique. MICP and EICP lead to the final product of calcium carbonate precipitation, which binds the soil grains together. The precipitate helps in the transition from a porous material to a solid form. MICP treatment involves using urease-producing bacteria like *Sporosarcina Pasteurii* for ureolytic action with a cementation solution consisting of urea and calcium chloride. Unfortunately, a few limitations in the application of MICP treatment on a field scale made EICP preferable compared to the former. The research focused on the studies of the drained triaxial strength and cyclic resistance in the EICP-treated soils. The historical developments in the application of the EICP technique in the improvement of mechanical behavior and factors influencing the treatment and

doi:10.6342/NTU202404421

methodology, and finally field scale improvement conducted by various researchers will be studied in the following sections

2.2 Urea Hydrolysis in EICP treatment

In EICP treatment, the ureolysis process is initiated by the urease enzyme and dissociates to ammonium and carbonate ions, which increases the pH of the solution. The presence of calcium ions in the cementation solution leads to the calcium carbonate precipitation shown in Figure 4. The chemical reactions involved in the mechanism are shown in the following equations.

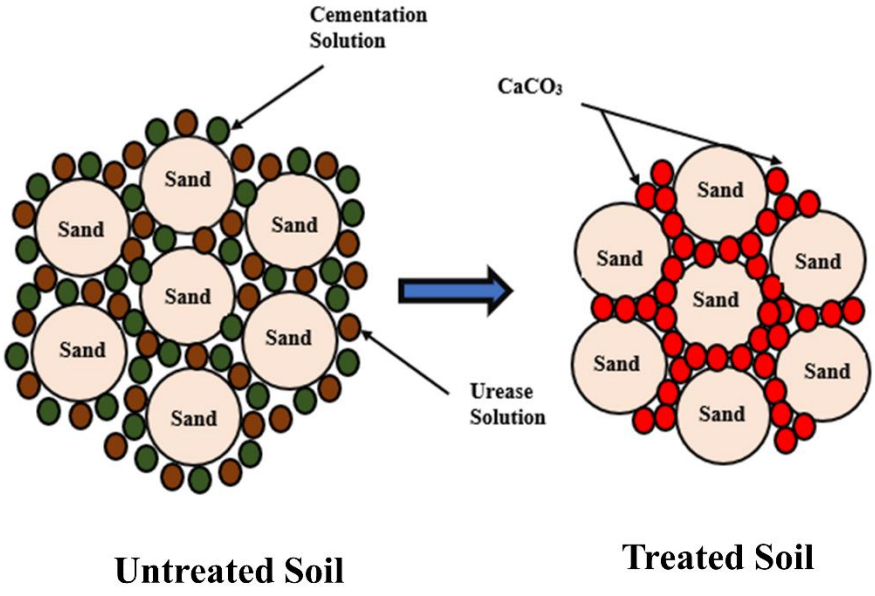

Figure 4: Soil Stabilization using Enzyme-Induced Calcite Precipitation (EICP)

$$CO(NH_2)_2 + H_2O \rightarrow NH_2COOH + NH_3 \quad [1]$$

$$NH_2COOH + H_2O \rightarrow NH_3 + H_2CO_3 \quad [2]$$

doi:10.6342/NTU202404421

$$2NH_3 + 2H_2O \rightarrow 2NH_4^+ + 2OH^- \quad [3]$$

$$2OH^- + H_2CO_3 \rightarrow CO_3^{-2} + 2H_2O \quad [4]$$

$$CO(NH_2)_2 + 2H_2O \rightarrow 2NH_4^+ + CO_3^{-2} \quad [5]$$

$$Ca^{2+} + CO_3^{-2} \rightarrow CaCO_3 \quad [6]$$

Equation 1 shows the hydrolyses of urea initiated by the urease enzyme to ammonia and carbamic acid, which increases the pH. The carbamic acid is further hydrolyzed to carbonic acid and ammonia, which can be seen in Equation 2. Under aqueous conditions, the ammonia further undergoes specific reactions and produces ammonium and carbonate ions under alkaline conditions, creating a favorable condition for precipitation (increase of pH). These reactions are shown in equation 3 and 4. Equation 5 summarizes all the four reactions and indicates that one mole of urea hydrolyses to two moles of ammonium and one of carbonate ions. The calcium chloride solution dissociates into calcium and chloride ions (Cl^-). The carbonate ions react with calcium ions, forming calcium carbonate precipitation. The chloride ions react with ammonium ions, leading to the formation of ammonium chloride. At this time, a reduction in the alkalinity of the solution is attained.

2.3 Factors influencing the formation of $CaCO_3$ precipitation

2.3.1 Electrical conductivity (EC) and pH

The formation of $CaCO_3$ precipitation is highly dependent on EC and pH of the EICP solution. Higher alkalinity in the pH of the solution creates a favorable condition for the precipitation. Hu *et al.* (2021) performed a series of test tube experiments of the ordinary EICP process and compared the carbonate precipitation from the ordinary EICP process to the modified EICP process with the addition of $MgCl_2$, NH_4Cl, and $CaCl_2$ concentration. The

doi:10.6342/NTU202404421

variation of EC and pH in the ordinary EICP process is shown in Figure 5. There is a minor EC change at the beginning of the ordinary EICP process due to the dissolution of urea. On adding $CaCl_2$ into the urea solution, the ionization of $CaCl_2$ produced more ions capable of carrying electric charges. Upon the addition of urease enzyme in the urea-$CaCl_2$ solution, two chemical reactions happen in the test tube a) Urea hydrolysis initiated by the urease enzyme to the formation of ammonium (NH_4^+) and carbonate ions (CO_3^{2-}) and calcium carbonate precipitation from the reaction between Ca^{2+} and CO_3^{2-} ions. Figure 5a shows the consistent increase in EC values and moves steadily until the end of the ordinary EICP process. The pH remains unchanged even after the addition of $CaCl_2$, whereas the pH significantly changes when the urease enzyme is added to the EICP process. The formation of OH^- ions induced by urea hydrolysis increases pH, and the consumption of OH^- in the carbonate precipitation process leads to the reduction of pH at the end of the EICP process. The pH value of the ordinary EICP process peaked at 8.9.

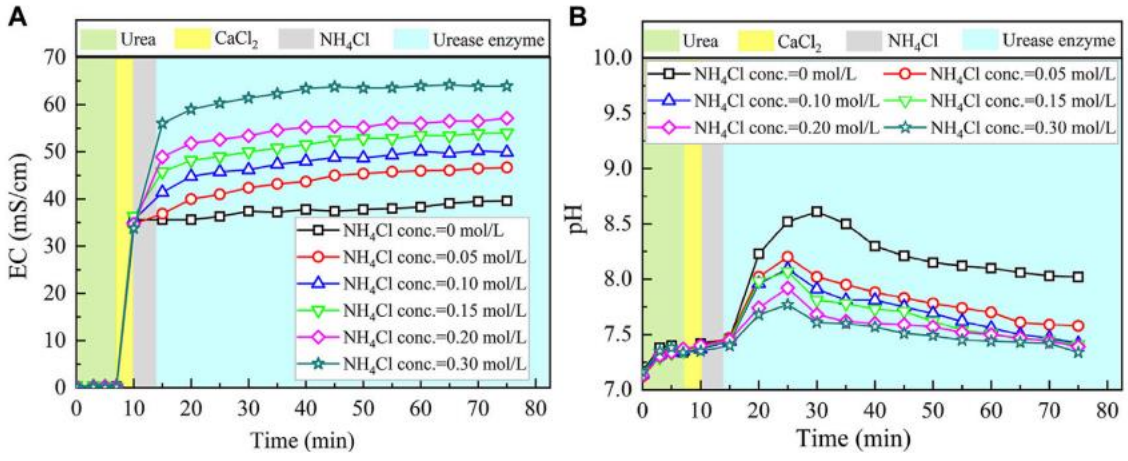

Figure 5: Temporal relations of EC and pH when subjected to the effect of NH_4Cl addition: (A) EC and (B) pH (Hu *et al.* 2021)

doi:10.6342/NTU202404421

Xie *et al*. (2023) investigated the environmental factors, cementation solution concentration, and urease activity in EICP treatment. The research explored pH's influence on calcium carbonate precipitation at different initial pH levels (7, 8, 9, 10, and 11). The variation of the consumption of Ca^{2+} and at various initial pH of the EICP solutions is shown in Figure 6a. Ca^{2+} consumption showed no significant difference with initial pH (6,7,8, 9, and 10) in the calcium carbonate precipitation and remained stable after 48 hours. Meanwhile, the EICP solution with an initial pH of 11 showed a remarkably lower consumption of Ca^{2+}. The possible reason could be due to the negative effect of high alkalinity inhibiting the formation of $CaCO_3$.

The influence of pH on the urease activity is shown in Figure 6b. The results show that the urease activity in pH 8-11 didn't significantly change the urease activity, whereas in pH 12, the urease activity dropped to the lowest activity. Extreme alkaline conditions inhibited the urease activity of the solution. The pH influences the dissociation of the substrate and coenzyme, affecting the enzyme's binding to the substrate. The optimum pH 8-11 maintains high activity; the dissociation of enzymes, substrates, and coenzymes was most suitable for them to combine and achieve high maximum reaction speed.

doi:10.6342/NTU202404421

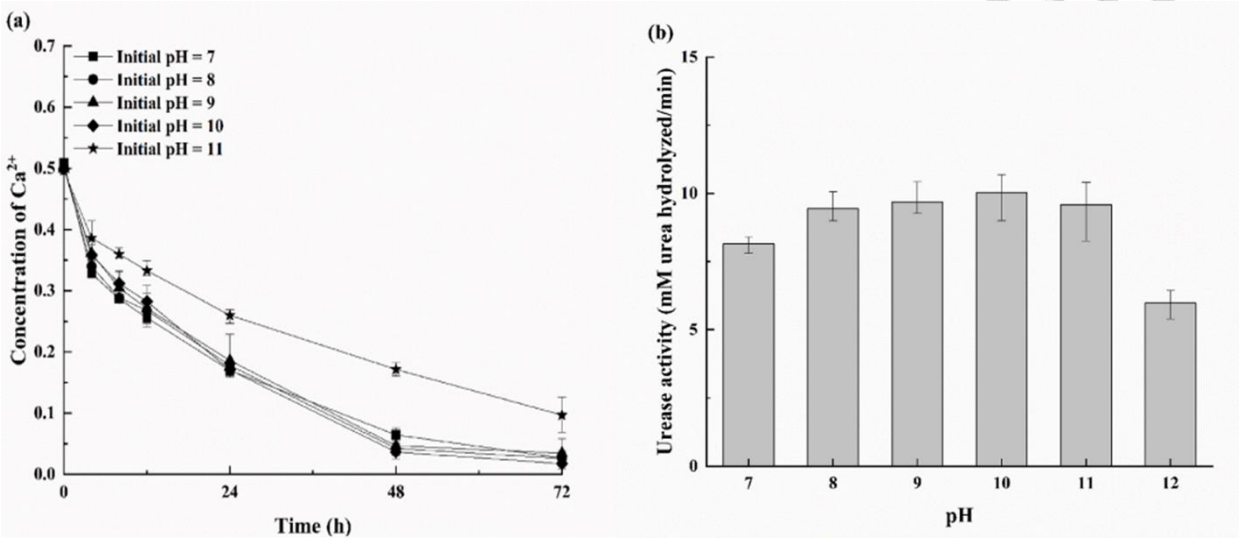

Figure 6: Variations of (a) concentration of Ca2+ with different initial pHs (b) pH on urease activity (Xie *et al*. 2023).

Jiang *et al*. (2016) studied the ureolytic efficiency in urease producing bacterium and purified urease enzyme under oxic and anoxic conditions. The purified urease enzyme and *Bacillus megaterium* were subjected to bench shaking ureolytic activity tests in both condition. The research studied various biochemical parameters like urea concentration, electric conductivity (EC), pH and optical density at 600 nm (OD_{600}) of the solution at different time interval were measured. Figure 7 shows the variation of EC and pH in the urease solution and bacterial solution. The increase of EC reflects the amount of electrolytic ions in the solution and affected by the magnitude and rate of ureolytic reactions. Both purified urease enzyme and bacterial urease showed higher EC value in anoxic condition than oxic conditions. Higher EC values in anoxic conditions could be due to the following factors (a) the ureolytic rate by the purified urease enzyme was faster in anoxic condition compared to oxic conditions (b) excess electrolytic substance formation apart from the ureolytic byproducts produced during bacterial cell growth in the anoxic conditions and (c) formation

doi:10.6342/NTU202404421

of the carbonate (CO_3^{2-}) and bicarbonate (HCO_3^-) ions in anoxic condition through bubbling with N_2 and CO_2. The variation of pH in purified urease enzyme and bacterial-derived ureases showed a sharp increase in pH with an initial time of 1 hour. This increase in pH could be due to the rapid hydrolysis of urea. Later, the pH of the solution increases marginally and reaches an equilibrium state. A notable observation was made in bacteria solution with anoxic conditions, which showed a slight reduction in the pH value due to the continuous production of acidic substances in the solution. The graph shows that the pH values in purified urease enzymes in anoxic conditions were slightly lower than in the oxic condition. This variation could be due to the deoxygenation caused by CO_2 gas. The graph shows that the pH in anoxic conditions in bacterial cases stabilized around 8.2-8.5, which is significantly lower than 9.4 in oxic conditions. This indicates that excess acidic electrolytic substances produced in the anoxic condition could reduce pH and increase EC values.

doi:10.6342/NTU202404421

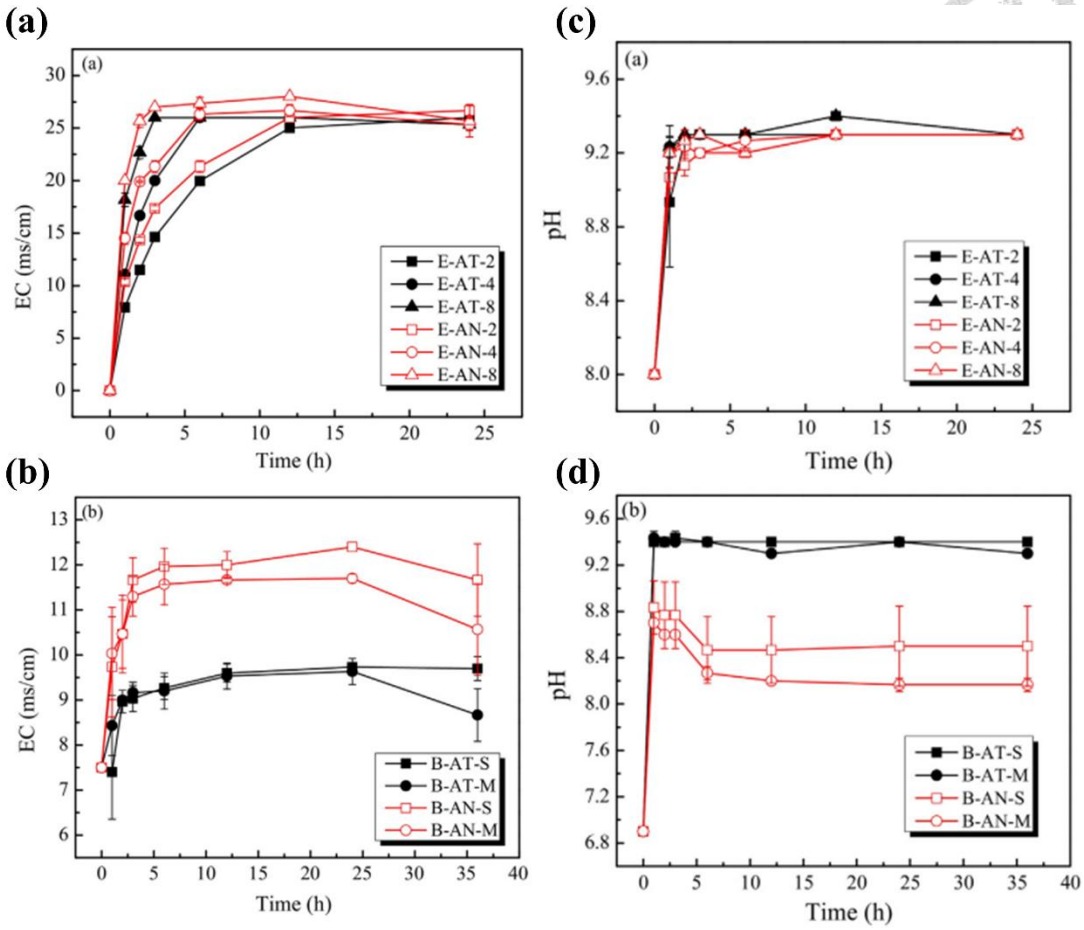

Figure 7: Variations of solution EC with time ((a) urease enzyme;(b) bacteria solution) Variations of solution pH with time ((c) urease enzyme;(d) bacteria solution) (Jiang *et al.* 2016).

2.3.2 Temperature

Urease is a protein and macromolecular biocatalyst. The temperature of the environmental condition greatly influences the enzymatic activity of the urease. The optimum temperature is essential for the maximum efficiency of the EICP process. If the temperature exceeds the optimum temperature, it could lead to the denaturation of the protein and inactivation of the enzymatic activity. Xie *et al.* (2023) studied the influence of urease activity with the increase of temperature in the range of 10-50ºC. Under 50 ºC, the reaction rate increased by binding

doi:10.6342/NTU202404421

higher energy molecules together from Figure 8a. When the temperature exceeds the optimum temperature, protein denaturation dominates the reaction rate, ultimately leading to the enzyme's inactivation.

Figure 8b shows the Ca^{2+} variation with time with three different temperatures: 20ºC, 28ºC and 37ºC. The research study confirms that the higher the temperature, the faster the $CaCO_3$ deposition rate. Both 20ºC and 28ºC took approximately 48 hours for the end of the reaction, whereas the 37ºC EICP solution took only 24 hours. Higher temperature increases the rate of ureolysis, which finally leads to a faster $CaCO_3$ deposition rate.

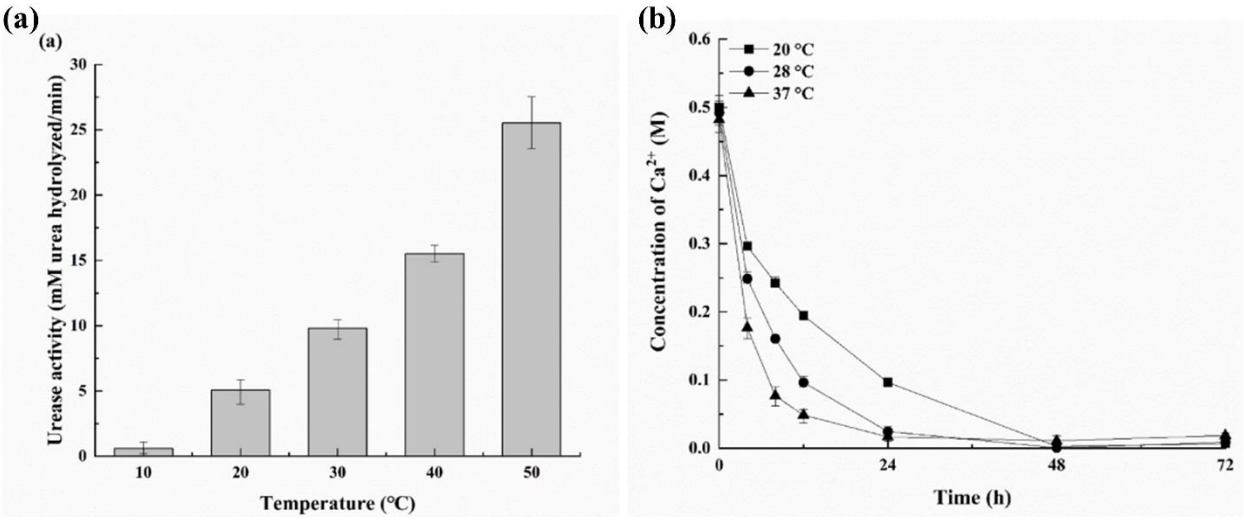

Figure 8: Influence of (a) temperature (b) Variations of concentration of Ca^{2+} at different temperatures (Xie *et al.* 2023).

Sahrawat (1984) mentioned the optimum temperature of the urease enzyme in the range of 10 - 60ºC and reached the maximum urease activity at 60ºC. Increasing the temperature to 100ºC, it had inhibited the urease activity. Nemati *et al.* (2003) studied the effect of temperature on the enzymatic formation of $CaCO_3$. The production rate of $CaCO_3$ increased from 0.038 to 0.34 g/L/hour with the temperature increase from 20 to 50ºC. On increasing

doi:10.6342/NTU202404421

the temperature range 30-50ºC, the conversion of 100% reached 120 hours, whereas at 20ºC the conversion at 100% took 300 hours. The enzymatic production of $CaCO_3$ at 20ºC and 50ºC was shown in the Figure 9.

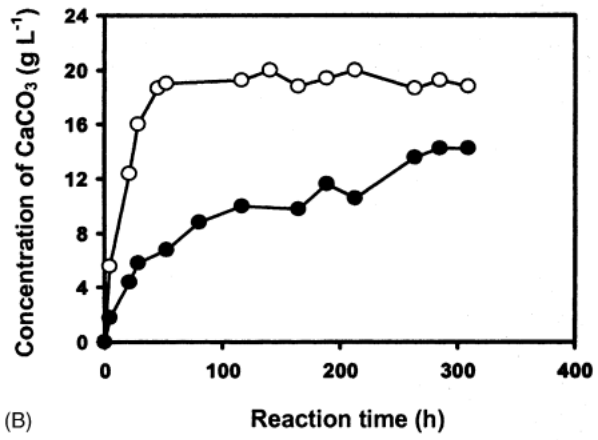

Figure 9: Effect of temperature on enzymatic $CaCO_3$ production: (●)22 ◦C, (○) 50 ◦C; (Nemati and Voordouw 2003).

2.3.3 Cementation Solution Concentration

Yasuhara *et al.* (2012) performed a tube test to examine the $CaCO_3$ precipitation depending on the concentration of the urea-$CaCl_2$. The amount of urease was fixed to 1g/100 ml, and the equimolar concentration of urea-$CaCl_2$ was 0.5,1 and 1.5 mol/L. The consumption of Ca^{2+} versus the concentration of urea-$CaCl_2$ is depicted in Figure 10. The average consumption of Ca^{2+} was 96.4%, 98.7%, and 79.1% at 0.5,1 and 1.5 mol/L urea-$CaCl_2$ EICP solution, respectively. The reduction in the consumption of Ca^{2+} was due to the supply of a high concentration of urea-$CaCl_2$ relative to the amount of urease supplied. This could restrain the activity of the urease and ultimately lead to a lesser amount of precipitation.

doi:10.6342/NTU202404421

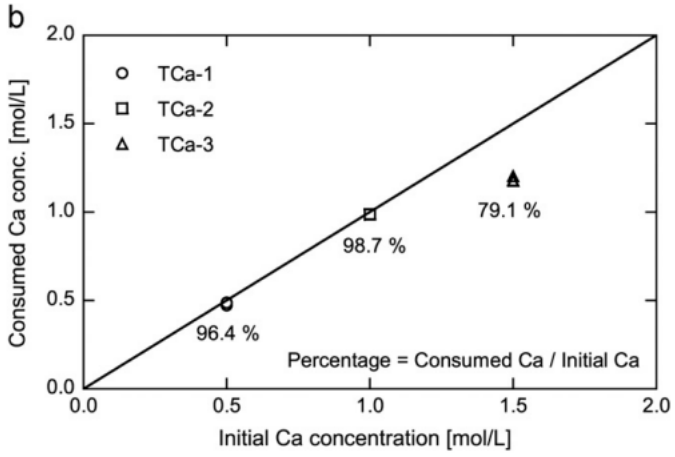

Figure 10: Results of test-tube experiments ((a) changes in pH with time and (b) relation between initial Ca and consumed Ca concentrations) (Yasuhara *et al.* 2012).

Similar results have been reported by Neupane *et al.* (2013). Several tube tests were performed with equimolar concentrations of urea-$CaCl_2$ with 0.5 and 1 mol/L. The amount of urease used in the tube test was fixed to 2 and 3.5 g/l. The EICP solution with 0.5 mol/L concentration yielded a higher precipitation ratio than 1 mol/L. The precipitation ratio in 0.5 mol/L increased tremendously with 2 g/l of urease; on further addition to 3.5 g/l, the precipitation ratio yielded 90%, as shown in Figure 11. Later on, an increase in the supply of urease showed a reduction in the precipitation ratio. This reduction could be due to the higher supply of urease showing an adverse effect or inhibiting the ureolytic reaction for $CaCO_3$ precipitation.

doi:10.6342/NTU202404421

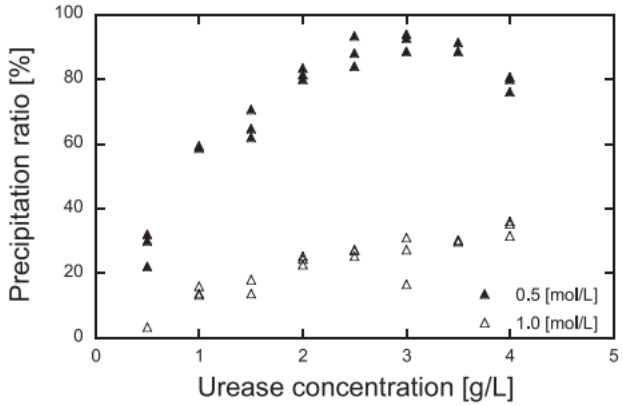

Figure 11: Correlation between urease concentration and $CaCO_3$ precipitation ratio (Neupane *et al*. 2013).

Carmona et al. (2016) aimed to analyze the impact of varying amounts of urea and calcium chloride on bio-cementation for soil improvement. Tube tests were carried out using equal amounts of urea and calcium chloride solutions (0.25, 0.5, 0.75, 1, and 1.25 mol/L) with a consistent urease concentration of 4 kU/L. Figure 12 depicted the results of the tube tests and confirmed that a lower concentration of urea-calcium chloride (0.25 mol/L) achieved a precipitation ratio of 95%, outperforming the higher concentrations, which implies that the urease supplied is sufficient to hydrolyze the urea completely. However, higher urea-$CaCl_2$ showed a reduction in precipitation ratio could be due to insufficient quantity of urease, which couldn't hydrolyze the urea completely, or higher urea-$CaCl_2$ inhibits the urease activity.

doi:10.6342/NTU202404421

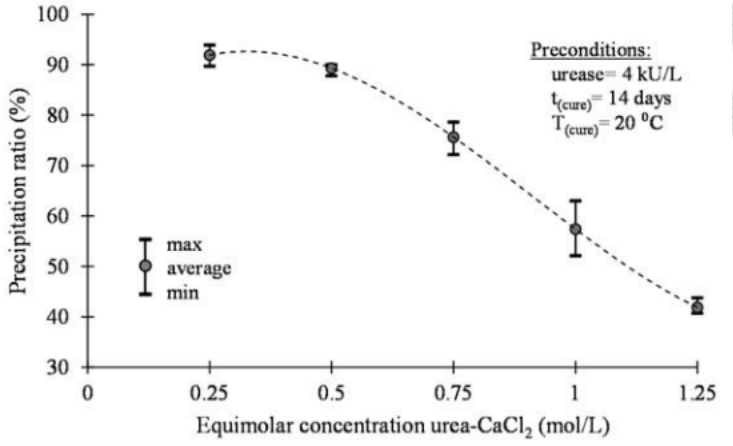

Figure 12: Test-tube experiments. Relation between urea-$CaCl_2$ concentration and $CaCO_3$ precipitation ratio (Carmona *et al.* 2016).

Ahenkorah *et al.* (2021b) studied the influence of the concentration of substrates [S_0] and enzyme [E_0] and enzyme activity (A_E) on the $CaCO_3$ precipitation ratio (PR). Two different types of urease were used in the study: high activity enzyme (HAE) with A_E = 40.15 kU/g and low activity enzyme (LAE) with A_E = 3.50 kU/g extracted from Jack bean and purchased by Sigma-Aldrich and Fischer Scientific respectively. The enzyme concentration was varied from 0 to 20 kU/l, corresponding to 0-0.42 g/l HAE and 0-5.10 g/l LAE. Figure 13a shows the precipitation ratio (PR) versus the equimolar concentration of urea-$CaCl_2$ [S_0]. In all the enzyme concentrations, PR decreased with a higher concentration of the substrate [S_0]. The reduction in PR could be due to an insufficient quantity of urease that could not hydrolyze the urea. Figure 13b shows the variation of PR with urease enzyme in different substrate concentrations [S_0]. PR increased with the increase of enzymatic activity [E_0]. A notable variation in PR is marked in both HAE and LAE urease enzymes.

doi:10.6342/NTU202404421

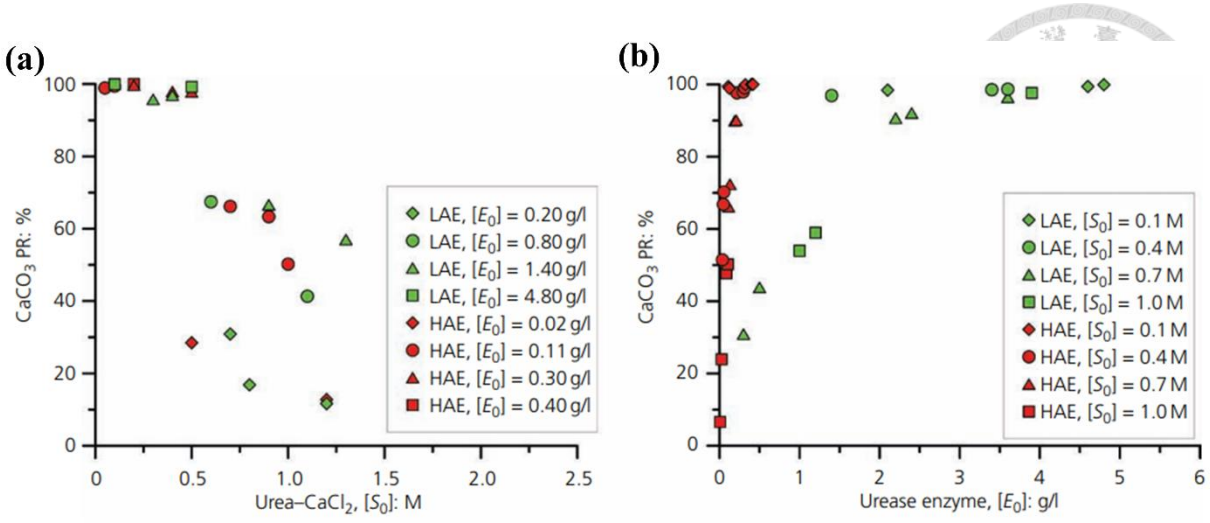

Figure 13: PR plotted against (a) urea–calcium chloride concentration, [S0]; (b) enzyme concentration, [E0] (g/l) (Ahenkorah *et al.* 2021b).

2.4 Prior Studies

Neupane *et al.* (2013) investigated the grouting technique in the porosity distribution by the precipitation of $CaCO_3$ in small-scale and in-situ tests. The optimal combined solution injected in a PVC cylinder and the porosity distribution within the soil are evaluated by sampling the treated sand at different locations. A small amount of enzyme achieved a precipitation ratio of up to 80%. The results show that the in situ enzymatic $CaCO_3$ precipitation technique may be feasible for large-scale applications. A Multiphysics simulator that considers the calcite precipitation reaction during the transport of the solution is adopted to predict the evolution of the porosity. The predicted porosities are compared with the measured porosities. The results show that the numerical predictions can replicate the actual changes in porosity relatively well and that the numerical model should help assume these changes are caused by the precipitated $CaCO_3$ induced by the grouting technique examined in this work. Neupane *et al.* (2015) worked on the insitu calcite grouting technique for a uniform distribution of calcite. This research carried out the grouting in the

doi:10.6342/NTU202404421

sand columns using an equimolar concentration of cementation solution and a mixed urease enzyme and enzyme reagent solution. The study also observed that the uniform distribution of the grout materials up to a distance of 1 m from the inlet is achievable and has a uniform distribution of calcite. Yasuhara *et al.* (2012) worked on the grouting technique by the enzymatically mediated calcite precipitation for the mechanical and hydraulic properties of treated sand samples through unconfined compression and permeability tests. The paper discusses the mechanical results showing that even a small percentage of calcium carbonate precipitated within the soils of interest brings about a drastic improvement in the strength of the soils compared to the untreated. The unconfined compressive strength treated with <10 vol% calcium carbonate precipitation against the initial pore volume ranges from ~ 400 kPa to 1.6 MPa. Also, the permeability of the treated soil was more than one order of magnitude smaller than that of the untreated soil. Neda Javadi *et al.* (2018) derived a lower cost of urease enzyme extracted from watermelon seeds used in the EICP for soil improvement. The extracted urease enzyme showed an activity of around 611 U/ml and was used to treat Ottawa 20/30 sand. A precipitation ratio of 64% was observed in the scanning electron microscope imaging results and energy-dispersive X-ray analysis.

2.5 Bio-cementation Techniques using EICP with additives

Almajed *et al.* (2021b) discussed the alternative stabilization of bio-stabilization methods like MICP and EICP. This paper reviewed the challenges, applicability, advantages, and disadvantages of MICP and EICP in soil treatment and their role in improving the geotechnical and geo-environmental properties. These bio-stabilization methods show their effectiveness in the remediation of soil contamination. This review intends to present a hands-on, adaptable treatment method for in-situ implementation depending on specific site

doi:10.6342/NTU202404421

conditions. Ahenkorah *et al.* (2021a) give a review and analysis of the EICP-based cementation. The study discusses the factors that influenced the EICP treatment, like the chemical constituents, the approach of the treatment, and the morphology of the calcite precipitation in the interlocking of the soil grains. The cost-effective approach in the extraction of urease enzyme and also the additives like magnesium chloride ($MgCl_2$), magnesium sulfate ($MgSO_4$), zeolite, dried non-fat milk, xantham gum, sisal fiber, and cabbage juice for the effectiveness of the treatment. Finally, the strength of the EICP-treated soil depends upon the particular polymorph, contact location, and distribution of precipitated $CaCO_3$, as well as the particle shape and size. Yuan *et al.* (2020) illustrated the preference for using organic materials in EICP treatment solutions. The additives like skim milk powder, glutinous rice powder, and brown sugar enhanced the soil strength by 33% compared to EICP-treated soil, which is nearly four times higher than untreated soil. The advantages of these inclusions provided nucleation sites for calcium carbonate deposition and improved the size, morphology, and structure of the calcium carbonate crystals. Almajed (2019) worked on the effect of adding biochar on the EICP-treated sand. Biochar was added at different temperatures (300, 500, and 700˚C) and applied at 1% to the soil. The outcome of the study illustrated that the addition of biochar will decrease the cementation bonding between particles, and strength, due to surface structure, and functional groups of biochar. However, the high pyrolysis temperature indicated that higher porosity would decrease the efficiency of precipitation. Putra *et al.* (2020) discussed the potential increase in the strength and stiffness of the soil, the additional materials for grouting, the effect of these materials on the treatment process, and the engineering properties of the EICP-treated soil. This paper also discussed the possible source of the urease enzyme and the applicability of the EICP method.

doi:10.6342/NTU202404421

The envisioned plans for application, as well as potential advantages and limitations of EICP for soil stabilization, were discussed. Chandra *et al.* (2020) demonstrated the effect of incorporating Mg^{2+} ions on crystal morphology and their direct influence on the mechanical properties of the soil. Soil specimens were prepared with EICP solutions, including urea, urease enzyme, and $MgCl_2/CaCl_2$ at various Mg^{2+}/Ca^{2+} molar ratios and subjected to unconfined compression test and microscopic studies (Field-emission scanning electron microscopy (FESEM) and X-ray diffraction (XRD) test). The undrained shear strength was improved for a lower molar ratio of Mg^{2+}/Ca^{2+}. He *et al.* (2022b) compared the influence of sand treated by EICP with either concrete-extracted or reagent calcium. Unconfined compressive test results with concrete extracted reached 833 kPa in the dry state compared to 204 kPa in the wet state by reagent calcium after 5 times of EICP treatment. Based on the scanning electron microscope (SEM) and X-ray diffractometer (XRD) analyses, calcite was the crystal type of calcium carbonate produced in the sand. Hu *et al.* (2021) studied the effect of the higher $MgCl_2$, NH_4Cl, and $CaCl_2$ in an EICP treatment solution to improve calcite precipitation. Tube test results were compared with the ordinary EICP process and the modified EICP process. The enhancement mechanism of carbonate precipitation is well interpreted by elevating the activity of the urease enzyme by introducing the magnesium ions. The degradation of carbonate precipitation was observed in higher NH_4Cl concentrations. The decreasing activity of the urease enzyme and the reverse EICP process play a leading role in the degradation of carbonate precipitation. Additionally, the exposure to higher $CaCl_2$ concentration, the slower rate of urea hydrolysis, and the decreasing activity of urease enzyme are primarily responsible for forming the hijacking phenomenon of carbonate precipitation. Putra *et al.* (2016) examined the mechanical properties of the EICP-treated

doi:10.6342/NTU202404421

soils by adding a small amount of magnesium chloride in the treatment solutions. the addition of magnesium chloride acts as a delaying agent. It is used to reduce the reaction rate of the precipitation, which may increase the volume of treated soil if used in the real field because of the slower precipitation rate and the resulting higher injectivity. The paper also presents the mineralogical analysis, which revealed that magnesium chloride decreases the crystal size of the precipitated materials and that another carbonate of aragonite is newly formed. Mechanical test results indicated that carbonate precipitates within the soils and brings about a significant improvement in strength. Lin *et al.* (2021) worked on EICP and MICP treatment in previous concrete piles to enhance the soil pile interaction and capacity. The research also focuses on the consolidated drained triaxial test on EICP and MICP treatments. The sand specimens were treated with similar levels of S-wave velocity using MICP and EICP treatment. EICP-treated specimens showed less calcium carbonate precipitation achieved. The MICP-treated specimen showed higher dilative and peak strength than the EICP-treated specimen. Iamchaturapatr *et al.* (2022) studied the influence of bio-cementation via EICP with natural hemp fibres for increasing the strength of the sandy soil. The results of bender tests evolved to a maximum shear modulus and shear wave velocity was achieved at natural hemp fibre at 2.5% as optimal amount. The cementation process peaked on the fourth day and ended on the sixth day. Using a spectrophotometer, the ammonification spiked on the fourth day and deteriorated later. Direct shear test results showed an increase in cohesion and friction angles, confirming that natural hemp fibre and the $CaCO_3$ precipitation improved the strength of the sand soil. Finally, the microscopic examinations via SEM imaging and XRD analysis showed the interlocking of the precipitation and natural hemp fibre for the strength enhancement in the sandy soil. Zhang *et al.* (2022a) investigated the EICP-lignin treatment

doi:10.6342/NTU202404421

in the silty soil in the Yellow River flood area, which is characterized by poor particle gradation, weak cohesion, and low strength. The research focused on studying the consolidated undrained triaxial test on them and found the cohesion and friction angle increased by 10 and 3 times, respectively, compared to the untreated silty soil. The shear strength parameter increased to 5% of lignin and decreased later with increasing lignin content. The SEM analysis showed the increasing aggregation of lignin and calcite. Figure 14 shows the advancement in the research involved in EICP over time.

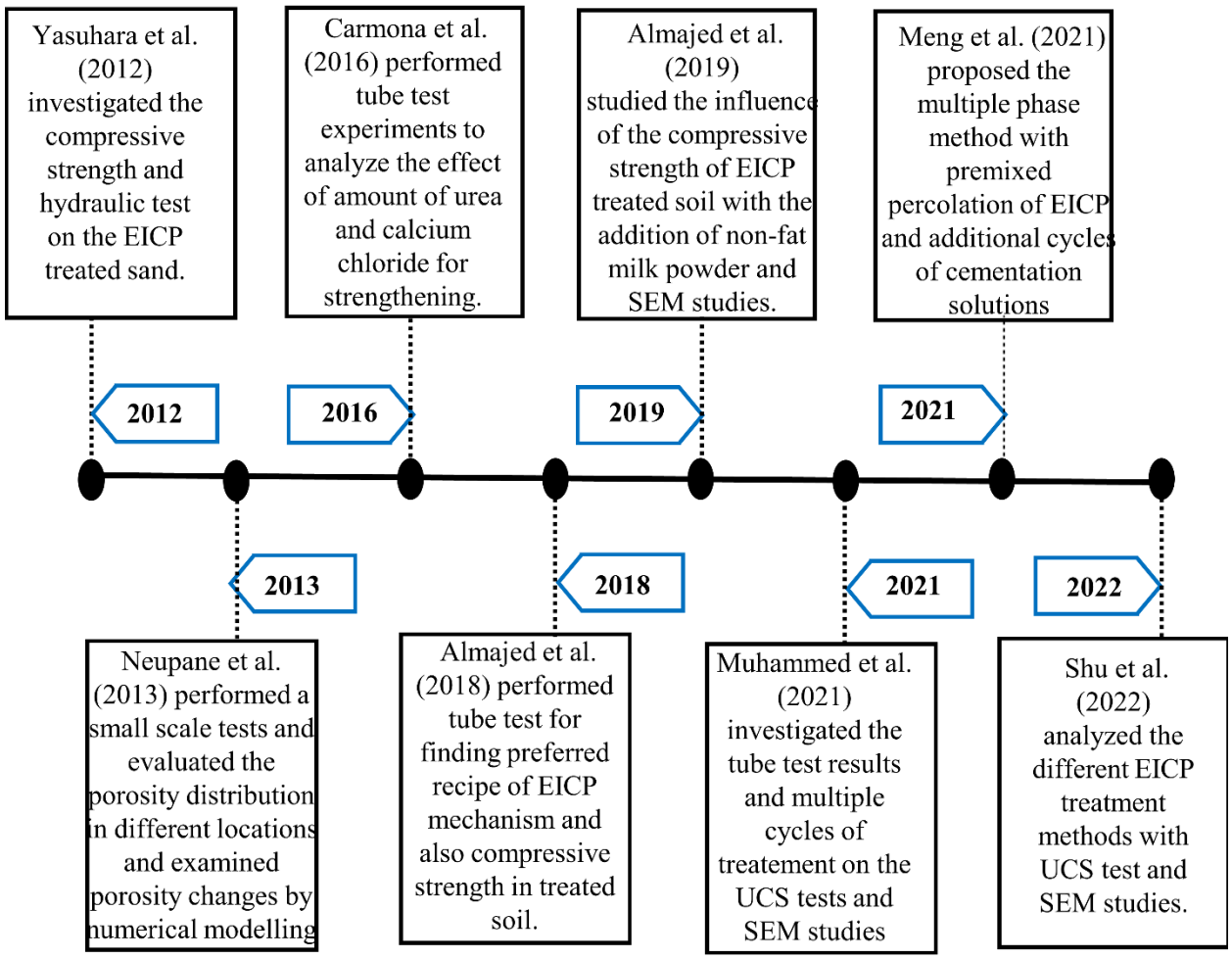

Figure 14: Timeline of research developments in EICP technique

doi:10.6342/NTU202404421

2.6 Compressive Strength Tests

2.6.1 Single-phase Treatment Cycle

Arab *et al.* (2021c) investigated jack bean meal urease with different EICP cementation solutions in one treatment cycle. The increase in the cementation concentration facilitates the dense calcite precipitation, leading to higher soil strength. The influence of bio-cementation under key environmental conditions like curing time, temperature, wetting and drying cycles, sulfate contamination exposure, and seawater exposure. Unconfined compressive strength in treated soils with a high molarity EICP-cementing solution was around 2.9 MPa at 5.6% $CaCO_3$. The EICP-treated soils showed higher resistance against seawater and wetting/drying cycles of fresh water, whereas less resistance was observed in the immersion of 5% sulfate solution. Martin *et al.* (2021) performed an unconfined compressive strength test in baseline EICP and modified EICP solutions (powdered milk used) in four cohesionless soils. The study found that the soils with modified EICP solution showed an increase in the strength of the baseline EICP solutions. Using this additive helps achieve greater target stress with a reduction in the cost of EICP treatment. Arab *et al.* (2021b) investigated the usage of EICP-based bio-cementation and sodium alginate biopolymer to produce bio-bricks in the construction industry. The bio-bricks produced have shown high compressive and flexural strength. The bio-bricks showed flexural strength comparable to 20% cement-treated sand and performed efficiently in the mechanical property and water absorption requirements. Wu *et al.* (2022) studied the influence of the mechanical properties of the desert aeolian sand with EICP treatment. The unconfined compressive strength, calcium carbonate content, and mercury intrusion capillary pressure tests. Higher compressive strength was achieved by increasing the urease activity and the concentration of the cementation solutions, and it also

doi:10.6342/NTU202404421

reduced the porosity of the solidified sand with calcite precipitation from EICP treatment. Xiao *et al.* (2019c) performed a series of unconfined compressive and splitting tensile tests in the basalt fiber-reinforced cemented sand specimens. Higher strength was achieved with the increase of calcite content, whereas the axial strain of the peak failure state decreases with the increase in calcite content. The improvement of ductility has implications for loading conditions in large deformations conditions. Almajed *et al.* (2019) demonstrated that the single-cycle treatment achieved a higher strength at a relatively low carbonate content by adding non-fat powdered milk to the EICP treatment solutions. The unconfined compressive strength results showed a higher strength in the samples treated with non-fat powdered milk. The use of additives can help reduce the number of treatments, thereby reducing the undesirable ammonium chloride by-product in an eco-friendly manner and reducing the treatment cost. Almajed *et al.* (2018) evaluated the influence of the composition of the EICP treatment solution on the efficiency of carbonate precipitation. The unconfined compression tests were performed in EICP-treated samples using two different types of treatment, percolation, and mixing methods, and they showed almost similar compressive strength in both treatments. To reduce the undesirable by-product of ammonium chloride, this study has rinsed the sample in deionized water to cause dissolution and flushing of organic matter or other by-products. Carmona *et al.* (2016) analyzed the effect of the amount of urea and calcium chloride on bio-calcification using EICP treatment. Tube test experiments and compression tests were performed in different urea – $CaCl_2$ concentrations, and the precipitation for $CaCO_3$ was evaluated. The increase of urea-$CaCl_2$ concentration inhibited the activity of urease and led to the reduction of the calcite precipitation. Cui *et al.* (2020) discussed the one-phase injection of low pH solution strategy in soil treatment. This method

doi:10.6342/NTU202404421

injects an EICP solution consisting of a mixture of urease solution of pH = 6.5, urea, and calcium chloride into the soil. Unconfined compression test results from the one-phase-low-pH method are much higher than those from the two-phase method, and the treatment is simplified with fewer injections. The experimental results proved that this method significantly improved the calcium conversion efficiency and the uniformity of calcium carbonate distribution in the sand samples compared with the conventional two-phase EICP method. Oliveira *et al.* (2017) examined the effect of the enzymatic calcium carbonate ($CaCO_3$) precipitation in five soil types (poorly graded sand, two silty sand, a silty soil, and organic soil). the result of the UCS test showed that EICP-treated soils improved compressive strength, but organic soil showed a detrimental bio-stabilization impact. Ahenkorah *et al.* (2021b) examined the influence of the concentration of the substrates and enzymes and the enzyme activity on the calcium carbonate precipitation ratio among 130 test tube experiments. An exponential function was developed to accurately capture the relationship between PR and enzyme concentration [Es]/concentration of substrates [So]. The established function was further correlated to predict the achieved strength gain from unconfined compressive strength [UCS] and splitting tensile strength [STS]. The scanning electron microscopy images, energy-dispersive X-ray spectroscopy, and X-ray powder diffraction showed that the precipitated calcium carbonate in test tubes and the treated soil were mostly calcite crystals with different morphologies. Putra *et al.* (2017) evaluated the effectiveness of magnesium as a substitute material in enzyme-mediated calcite precipitation. Magnesium sulfate was added to the urea, urease, and calcium chloride injecting solution. X-ray powder diffraction and scanning electron microscopy analyses were conducted to examine the mineralogical morphology of the precipitated minerals. In addition to calcite, aragonite and

doi:10.6342/NTU202404421

gypsum were formed as the precipitated minerals. The effect of the presence of aragonite, gypsum, and calcite was evaluated in unconfined compressive strength tests. the presence of the precipitated materials, comprising 10% of the soil mass within treated sand, generated a strength of 0.6 MPa.

2.6.2 Multiple-phase Treatment Cycles

Shu *et al.* (2022) performed a comparative study of different types of EICP treatment in sandy soil. Soybean crude urease was used as a catalyst for calcite precipitation. The four treatment methods include the one-phase, two-phase, premix and compact, and multiple-phase methods. The study confirmed that the samples from the multiple-phase method showed a high chemical conversion efficiency and uniform distribution of $CaCO_3$, which also helped efficiently utilize urease. Meng *et al.* (2021b) proposed a multiple-phase method consisting of premixed soybean crude urease and cementation solution followed by several percolations of cementation solution in one cycle of bio-cementation. In insitu-EICP treatment, a one-phase premixed percolation method using purified urease enzyme is adopted widely, which is expensive, involving the consumption of large amounts of urease. The treatment has increased the utilization of the urease by at least four times compared to the one cycle of treatment. This method has also weakened the clogging of the calcium carbonate precipitation and produces relatively uniform calcite precipitation. After four cycles of EICP treatment, the compressive strength of the ASTM C778-graded sand exceeded 10 MPa with a $CaCO_3$ of 20%. Cui *et al.* (2021a) proposed an alternative method, a modified one-phase-low-pH MICP or EICP method used to simplify the treatment procedure in improving the bio-treatment in real constructions. In this method, low-pH bacteria or urease solution is only used with the cementation solution (i.e., $CaCl_2$ and urea) for the first treatment. For the

doi:10.6342/NTU202404421

subsequent treatment, only cementation solution is used. The test results show that using the modified one-phase-low-pH MICP method with a bacterial solution of a volume ratio of 0.75 is comparable to that using the original one-phase-low-pH method, and 80% of the calcium conversion efficiency can be maintained for up to 5 treatments. However, the modified one-phase-low-pH EICP method may only be used for the first 2 or 3 treatments due to the relatively poor durability of the urease enzyme in inducing calcium carbonate during the subsequent injections of cementation. Muhammed *et al.* (2021) evaluated the effects of the multiple treatment cycles on the unconfined compressive strength (UCS) of the EICP-treated soil. The effectiveness of the bio-cementation revealed higher compressive strength with increased treatment cycles. The highest UCS was 1712 kPa at 1M after the 3rd treatment cycle, with 8.21% $CaCO_3$ content. The paper confirmed that the higher number of treatment cycles demonstrated that increased deposition of $CaCO_3$ precipitates increases the bonding effects and the strength of the treated soil. Qian *et al.* (2022) discussed the cementation mechanisms of MICP/EICP in the influence of soil pore structures, bacterium, urease, and cementation solution properties, and cementation methods on characteristics of calcium carbonate. The results indicated that the smaller the pore size, the more complex the infiltration of microorganisms or urease creates a random distribution of calcium carbonate. More contact points among the soil particles will produce more deposition points for $CaCO_3$, resulting in stronger bonding and bridging effects and better cementation effects. The generation rate and total amount of $CaCO_3$ increase as the concentration of bacterium or urease and the activity of urease increase in a certain range. However, too-high concentration or activity will induce a too-high generation rate of $CaCO_3$, resulting in clogging near the injection end. The calcium carbonate crystals obtained from low-concentration cementation

doi:10.6342/NTU202404421

solution are relatively small and evenly distributed. Multilayer alternating injection or one-phase low pH injection improves the distribution uniformity of $CaCO_3$ in the sample.

2.7 Static Triaxial Studies

He *et al.* (2020) demonstrated bio-cementation on silty sand with crude urease extracted from the lysis of ureolytic bacteria and live bacteria and evaluated their stress-strain response and volumetric strain response. The monotonic undrained triaxial test results of samples treated with urease showed higher shear strength and more dilative stress-strain responses than the samples treated by live bacteria. A major shortcoming of using live bacteria is that $CaCO_3$ precipitation accumulates on the injection side of the sample. This problem can be alleviated using crude urease, which showed higher $CaCO_3$ even at deeper locations. He *et al.* (2021) performed a laboratory model experiment in EICP treatment using crude urease extracted from soybean. Triaxial samples were taken from the model, and consolidated drained triaxial tests were performed on them. The EICP-treated specimens showed a 5.4 to 34.7% increase in the peak deviatoric stress compared to the untreated soil. Also, an improvement in shear strength parameters was observed. The effective friction angle increased from 24˚ to 28.9˚, and cohesion increased from 0 to 3.5 kPa. The XRD analysis of the treated soil sample showed calcite and vaterite crystals with more calcite crystals in the soil. Gao *et al.* (2019b) studied the mechanical behavior of soil treated with EICP via soybean urease, which was examined on silty sandy soil. The treated soil exhibited higher peak deviatoric stress and a more dilative response than untreated soil. Moreover, the treatment process led to a continuous increase in calcium carbonate content. Notably, no soil pore clogging occurred during multiple treatment processes, indicating the potential applicability of EICP treatment to fine-grained soils. Cui *et al.* (2021b) conducted drained triaxial tests and scanning electron

doi:10.6342/NTU202404421

microscopy observations in calcareous sand, which has abundant interparticle pores and is prone to particle breakage. Experimental results confirmed higher shear strength in EICP-treated calcareous sand. The strength enhancement in the bio-cemented calcareous sand is significantly lower than that of bio-cemented silica sand at the same calcium carbonate content, which the differences in the following may cause: (a) soil skeleton strength; (b) the amount of effective calcium carbonate; (c) interparticle pore filling of calcium carbonate. Gao *et al.* (2019a) conducted a triaxial consolidated drained test, and K_0 consolidation tests were carried out on ASTM-graded Ottawa and relative densities to study the failure and drained stress-strain behavior and compressibility of bio-cemented sand. Even a small amount of bio-cement treatment showed better densification treatment regarding strength improvement and deformation control. In triaxial tests, the shear strength, the slope of failure in the p'-q space, and the peak dilation rate increase with every increase of treatment at various levels of relative density. In the K_0 consolidation test, the K_0 value showed a smaller value due to a bio-cementation effect. Scanning electron microscopy was also conducted on the sand samples to investigate the particle-level structure of the bio-cemented sand and its correlation to mechanical behavior. Feng and Montoya (2016) illustrated the monotonic mechanical response of MICP cemented sand in four cementation levels (untreated, lightly treated, moderately treated, and heavily treated) and three levels of effective confining pressure (100, 200, and 400 kPa). The experimental results indicated that the stiffness, peak shear strength, and dilation increase with an increase in calcite content at a given effective confining pressure, and the dilation is suppressed with an increase in effective confining pressure. The mechanical properties of the MICP-treated soils, like peak and residual friction angles and initial elastic modulus, *Ei*, depend on the cementation levels and effective

doi:10.6342/NTU202404421

confining pressure. Montoya *et al*. (2015) examined the evolution of the shear strength and the stiffness of sand subjected to undrained and drained shearing using triaxial tests. MICP-treated sands with cementation levels ranging from young, uncemented sand to a highly cemented sandstone-like condition are subjected to undrained shear. A transition from strain hardening to strain softening behavior and a corresponding transition of global to localized failure as cementation is increased is observed. Shear wave velocity is used to monitor the change in small strain stiffness nondestructively during shearing, indicating cementation degradation as a function of strain level. This is because the shear wave velocity gets influenced by both the level of cementation and the change in effective mean stress during shearing. He *et al*. (2022c) performed a model test using a meter-scale soil model to evaluate the performance of the EICP method for the improvement in silty sand. Crude urease derived from soybean and industrial grade calcium chloride and fertilizer urea are used for soil treatment. In the treatment process, 1.5 times the pore volume treatment was circulated in the soil model through four perforated treatment pipes at one treatment time. The soil model has been treated a total of 5 times. Penetration resistance tests with a cone-shaped penetrometer were conducted in the soil model. It was found that the penetration resistance increased with more treatment times. The distribution of calcium carbonate content was consistent in the model. Soil samples taken from the model box for triaxial CD tests showed higher peak deviatoric stress, 34.7% improvement, and friction angle increased from 24.0˚ to 28.9˚, and cohesion increased from 0 to 3.5 kPa. Nafisi *et al*. (2019) investigated the shear behavior of moderately treated specimens using EICP and MICP on different sands - Ottawa 20-30 and Ottawa 50-70. The improvement in calcium carbonate precipitation and the shear wave velocity was faster in EICP than in the MICP-treated specimen. Even among specimens with

doi:10.6342/NTU202404421

similar shear wave velocities, the EICP-treated specimens exhibited less calcium carbonate precipitation than the MICP-treated specimens. Both EICP and MICP-treated specimens exhibited improvement in terms of shear strength. At a similar shear velocity, the EICP-treated specimen showed lower strength and dilative strain than the MICP-treated specimen. Still, this claim could change when the calcium carbonate for EICP and MICP-treated specimens were similar. The SEM studies on the EICP and MICP-treated samples showed vaterite and calcite to be the predominant crystal shapes, which influenced the shear strength of the sand.

2.8 Dynamic Response Studies

2.8.1 MICP Treatment

Xiao *et al.* (2018a) studied the cyclic resistance of the calcareous sand using MICP treatment to mitigate their liquefaction potential. This research paper examines the effectiveness of MICP on cyclic resistance as a function of cementation solution (CS) content, effective confining pressure, and cyclic stress ratio (CSR). The generation and accumulation of excess pore pressure and corresponding axial strains are compared with treated and untreated sand. Xiao *et al.* (2019b) explored the effect of relative density on bio-cemented sand treated with MICP. The study evaluated the efficiency of cementation, liquefaction mitigation, and cyclic behavior in bio-cemented calcareous soils. As the relative density of untreated loose calcareous sand increased from 50% to 80%, it shifted from a flow failure liquefaction mode to cyclic mobility. The liquefaction curve rose as relative density increased, mirroring trends observed in MICP-treated bio-cementation. However, when comparing untreated calcareous sand specimens to MICP-treated ones with the same unit dry weight, the cyclic resistance of the MICP-treated specimens was notably higher. This improvement was attributed to the

doi:10.6342/NTU202404421

influence of calcium carbonate precipitation between the voids, enhancing the overall strength and resistance to cyclic loading instead of densification. Sun *et al.* (2021) applied MICP treatment to stabilize loess soil and assess its liquefaction resistance using two methods: simultaneous supply of bacterial suspension and cementation solution (AT) and separate supply (AS). In MICP-treated samples, AT treatments with an initial density of 1.4 g/cm³ showed greater liquefaction resistance compared to AS treatments with initial densities of 1.5 and 1.6 g/cm³. The AT method proved more effective for soils with lower initial density, minimizing bio-clogging during the treatment. MICP treatment also reduced soil permeability by filling voids with calcium carbonate precipitation. As the number of treatment cycles increased, so did the number of cycles required to induce liquefaction. The results showed an exponential relationship between the calcium carbonate content, the number of cycles to liquefaction (NL), residual strength, and the reduction in damping ratio (*D*). Linear correlations were also identified between Specific Gravity (SG), $CaCO_3$ content, NL, residual strength (τr), and damping ratio (*D*) in the solidified loess soil. These findings offer valuable insights into mitigating liquefaction in loess soil through MICP treatment. Sasaki *et al*. (2016) investigated the sandy materials with or without the fineness content in the sand recovered from Urayasu City after the 2011 Great East Japan Earthquake. Bio-cementation using MICP treatment on the sand solidified with $CaCO_3$ produced by a bacterial species named Sporosarcina Pasteurii. The MICP-treated sand was subjected to undrained cyclic loading. The experimental results confirmed the effectiveness of MICP to sand with a non-plastic fines content in mitigating the liquefaction potential. Karakan *et al*. (2019a) examined the evaluation of the cyclic behavior of silts in a pore water pressure ratio of less than 50%. The inclusion of non-plastic silt was used to eliminate the effects of plasticity and

doi:10.6342/NTU202404421

also inferred that volume changes in silt due to the reconsolidation after cyclic loading with an induced pore water pressure (r_u) less than 50% shows limited liquefaction. Karakan *et al.* (2019b) evaluated the effect of the liquefaction and post-liquefaction behavior of non-plastic silt under cyclic loading. The cyclic triaxial tests revealed that the axial strains of specimens in lower relative densities increased at a higher CSR level. Post-liquefaction volumetric strain and relative density were established to predict liquefaction. These curves, along with the calculation of post-liquefaction volumetric strain, are helpful in the estimation of settlements of silt after being subjected to cyclic loading. Han *et al.* (2016) explored different grouting schemes during specimen preparation and analyzed the dynamic response of MICP-treated specimens. Dynamic triaxial tests conducted on solidified sand samples showed enhanced liquefaction resistance. The study employed four grouting schemes (MP10, MP11, MP12, and MP13), as detailed in Table 2, and the experimental results highlighted significant improvements in liquefaction resistance across the treatments.

Table 2: Grouting Scheme

Sample No.	10^8/ mL	Bacteria Batches	Nutritive Salt Batches
MP10 group	0.55	1	1
MP11 group	1.10	1	1
MP12 group	0.55	2	2
MP13-1	0.55	4	4

The grouting schemes MP10 and MP11 produced similar results, with the only difference being the bacterial cell concentration, indicating that the concentration used was sufficient

doi:10.6342/NTU202404421

for effective calcium carbonate precipitation. MP12 demonstrated a better transition from loose to dense sand, which significantly reduced the soil's vulnerability to earthquake-induced liquefaction. Notably, MP13-1 outperformed the other specimens, suggesting that once the soil attains a certain strength, further reductions in bacterial concentration may no longer be economically or environmentally justified. The new MICP formula and grouting method used in the study proved to be more efficient overall. Xiao *et al*. (2019a) performed an extensive experimental study on the influence of initial relative density on the efficiency of the cementation process, the reduction of liquefaction susceptibility, and the cyclic response in the calcareous soil. The cyclic experiments revealed that the MICP treatment can change the liquefaction failure mechanisms from flow failure to cyclic mobility and significantly change the excess pore pressure generation response of initially loose specimens. The effect of bio-cementation using MICP was contrasted against the effect of relative density alone, and MICP treatment showed greater efficiency in improving the cyclic resistance than densification. Montoya *et al*. (2013) conducted an assessment of cementation effects through centrifuge testing and investigated the behavior of MICP-treated sands under dynamic loading. Three levels of cementation treatment (light, moderate, and heavy) were subjected to ground motions, including sine waves with increasing amplitude. In dynamic testing, soils treated with MICP exhibited a reduced excess pore pressure response at all accelerations, decreased settlements, and greater peak surface accelerations compared to untreated loose saturated sand. Shaking-induced settlements were lower in MICP-treated sand than in untreated loose sand models. Centrifuge test results indicated lower pore pressure ratios, reduced shaking-induced settlements, and increased peak accelerations at the ground surface with heavy cementation. These findings underscore the importance of

doi:10.6342/NTU202404421

conducting a thorough site response study before MICP treatment and the need to minimize the amplitude of higher surface acceleration, which is undesirable. Rui *et al.* (2022) investigated the liquefaction resistance of calcareous sand and fiber-reinforced sand of MICP-treated sand. Dynamic triaxial testing results in MICP-treated sand showed that the dynamic strain and dynamic pore pressure decreased by 95.74% and 92.43%, respectively. Similarly, the dynamic strain and dynamic pore pressure of the fiber-reinforced MICP specimens decreased by 74.32% and 74.18%, respectively. Both treatments, with or without fiber reinforcement, increased the dynamic modulus of elasticity and reduced its attenuation rate. The inclusion of fibers in the MICP treatment specimen increased spots for bacterial adhesion and promoted the formation of calcium carbonate crystals.

2.8.2 EICP Treatment

There have been very few studies investigating the dynamic response of EICP treatment. Figure 15 shows the research developments of MICP and EICP treatments in studying the dynamic response toward liquefaction resistance. Simatupang *et al.* (2018) performed undrained cyclic triaxial tests on EICP-treated sand to investigate how particle size, calcite content, and degree of saturation affect liquefaction resistance and small strain stiffness. Two key factors were found to significantly impact both liquefaction resistance and small strain stiffness. First, calcite precipitation during treatment bonded the soil grains together, enhancing the mechanical properties of the treated sand. However, these calcite bonds began to degrade when the double amplitude axial strain (DA) reached approximately 0.5%. Second, the treated sand demonstrated improved dilative behavior due to the relative angularity, which was influenced by the ratio of calcite crystal size to sand grain size. This angularity also affected the number of cycles required to reach DA = 5% after achieving DA

doi:10.6342/NTU202404421

= 0.5%. Small strain stiffness was found to increase with higher confining pressure and calcite content, while sand particle size had little effect on the improvement. An empirical relationship was established between liquefaction resistance and normalized shear wave velocity, offering a valuable tool for field applications in mitigating liquefaction. Singh *et al.* (2021) worked on the effect of EICP treatment on the cyclic response of silty sands containing petroleum hydrocarbon compounds. The strain-controlled cyclic triaxial tests revealed that petroleum contamination moderately increases the cyclic resistance up to a transition point beyond which it falls off sharply. The coupled effect of increasing oil content and curing time of EICP treatment was assessed. The variation of cyclic strength with crude oil content results in a single-peaked profile for both untreated and treated specimens. EICP treatment increases the cyclic resistance of oil-contaminated sand up to 1.5 times by suppressing the excess pressure build-up. Finally, with the increasing oil content and shear strain levels, the efficacy of EICP treatment exhibited a remarkable decline. Simatupang *et al.* (2017) investigated the effects of the degree of saturation during the precipitation of calcite on the behavior of sand that has been lightly cemented using EICP and evaluated through a series of undrained cyclic triaxial tests. Liquefaction strength curves correlating the cyclic stress ratio with the number of cycles needed to cause 5% double amplitude (DA) axial strain were compared for treated and untreated sand. The research study found that the lower the degree of saturation during calcite precipitation and the higher the calcite content in the samples, the higher the liquefaction resistance of the EICP-treated sand. The paper confirmed that the precipitated calcite precipitation at a lower degree of saturation (30%) can double the liquefaction resistance. However, excessive strain in the order of 1% degrades the bonding between sand particles. Simatupang (2020) conducted a comparative study utilizing

doi:10.6342/NTU202404421

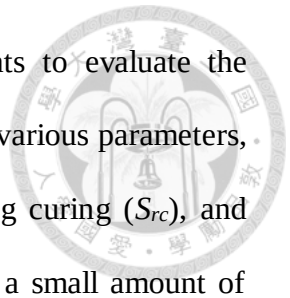

laboratory cyclic triaxial experiments combined with bender elements to evaluate the liquefaction resistance (*RL*) of EICP-treated sand. The study examined various parameters, including sand particle size, confining pressure (CP), saturation during curing (S_{rc}), and calcite content (CC). The experimental results demonstrated that even a small amount of calcite precipitation significantly enhanced the soil's shear modulus (G_o), which was linked to improvements in the shear wave velocity (V_{sl}) of the treated sand. However, when the test results were compared with standard liquefaction charts, it was found that the corrected cyclic resistance ratio (CRR) and V_{sl} of EICP-treated sand exhibited distinct behaviors compared to untreated sand. Consequently, the existing liquefaction potential curves were determined to be unsuitable for evaluating liquefaction resistance in the context of bio-cementation (EICP) treatment.

doi:10.6342/NTU202404421

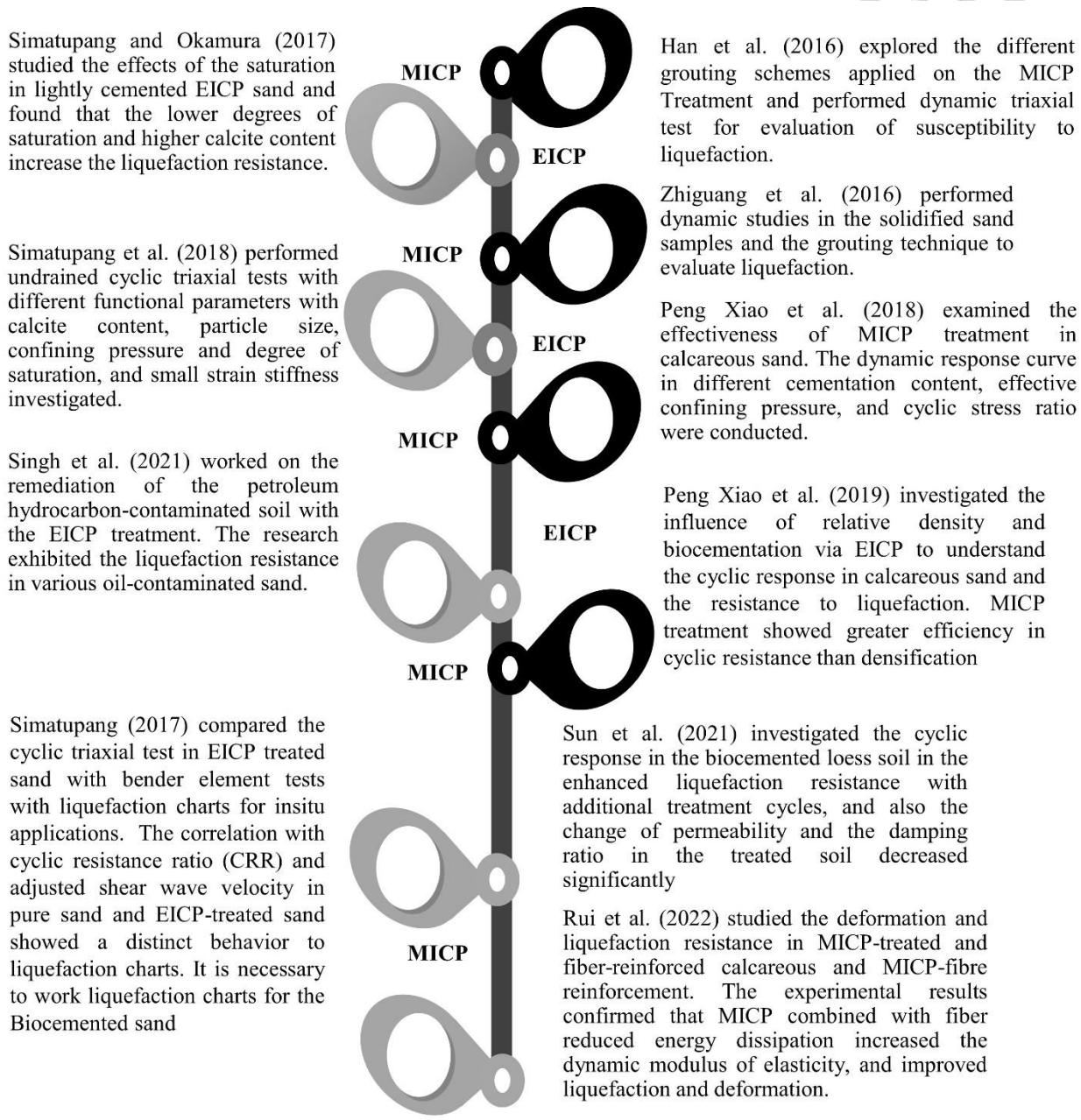

Figure 15: Timeline of research developments for the dynamic behavior of EICP and MICP treatments in cyclic triaxial testing.

doi:10.6342/NTU202404421

Chapter 3 EXPERIMENTAL PROGRAM

3.1 Materials

3.1.1 Sand

Silica sand was used in this study. The particle size distribution curve is shown in Figure 16. The coefficient of uniformity C_u was 1.403, while the coefficient of curvature C_c was 0.977. The specific gravity is 2.66. Some of the other geotechnical parameters include D_{60} = 0.205 mm, D_{30} = 0.171 mm, D_{10} = 0.146 mm, e_{max} = 0.911, e_{min} = 0.574, and ρ at 50% relative density = 1.527 g/cm^3. According to the Unified Soil Classification System (ASTM_D2487−17 2018) , the soil adopted in the study is classified as poorly graded sand (SP). From Figure 16, the liquefaction boundaries for potentially liquefiable soils and most liquefiable soils were adopted from Tsuchida (1970) and shows that the sand used in the research falls between the most liquefiable soil.

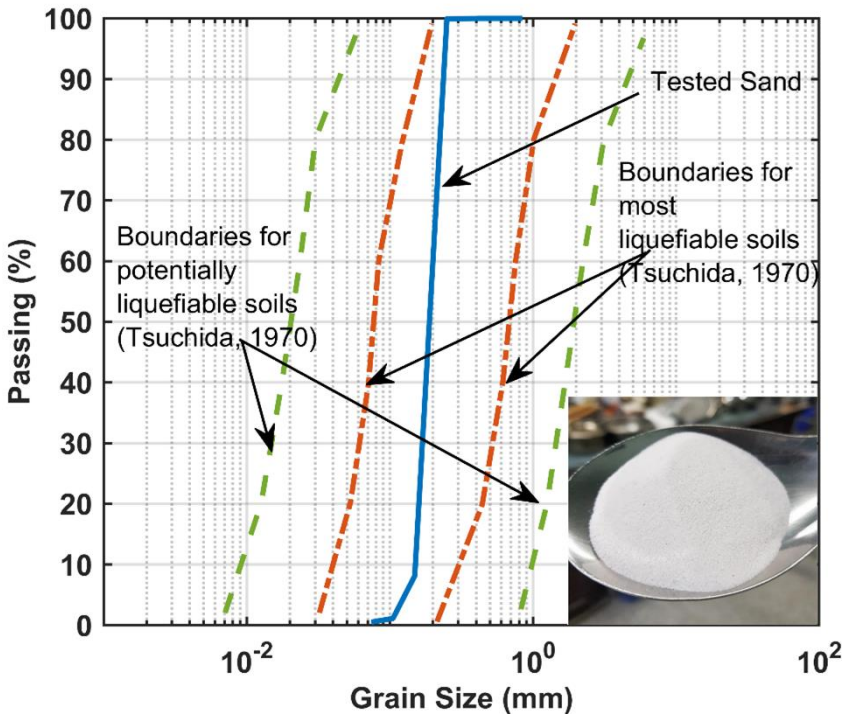

doi:10.6342/NTU202404421

Figure 16: Grain Size Distribution Curve

3.1.2 Characteristics of Urease Enzyme and Reagents

Two types of urease enzymes were used in this study were extracted from the agricultural source, i.e., *Canavalia ensiformis* (jack beans) was purchased. The urease enzyme used in this study was extracted and purchased from Sigma-Aldrich Company Ltd (Figure 17a). The activity rate of this enzyme used in the research is 5 U/mg (powder form). After using the enzyme, it is stored in the refrigerator at 4ºC for future use. The second urease was extracted from an agricultural source (jack beans) and was purchased from CDH Chemicals Pvt Ltd, India. (Figure 17b) The urease enzyme has an activity rate of each mg of urease active meal will hydrolyze 3 mg urea in 30 minutes at 37˚C. Two types of cementation solution were used in the study: Calcium chloride ($CaCl_2$) and Urea ($CO(NH_2)_2$) with 99% purity was purchased from Sigma-Aldrich Company Ltd and also calcium chloride dihydrate ($CaCl_2.2H_2O$) and Urea ($CO(NH_2)_2$) with 99% purity was purchased from Bioman Scientific Co., Ltd shown in the Figure 18.

doi:10.6342/NTU202404421

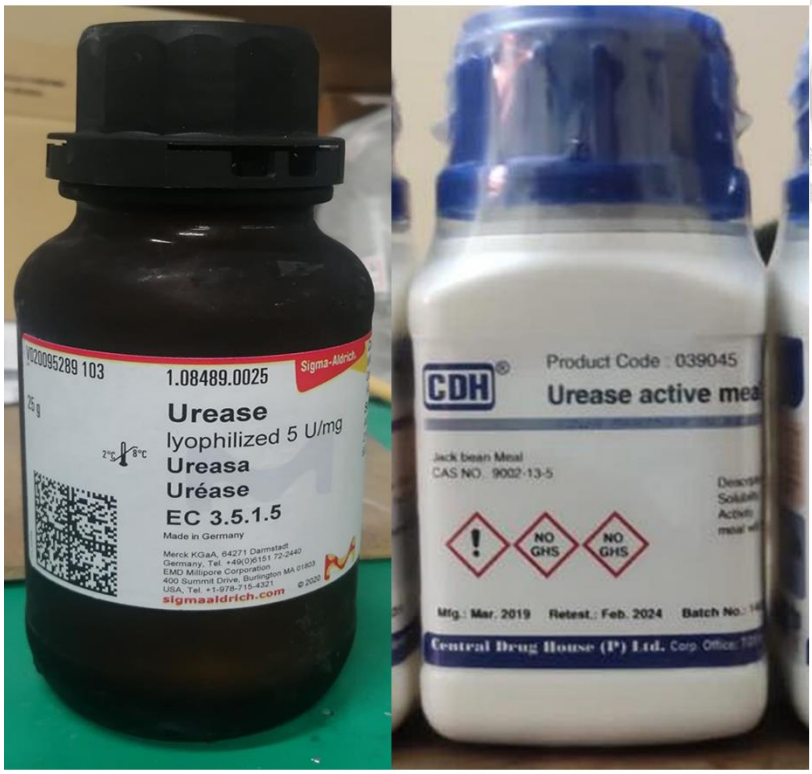

(a) (b)

Figure 17: Types of Urease used in the study (a) Sigma Aldrich urease with 5 U/mg (b) CDH urease

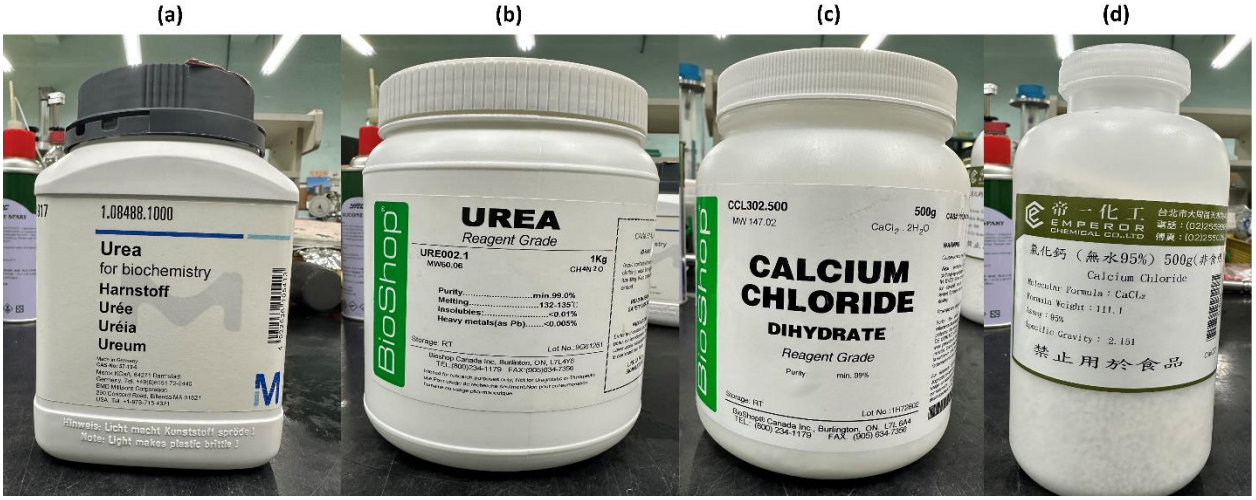

Figure 18: Chemical Reagents used

doi:10.6342/NTU202404421

3.1.3 Paper Mould

The paper mold was used for EICP treatment, and the soil remolding specimen is shown in Figure 19. The paper mold has a diameter of 73 mm and a height of 150 mm, as per (ASTM_D7181-11 2011). Before remolding, the aerosol was sprayed inside to prevent any loss of sand. Holes are drilled at the bottom of the mold for open-ended soil columns and the holes are taped tightly for closed-ended soil columns.

Figure 19: Paper mold

3.1.4 Magnetic stirrer

A magnetic stirrer was used to prepare a uniform EICP solution for treatment, as shown in Figure 20. At first, the cementation solution at the required concentration is prepared, and the stirrer runs at 5 rpm for 30 to 60 seconds. Then, the urease enzyme is added to the cementation solution. The urease enzyme activation starts immediately, so the stirrer is made

doi:10.6342/NTU202404421

to rerun till a milky solution is observed. This stage reaches approximately after 30-40 seconds.

Figure 20: EICP solution

3.1.5 Whatman Ashless Filter Papers

The filter paper used for the research study is shown in Figure 21. Filter paper with grade 40 with ashless Whatman filter paper was used in the preliminary investigation of the Falcon tube test, and Filter paper with grade 541 hardened Whatman filter paper was used in triaxial testing. The properties of filter paper are mentioned in Table 3.

doi:10.6342/NTU202404421

Figure 21: Filter papers used

Table 3: Properties of filter papers

Specifications	Falcon Tube Test	Fall Cone Test	Static and Dynamic Triaxial Test
Brand	GE Healthcare Life Sciences Whatmann	GE Healthcare Life Sciences Whatmann	GE Healthcare Life Sciences Whatmann
Grade	40	541	541
Type	Ashless	Hardened Ashless	Hardened Ashless
Diameter	125 mm	70mm	70mm
Particle Retention in Liquid	8 µm	22 µm	22 µm
Thickness	210 µm	155 µm	155 µm

doi:10.6342/NTU202404421

Basis Weight	95 g/m^2	78 g/m^2	78 g/m^2
Ash Content	≤ 0.007 %	0.005 %	0.005 %
Product Code	CAT No. 1440-125	CAT No. 1541-070	CAT No. 1541-070

3.1.6 Hydrochloric Acid

4M of hydrochloric acid is used to wash the calcium carbonate-precipitated soil. The weight change in before and after acid washing symbolizes the weight of calcite precipitated in the soil.

3.1.7 Falcon Tubes

The test tubes were bought from Labcon Corporation Ltd. This tube is used for calcium carbonate formation from urease and cementation solution (urea and calcium chloride). The tube is shaken periodically by hand for reaction and filtered with Whatman ashless filter paper. A 50 ml falcon test tube was used to estimate the $CaCO_3$ precipitation, as shown in Figure 22. The properties of the test are mentioned in Table 4.

doi:10.6342/NTU202404421

Figure 22: Falcon Tubes

Table 4: Properties of Falcon Tube

S.No	Specifications	
1	Material	100% Propylene
2	Grade	Medical
3	Rating	USP Class VI
4	Sterility	Sterile
5	Color	Natural Clear with Teal Cap
6	Bottom Shape	Conical
7	Capacity	50 ml
8	Diameter	30 mm

doi:10.6342/NTU202404421

9	Length	115 mm
10	Lot Expiration	4 years
11	Sterile Expiration	3 years

3.1.8 Monitoring of Urease activity in solution

Electrical conductivity (EC) and pH meter were measured at different sets of intervals using Thermo Scientific Orion Star A 329 (Figure 23) and A 111(Figure 24), respectively. The electrical conductivity meter and pH meter were calibrated before making measurements. The electrode was placed in the falcon tube at specified intervals and monitored for 7 days.

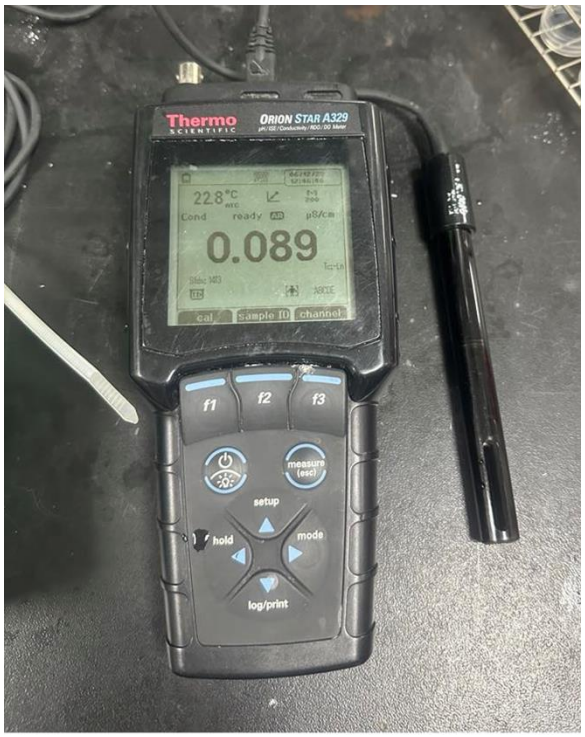

Figure 23: Electrical Conductivity (EC) meter

doi:10.6342/NTU202404421

3.1.8.1 Calibration of Electrical Conductivity Meter

A premium quality standard buffer solution with 1413 µS/cm conductivity prepared against a NIST traceable potassium chloride solution was calibrated before initiating the tests.

Standard Procedure for Measuring Electrical Conductivity

1. Turn on the EC meter. It is essential to wash the electrode with deionized water carefully. The sensor bulb in the electrode should be placed in the calibration liquid.
2. After placing the electrode, the electrode is standardized to 1413 µS/cm by clicking the calculate button in the meter.
3. The electrode was rinsed again and placed on the test samples. The electrical conductivity of the solution was calculated respectively.

Figure 24: pH meter

3.1.8.2 Calibration of pH meter

Buffer solutions of pH 4.01, 7, and 10.01 were used to calibrate the instrument, and the three points were plotted, and the slope was calculated. The obtained slope ≥ 96% from the calibration implies the best fit of calibration.

doi:10.6342/NTU202404421

Standard Procedure for Measuring Electrical pH

1. Turn on the pH meter. It is essential to wash the electrode with deionized water carefully. The sensor bulb in the electrode should be placed in the calibration liquid at pH 4.01
2. After placing the electrode, by clicking the calculate button in the meter, the electrode is standardized to 4.01.
3. Repeat steps 1 and 2 by standardizing at pH 7 and 10.01
4. Press slope calculation. Slope ≥ 96% is the best fit for calibration
5. The electrode was rinsed again and placed on the test samples. The electrical pH of the solutions was calculated respectively.

3.1.9 Microscopic Examination

3.9.1.1 Field Emission Scanning Electron Microscopic (FESEM) Analysis and Energy Dispersive Spectroscopic (EDS) Mapping

Microscopic examinations were performed on both EICP-treated samples and pure sand to gain insights into morphological changes from the calcium carbonate precipitation. Initially, the samples were collected and dried in the oven at 110˚C for 24 hours. The sample was examined using the high-resolution Hitachi S-4800 cold field emission SEM coupled with EDS (Figure 26). Before performing SEM and EDS analysis, the samples were collected on the carbon paper, as shown in Figure 25a. To enhance the charge dissipation in the samples, sputtering was done on the samples with platinum using Quorum Q150R-S rotatory pump coater, as shown in Figure 25b. Silica (Si) and Calcium (Ca) are the vital minerals considered in the study and discussed the elemental mapping for understanding the distribution of the calcium carbonate precipitate.

doi:10.6342/NTU202404421

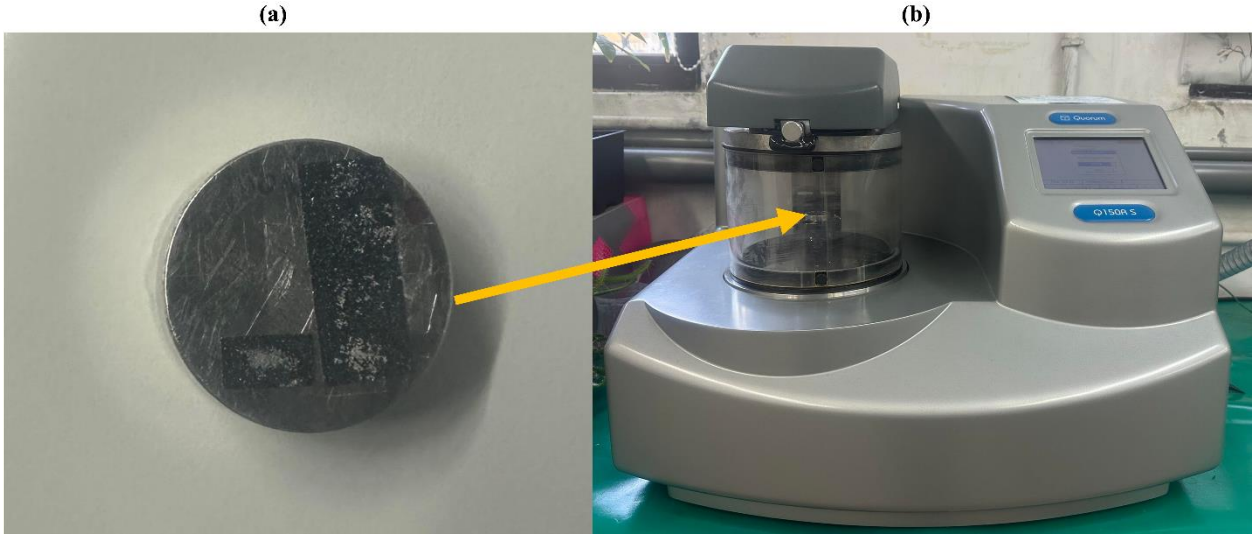

Figure 25: (a) Sample collected in Carbon Paper (b) Process of Sputtering

Figure 26: Field Emission- Scanning Electron Microscopy (FE-SEM) Hitachi S-4800 coupled with Energy Dispersive Spectroscopy (EDS)

doi:10.6342/NTU202404421

3.9.1.2 X-ray Diffraction (XRD) analysis

The oven-dried samples were collected in the plate and filled perfectly inside the plate without scattering. They were then subjected to an X-ray diffraction study to identify the type of calcium carbonate crystal formed from the EICP treatment. XRD diffraction in soil samples was conducted using the Bruker D8 Venture instrument with Cu-Kα (30 kV and 10 mA) in increments of 0.02˚, as shown in Figure 27b. The 2θ scanning angle ranged from 10 - 80˚. The samples were filled on the standard glass slides and positioned within the chamber for testing.

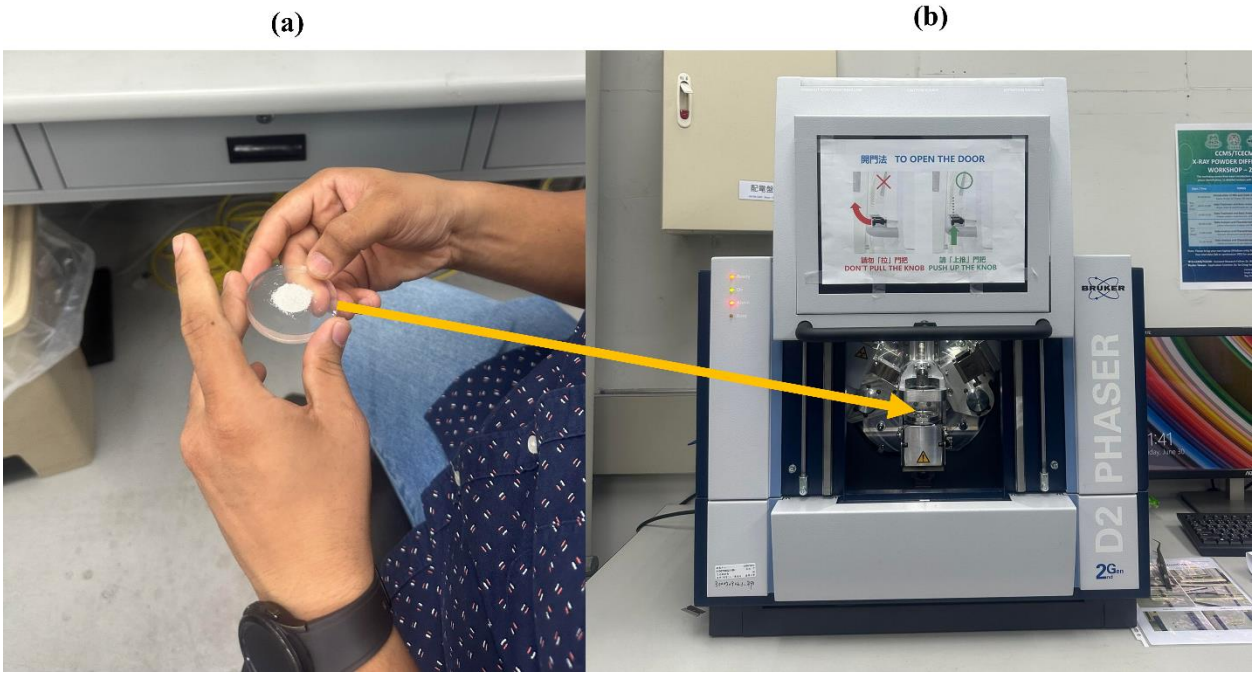

Figure 27: (a) Sample collected in the holder (b) X-ray Diffraction (XRD) Bruker D8 Venture

doi:10.6342/NTU202404421

3.2 Specimen Preparation

3.2.1 Fall Cone Test

A fall cone test was conducted using a paper mold measuring 65 mm in diameter and 55 mm in height. Silicone aerosol was sprayed on the sides of the mold to prevent the sand particles from adhering to the mold's sides. Four drainage holes were drilled at the bottom using a screw for adequate drainage. Based on these dimensions and a maximum dry unit weight corresponding to 50% relative density, the required weight of sand was computed and compacted into three layers. The filter paper was placed on the top and bottom of the compacted sand.

For the treatment, 75 ml of EICP cementation solution was employed. The cementation solution was initially dissolved in deionized water at specific concentrations, and the urease enzyme was added. This study used a one-phase EICP treatment. The EICP solution underwent a brief agitation period on a magnetic stirrer for 5-10 seconds before being poured onto the paper mold from top to bottom, as illustrated in Figure 28. The solution drained naturally due to gravity, and excess solution collected at the bottom holes was recycled by pouring it again from top to bottom. The same procedure was followed for the pure sand specimen, where an equivalent solution with deionized water was added, repeating the process three times to ensure a uniformly distributed EICP solution.

Figure 28 depicts the specimen preparation for the fall cone test, with four combinations selected from the falcon tube test, as detailed in Table 5. After specimen preparation, the paper mold was covered with a plastic sheet to prevent evaporation loss, which could impact calcium carbonate precipitation in the top part of the specimen. All specimens were placed in an airtight box for curing. Following 3 and 7 days of curing, a fall

doi:10.6342/NTU202404421

cone test was conducted on each specimen. Penetration depth readings were taken at the middle and average of all four sides of the specimen.

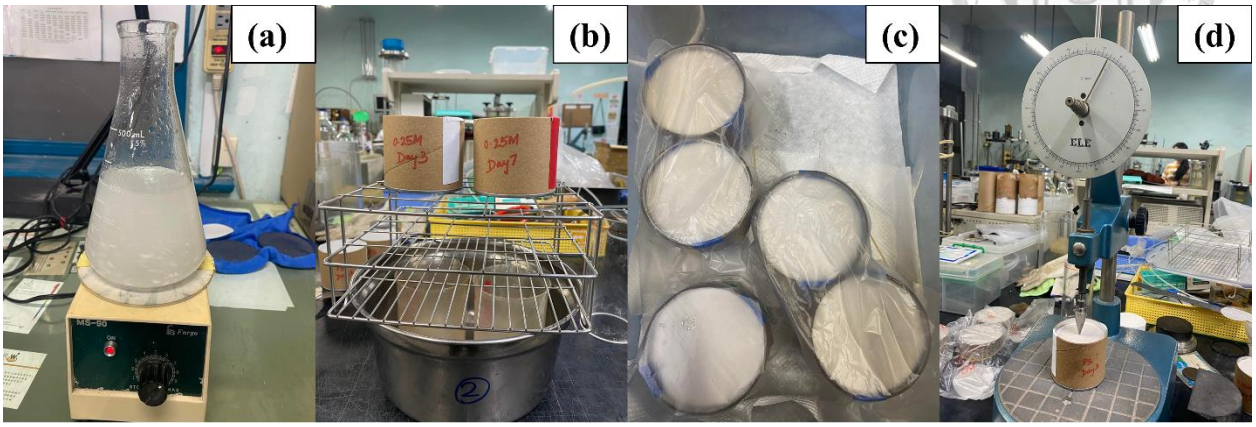

Figure 28: Fall cone test (a) EICP Solution (b) One-phase EICP treatment (drained) soil columns (c) Curing of treated samples (d) Testing

Table 5: Summary of Different Combinations of EICP Technique

S.No	Urea (M)	$CaCl_2$ (M)	Urease (g/l)	Ratio ($CaCl_2$:Urea)	Notations
1	0.25	0.14	3	1:1.75	Combination 1
2	0.5	0.5	3	1:1	Combination 2
3	0.61	0.35	3	1:1.75	Combination 3
4	1	0.67	3	1:1.5	Combination 4

doi:10.6342/NTU202404421

3.2.2 Triaxial Testing

Generally, two types of EICP treatment in soil improvement, (1) mixing and (2) percolation for laboratory investigations were adopted. The percolation method comprises the infiltration of EICP solution into the remolded specimen by gravity or motor. In contrast, the former combined urea, calcium chloride, and free urease enzyme into the soil and remolded. The former method is quite difficult to control while treating the soil in situ (Yasuhara et al., 2012). As a result, the percolation method is considered more convenient because it causes less perturbance in the soil structure. The surface percolation method is a low-cost method that eliminates the need for cumbersome equipment, simplifies sample preparation, and lowers the expenses associated with personnel and expensive technology.

In this study, all EICP-treated soil specimens were prepared using a paper mold consisting of 73 mm in diameter and 160 mm in height. The percolation method of EICP solutions in the pure sand soil was adopted to mimic the field conditions and ensure ease of application. The formulation for the EICP treatment solution was derived from the outcomes of the falcon tube tests. EICP solutions consist of 1 M Urea, 0.67 M $CaCl_2$, and 3 g/l of urease enzyme. Specimens were prepared under two distinct conditions: drained and undrained.

For drained conditions, drainage holes were created at the base of the paper mold. In contrast, undrained conditions retained the EICP solutions without any drainage. Before introducing dry sand into the paper mold, a silicone aerosol was sprayed to prevent sand particles from adhering to the surface. The volume of dry sand was determined based on the dry density of sand at 50% relative density. The soil column was compacted into five layers, with interlayer scratches to mitigate interface effects.

doi:10.6342/NTU202404421

Under drained conditions, the EICP solution percolated from top to bottom, gauging the water retention in the soil specimen. A volume of 270 ml of EICP treatment solutions ensures that a small amount of solution remains above the soil specimen to soak thoroughly. After 4 to 5 days, any excess solution either absorbed in the paper mold or leaked from the end of the mold, leaving the specimen intact in proper shape without any defects.

Subsequently, a one-phase EICP treatment solution was poured from top to bottom and allowed to drain through gravity, both in drained and undrained conditions. In the case of undrained conditions, the solution remained in the paper mold curing in a soaked condition. For drained conditions, the solution was permitted to flow thrice from top to bottom to fill the pore void with EICP treatment solution thoroughly. After EICP treatment, the paper mold was covered with plastic sheeting to prevent evaporation and left to cure for 7 days.

After a specified curing time, the triaxial specimens were cut open and transferred to the triaxial chamber for monotonic drained triaxial testing. Before proceeding to the testing, it is essential to study the uniformity of the soil column for a better result. The specimen preparation for the static triaxial and undrained triaxial testing were illustrated in the following Figure 29.

doi:10.6342/NTU202404421

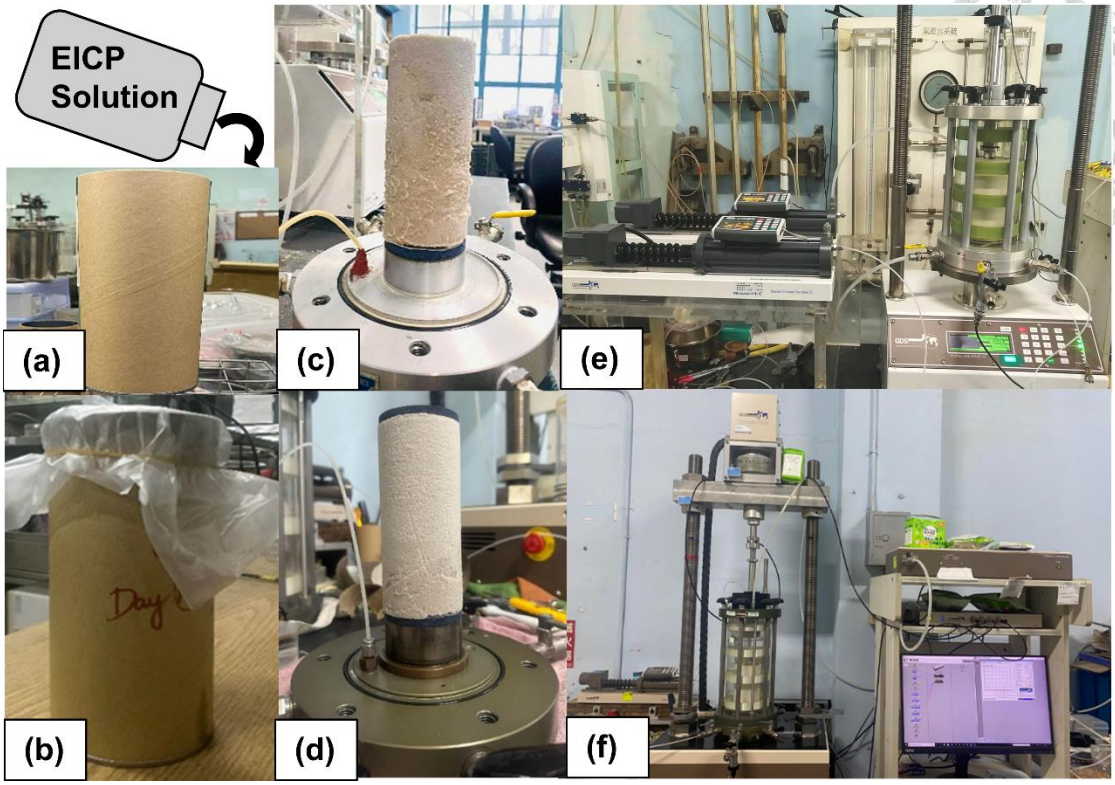

Figure 29: (a) Pouring of EICP treatment solution (percolation method) (b) EICP-treated specimen (Curing) (c) EICP-treated specimen on Monotonic Triaxial plate (d) EICP-treated specimen on Cyclic Triaxial plate (e) Monotonic Triaxial Setup (f) Cyclic Triaxial Setup

3.3 Laboratory Tests

3.3.1 Falcon Tube Test

Falcon Tube tests were conducted with 1 M urea concentration and different ratios ranging from 1:1 to 1:1.75 ($CaCl_2$: Urea), while the urease enzyme concentration ranged from 1 to 6 g/l. The EICP solution is a blend of urease and cementation solutions. EICP solution is created by dissolving calcium chloride and urea into deionized water, followed by the addition of urease enzyme. Within a 50 ml test tube, 20 ml of EICP solution is introduced without soil. The instantaneous reaction of the urease enzyme in the cementation solution

doi:10.6342/NTU202404421

marks the initiation of the favorable conditions of the precipitation, and leaving the test tubes left to cure for 24 hours is sufficient to complete the EICP reaction.

A milky appearance immediately becomes visible to the naked eye after adding urease to the cementation solution. Gentle shaking of the test tube for a few minutes results in a thick, milky solution due to the higher activity of the urease enzyme. Within a few hours, the interaction of the urease enzyme with the cementation solution initiates the precipitation of calcium carbonate, which settles at the bottom of the test tube. Subsequently, the test tube is shaken randomly to ensure complete precipitation during the 24-hour curing period.

At the end of the curing period, the solution is collected and filtered using ashless filter paper. The tube and filter paper were oven-dried to calculate the quantity of calcium carbonate precipitation, which is determined by combining the mass of rainfall on the filter paper with that remaining at the bottom of the test tube. The process of the falcon tube test is depicted in Figure 30. The precipitation ratio is defined as the ratio of the mass of the calcium carbonate precipitated to the theoretical mass of the calcium carbonate. The theoretical mass of calcium carbonate can be calculated using the formula C*V*M (Ahenkorah *et al.* 2021b; Chandra and Ravi 2020).

Where C represents the concentration of the solution (moles per liter), V is the volume of the solution in the tube (ml), and M stands for molar mass of calcium carbonate (grams)

Miftah *et al.* (2019) mentioned that rhombohedral calcite predominates the crystal structure in the enzyme-induced precipitation within the sand. Later on, the type and shape of the calcium carbonate crystal were explored through Field Emission-Scanning Electron Microscopic (FE-SEM) analysis, Energy Dispersive Spectroscopy (EDS) analysis, and X-ray Diffraction (XRD) analysis

doi:10.6342/NTU202404421

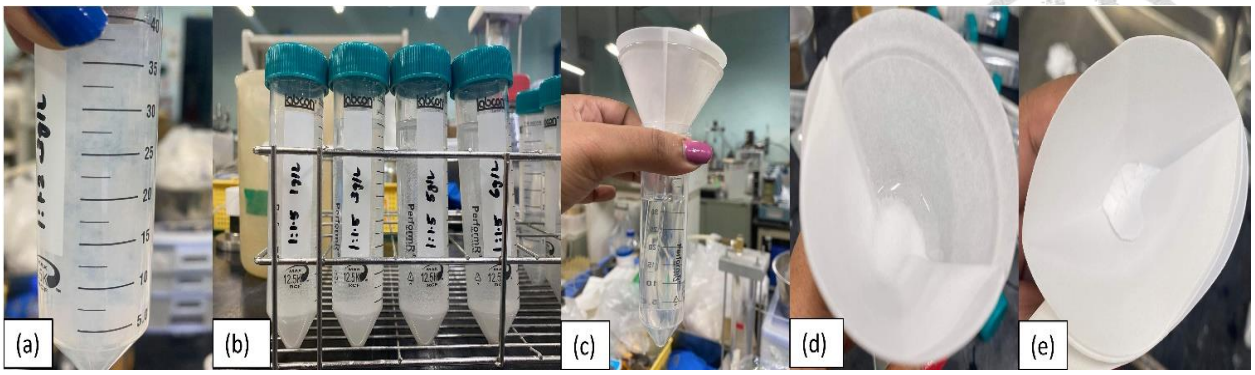

Figure 30: Falcon Tube test procedure (a) Light milky patches at the initial point of EICP reactions (b) Deposits of $CaCO_3$ after 24 hours (c, d) $CaCO_3$ filtration (e) Dried $CaCO_3$

3.3.2 Fall Cone Test

This rapid and straightforward testing method involves driving a cone into a soil specimen using its weight, with subsequent determination of its penetration depth. The primary parameters assessed through this test include undrained shear strength (S_u), Atterberg limits (Liquid limit (W_L) and Plastic limit (W_P)), and sensitivity (S_t). The Fall Cone Test (FCT) was conducted using a fall-cone penetrometer following the guidelines outlined in ISO 17892–6. The FCT apparatus features a measurement gauge with an accuracy of 0.1 mm, incorporating a standardized stainless-steel cone possessing a cone tip aperture of 30º and a mass of 80 grams. The testing procedure involves placing a specimen and positioning the FCT cone so that its tip makes contact with the specimen. The gauge is then adjusted to zero, and the cone is released for five seconds. The resulting penetration value is carefully recorded for analysis.

3.3.3 Consolidated Drained Triaxial Testing

Consolidated drained triaxial tests were performed according to (ASTM_D7181-20 2020) to assess the impact of bio-cementation on the sand. A displacement-controlled triaxial apparatus equipped with a data acquisition system was utilized for conducting both

doi:10.6342/NTU202404421

consolidation and drained triaxial compression tests. The EICP-treated specimen was placed on the triaxial base, aligned with filter paper and porous stone at the bottom. It was then encased in a latex membrane and positioned within the triaxial chamber. Initially, a vacuum pressure of 20 kPa was applied to the specimen, followed by a cell pressure of 20 kPa to support it. To facilitate saturation, the specimens were first flushed with de-aired water under an effective stress of 20 kPa, after which an ultimate back pressure of 700 kPa was applied to achieve a B-value of 0.97 or higher, indicating that the specimen was fully saturated. The confining pressure considered in the study corresponding to the pressure at a depth of 5-20m below ground surface. The specimen was subjected to three different confining pressures: 50 kPa, 100 kPa, and 200 kPa. Each sample was monotonically sheared until the axial strain reached 20%, at which point the test was stopped, and data were collected. Triaxial tests were carried out at these varying confining pressures. The same method was used to determine the calcium carbonate content (CCC) at different curing periods—on the 3, 7, and 14 days. After curing, the specimen was divided into three sections: top, middle, and bottom. The average calcium carbonate content (CCC) results were calculated by three samples taken from the top, middle, and bottom of each specimen.

3.3.4 Undrained Cyclic Triaxial Testing

The tests were carried out per (ASTM_D5311-11 2012), standard, using a saturation procedure similar to the one described in the experimental method for static triaxial testing. Each specimen was consolidated under an effective confining pressure of 100 kPa, after which a specified cyclic stress ratio (CSR) was applied to assess liquefaction resistance. A cyclic loading frequency of 0.1 Hz was chosen to align with ASTM requirements, ensuring the excess pore water pressure developed fully during shearing. To evaluate liquefaction

doi:10.6342/NTU202404421

resistance, a plot of CSR versus the number of loading cycles (N_L) on a logarithmic scale was created. Liquefaction, denoted as N_L, was defined in this study by an excess pore water pressure ratio ($r_u = \Delta u/\sigma'_3$) of 1.0, marking the onset of initial liquefaction in the cyclic triaxial tests.

3.4 Acid Digestion

3.4.1 Determination of Calcium Carbonate Content (CCC)

The acid digestion method was used for the determination of calcium carbonate content after the EICP treatment. The specimen was cut into three sections (top, middle, and bottom) and dried in the oven at 105ºC for 24 hours. After the drying process, 10 grams of dried sand were placed in a glass tube to initiate the acid digestion procedure. A 4 M hydrochloric acid (HCl) solution was prepared for the purpose of digesting the precipitated calcium carbonate in the soil specimens.

Three separate 10 gram samples were collected from the specimen's top, middle, and bottom sections. In the glass tube, 10 ml of HCl acid was added and left to interact for 24 hours. During this period, the precipitated calcium carbonate within the soil reacts with acid, resulting in a noticeable carbonation effervescence, as shown in Figure 31. After 24 hours, an additional 10 ml of acid was added to the tube to ensure complete digestion of the calcium carbonate precipitation within the sand.

The supernatant of the solution was carefully decanted, and the sample was rinsed with deionized water. After washing, the glass tube was placed in an oven at 60˚C for 24 hours. Subsequently, the dry weight was measured again. The difference in weight of the sample before and after the acid digestion process yielded the quantity of calcium carbonate present

doi:10.6342/NTU202404421

in the soil (Cui *et al*. 2017). The process of acid digestion of the precipitated calcium carbonate in the soil can be outlined in the following equations.

$$CaCO_3 + 2\,HCl \rightarrow CaCl_2\,(aq) + H_2O\,(l) + CO_2\,(g) \quad [7]$$

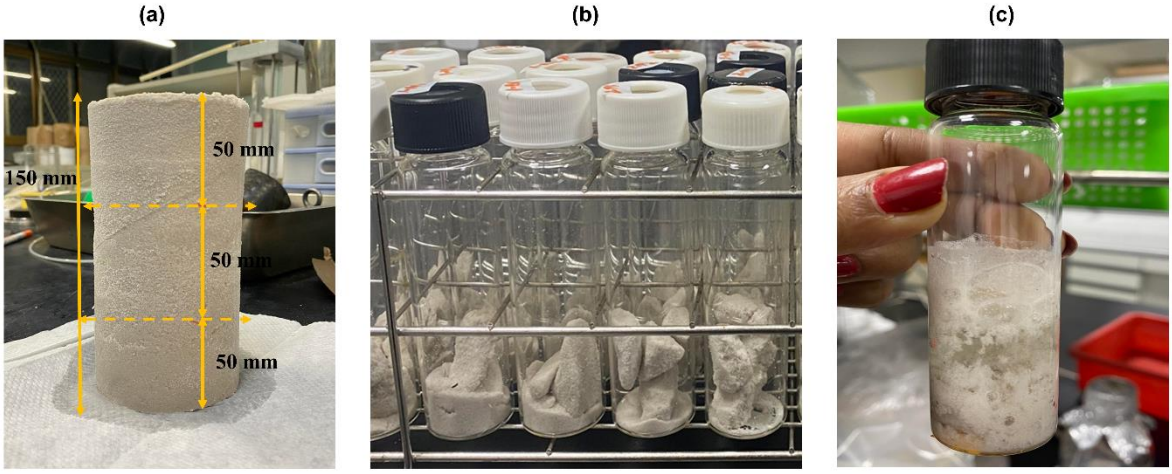

Figure 31: Acid Digestion (a) EICP-treated specimen (b) Sand samples before acid digestion (c) Effervescence in the sand

The following equation is used for the determination of the calcium carbonate content (CCC).

$$CCC\ (\%) = \frac{w_1 - w_2}{w_1} * 100 \quad [8]$$

w_1 = weight of the soil sample before acid washing, and w_2 = weight of the oven-dried soil sample after acid washing.

3.4.2 Assessment of Uniformity in Triaxial Specimen

Two conditions were employed in the EICP treatment process using Sigma urease enzyme: pouring the treatment solution into sand specimens with drainage and without drainage at the bottom of the paper mold. This approach aimed to determine which condition resulted in uniform treatment and higher induced precipitation of the treated specimens by

doi:10.6342/NTU202404421

conducting acid digestion. This study employed the drained condition and undrained condition to simplify the description of the two conditions and enhance clarity in the result.

3.4.2.1 Method 1 – Drained Conditions

One-phase of the EICP treatment solution using Sigma urease was poured into the pure sand triaxial specimen. 270 ml of EICP treatment solution were drained through holes at the bottom of the paper mold. The drained solution was collected at the bottom of the paper mold, as shown in Figure 32. The collected liquid is poured again into the specimen and followed thrice for a thorough filling of EICP treatment solution in the voids of the pure sand for uniform $CaCO_3$ precipitation.

doi:10.6342/NTU202404421

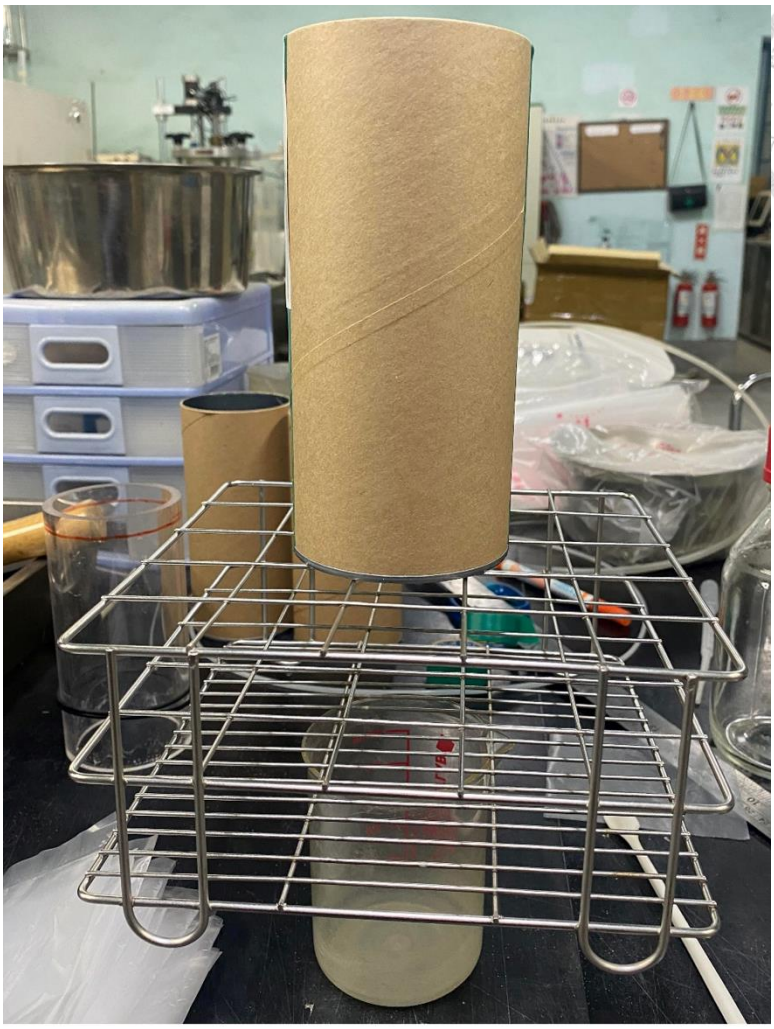

Figure 32: Sigma-treated specimen preparation under drained conditions

3.4.2.2 Method 2- Undrained Conditions

A similar procedure was followed as in drained conditions. In the case of undrained conditions, the solution remained in the paper mold curing in a soaked condition. 270 ml of EICP treatment solution were poured into the triaxial specimen. The EICP solutions were retained without drainage in undrained conditions, as shown in Figure 33.

doi:10.6342/NTU202404421

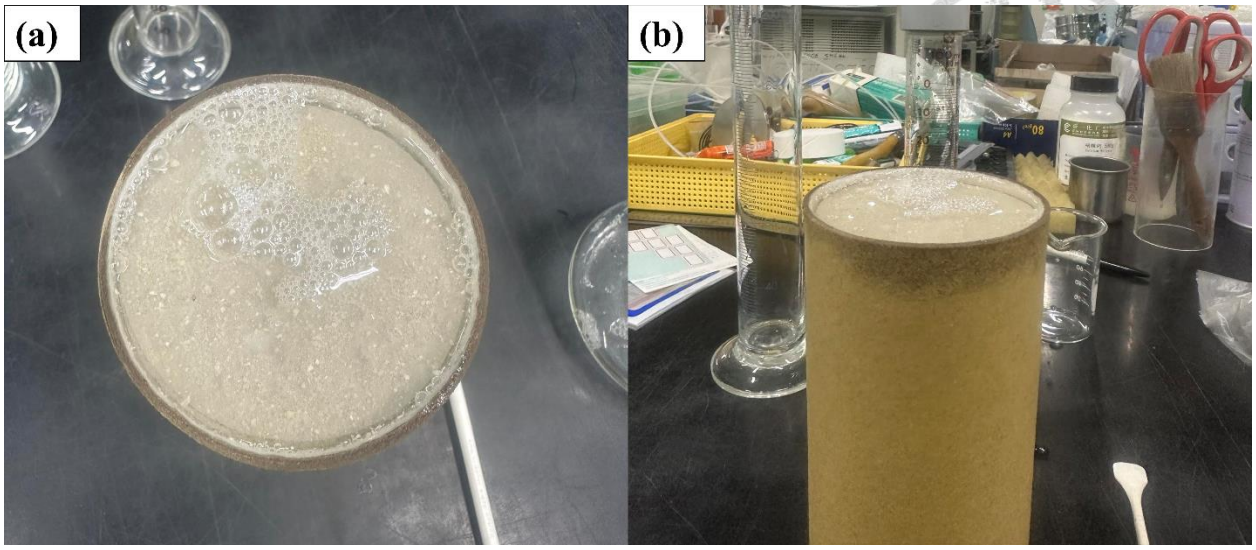

Figure 33: CDH-treated specimen preparation under undrained conditions

After the respective curing time, the specimen was cut into three sections (top, middle, and bottom) for both drained and undrained conditions and dried in the oven at 105ºC for 24 hours. Similar procedure is followed as mentioned in Section 3.4.1

Figure 34 illustrates the acid digestion results for both pouring treatment solution into sand specimen with drainage (drained condition) and without drainage (undrained condition) at the bottom of the paper mold, aiming to quantify the amount of calcium carbonate precipitation in each section. The Sigma-treated specimen under undrained conditions showed almost uniform and induced higher calcium carbonate precipitation. This could be due to the arresting of the drainage condition at the bottom of the mold, the soil gets stagnated or completely drenched in the EICP solution for more uniform precipitation. Based on the acid digestion results, the research study opted to utilize EICP-treated specimens prepared with undrained conditions.

doi:10.6342/NTU202404421

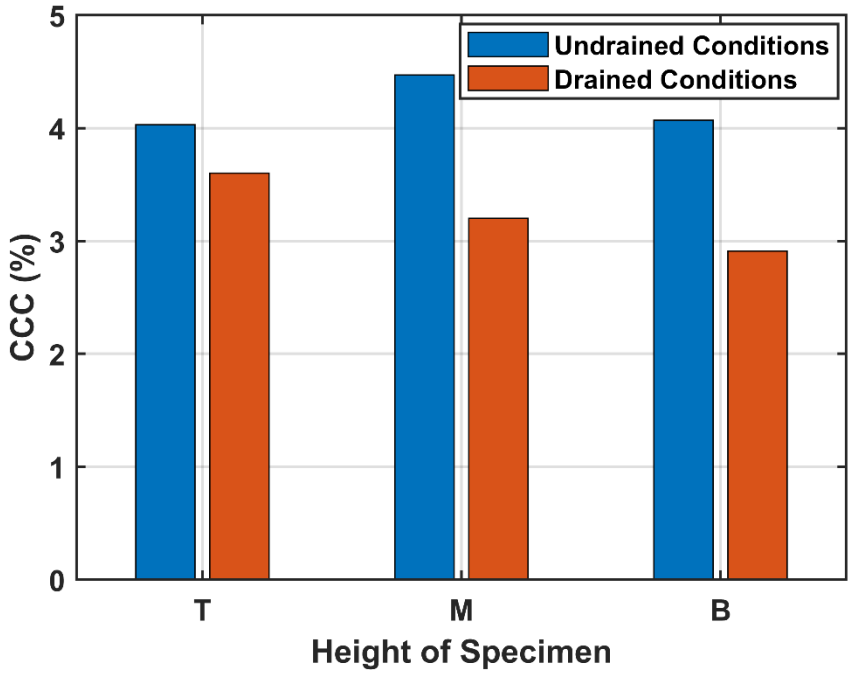

Figure 34: Acid digestion of Sigma-treated specimen at drained and undrained conditions at 3 days of curing

Similarly, the CDH urease enzyme was applied to the treatment solution with Combo 4 reactant concentrations. As the CDH urease enzyme is a lower-activity urease enzyme, the acid digestion test was performed at seven days of curing time. To check the uniformity of the CDH-treated specimen, the specimen was cut into five parts (top, intermediate 1, intermediate 2, intermediate 3, and bottom). In every section, approximately 5 grams of sand was taken in nine dissected areas shown in Figure 35 and kept for oven drying at 110˚C for 24 hours.

doi:10.6342/NTU202404421

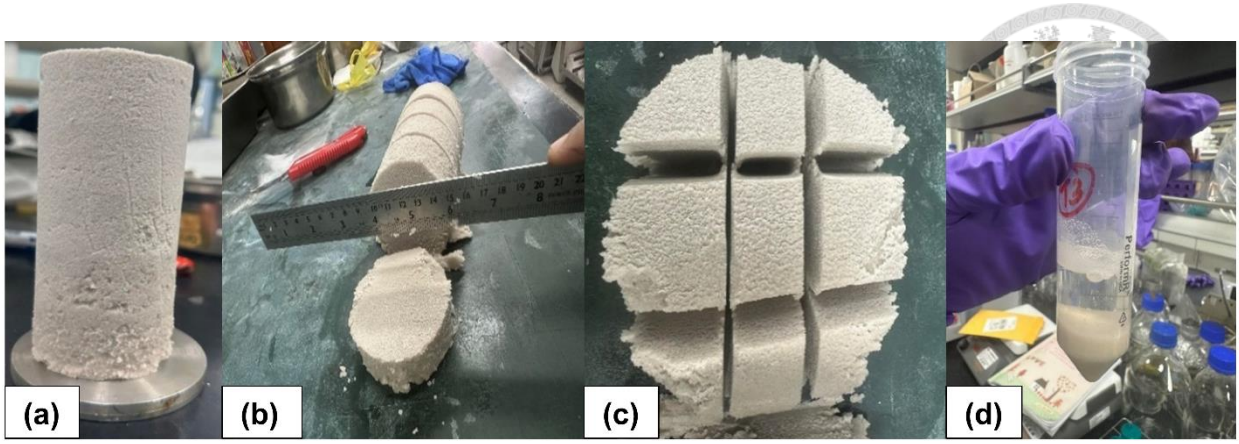

Figure 35: Uniformity study of CDH-treated specimen (a) CDH-treated specimen (b) Specimen cut in five parts (c) Samples taken for acid digestion (d) Effervescence from acid digestion

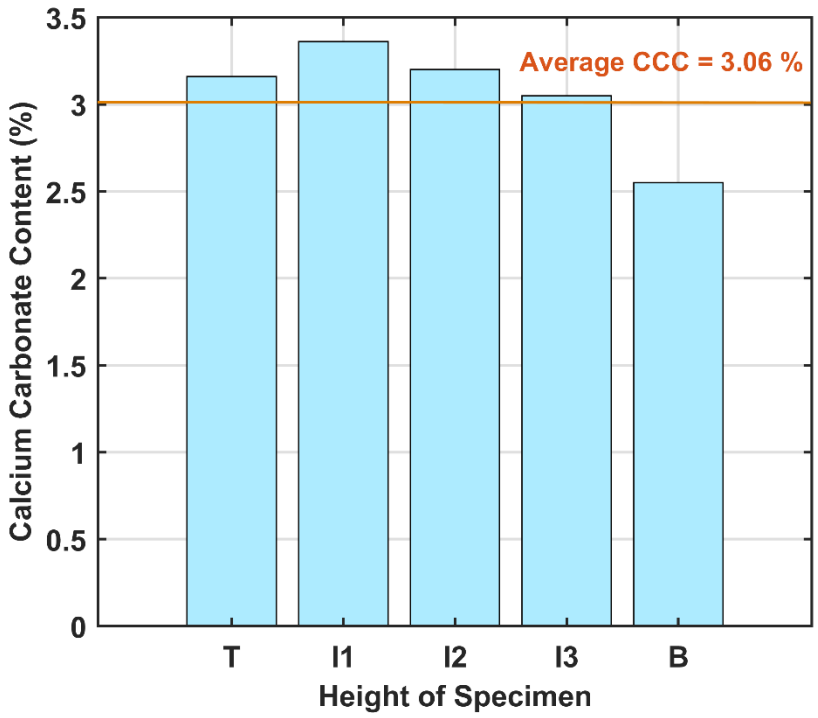

Figure 36: Acid digestion of CDH-treated specimen at 7 days of curing.

The average calcium carbonate content (CCC) of nine samples in the top, intermediate 1 (I1), intermediate 2 (I2), intermediate 3 (I3), and the bottom was shown in Figure 36 in the

doi:10.6342/NTU202404421

CDH-treated specimen at 7-days of curing. All the parts showed almost uniform calcium carbonate precipitation along the height of the specimen.

The concentration of the cementation solution and the quantity of urease enzyme can significantly affect the $CaCO_3$ content and precipitation ratio in EICP treatment. In this study, the urease enzyme used, derived from *Canavalia ensiformis* and purchased from Sigma Aldrich with an activity rate of 5U/mg, was applied at an optimal formulation of 1M urea, 0.67M $CaCl_2$, and 3g/L of urease enzyme, in a $CaCl_2$: Urea ratio of 1:1.5. This combination yielded the highest precipitation ratio for the study, with 1.77g of $CaCO_3$ content and a 100% precipitation ratio from 20ml of EICP treatment solution.

Using a different urease enzyme, even with the same cementation solution concentration, could result in variations in both $CaCO_3$ content and precipitation ratio. It is, therefore, essential to perform tube tests to determine the optimal formulation for the desired $CaCO_3$ content, depending on the research objectives. The acid digestion results indicated average calcium carbonate contents of 3.06% in the CDH-treated specimen and 4% in the Sigma-treated specimen were obtained from the above mentioned formulation which could defer from a different EICP formulation when used. Higher $CaCO_3$ precipitation generally enhances both shear strength and liquefaction resistance in treated soils, making this formulation can be crucial for soil improvement.

doi:10.6342/NTU202404421

Chapter 4 RESULTS AND DISCUSSIONS

4.1 Falcon Tube Test Results from Sigma Urease

4.1.1 0.25 M Urea Concentration

Figure 37 provides a comprehensive overview of the assessed $CaCO_3$ content and precipitation ratios at a 0.25 M urea concentration across varied $CaCl_2$: Urea ratios (ranging from 1:1 to 1:1.75) combined with different urease enzyme concentrations (1 to 5 g/l). The combinations featuring 0.25 M urea and 0.25 M $CaCl_2$, with 1 g/l urease enzyme in a 1:1 ratio, exhibit the lowest $CaCO_3$ content (0.42 g) with a precipitation ratio of 0.84. Similarly, an identical $CaCO_3$ content (0.42 g) with a precipitation ratio 1.00 is observed in the combination of 0.25 M urea and 0.17 M $CaCl_2$, with 1 g/l urease enzyme in a 1:1.5 ratio. In contrast, the combination of 0.25 M urea, 0.14 M $CaCl_2$, and 3g/l urease in a 1:1.75 ratio displays the highest $CaCO_3$ content (0.62 g) and a precipitation ratio of 1.00 compared to other combinations. The second-highest $CaCO_3$ content (0.62 g) and precipitation ratio (1.00) are found in 0.25 M urea and 0.25 M $CaCl_2$ with 5g/l urease enzyme. Notably, an excess urease enzyme produces a sharp decline in $CaCO_3$ content. It is crucial to highlight that higher urease enzyme consumption does not necessarily translate to increased calcium carbonate precipitation, as evidenced in the combination of 0.25 M urea and 0.17 M $CaCl_2$ in a ratio of 1:1.5 with both 3 g/l and 5 g/l urease enzyme.

doi:10.6342/NTU202404421

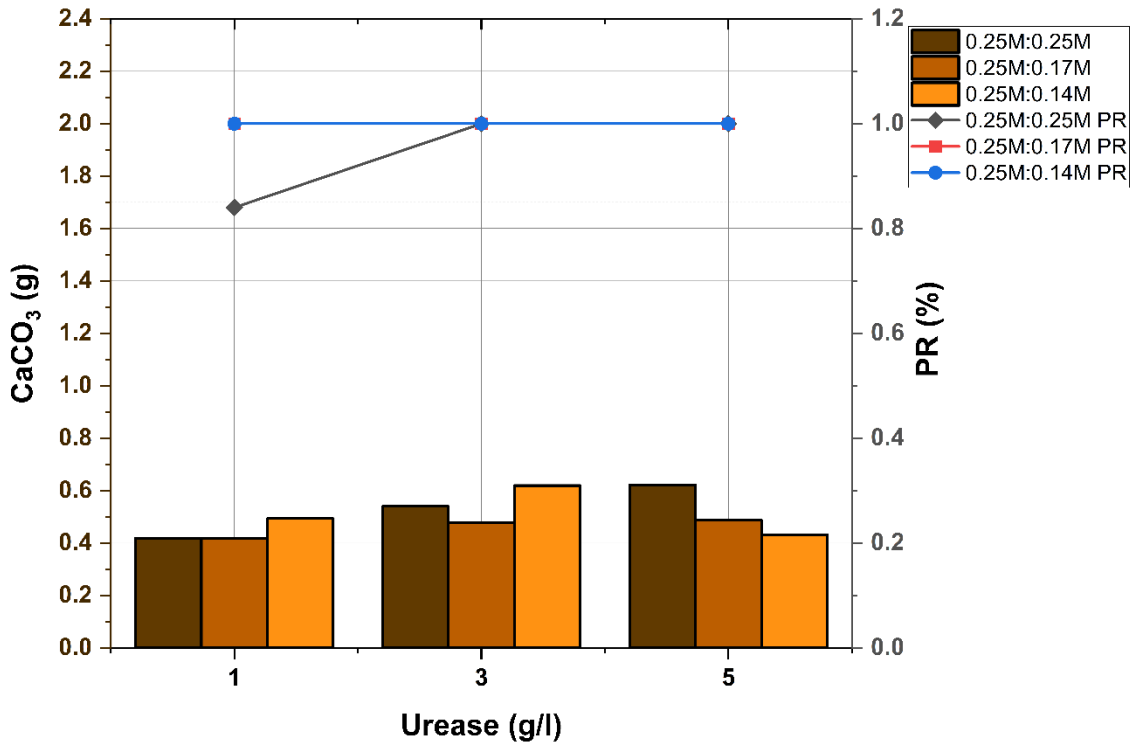

Figure 37: Falcon Tube test results of 0.25 M Urea Concentration

4.1.2 0.5 M Urea Concentration

Figure 38 comprehensively summarizes the evaluated $CaCO_3$ content and precipitation ratio at a 0.5 M urea concentration with a 1:1 ratio, considering various urease enzyme concentrations. The combination of 0.5 M urea, 0.5 M $CaCl_2$, and 3 g/l urease enzyme in a 1:1 ratio demonstrates the highest $CaCO_3$ precipitation (1.14 g) and a precipitation ratio of 1.00. However, an excess urease enzyme beyond 3 g/l inhibits its activity, impacting urea hydrolysis and resulting in a decline in precipitation ratio and $CaCO_3$ content. In Figure 38, the combination of 0.5 M urea and 0.5 M $CaCl_2$ exhibits a slight reduction in $CaCO_3$ content (1 g), with the precipitation ratio (1.00) showing a decline after a urease enzyme concentration of 3 g/l. Higher urease enzyme concentrations may not have

doi:10.6342/NTU202404421

sufficient urea-$CaCl_2$ concentration to promote the urea hydrolysis, leading to reduced precipitation ratio and $CaCO_3$ content.

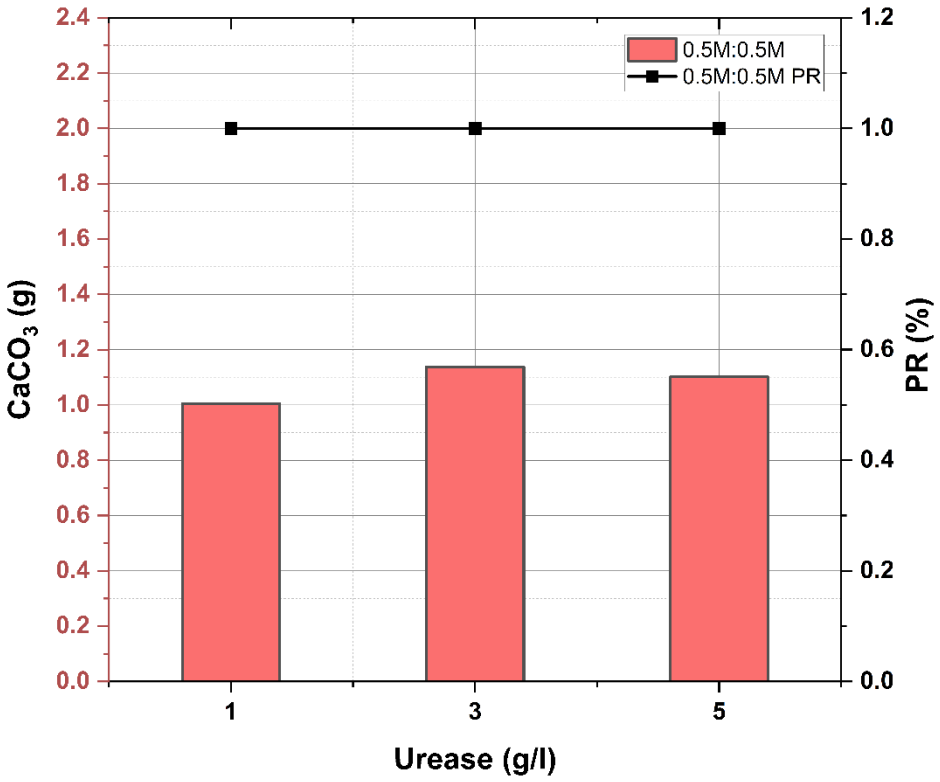

Figure 38: Falcon Tube test results of 0.5 M Urea Concentration

4.1.3 0.61 M Urea Concentration

Figure 39 explores a 0.61 M urea concentration with 1:1.5 and 1:1.75 ratios, examining different urease enzyme concentrations. The combination of 0.61 M urea, 0.35 M $CaCl_2$, and 3 g/l urease enzyme in a 1:1.75 ratio demonstrates the highest $CaCO_3$ precipitation (1.05 g) and a precipitation ratio of 1.00. This mirrors the findings in the combination of 0.61 M urea, 0.41 M $CaCl_2$, and 1 g/l urease enzyme, exhibiting similar $CaCO_3$ content (1.05 g) and a precipitation ratio of 1.00. The study maintains a fixed 3 g/l urease enzyme concentration across different combinations. In the case of 0.61 M urea and 0.41 M $CaCl_2$

doi:10.6342/NTU202404421

with a 1:1.5 ratio, there is a downward trend in $CaCO_3$ content and precipitation ratio with 1 g/l, 3 g/l, and 5 g/l urease enzyme concentrations. Carmona *et al.* (2016) conducted a falcon tube test with varying concentrations of urea-$CaCl_2$ (0.25, 0.5, 0.75, 1, and 1.25 mol/L) and 4kU/L of urease enzyme for evaluating calcium carbonate precipitation. Their results indicated the highest precipitation at lower concentrations (0.25 mol/L) of urea-$CaCl_2$, showcasing complete urea hydrolysis by urease enzyme. Higher urea-$CaCl_2$ concentrations inhibited ureolytic activity, resulting in reduced precipitation, aligning with the trends observed in our research with lower concentrations yielding maximum precipitation ratios.

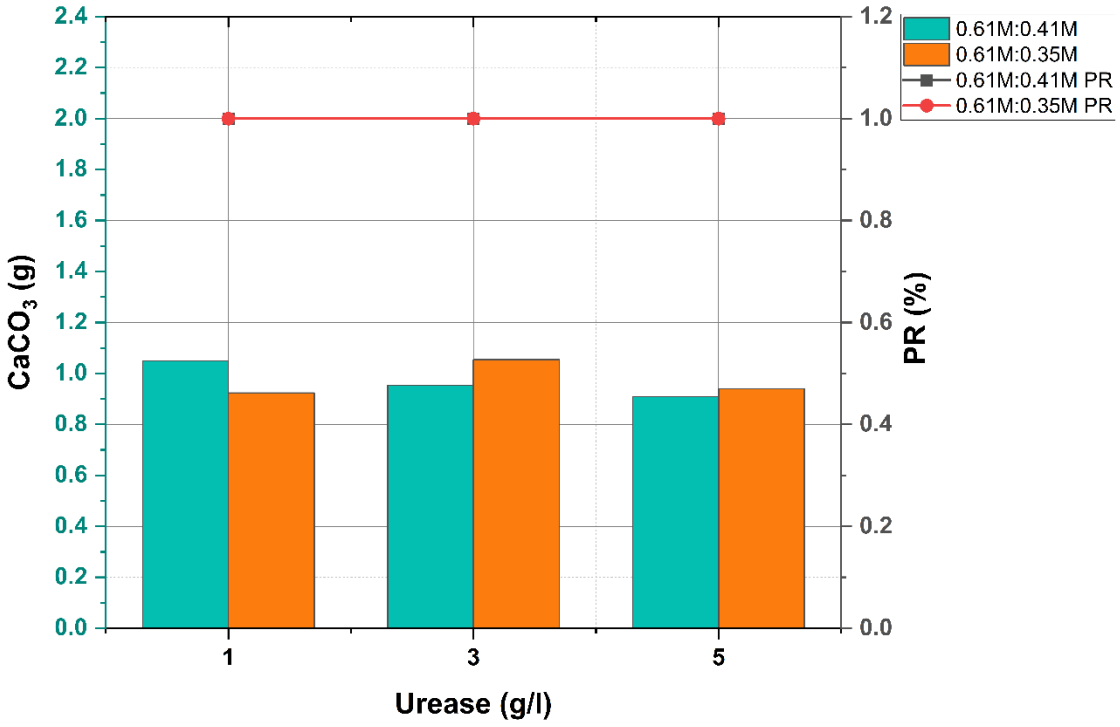

Figure 39: Falcon Tube test results of 0.61 M Urea Concentration

4.1.4 1 M Urea Concentration

The combination of 1 M urea and 1 M $CaCl_2$ with 5 g/l urease enzyme stands out, yielding the highest $CaCO_3$ precipitation (1.98 g) and a precipitation ratio of 0.99. Following

doi:10.6342/NTU202404421

closely, the combination of 1 M urea, 0.67 M $CaCl_2$, and 5 g/l urease enzyme in a 1:1.5 ratio demonstrates the second-highest $CaCO_3$ content (1.91 g) with a precipitation ratio of 1.00. Intriguingly, maintaining the same combination but with 3 g/l urease enzyme results in a $CaCO_3$ content of 1.77 g and a precipitation ratio of 1.00. Notably, the difference in $CaCO_3$ precipitation ratios between 3 g/l and 5 g/l urease enzyme concentrations is minimal, prompting the selection of 3 g/l for economic considerations. As Urea and $CaCl_2$ concentrations increase with ratios of 1:1, 1:1.2, and 1:1.75, there is a reduction in the precipitation ratio. Both combinations (1 M urea, 0.83 M $CaCl_2$) and (1 M urea, 0.57 M $CaCl_2$) exhibit a similar trend in precipitation ratios with varying enzyme concentrations. The reduction in the precipitation ratio may be attributed to two factors: (1) the quantity of urease enzyme for urea hydrolysis and (2) excess urea and calcium ions in EICP solutions. Carmona *et al.* (2016) also noted that either or both of these factors could inhibit $CaCO_3$ precipitation. Higher concentrations of urea and $CaCl_2$ lead to increased precipitation; however, haphazard concentration increases could induce salinity in the EICP solution, potentially restraining urease activity and reducing precipitation (Chiet *et al.* 2015).

doi:10.6342/NTU202404421

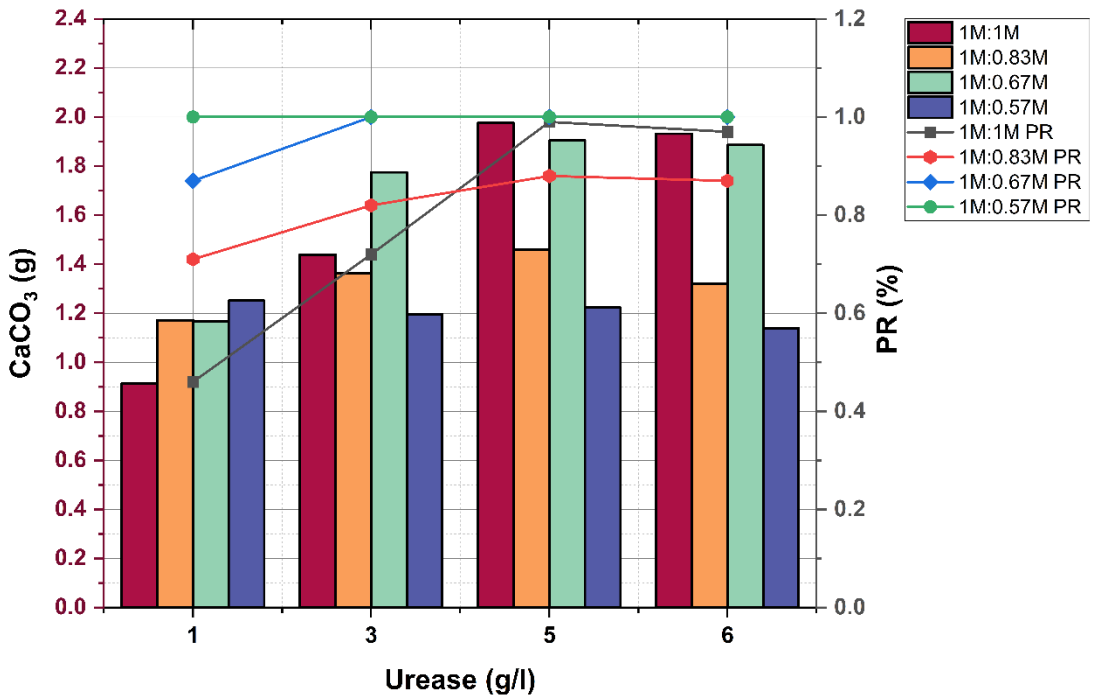

Figure 40: Falcon Tube test results of 1 M Urea Concentration

Figure 40 highlights that the combination of 1 M urea, 0.67 M $CaCl_2$ with 3 g/l in a 1:1.5 ratio emerges as a preferred combination for soil stabilization techniques. In a related study, Song *et al.* (2020b) employed two urease enzymes with varying activity levels (Sigma Aldrich and a lower activity enzyme from soybeans). They assessed reaction efficiency for calcium carbonate precipitation with different urea: $CaCl_2$ molar ratios from 1 to 2.5. Higher and lower activity urease enzymes exhibited higher reaction efficiency at a molar ratio 1.5. The study concluded that a 1.5 molar ratio of urea: $CaCl_2$ is identified as the optimal concentration, aligning with our research findings.

doi:10.6342/NTU202404421

4.2 Fall Cone Test from Sigma Urease

4.2.1 Variation of Penetration Depth at One Treatment Cycle

4.2.1.1 3 Days of curing

The fall cone test was conducted in pure sand and in all four combinations derived from the falcon tube test, each characterized by higher $CaCO_3$ and precipitation ratios. Figure 41 presents the penetration depths after three days of curing. The pure sand exhibited a penetration depth of 5 mm. Among the different combinations, Combo 4 displayed the lowest penetration depth in the paper mold, indicating a higher level of calcium precipitation in the soil at 0.9 mm. The second most minor penetration depth was observed in Combo 2 at 1.3 mm. Combo 1 and 3 exhibited penetration depths of 2.05 mm and 2.1 mm, respectively, demonstrating a nearly equal impact on the soil. The calcium carbonate precipitated during the EICP treatment fills the void spaces within the soil particles, transitioning from a porous to a solid form. This transformation significantly enhances the shear strength of the soil.

doi:10.6342/NTU202404421

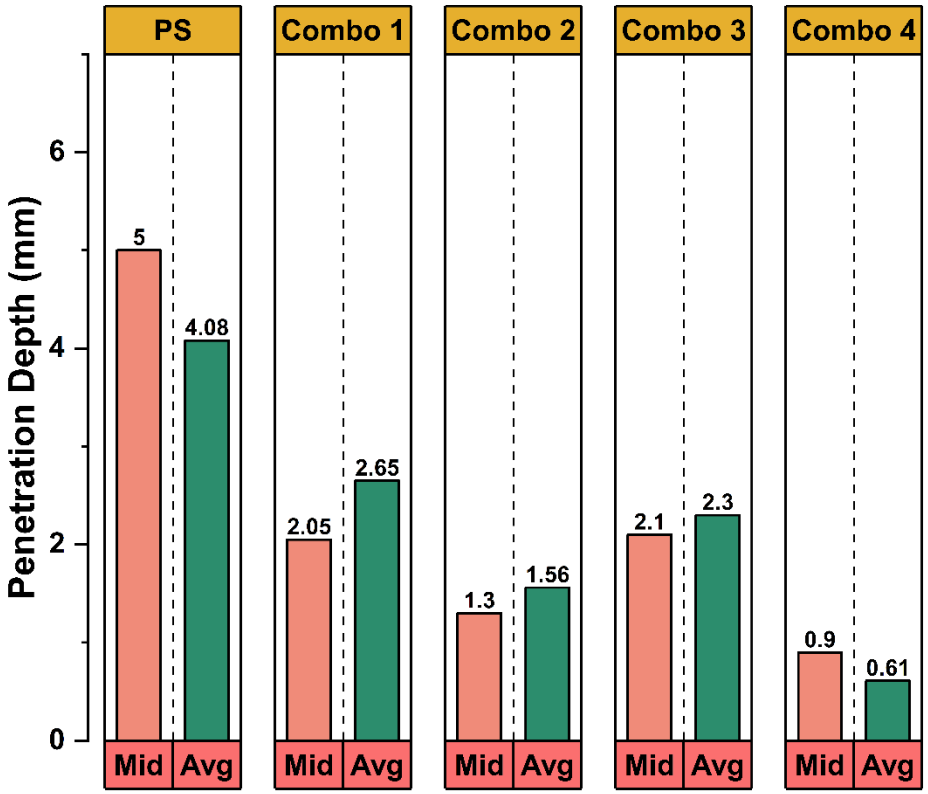

Figure 41: Fall cone test result at 3-days of curing

4.2.1.2 7 Days of curing

Figure 42 presents the penetration depths after 7 days of curing. The curing duration was extended to 7 days to explore the effects of a prolonged curing period. The penetration depth in pure sand is measured at 4.85 mm. Among the different combinations, Combo 4 exhibited the smallest penetration depth in the paper mold, indicating a higher level of calcium precipitation in the soil at 1 mm. The second most minor penetration depth is noted in Combo 2 at 1.7 mm. Combo 1 and 3 show penetration depths of 2.65 mm and 3.15 mm, respectively. Comparing the results with day 3, variations in penetration depths were observed in the four combinations on day 7. However, the trend remains consistent with the one-cycle fall cone test observations on day 3. This discrepancy could be attributed to potential evaporation

doi:10.6342/NTU202404421

losses during the extended curing period or inverse ureolytic actions. Despite these variations, the overall trend in penetration depth among all four combinations and pure sand remains consistent.

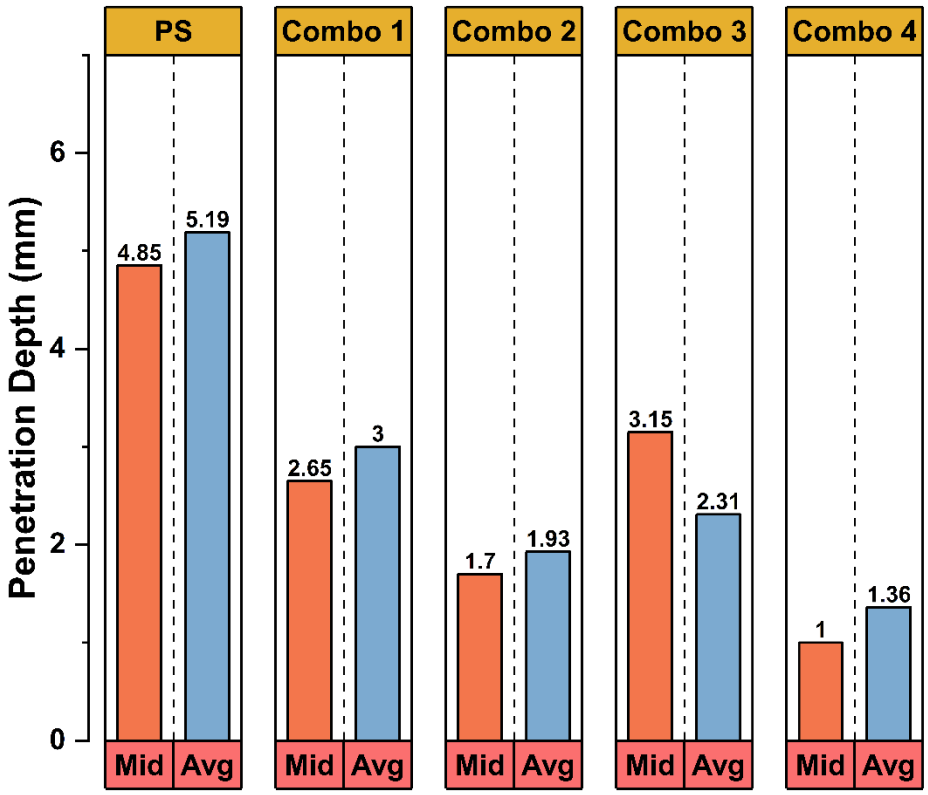

Figure 42: Fall cone test result at 7 days of curing

4.2.2 Variation of Penetration Depth at Two Treatment Cycles

4.2.2.1 7 Days of curing

Based on findings from the literature, increased treatment levels are associated with elevated $CaCO_3$ precipitation in the soil. Figure 44 illustrates one cycle of EICP treatment and one cycle of cementation solution without urease enzyme in the treated specimen. Following a 3-day curing period, 50 ml of cementation solution was introduced in all combinations.

doi:10.6342/NTU202404421

Subsequently, the drained cementation solution undergoes three cycles within the specimen before being covered with plastic to prevent evaporation loss. After a total curing time of 4 days, the fall cone test is conducted on the specimen. In contrast to prior instances where pure sand displayed a 5 mm penetration depth, it marked at 2.85 mm under these conditions. This discrepancy underscores the dependence of penetration depth on soil dry density and saturation effects (Likos *et al.* 2014). Combo 4 exhibits the most minor penetration depth at 0.3 mm, indicating a higher calcium precipitation. Following closely, Combo 2 records 0.5 mm. The decreasing trend in penetration depth from one treatment cycle to two cycles is elucidated in Figure 43. Combo 4 and 2, after two cycles, exhibit nearly identical penetration depths, suggesting a stabilizing effect. Repeated treatment cycles may further limit penetration depth, as evidenced by Combo 1 and 3 at 1.4 mm and 1.1 mm, respectively.

doi:10.6342/NTU202404421

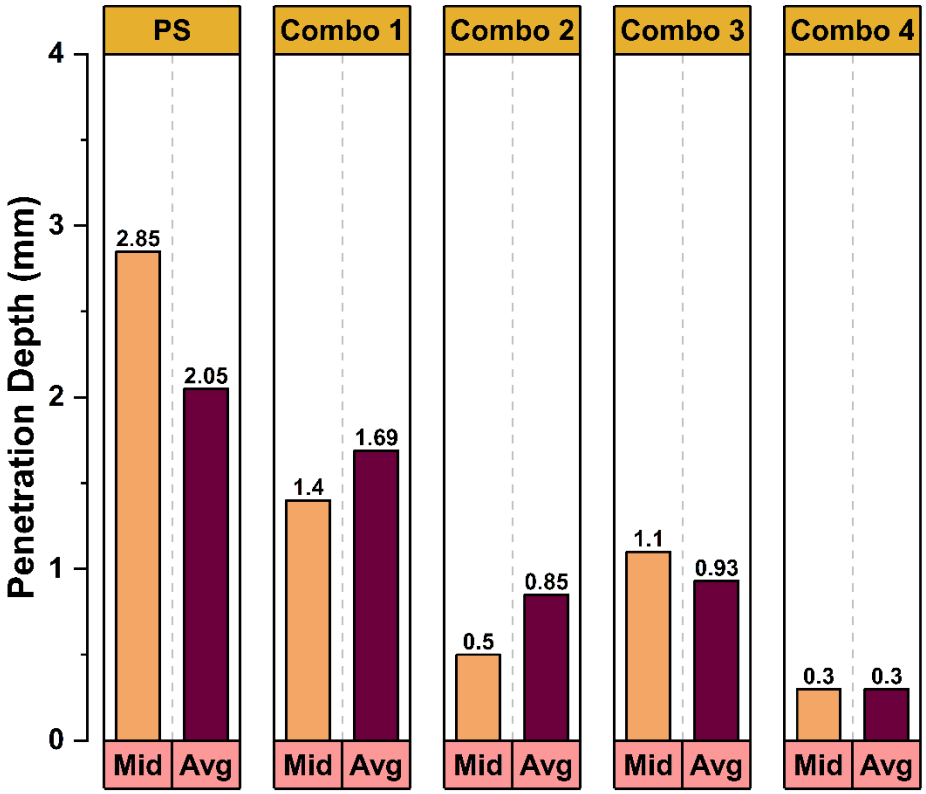

Figure 43: Fall cone test result at 7 days of curing at two treatment cycles

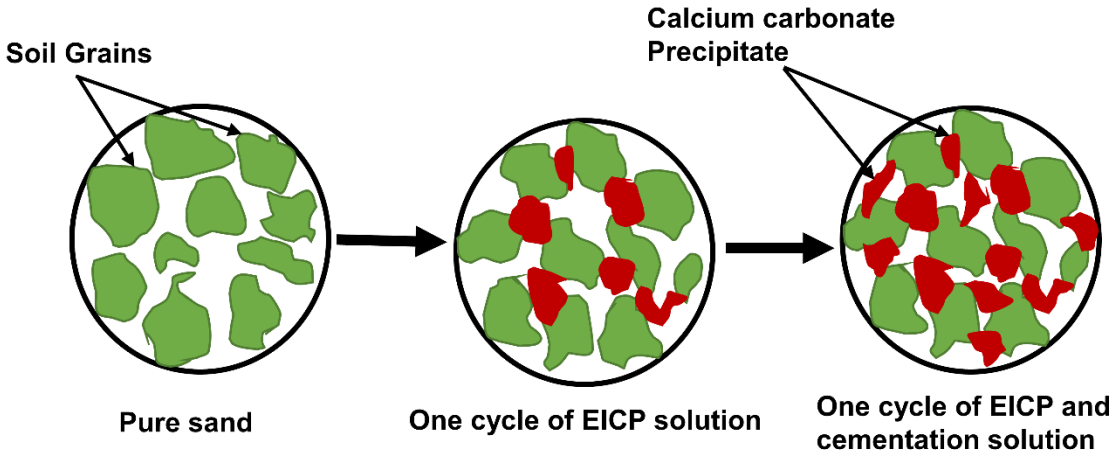

Figure 44: Schematic illustration at two cycles of bio-cementation

doi:10.6342/NTU202404421

4.2.3 Analysis of Acid Digestion Outcomes from Fall Cone Testing

4.2.3.1 3 Days and 7 Days of Curing at One Treatment Cycles

After the fall cone test at 3 days of curing, the respective CCC can be seen in Figure 45. Combo 4 exhibited the highest CCC (3.97%) at the top part of the specimen. The second highest CCC could be seen in Combo 2, with 2.75%. Combo 4 and 2 have more CCC in the topmost part and less in the bottom part, whereas Combo 1 and 3 showed the opposite pattern. Combo 1 and 3 have the least precipitation at the top and highest in the bottom part. Combo 4 showed a non-uniform with higher CCC at the top and lowest at the bottom. The other combo 1, 2, and 3 revealed approximately uniform precipitation. A similar trend can be seen in Figure 46 from the acid digestion results at 7 days of curing. Combo 4 observed the highest CCC (3.79%), and Combo 2 had a CCC of 2.86%. In contrast to the acid digestion results from day 3, the prolonged curing period may have impacted CCC. The trend line for combo 4 fluctuates more because the high concentration of urea and $CaCl_2$ may lead to non-uniform $CaCO_3$ precipitation throughout the specimen. Al Qabany *et al.* (2012) investigated the treatment factors such as chemical concentration and retention times on the calcium carbonate precipitation in MICP treatment. Scanning Electron microscopy analysis with lower urea-$CaCl_2$ concentration (0.25M) resulted in a uniform calcium carbonate distribution with an even distribution. An intermediate concentration (0.5M) in urea-$CaCl_2$ caused a random, non-uniform calcium carbonate distribution with more $CaCO_3$ crystal accumulation rather dispersed. Higher urea-$CaCl_2$ (1M) larger calcium carbonate crystals formed, leading to a lesser uniform calcium carbonate distribution. Cui *et al.* (2016) evaluated the EICP treatment using three different treatment methods: high concentration (1M), low concentration (0.5M), and mixed high - low concentration (1M+0.5M). The maximum

doi:10.6342/NTU202404421

unconfined compressive strength was achieved by mixing high – low concentrations with fewer injections.

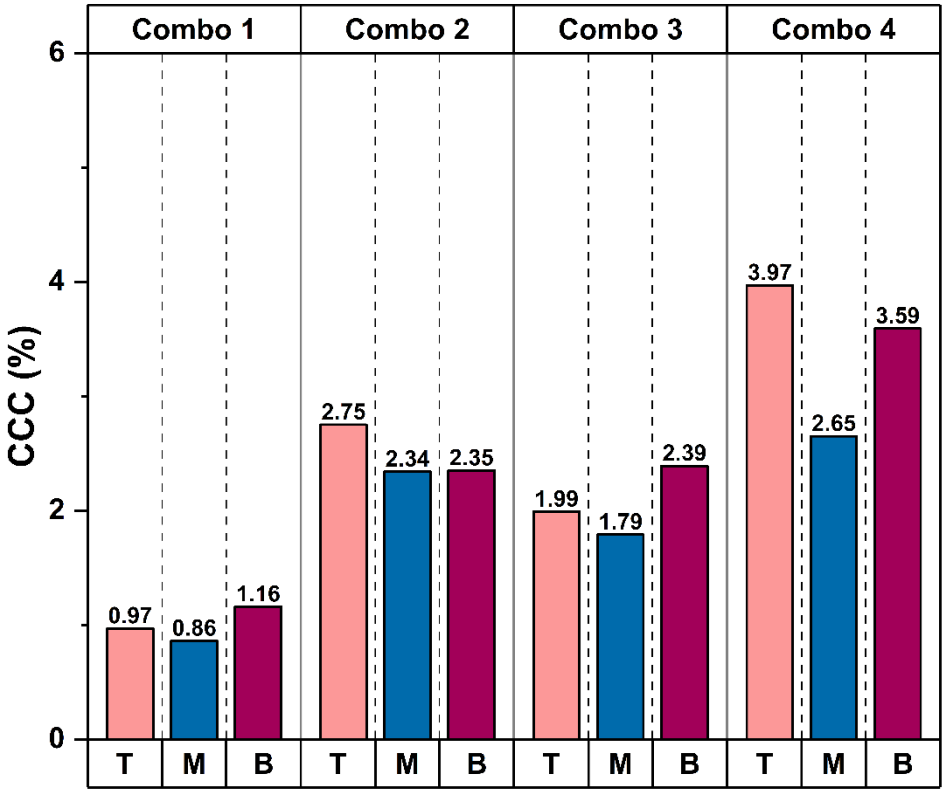

Figure 45: Acid Digestion results at 3 days of curing

doi:10.6342/NTU202404421

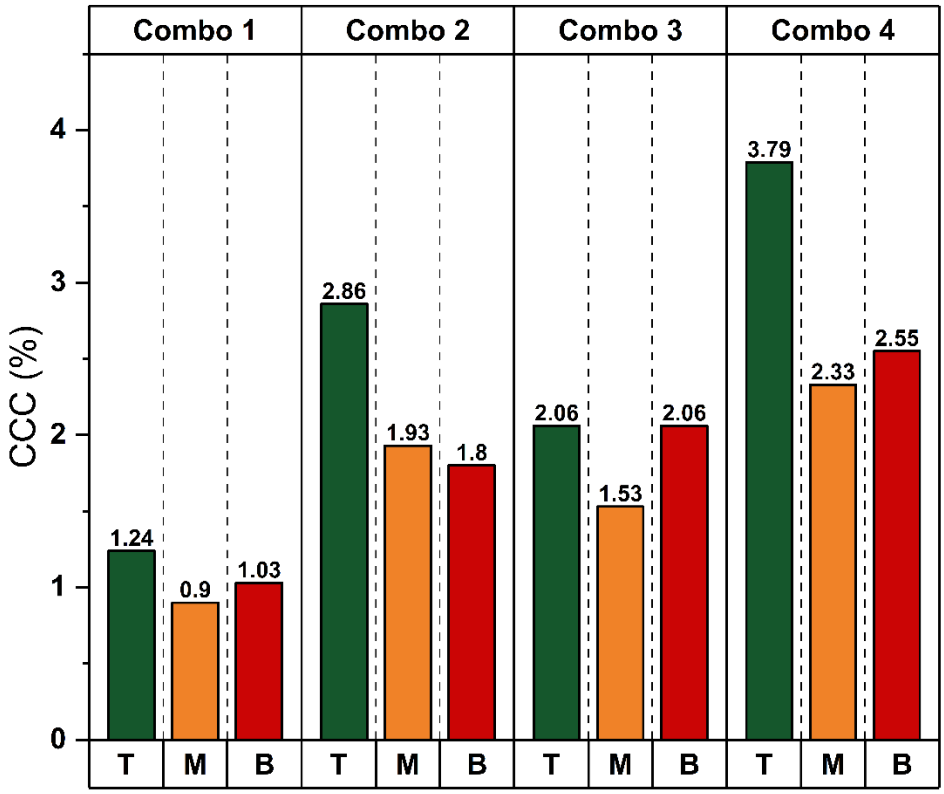

Figure 46: Acid Digestion results at 7 days of curing

4.2.3.2 7 Days of Curing at Two Treatment Cycle

Figure 47 illustrated the two treatment cycles at 7 days of curing time. The CCC in the top part of the soil specimen produced in Combo 2 and 4 with 3.36% and 4.02%. Similar to Figure 45 and 46, a non-uniform specimen can be seen in combos 2 and 4. Combo 1 and 3 showed a uniform CCC. The high urease concentration and urease activity lead to the rapid formation of $CaCO_3$. Therefore, the precipitated $CaCO_3$ accumulates in the injection, resulting in the non-uniform $CaCO_3$ distribution in the specimens. The precipitation of $CaCO_3$ occurs immediately after the injection of the EICP treatment solution, narrowing the pore throats. As a result, it becomes more challenging for the EICP solution to penetrate

doi:10.6342/NTU202404421

further. Zhang *et al.* (2014) found that the pore size distribution of calcium chloride resulted in a non-uniform distribution and identified an alternative calcium source of calcium acetate, which resulted in a more uniform distribution. The non-uniformity can be reduced when the soluble calcium reactant concentration is reduced (Gomez *et al.* 2017).

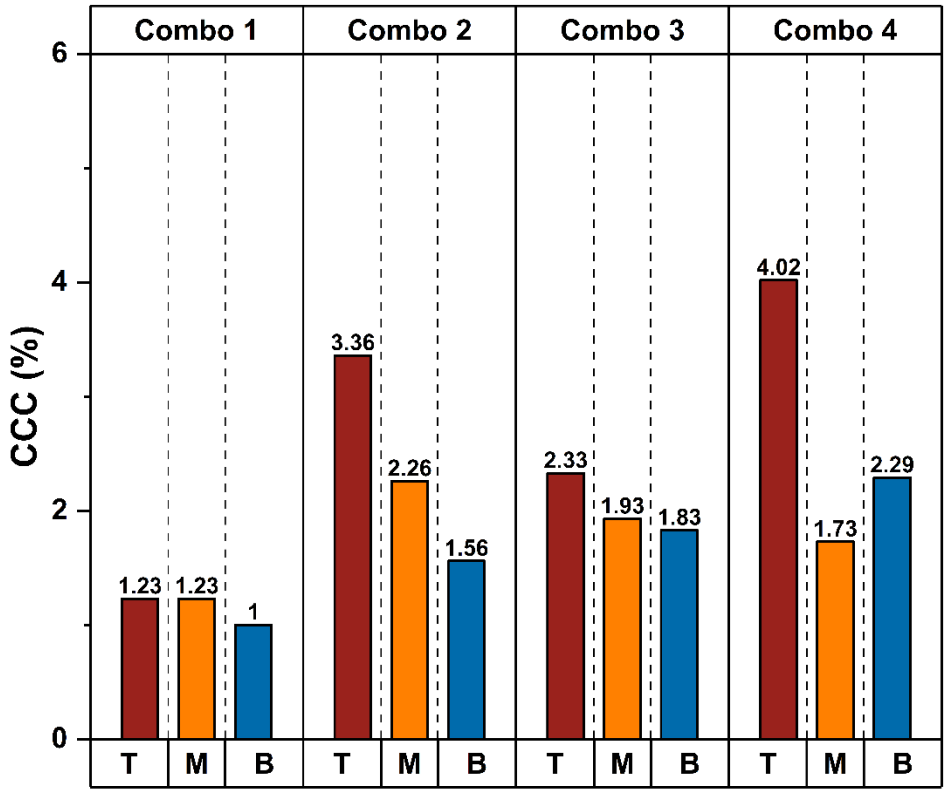

Figure 47: Acid Digestion results at 7 days of curing in two treatment cycles

4.2.4 Analysis of Acid Digestion of Triaxial Specimen

Figure 48 shows the triaxial acid digestion results in four combinations at 3 days of curing. The percolation in the increased height in the triaxial specimen could influence the $CaCO_3$ precipitation. The lower concentrations in Combo 2 and 3 showed almost uniform $CaCO_3$ precipitation. Higher concentration leads to rapid precipitation, which leads to non-uniform $CaCO_3$ precipitation. Similar results were achieved in the acid digestion results from fall cone

doi:10.6342/NTU202404421

test results at 3 days of curing. A higher amount of $CaCO_3$ precipitation in the specimen increases the strength and stiffness of the soil. Combo 4 shows the highest $CaCO_3$ precipitation, which uses triaxial testing for experimental study. Further research was employed on combo 4 for uniform $CaCO_3$ precipitation.

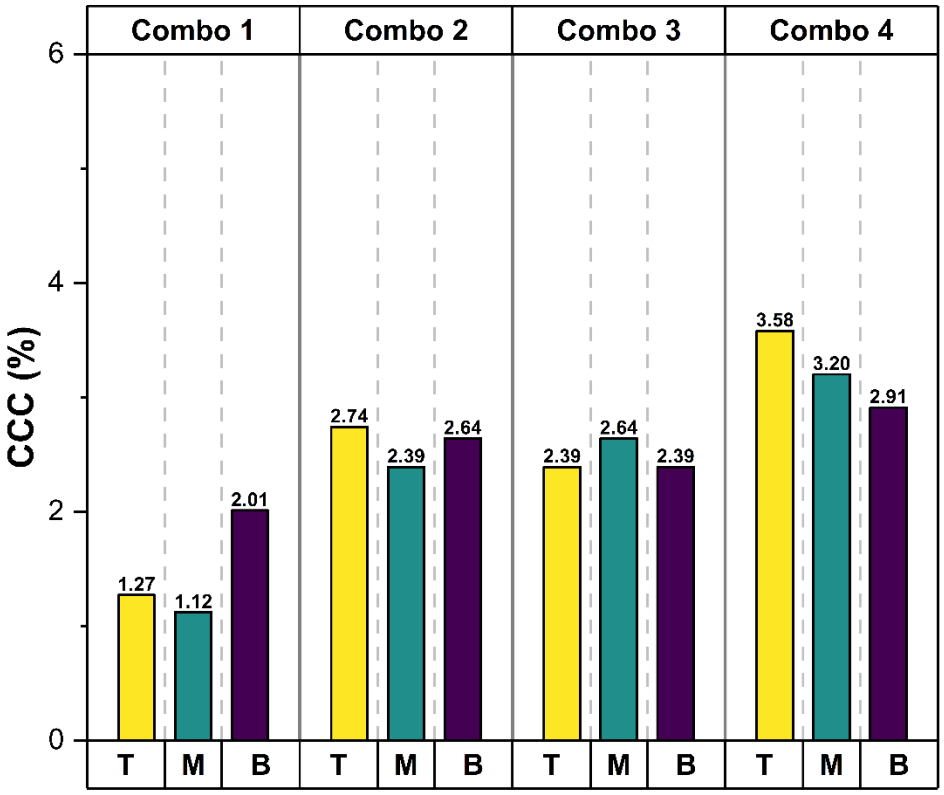

Figure 48: Triaxial acid digestion results in four combinations

4.3 Monitoring of Electrical Conductivity (EC) mS/cm and pH

4.3.1 Sigma Urease

The urease activity in the EICP solution is influenced by environmental conditions such as electrical conductivity, pH, and temperature. Temperature stands as a vital parameter within EICP treatment, and the activity is affected by different temperatures. The EICP solution was

doi:10.6342/NTU202404421

assessed at room temperature (approximately 25˚C) under oxic conditions at various intervals. Electrical conductivity represents the ionic strength in the EICP solution, and it serves as an indicator of ureolytic activity. The electrical conductivity escalates with increased enzyme reactivity, with variations over time. The progression of the reaction in the treatment is captured through electrical conductivity measurements because the electrical conductivity of the solution increases due to hydrolysis of urea and the associated precipitation of calcium carbonate (Whiffin 2004). Electrical conductivity and pH were calculated for 7 days at certain intervals to understand the hydrolysis of urea and favorable conditions for calcium carbonate precipitation.

The electrical conductivity in the EICP solution increases faster due to the higher concentration of ions in the treatment. Xie *et al.* (2023) explored the urease activity concerning pH and temperature in EICP treatment, affirming that the optimal temperature range of ureolytic activity lies between 10-50˚C. Beyond this range, the urease activity diminishes, and protein desaturation occurs, leading to reduced calcium carbonate precipitation. The initial electrical conductivity and pH values before the urease enzyme addition were approximately 78-79 mS/cm and 8.8 to 9.2, respectively. Figures 49 and 51 illustrate that the EICP treatment solution with Sigma-treated and CDH-treated EICP solution showed no degradation effects by manifesting any drop in the values of electrical conductivity of the solution. Zhao *et al.* (2014) confirmed that the increase in the rate of electrical conductivity depends upon the rate of ureolysis, which agrees with the present study.

After introducing the urease enzyme in the EICP solution, an inevitable drop in the pH can be seen in the initial stages, followed by an increase over the next few days. The

doi:10.6342/NTU202404421

initial drop could be attributed to the higher concentration of the cementation solution or the neutralizing effect on pH from its starting conditions during the first stage of the EICP treatment, involving carbonic acid decomposition. Subsequent hydrolysis of ammonia leads to a gradual pH increase (Ng *et al.* 2012). The optimal pH range for urease activity is within 7.5 – 10, creating conducive conditions for precipitation, as the pH of the solution considered here falls within the mentioned range (Arab *et al.* 2021a; Stocks-Fischer *et al.* 1999). However, exceeding this range could affect the dissociation of calcium carbonate precipitation and the coenzyme by affecting the binding between the precipitation and the enzyme (Piumetti *et al.* 2022). Both the urease enzymes showed a drop in the pH value after adding the urease enzyme in the urea-$CaCl_2$ solution. Figure 50 shows the visible changes in the EICP solution (Sigma-treated) at the initial and end of the test. The addition of the urease enzyme in the urea-$CaCl_2$ solution causes a milky formation, as can be seen in Figure 50a. Figures 50b and c show the deposition of the $CaCO_3$ precipitate at the bottom of the tube and around the sides of the tube, respectively. Similarly, Figure 52 shows the test's initial and end at 7 days of observation. Similar to the Sigma-treated EICP solution, a milky formation was observed immediately upon the addition of urease in the urea-$CaCl_2$ solution. The ureolytic actions get started immediately, and frequent handshaking of the falcon tube could enhance the reaction rate over time. Finally, after 7 days of EC and pH observation, $CaCO_3$ precipitate flocculates can be seen in the test tube and some settled at the bottom.

doi:10.6342/NTU202404421

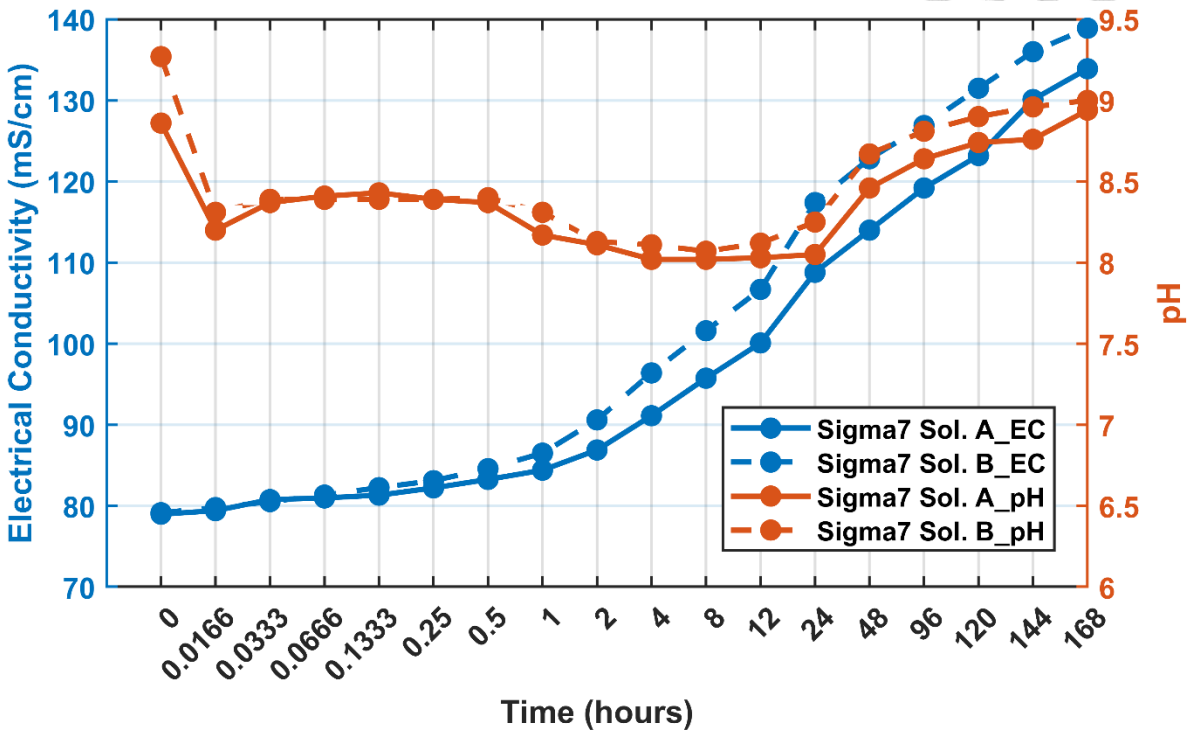

Figure 49: Electrical conductivity and pH Versus Time in EICP solution (Sigma Urease)

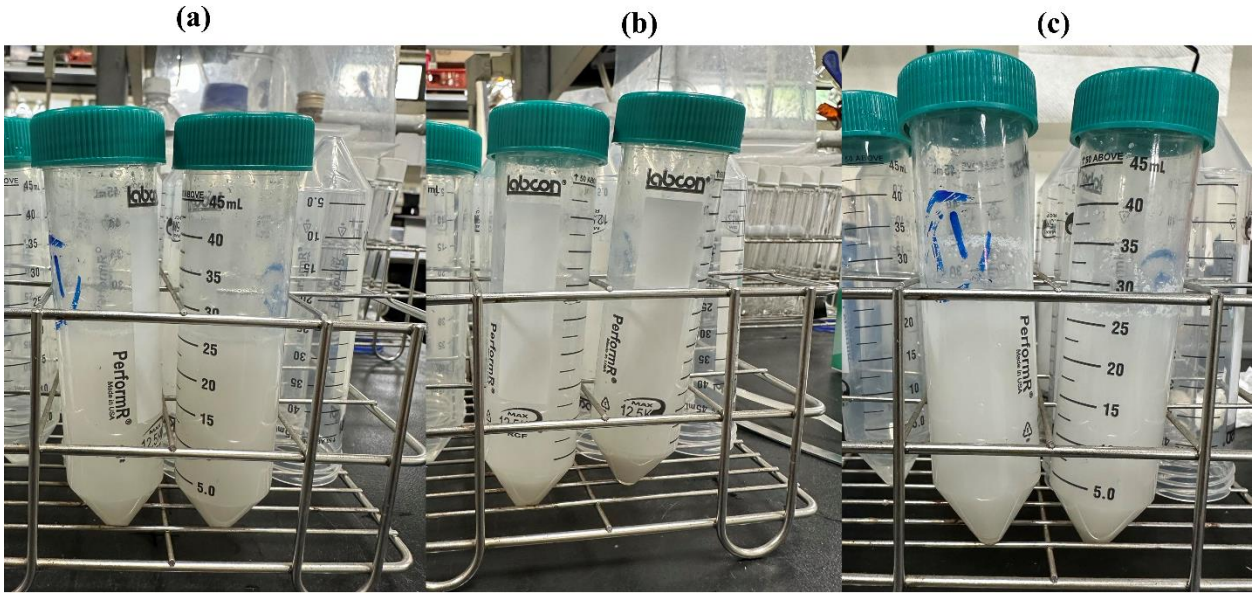

Figure 50: EICP solution (a) After the addition of urease (b) deposition of $CaCO_3$ at the bottom (c) end of the test

doi:10.6342/NTU202404421

4.3.2 CDH Urease

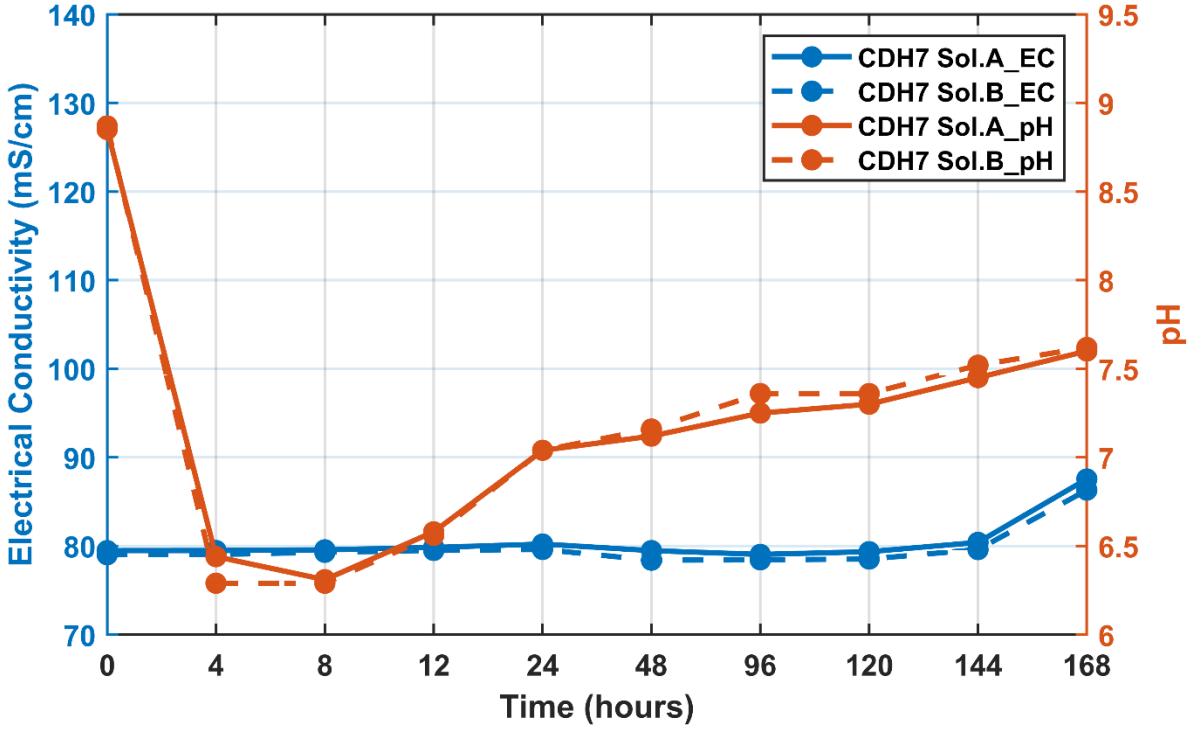

Figure 51: Electrical conductivity and pH Versus Time in EICP solution (CDH Urease)

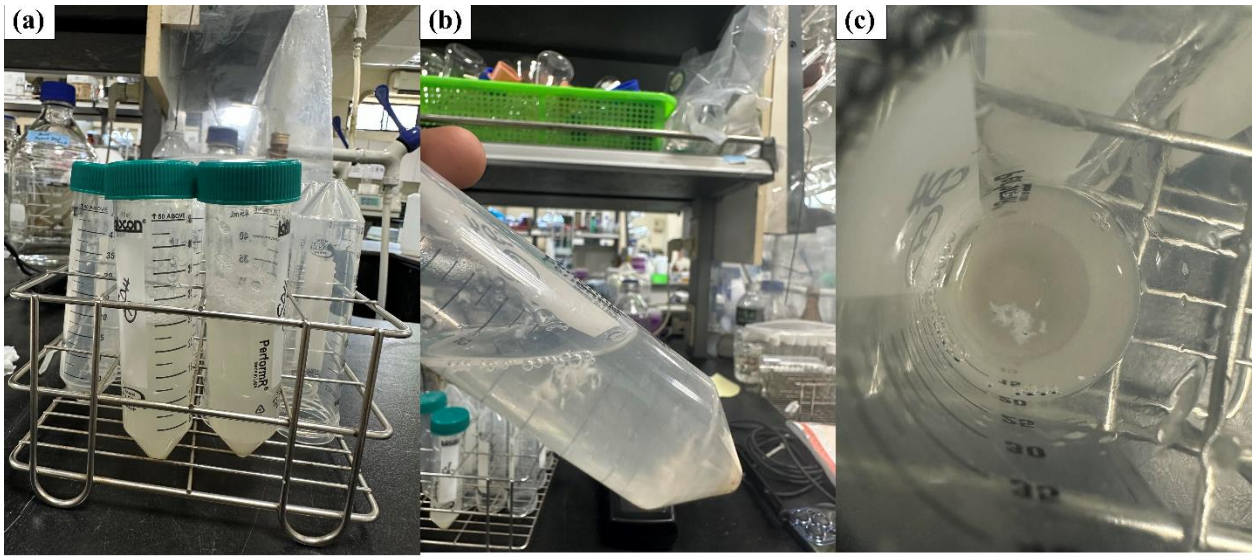

Figure 52: EICP solution (a) After the addition of urease (b and c) end of the test

doi:10.6342/NTU202404421

4.4 Isotropic Consolidated Drained (CID) Triaxial Tests

4.4.1 Stress-Strain Behavior

4.4.1.1 CDH-Treated Specimen

The stress-strain curves of pure sand and EICP-treated consolidated drained triaxial shear response curves at effective confining pressures of 50, 100, and 200 kPa and 3 curing times (3, 7, and 14 days) are shown in Figure 53. The peak deviatoric stress measured on day 3 and day 7 was lower compared to pure sand. However, after one EICP treatment cycle, the peak deviatoric stress observed on day 14 was significantly higher than on days 3 and 7. To achieve even greater strength, it is recommended to implement multiple treatment cycles, as this could result in further increases in peak deviatoric stress.

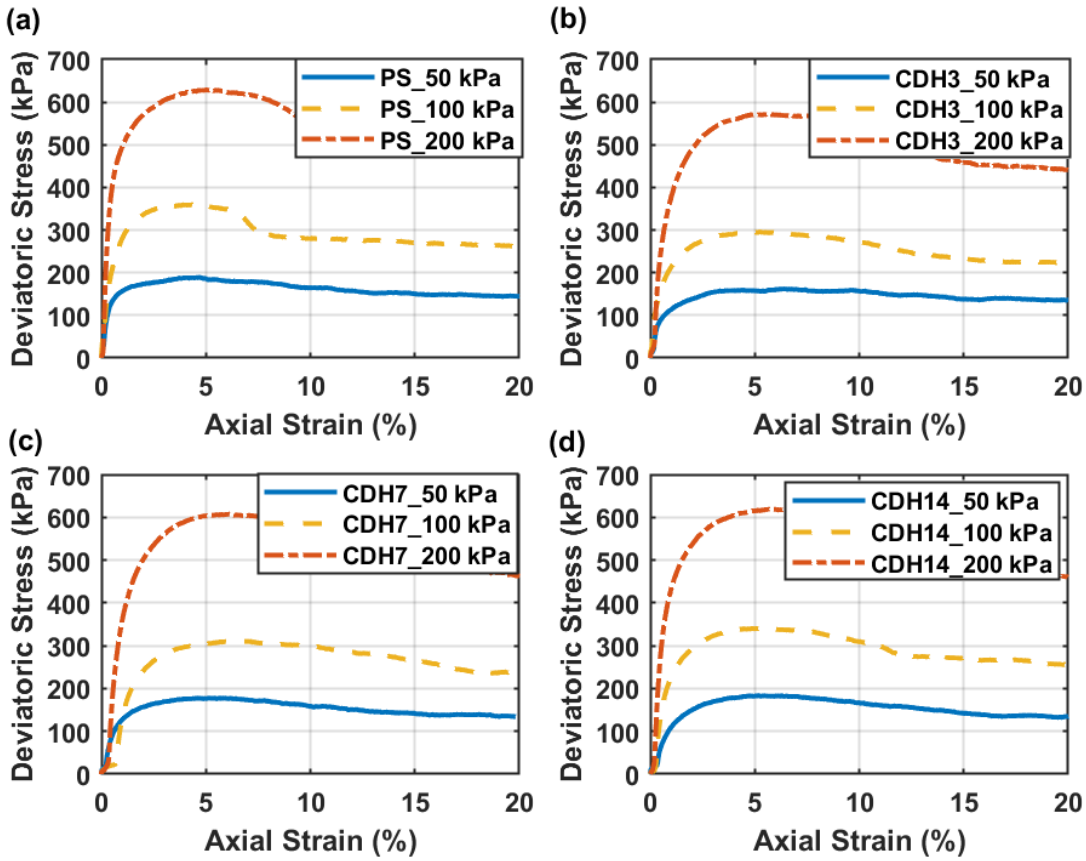

doi:10.6342/NTU202404421

Figure 53: Results of Drained Triaxial test (CDH Urease)- Stress-Strain Behavior at 50 kPa, 100 kPa, and 200 kPa effective confining pressure (a) Pure sand (PS) (b) CDH-treated specimen at 3 days curing (c) CDH-treated specimen at 7 days curing (d) CDH-treated specimen at 14 days curing

The bonding between precipitated calcium carbonate particles weakens when the specimen is subjected to larger strains during shearing. One notable behavioral change, shown in Figure 53, is that the deviatoric stress peaks at around 3% to 5% axial strain in untreated specimens. In contrast, all CDH-treated specimens reached their peak deviatoric stress beyond 5% axial strain, regardless of the confining conditions. This is likely due to particle interlocking in treated specimens, which helps sustain the load as axial strain increases. After reaching 10-12% axial strain, the deviatoric stress decreased to a residual level. The deviatoric stress at the residual stage at 3 days of curing was adjusted from 185 kPa to 180 kPa at 50 kPa so that the deviatoric stress kept increasing at 7 and 14 days to 184.32 and 184.61 kPa so that increase of curing time could increase the higher shear strength envelope.

The failure of pure sand and CDH-treated sands showed brittle failure (dilative behavior) at 20% axial shear strain. Similar results can be seen in other research papers (Cui *et al*. 2017; Yuan *et al*. 2020; Zhang *et al*. 2022b). The EICP particle-particle contact highly influences the peak deviatoric strength. The peak deviatoric stress at different curing times increases with an increase in effective confining pressure.

Figure 54 presents the stress ratio versus axial strain from monotonic drained compression triaxial tests on both untreated and CDH-treated sand. The bio-cementation

doi:10.6342/NTU202404421

process using EICP resulted in an increase in the stress ratio, which can be attributed to the higher calcium carbonate content (CCC), enhancing the dilatancy of the specimens (Choi *et al.* 2019). Both untreated and treated specimens showed a peak in the stress ratio, followed by a slight decrease as the effective confining pressure increased (Amini *et al.* 2014). Additionally, the stress ratio showed a significant increase with curing on days 3, 7, and 14. However, the reduction in the stress ratio may be due to the breakage of calcium carbonate bonds between soil particles as confining pressure increases.

At 20% strain, the stress ratio at the residual state was lower than that of untreated sand. This behavior could be explained by the weak cementation of calcium carbonate in the soil, which breaks down under higher strain levels and confining pressure (Montoya and DeJong 2015).

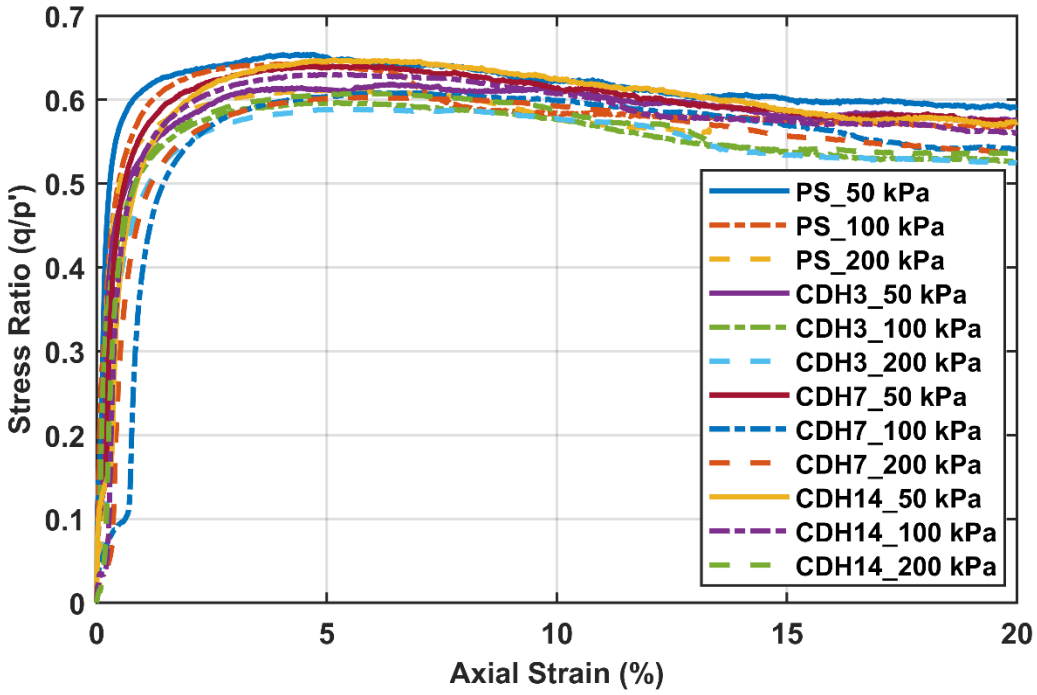

doi:10.6342/NTU202404421

Figure 54: Summary of CD triaxial test in untreated and CDH-treated specimens - Stress ratio (Deviatoric stress (q)/ Mean effective stress (p')) versus axial strain (%)

4.4.1.2 Sigma-Treated Specimen

Figure 55 presents the results of deviatoric stress versus axial strain from consolidated drained triaxial tests on pure sand and Sigma-treated specimens after 7 days of curing, under effective confining pressures of 50, 100, and 200 kPa. The calcium carbonate precipitation, which occurs at particle-to-particle contacts and on the surface of sand grains, enhances both the shear resistance and surface roughness, thereby improving the overall strength of the soil. The increased deviatoric stress observed in the Sigma-treated specimens, compared to the pure sand, highlights the influence of calcium carbonate content across all confining pressure conditions. Both the pure sand and Sigma-treated specimens display a strain-hardening behavior, with strength continuing to increase as axial strain progresses.

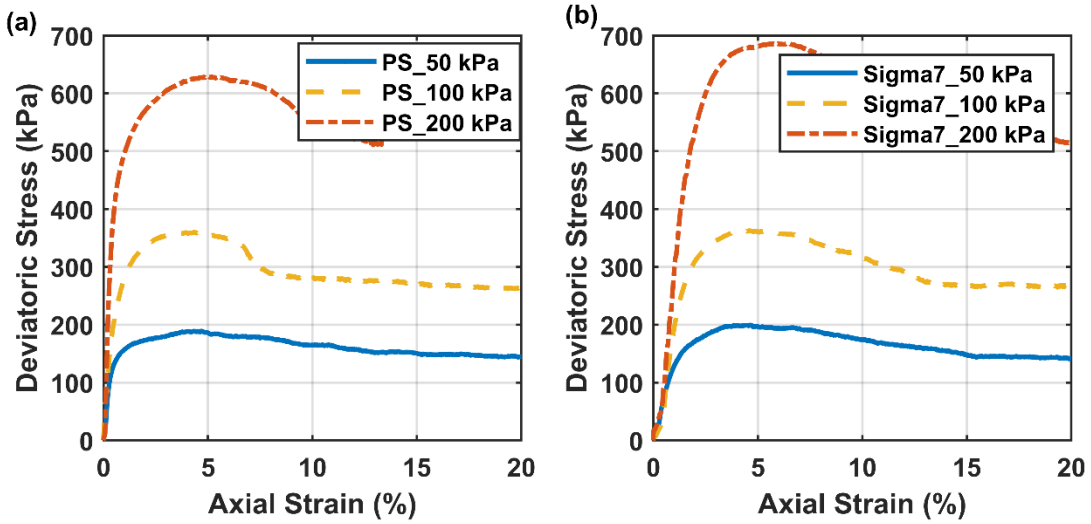

Figure 55: Summary of Drained Triaxial test (Sigma Urease) – Stress-Strain Behavior of pure sand and Sigma-treated specimen at 7 days of curing under 50 kPa, 100 kPa and 200 kPa effective confining pressure

doi:10.6342/NTU202404421

Both pure sand and Sigma-treated specimens reach peak deviatoric stress at around 4 to 5% axial strain, followed by a decline as the stress decreases post-peak, stabilizing at a residual state around 20% axial strain. This reduction in peak deviatoric stress is likely due to weakened bonding between soil particles, resulting from calcium carbonate precipitation when subjected to high axial strain. At larger strains, the residual deviatoric stresses in both pure sand and Sigma-treated specimens converge to nearly the same level. Gao *et al.* (2022) demonstrated a similar trend using a large-volume circulation technique to induce calcium carbonate precipitation through MICP treatment via denitrification. Their consolidated drained triaxial tests showed improved mechanical behavior in treated sand, primarily through increased shear strength parameters, although the residual deviatoric stresses in treated and untreated sand were similar. By the time 20% axial strain is reached, both pure sand and Sigma-treated specimens undergo brittle failure, characterized by a distinct shear plane failure.

The calcium carbonate content in Sigma-treated specimens increases the stress ratio compared to pure sand, as shown in Figure 56. Initially, the stress ratio peaks during shearing and then decreases until reaching 20% axial strain. The stress ratio reduction is more pronounced under higher effective confining pressures, likely due to the weakening of interparticle contacts caused by calcium carbonate precipitation, particularly under higher confining pressures and larger strains.

doi:10.6342/NTU202404421

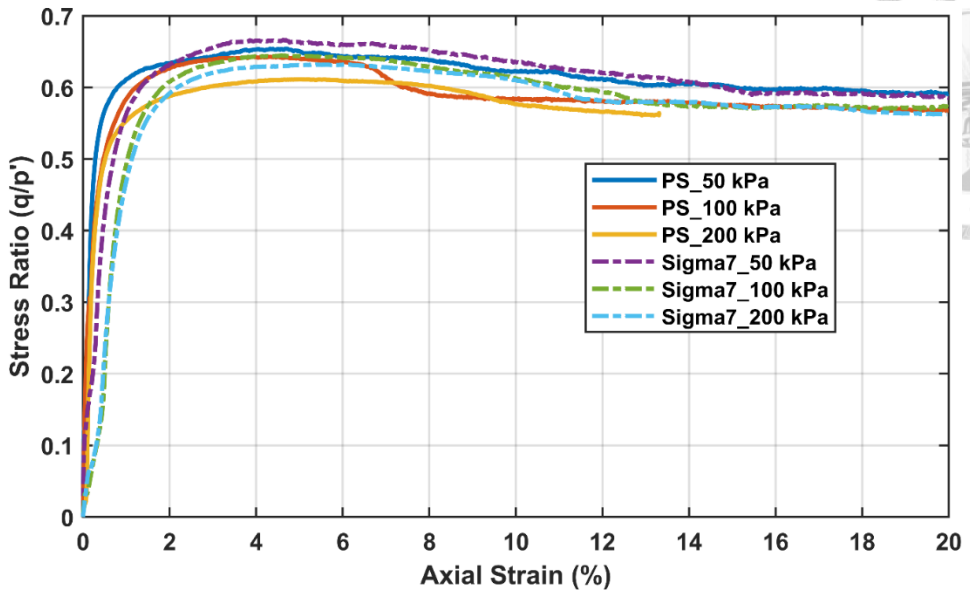

Figure 56: Summary of CD triaxial test in untreated and Sigma-treated specimens - Stress ratio (Deviatoric stress (q)/ Mean effective stress (p')) versus axial strain (%)

As mentioned previously, all the triaxial specimens were prepared at 50 % relative density. The increase in deviatoric stress in EICP-treated soil depends upon the relative density. A relative density below 50% may result in lower strength compared to higher-density soils, as EICP treatment is influenced by both relative density and $CaCO_3$ content. Increasing the number of treatment cycles will enhance $CaCO_3$ precipitation, improving the shear strength of soils with lower relative densities. This finding aligns with the research of Gao *et al.* (2019a), which conducted consolidated drained triaxial tests on sand with varying treatment cycles and densities. The results showed that even a few treatment cycles on loose and medium-density sand could significantly improve strength, without the need for densification, while also controlling deformation in the treated soil. Uniformity in EICP treatment is crucial for its efficiency, and studies have shown that a more uniform $CaCO_3$ distribution can be achieved in loose soils compared to dense (Xiao *et al.* 2019b).

doi:10.6342/NTU202404421

4.4.2 Peak and Residual Strength Parameters

4.4.2.1 CDH-Treated Specimen

The effective shear strength parameters (effective friction angle and effective cohesion) are derived from the Mohr-Coulomb failure envelopes. The shear strength parameters were determined at peak and residual state for pure and CDH-treated sand at 3, 7, and 14 days of curing, as shown in Figure 57.

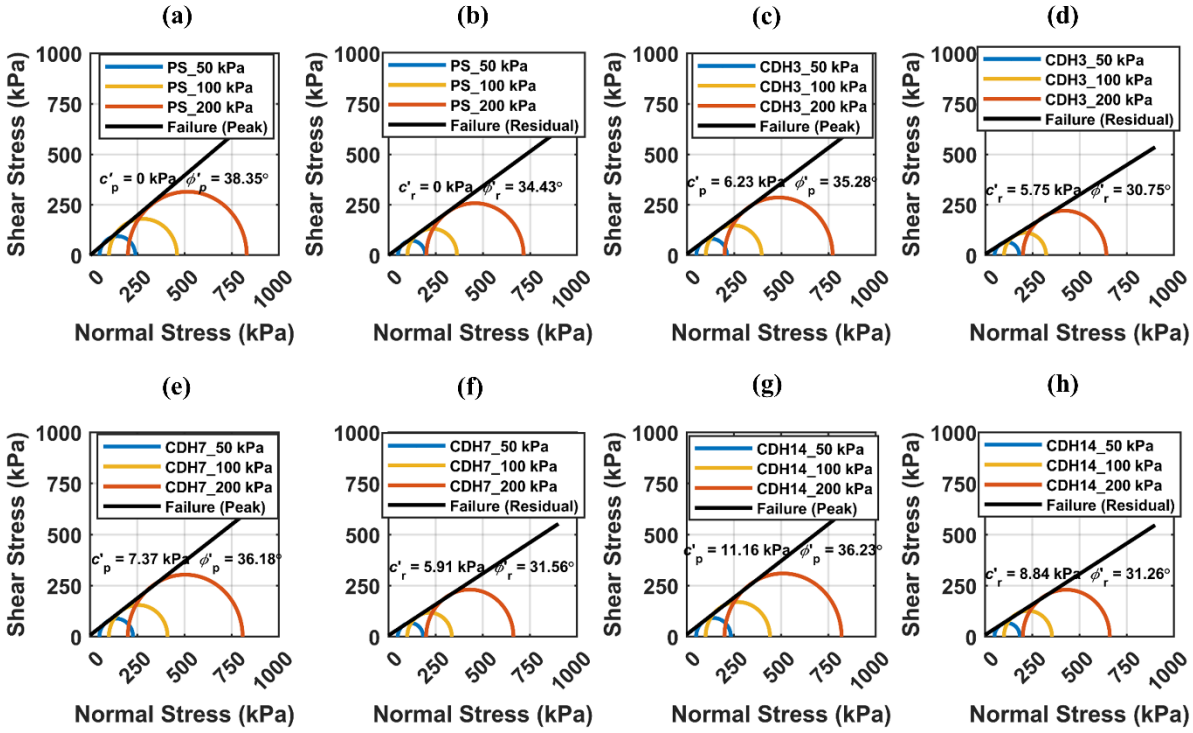

Figure 57: Mohr-Coulomb failure envelopes for untreated and CDH-treated sand (a) Pure Sand – Peak Strength (b) Pure Sand – Residual Strength (c) CDH Day 3 – Peak Strength (d) CDH Day 3 – Residual Strength (e) CDH 7 – Peak Strength (f) CDH Day 7 – Residual Strength (g) CDH Day 14 – Peak Strength (h) CDH Day 14 – Residual Strength.

The increase in bio-cementation positively impacts the cohesion of CDH-treated specimens, aligning with findings from the literature that bio-cementation enhances the

doi:10.6342/NTU202404421

effective cohesion of soil without altering the friction angle (Iamchaturapatr *et al.* 2022; Putra *et al.* 2018; Song *et al.* 2020a; Wu *et al.* 2021a). The bonding between particles due to bio-cementation contributes to this cohesion increase (Liu *et al.* 2019a). As the cementation level in treated specimens rises, both peak and residual friction dilation angles improve (Feng and Montoya 2016). Notably, effective cohesion continues to increase up to day 14 with EICP treatment.

Similarly, the effective cohesion in the residual strength increases as curing time progresses. However, both the peak and residual friction angles in untreated and CDH-treated soil show a reduction in CDH-treated soil compared to pure sand. This decrease in friction angle is offset by the increase in effective cohesion, which compensates for the strength loss in CDH-treated soil across various curing times.

Bio-cementation enhances frictional resistance by filling voids and providing inter-particle bonding within the soil (Lade *et al.* 1989). Additionally, the roughness of particles due to calcium carbonate precipitation, along with the degradation of cementation during shearing, affects the residual strength of CDH-treated specimens (Montoya and DeJong 2015).

4.4.2.2 Sigma-Treated Specimen

The Mohr-Coulomb failure envelope was employed to calculate the effective shear strength parameters, including effective cohesion and friction angle, for pure sand and Sigma-treated specimens. The failure envelope at peak and residual state for pure sand and Sigma-treated specimen is depicted in Figure 58.

doi:10.6342/NTU202404421

In pure sand, which lacks cementation effects, the deviatoric stress increases linearly under axial loading. In contrast, Sigma-treated specimens initially resist axial loading due to cementation, but as the bond from calcium carbonate precipitation weakens, localized failure planes develop within the triaxial specimen, leading to greater strain at the failure point. Beyond 10-15% axial strain, the deviatoric stress declines to a residual state. These findings are consistent with those reported by (Gitanjali *et al.* 2024) in CDH-treated specimens as well.

As shearing progresses and larger axial strains are applied, the degradation of calcium carbonate precipitation at particle contacts becomes a critical factor, affecting the residual strength in both pure sand and Sigma-treated specimens. Similar to our research findings, Liu *et al.* (2019a) investigated MICP-treated specimens under varying cementation solution-to-sample volume ratios and observed, through consolidated drained triaxial tests, that the peak effective cohesion increases with a higher cementation solution volume, while the peak friction angle remains constant. This aligns with the shear strength parameters observed in our research.

doi:10.6342/NTU202404421

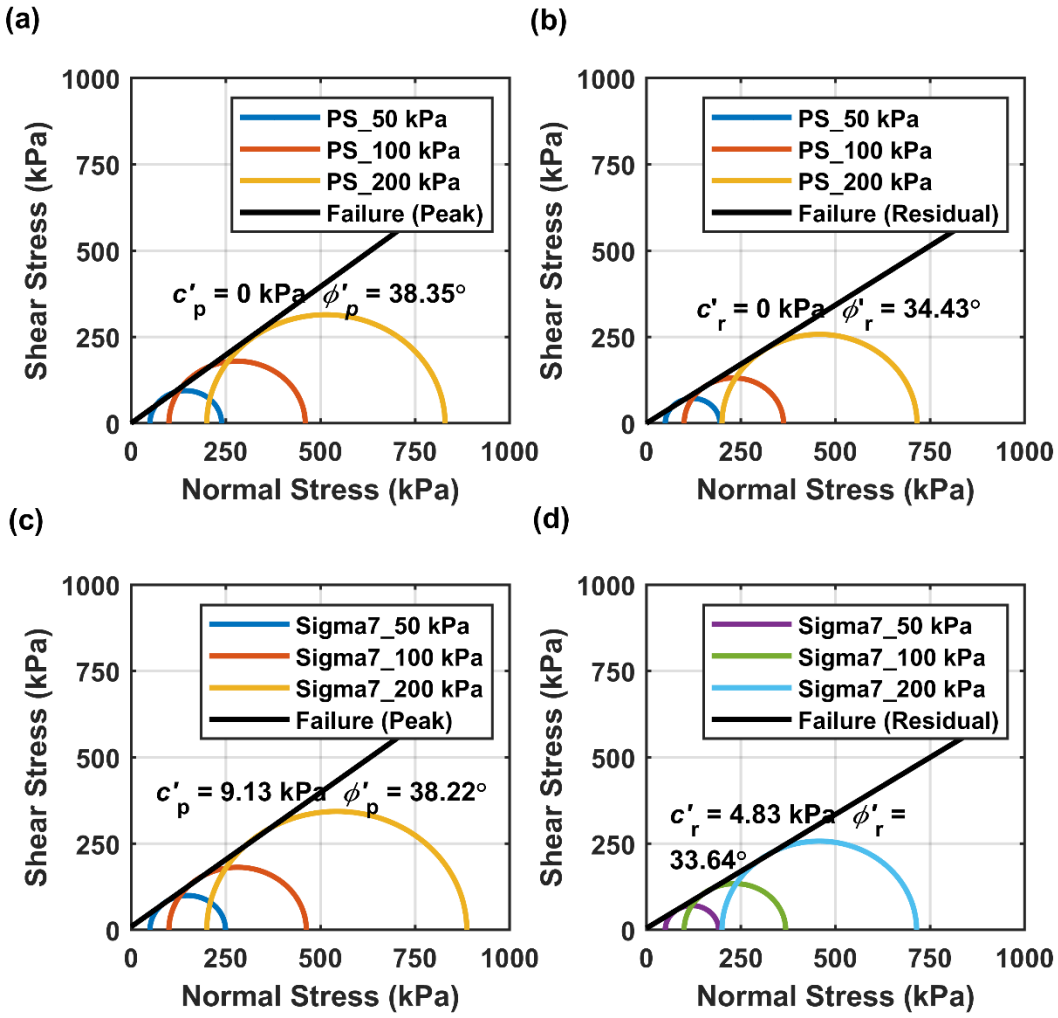

Figure 58: Mohr-Coulomb failure envelope for pure sand and Sigma-treated specimen (a) Pure Sand – Peak Strength (b) Pure Sand - Residual Strength (c) Sigma Day 7 – Peak Strength (d) Sigma Day 7 – Residual Strength

The improvement in shear strength parameters in both CDH and Sigma-treated specimens is attributed to a single cycle of treatment. However, increasing the number of treatment cycles would significantly enhance $CaCO_3$ precipitation, leading to a greater improvement in shear strength compared to just one cycle. Achieving the desired strength may require multiple treatment cycles. Two key factors—particle roughness and porosity—

doi:10.6342/NTU202404421

play a crucial role in enhancing the effective friction angle. Bio-cementation reduces porosity and increases particle roughness, which helps improve the effective friction angle (Cui *et al.* 2021b). Additionally, EICP bio-cementation strengthens the bonds between sand grains, resulting in an increase in effective cohesion (Wu *et al.* 2021a).

From the literature reviews, it can be seen triaxial test on the biocemented soil were perfomed under 400 kPa (Cui *et al.* 2021b; Liu *et al.* 2019a). More research is needed to explore EICP treatment under higher confining pressures. Zhang *et al.* (2024) conducted a series of drained triaxial tests with effective confining pressures ranging from 400 kPa to 1800 kPa, investigating shear strength parameters, volumetric deformation, and dilatancy in EICP-treated calcareous sand. The results showed that increasing the cementation level heightened the brittleness of the treated soil, resulting in higher peak strength and more pronounced dilative deformation. However, at higher confining pressures, dilation decreased while contraction-induced deformation increased, with yield stress improving as cementation levels rose. At very high confining pressures, particle breakage and bonding degradation becomes significant (Wu *et al.* 2021b). The impact of high confining pressure on treated soils could potentially be mitigated by increasing $CaCO_3$ precipitation. This study found that even a single cycle of EICP treatment in pure sand produced considerable improvements in effective shear strength. Applying multiple cycles of treatment could further enhance $CaCO_3$ precipitation, leading to increased soil strength. Higher $CaCO_3$ content promotes stronger interlocking between soil grains, increases particle roughness, and thus contributes to more effective soil improvement.

doi:10.6342/NTU202404421

4.4.3 Volumetric Behavior

4.4.3.1 CDH-Treated Specimen

All the drained triaxial specimens exhibited brittle behavior at 20% axial strain, showing dilatancy characteristics indicative of a brittle behavior mechanism. Both CDH-treated and pure sand exhibited volumetric behavior involving compression and dilation during shearing. The general trend of volumetric strain in the CDH-treated specimens tends to be higher than in pure sand. A notable observation can be seen in the CDH-treated specimen at 14 days of curing at 50 kPa, where it exhibited maximum dilation compared to the pure sand. Figure 59 shows a decrease in volumetric strain with increasing effective confining pressure, consistent with prior findings (Torsten Wichtmann *et al.* 2015). The volumetric strain response graph indicates the dilatancy to the monotonic loading due to calcium carbonate precipitation in the CDH-treated specimens, which aligns with other research papers (He *et al.* 2022c; Lin *et al.* 2021; Nafisi *et al.* 2019) .

doi:10.6342/NTU202404421

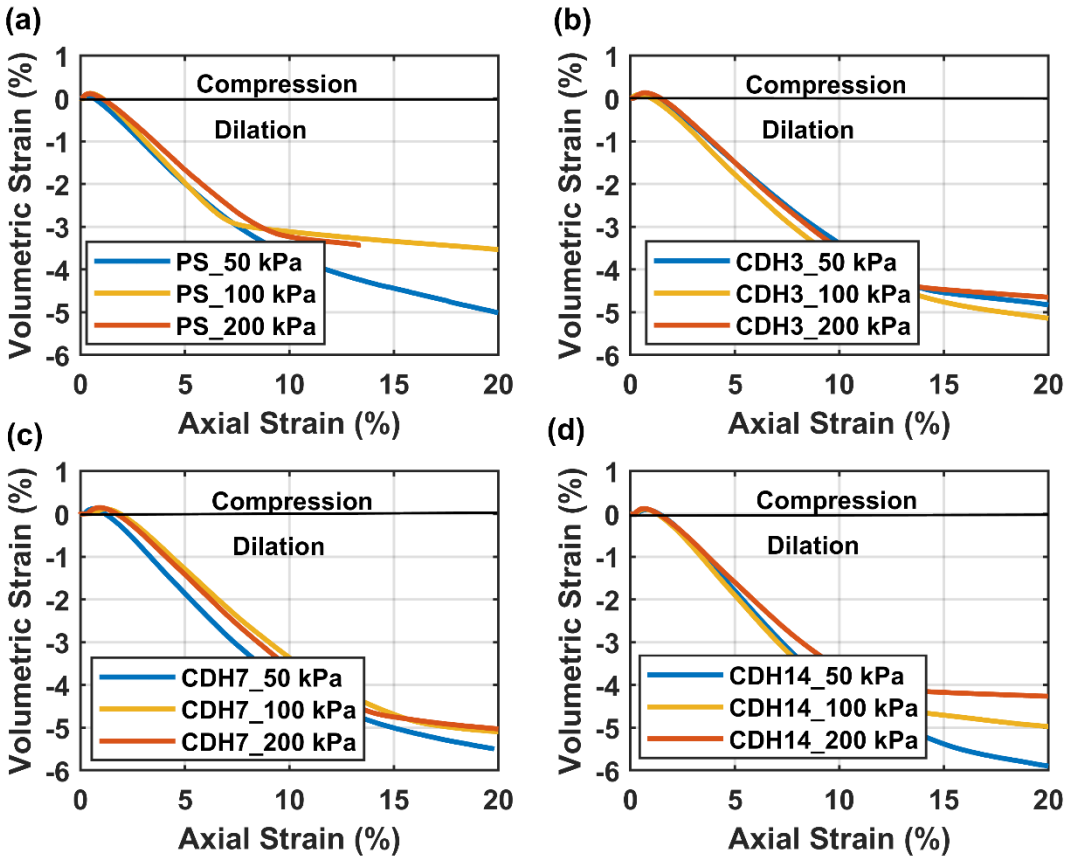

Figure 59: Results of Drained Triaxial test – Volumetric Strain Behavior at 50 kPa, 100 kPa, and 200 kPa effective confining pressure (a) Pure sand (PS) (b) CDH-treated specimen at 3 days curing (c) CDH-treated specimen at 7 days curing (d) CDH-treated specimen at 14 days curing

The volumetric strain response initially shows contraction, followed by significant dilation. The CDH-treated specimen displays increased initial contraction, consistent across triaxial tests at varying confining pressures and curing times. The influence of cementation in the CDH-treated specimens results in higher compressibility during the initial shearing stage, likely due to the breakage of weak calcium carbonate cemented particle contacts.

doi:10.6342/NTU202404421

All the CDH-treated specimens transitioned from contractive behavior to dilative behavior after a particular stage of initial shearing. The increase of calcium carbonate content in CDH-treated specimens induces dilative behavior compared to the untreated specimens. EICP bio-cementation enhances the particle interlocking soil grains by gelling calcium carbonate precipitation.

The volumetric strain response curve demonstrated increased dilatancy at 14 days of curing time compared to pure sand. Initially, all specimens exhibit consistent contractive behavior before shifting to dilative behavior. CDH-treated specimens consistently show a higher dilative behavior rate than the untreated sand. At the residual stage, the calcium carbonate precipitation in the specimen leads to significant dilation compared to pure sand. The higher amount of calcium carbonate content increases initial stiffness and dilative behavior compared to untreated specimen. (Wu *et al.* 2021a).

4.4.3.2 Sigma-Treated Specimen

Figure 60 illustrates the relationship between the volumetric and axial strain as observed from the monotonic drained triaxial test conducted on pure sand and Sigma-treated specimens at 7 days of curing under 50,100 and 200 kPa effective confining pressure. A negative volumetric strain indicates dilation. The volumetric behavior of the Sigma-treated specimen demonstrated greater dilation compared to pure sand, largely due to the effects of calcium carbonate precipitation from the treatment.

Both pure sand and Sigma-treated specimens initially underwent compression during the early stages of shearing, followed by significant dilation at larger strain levels. However, Sigma-treated specimens exhibited more pronounced compression than pure sand, which can be attributed to the disruption of unstable calcium carbonate bonds at the bridging points

doi:10.6342/NTU202404421

between soil grains. This trend was observed consistently across all Sigma-treated specimens. The increased dilation in the Sigma-treated specimen is likely due to the enhanced roughness on the sand particle surfaces caused by calcium carbonate precipitation. Wu *et al.* (2021a) explored stress-dilatancy in MICP-treated sand through consolidated triaxial compression tests, and their findings align with the volumetric strain response observed in this research.

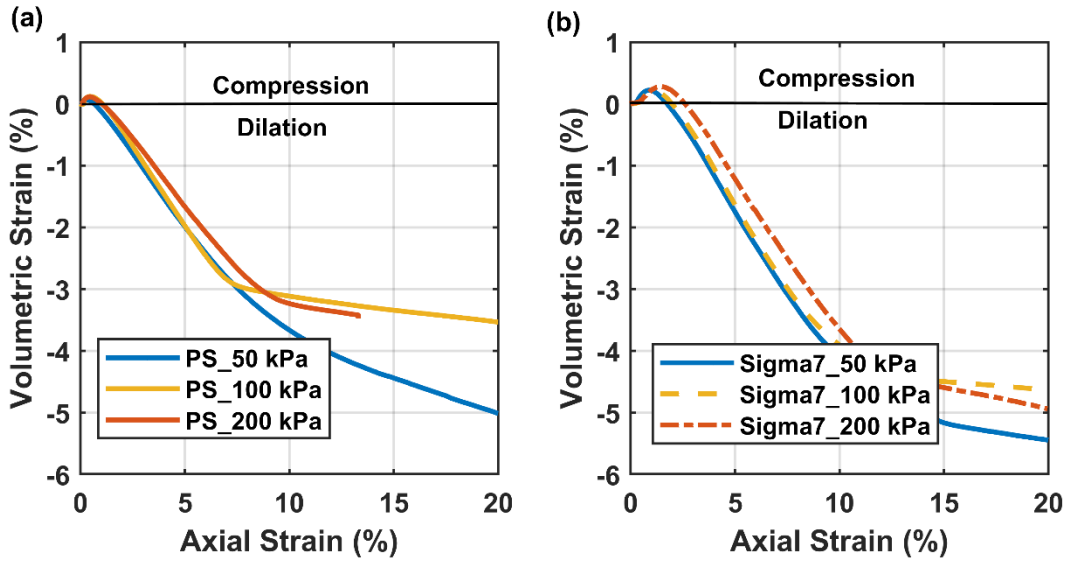

Figure 60: Summary of Drained Triaxial test – Volumetric Strain Behavior of Pure sand and Sigma-treated specimen at 7 days of curing under 50 kPa, 100 kPa, and 200 kPa effective confining pressure

4.5 Study of Liquefaction Resistance

4.5.1 Cyclic Triaxial Testing and Discussion with CDH-Treated Specimen

The undrained cyclic triaxial tests were conducted in both pure sand and CDH-treated specimens to examine the effectiveness of the EICP treatment against soil liquefaction. The axial strain (ε_a), excess water pore pressure ratio (r_u), and the number of cycles (N_L)

doi:10.6342/NTU202404421

corresponding to the cyclic stress ratio for pure sand and EICP-treated sand of 7-day curing are listed in Table 6.

Table 6: Test Scheme in Cyclic Triaxial (CDH-Treated Specimen)

Tests	EICP Recipe	Curing Days	CSR	Axial Strain (%)	Number of Cycles (N_L)
Pure Sand	N/A	N/A	0.206	-0.87	200.03
			0.258	-0.70	7.05
			0.308	-1.48	4.03
CDH	1 M Urea 0.67 M $CaCl_2.2H_2O$ 3 g/l Urease	7 days	0.212	-0.55	991.05
			0.258	-0.57	17.07
			0.31	-1.48	9.05

4.5.1.1 Cyclic Strain Response and Pore Pressure Development

The effectiveness of EICP treatment in enhancing liquefaction resistance was evaluated by comparing pure sand with CDH-treated specimens after 7 days of curing under stress-controlled conditions. The deformation response and excess pore water pressure ratio reveal the impact of EICP treatment on the shear strength and stiffness of the specimens. Both pure and CDH-treated sand exhibited compression and extension strains during cyclic loading. Figure 61 illustrates the axial strain versus the number of cycles for both types of sand, which can be divided into three stages: (i) Stage 1 – Compaction, (ii) Stage 2 – Shearing, and (iii) Stage 3 – Failure.

doi:10.6342/NTU202404421

In the compaction stage, the soil structure undergoes initial changes, resulting in slight deformation due to vertical displacement caused by cyclic loading. During the shearing stage, axial strain gradually increases with the number of cycles, as dynamic strain and the shearing effect on soil grains become dominant. In the final failure stage, cyclic loading exceeds the dynamic strength of both pure and CDH-treated sand, causing a significant increase in axial strain as the number of cycles grows until the specimen either withstands the loading or fails. These trends were consistently observed across all tests, in line with previous research (Rui *et al.* 2022).

Figure 61 shows the compression strain at the point of liquefaction, where EICP treatment led to a noticeable reduction in compression strain in CDH-treated specimens compared to pure sand under three different cyclic stress conditions. This suggests that CDH-treated specimens exhibit more dilative behavior due to calcium carbonate precipitation. Enhanced cementation through EICP may further reduce compression strain and push the specimen toward a dilation hardening phase. Similar dilative behavior was observed during monotonic drained triaxial testing at 7 days of curing, as reported in earlier studies (Xiao *et al.* 2018a).

doi:10.6342/NTU202404421

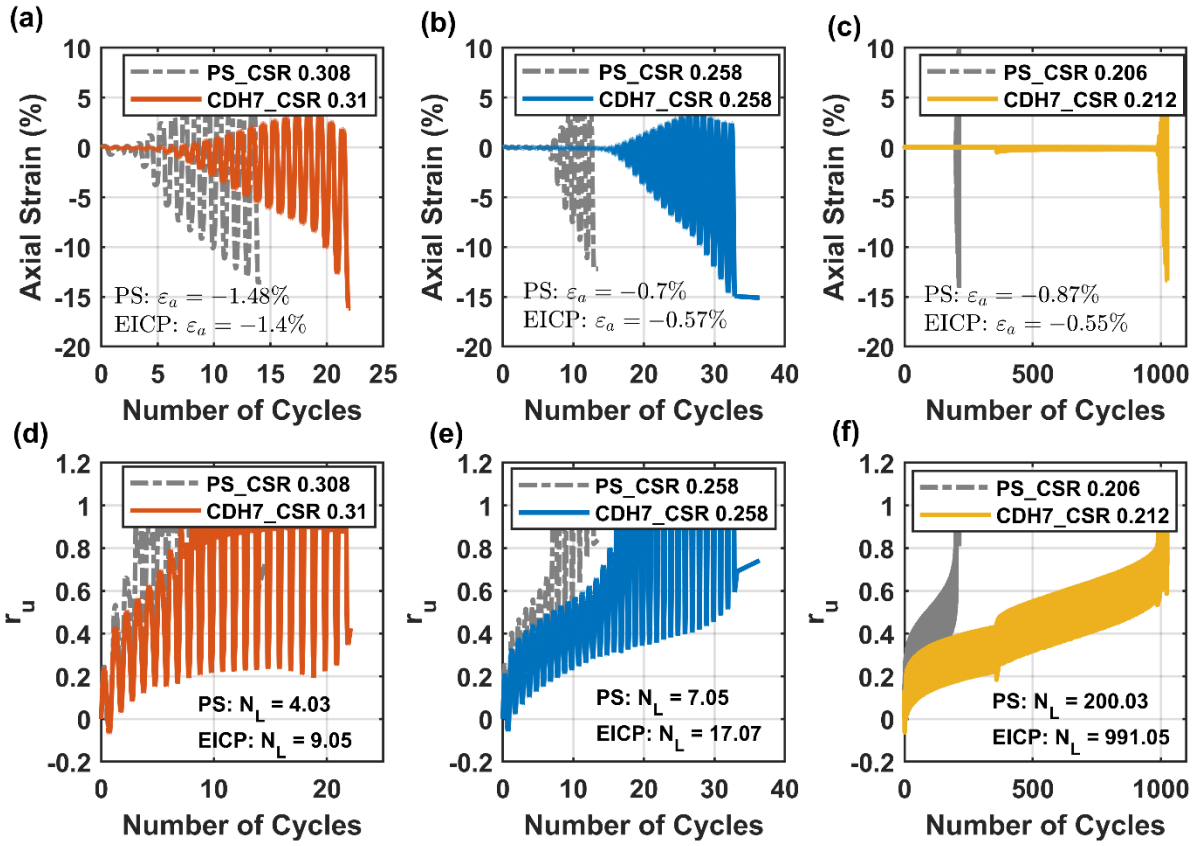

Figure 61: Relationships of axial strain, excess pore water pressure ratio, and number of load cycles

During liquefaction, the axial strain in the pure sand was measured at -1.48% for CSR 0.308. However, in the EICP-treated specimen at CSR 0.31, this value was reduced to -1.4%. A similar trend was observed with compression strains, which decreased to -0.57% and -0.55% in the EICP-treated specimens at CSR 0.258 and 0.212, respectively. Under all stress-controlled conditions, cementation via EICP showed a diminishing trend in compression as the number of liquefaction cycles increased, while also reducing the sudden dissipation of pore water pressure. Additionally, multiple EICP treatment cycles lowered the cyclic strain rates in CDH-treated specimens, indicating a shift toward dilation hardening. This suggests

doi:10.6342/NTU202404421

that the interlocking of calcium carbonate crystals contributed to a rock-like structural behavior in the treated samples. Calcium carbonate precipitation both among particles and on the surface of soil grains enhanced the strength and cyclic resistance of treated specimens, as confirmed by SEM and EDS mapping.

The number of load cycles required to reach liquefaction increased in the CDH-treated specimens compared to pure sand due to the interparticle binding from calcium carbonate precipitation and the impermeable nature of the cemented soil. The excess pore water pressure response during cyclic loading plays a critical role in soil instability under liquefaction conditions. The pore water pressure ratio response initially rises rapidly during the early stages of cyclic loading, followed by a slower increase at the liquefaction stage. This trend was consistent across all tests, aligning with previous studies (Ghionna *et al.* 2006; Han *et al.* 2020).

In untreated loose sand, cyclic shear typically produces an S-shaped pore pressure response. However, bio-cementation and the resulting increase in soil density shift this response to a hyperbolic-type curve (Xiao *et al.* 2019a). Near liquefaction, both pure sand and CDH-treated sand exhibited a small notch in the response curve, indicating cyclic behavior under loading. The area enclosed between two peaks in these notches represents cyclic activity within the specimen. As axial strain increases, the location of these notches shifts, signifying a rise in cyclic activity as the number of cycles grows. This phenomenon reflects alternating shear-induced contraction, shear-induced expansion, and unloading-induced contraction in both pure and CDH-treated sand under cyclic loading. These findings are consistent with prior research (Han-Long *et al.* 2018; Yanli *et al.* 2009). The magnitude of the cyclic stress ratio significantly influences the number of cycles to liquefaction. The

doi:10.6342/NTU202404421

number of load cycles to liquefaction increased from 4.03 to 9.05 in the pure sand and CDH-treated specimens at CSR 0.308 and 0.31, respectively. Similarly, the number of load cycles increases from 7.05 to 17.07 cycles and 200.03 to 991.05 in pure sand and CDH-treated specimens at CSR 0.258 and CSR 0.212. Thus, it is evident that the liquefaction resistance increases with the decrease in CSR.

4.5.1.2 Cyclic Stress-Strain Characteristics

The hysteresis loops and the stress paths of the untreated and CDH-treated specimens at different CSR levels are shown in Figure 62. The number of load cycles to liquefaction significantly increased in CDH-treated sand under all stress conditions.

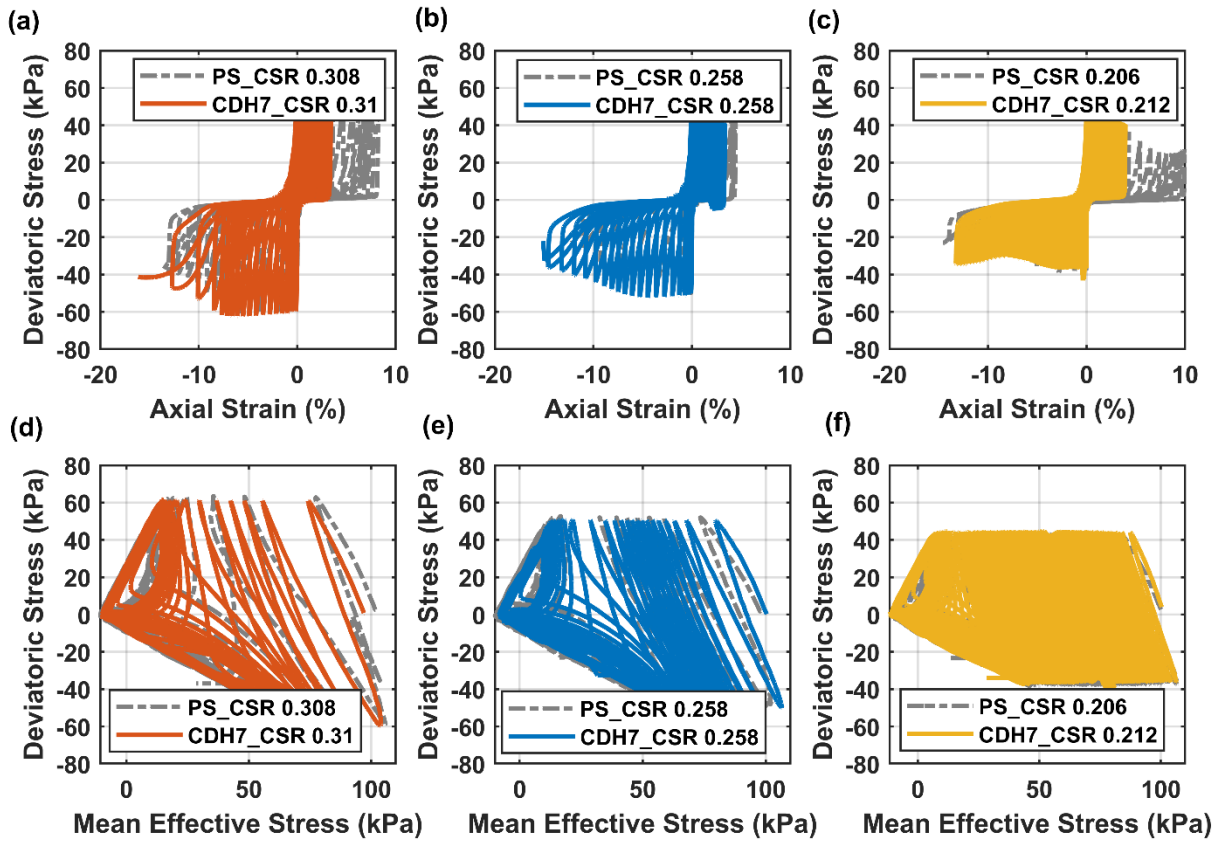

Figure 62: Cyclic stress-strain curves and stress paths

doi:10.6342/NTU202404421

During cyclic loading, the specimen gradually loses stiffness, leading to dilation hardening. As excess pore water pressure accumulates, the effective stress path shifts toward the origin due to a reduction in mean effective stress. Once liquefaction is reached, the effective stress path aligns with the failure envelope, achieving a state of non-zero mean effective stress, at which point the specimen can no longer sustain the applied load (Xiao *et al.* 2018a). The number of load cycles to liquefaction is higher in CDH-treated sand than in untreated sand, a result of the cementation effect from calcium carbonate precipitation, which strengthens the interparticle binding. Neither CDH-treated nor pure sand specimens exhibit flow failure liquefaction. Instead, they demonstrate a gradual loss of stiffness associated with a cyclic mobility failure mode (Xiao *et al.* 2019b).

During cyclic loading, some of the external work applied to the specimen is stored as elastic deformation energy, while the remainder dissipates into other forms of energy. When the deviatoric stress reverses, the stored elastic energy is released, while the dissipated energy is used to rearrange soil grains, leading to the accumulation of plastic strain. The repetitive loading and unloading cycles produce stress-strain hysteresis loops, with the area enclosed by each loop representing the energy dissipated during a single loading cycle (Han *et al.* 2020). Compared to pure sand, CDH-treated sand withstands cyclic loading for a greater number of cycles, likely due to the bonding effect between the sand grains and calcium carbonate precipitate.

Figure 63 compares the liquefaction resistance curves for pure sand and CDH7-treated sand at an effective confining pressure of 100 kPa. EICP treatment has increased the cyclic resistance to approximately 2 to 5 times by suppressing the excess pore water pressure ratio.

doi:10.6342/NTU202404421

The liquefaction resistance curves show a significant enhancement for one cycle of EICP treatment.

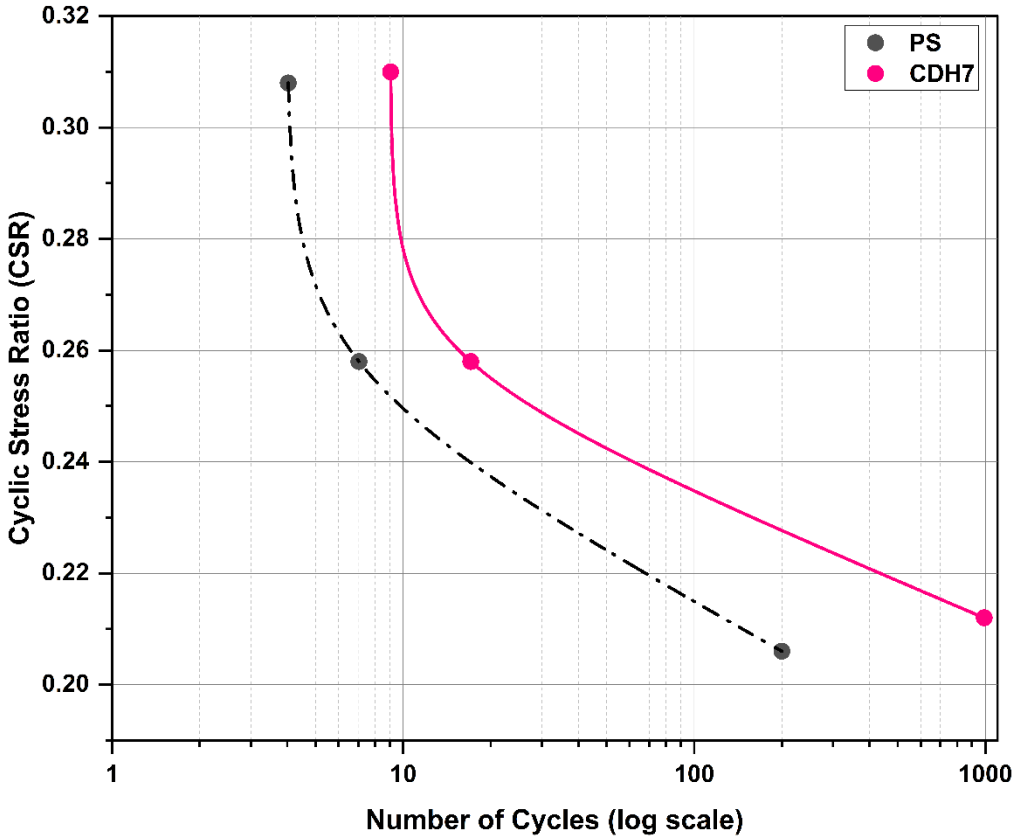

Figure 63: Liquefaction resistance curves for pure sand and treated sand at an effective confining pressure of 100 kPa

The liquefaction resistance of EICP-treated soil is significantly affected by confining pressure conditions. At low confining pressures, the EICP-treated sand exhibits high liquefaction resistance, but this resistance decreases as confining pressure increases (Simatupang and Okamura 2017). Under low confining pressure, the treated soil tends to dilate and behave in a brittle manner. Conversely, at higher confining pressures, the soil

doi:10.6342/NTU202404421

contracts and exhibits ductile failure behavior, likely due to particle breakage and the degradation of calcium carbonate ($CaCO_3$) precipitation. Implementing multiple cycles of EICP treatment could further enhance the liquefaction resistance, as increased $CaCO_3$ precipitation would better resist the effects of confining pressure under cyclic stress conditions, improving the soil's overall stability.

4.5.2 Cyclic Triaxial Testing and Discussion with Sigma-Treated Specimen

The undrained cyclic triaxial tests were conducted in both pure sand and Sigma-treated specimens to examine the effectiveness of the EICP treatment against soil liquefaction. The axial strain (ε_a), excess water pore pressure ratio (r_u), and the number of cycles (N_L) corresponding to the cyclic stress ratio for pure sand and EICP-treated sand of 7-day curing are listed in Table 6.

Table 7: Test Scheme in Cyclic Triaxial (Sigma-Treated Specimen)

Tests	EICP Recipe	Curing Days	CSR	Axial Strain (%)	Number of Cycles (N_L)
Pure Sand	N/A	N/A	0.258 0.308	-0.70 -1.48	7.05 4.03
Sigma	1 M Urea 0.67 M $CaCl_2.2H_2O$ 3 g/l Urease	7 days	0.258 0.31	-0.57 -1.48	17.07 9.05

doi:10.6342/NTU202404421

4.5.2.1 Deformation Response

Bio-cementation via EICP controls the deformation response in the Sigma-treated specimen by facilitating the deposition of calcium carbonation precipitation at the particle-to-particle contact and on the surface of the sand grains. The deformation response of the pure sand and Sigma-treated specimen includes both compression and dilation strains. Figures 64a and 64b shows the axial strain versus the number of cycles in the pure sand and Sigma-treated specimen can be classified into three stages: a) Stage 1 – Compaction, b) Stage 2 – Shearing, c) Stage 3 – Failure. In the initial stage of cyclic loading, smaller axial strains were achieved due to the compaction effect from the vibration or loading. This is followed by the shearing stages, where the axial strain increases significantly, and also, the cyclic strength of the specimen dominates the cyclic loading with the increasing number of cycles to liquefaction. Finally, at the failure stage, cyclic loading intensifies the cyclic strength of the specimen. As liquefaction occurs, the axial strain reaches higher levels with an increasing number of cycles. A similar trend is observed in all other tests and also aligns with previous findings (Rui *et al.* 2022). Sigma-treated specimen exhibited lesser compression strains compared to the compression strain achieved by the pure sand while sustaining cyclic loading for a larger number of cycles. The reduction in compression strains in the Sigma-treated specimen indicates the accumulation of dilation hardening signifying a reduction of pore spaces due to calcium carbonate precipitation. This research finding is also consistent with previous studies (Xiao *et al.* 2018b).

4.5.2.2 Pore Pressure Development

Figure 64c and 64d illustrates the relationship between the number of cycles and r_u for both pure sand and Sigma-treated specimen. The assessment and monitoring of the pore

doi:10.6342/NTU202404421

pressure accumulation within the treated specimen provide insights into the mechanical response during EICP treatment. As the specimen approaches liquefaction, a distinct notch becomes apparent, signifying the cyclic behavior of the specimen under cyclic loading conditions. The area enclosed by this notch between two peaks serves as an indicator of the cyclic activity of the specimen. Notably, as the axial strain increases, so does the area of the notch, indicating a corresponding increase in cyclic activity with a higher number of cycles. This finding is consistent with prior research (Rui *et al.* 2022; Yong 2009). A notable trend emerges in the slower accumulation of pore pressure leading up to the liquefaction stage, followed by a rapid increase in pore pressure after liquefaction occurs. The number of cycles required for liquefaction increases with the rise in calcium carbonate precipitation. The deposition of calcium carbonate within the treated specimen effectively interlocks the pore spaces, hindering the dissipation of pore pressure and leading to a more significant number of cycles required for liquefaction. The EICP treatment using sigma urease has improved the cyclic resistance to liquefaction by 3 times (approximately) by suppressing the excess pore water pressure buildup in the treated soil.

doi:10.6342/NTU202404421

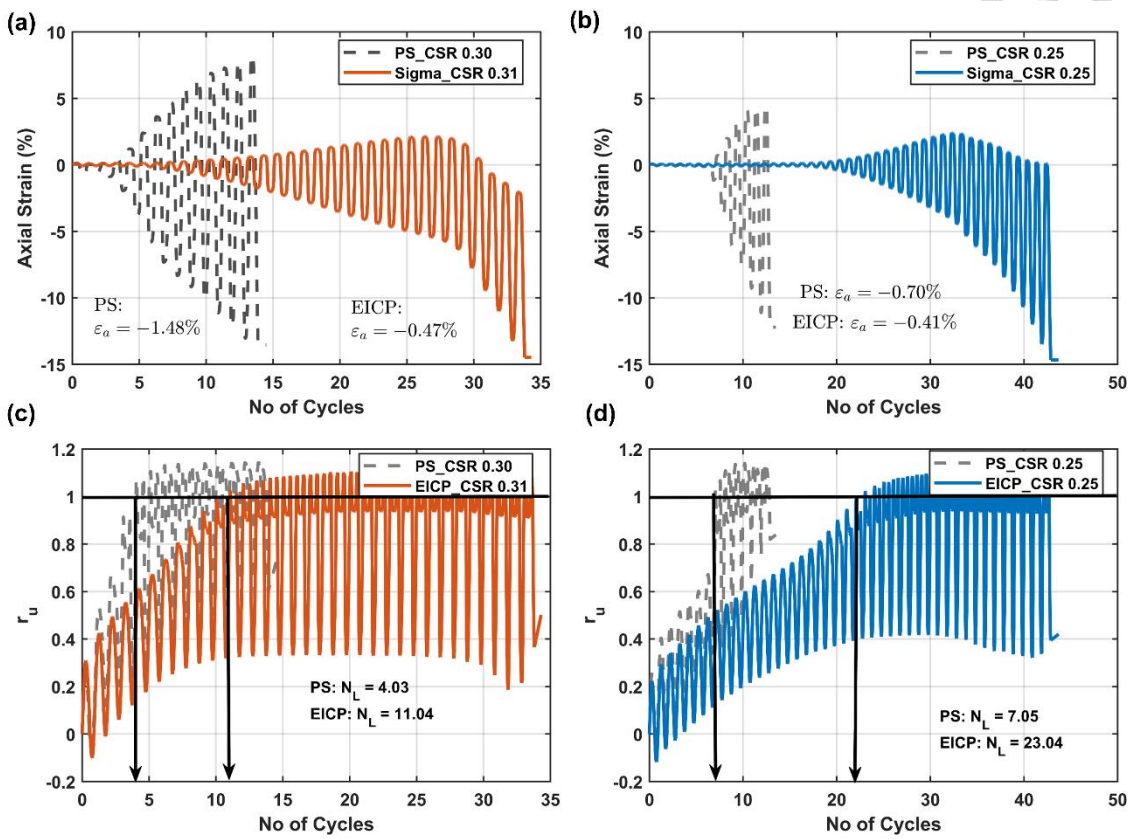

Figure 64: (a and b) Strain development at pure sand and Sigma-treated specimen in CSR 0.3 and 0.25 (c and d) Pore pressure development at pure sand and Sigma-treated specimen in CSR 0.3 and 0.25

The eccentric pore pressure response curve observed in both CDH-treated soil and Sigma-treated soil can be attributed to the calcium carbonate precipitation that occurs during the treatment. The calcium carbonate precipitation enhances the shear strength and resistance to liquefaction in the treated soil. However, when the interlocking between soil particles and the precipitated material is unable to withstand cyclic loading, particle bonds break, leading to concentrated forces in specific areas. This causes the formation of localized shear bands, and the biocemented sand exhibits greater volumetric dilation compared to untreated sand (Jiang *et al.* 2011). Additionally, the size of sand particles

doi:10.6342/NTU202404421

coated with calcium carbonate, or the aggregation of these particles, becomes larger than that of untreated sand, contributing to increased dilation in the treated soil (Wu *et al.* 2021a). Similar observations can be found in the following research paper. Gao *et al.* (2019b) performed undrained triaxial tests on EICP-treated soil showed higher dilation and peak deviatoric stress compared to untreated soil. Furthermore, increasing the number of treatment cycles led to greater $CaCO_3$ content in the soil. After 15 treatment cycles, excess pore pressure was higher than in samples with only 5 to 10 cycles, likely due to the non-uniform distribution of $CaCO_3$, particularly lower concentrations at the bottom of the specimen. Another hypothesis mentioned by Ahenkorah *et al.* (2021a), the generation of excess pore water pressure is influenced by the void ratio (e_0) of the sample after consolidation. At low consolidation pressures, highly cemented soil samples exhibited smaller void ratios than lightly cemented samples. However, the more highly cemented samples experienced a significant increase in pore water pressure, indicating that the level of cementation impacts the soil's response to cyclic loading and pore pressure generation.

4.5.2.3 Cyclic Stress-Strain Development

Figure 65a and 65b depicts the hysteresis loop of deviatoric stress versus axial strain for pure sand and Sigma-treated specimens. As mentioned by (Han *et al.* 2020; Wei-zhong 2005), during cyclic loading, a portion of the work done by the cyclic load on the specimen is consumed by elastic deformation and stored as elastic deformation energy, while the other part of the work is dissipated in the form of energy. During unloading or reversing the cyclic loading, the elastic deformation is restored, but the other part of the work is done by the rearrangement of the soil structure, which leads to the accumulation of axial strain. The non-

doi:10.6342/NTU202404421

coincidence of the loading and unloading paths in the cyclic loading of the specimen gives rise to the formation of a hysteresis loop. Therefore, the area enclosed by the hysteresis loop in both pure sand and Sigma-treated sand serves as a measure of the energy dissipated by the specimen during one loading cycle. Notably, the Sigma-treated specimen exhibits a larger hysteresis loop, attributed to the bio-cementation effect, which becomes more pronounced with increasing cycles.

4.5.2.4 Cyclic Deformation Characteristics

Figure 65c and 65d illustrates the deviatoric stress and the effective stress path for pure sand and Sigma-treated specimens. A noticeable trend emerges as the effective stress path moves from right to left, primarily driven by the reduction in the mean effective stress as pore water pressure increases during the cyclic loading. When the mean effective stress eventually reaches a non-zero state and intersects with the effective failure envelope, it signifies the onset of liquefaction. At this point, the specimen loses all its stiffness, rendering it unable to sustain any further deviatoric stress. Comparatively, the Sigma-treated specimen exhibited more cycles required for liquefaction compared to pure sand. This indicates that the EICP-treated specimen offers greater cyclic shear resistance due to the influence of calcium carbonate precipitation from particle-to-particle contact and particle-to-calcite precipitation.

doi:10.6342/NTU202404421

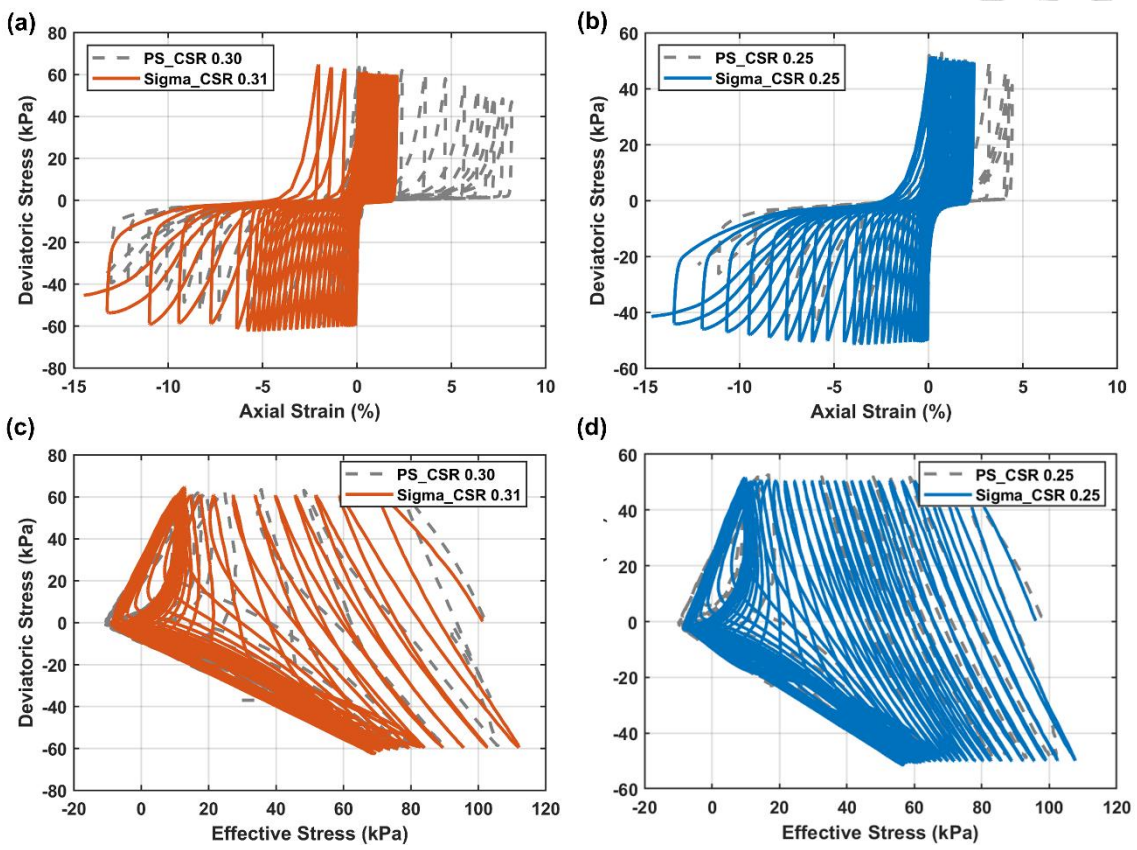

Figure 65: (a and c) Stress-Strain development at pure sand and Sigma-treated specimen in CSR 0.3 and 0.25 (b and d) Cyclic Deformation characteristics at pure sand and Sigma-treated specimen in CSR 0.3 and 0.25

4.6 Microscopic Examination

4.6.1 Field Emission – Scanning Electron Microscopy (FE-SEM) analysis

Field Emission Scanning Electron Microscopy (FE-SEM) images were taken for both pure sand and EICP-treated specimens using an accelerating voltage of 10 kV and a working distance of 15 mm. The calcium carbonate distribution in the EICP-treated specimen varied depending on the type of sand used. In silica sand, the calcium carbonate was sparsely distributed, with some areas of the sand grains remaining uncemented, consistent with the findings of (Cui *et al.* 2021b). Cui *et al.* (2021b) investigated the distribution of nucleation

doi:10.6342/NTU202404421

sites in both calcareous sand and silica sand and its impact on the growth pattern of calcium carbonate precipitation. Silica sand has a characteristic of preferential deposition pattern for the growth of the calcium carbonate formation in distinct preferential location.

The EICP treatment showed two distinct cementation effects: (a) calcium carbonate precipitation at particle-to-particle contacts, and (b) precipitation at particle-to-calcite interfaces. Both forms of precipitation contributed to improving the soil's shear strength. A higher $CaCO_3$ content does not always result in increased soil strength and stiffness (Cheng *et al.* 2013; Cheng *et al.* 2017; Whiffin *et al.* 2007). The calcium carbonate precipitate can either bond soil particles together or form on the surface of particles, enhancing their roughness. This occurs either through bridging crystals that connect adjacent soil grains at their contact points or surface crystals that increase particle roughness. While both mechanisms improve soil strength, the interparticle bonding is expected to produce a much greater effect on the treated soil (Cheng *et al.* 2013; Cheng *et al.* 2017).

4.6.1.1 Particle-to-Particle Contact Precipitation

FE-SEM images of pure sand reveal a mixture of sub-angular and sub-rounded grains, with textures that vary between smooth surfaces and rough patches. The sand grains also display distinct cleavage patterns. In Figure 66a, the sand particles are clearly separated, with visible pore spaces and no foreign materials attached to the grain surfaces. However, with EICP treatment, calcium carbonate precipitation improves the bonding between sand particles. Figures 66(b-d) illustrate this effect, showing particle contacts formed through calcium carbonate precipitation. This bonding reduces the void ratio and enhances the shear strength of the soil. The calcium carbonate bridges between particles provide cohesion, contributing to increased shear resistance. Despite this, the images indicate that not all

doi:10.6342/NTU202404421

particle contacts were fully cemented after a single EICP treatment cycle. Higher calcium carbonate content could improve interparticle contact more effectively, leading to further increases in sand shear strength.

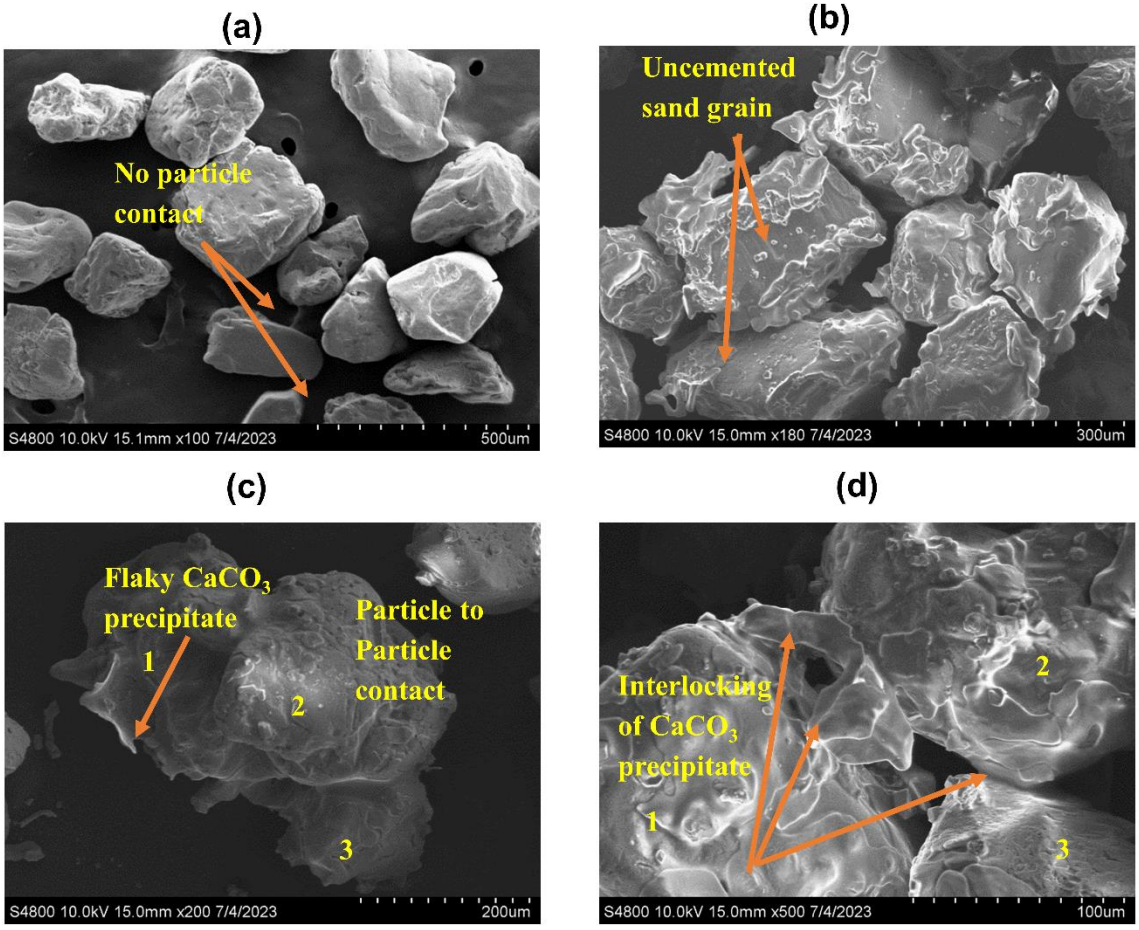

Figure 66: Particle to Particle Contact Precipitation (a) pure sand (b-d) Sigma-treated

Similar to Sigma treated sample, the CDH-treated sample at 7 days of curing showed the precipitation at the particle contact of the soil grains with no precipitation on the surface of the soil grain in the Figure 67. The transition from a porous (pure sand) state to a solid state (EICP-treated).

doi:10.6342/NTU202404421

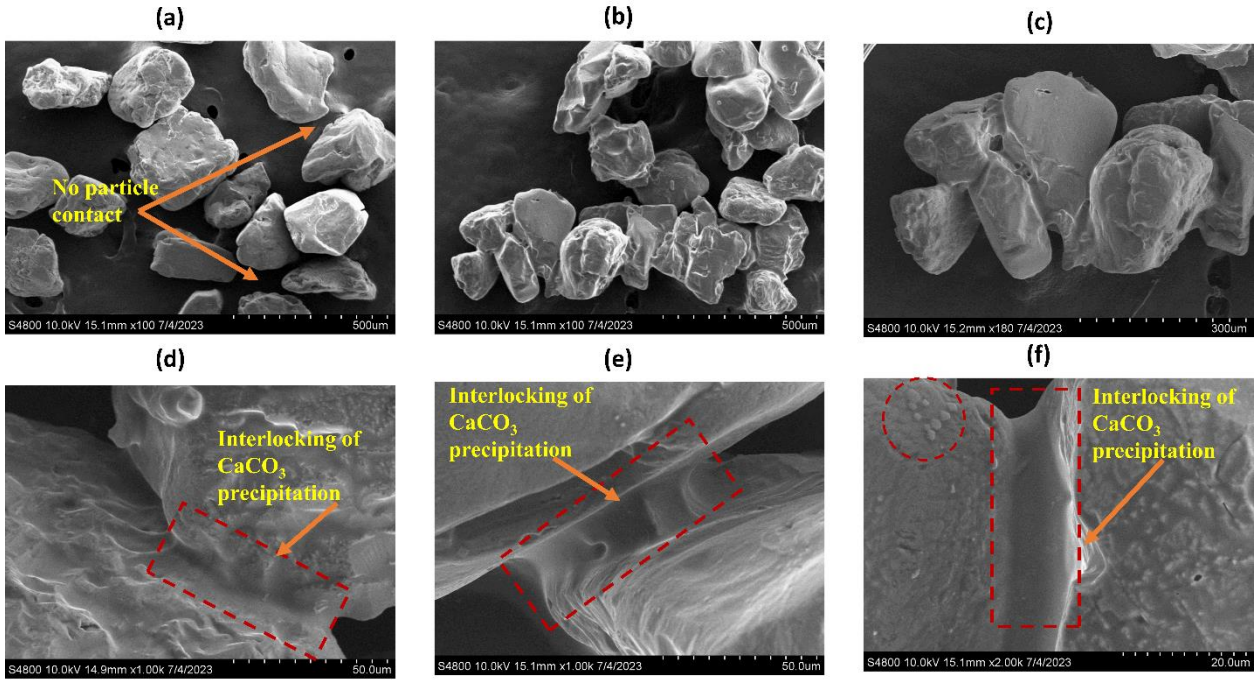

Figure 67: Particle to Particle Contact Precipitation (a) pure sand (b-f) CDH-treated

4.6.1.2 Particle-to-Calcite Precipitation

The pure sand lacks the cementation effects seen in the EICP-treated samples, such as the Sigma-treated and CDH-treated specimens, as depicted in Figures 68 and 69. In the Sigma-treated specimen, flaky calcium carbonate precipitation is visible on the sand grain surfaces. This precipitation tends to adhere to the sand particles, forming a layered deposit without direct particle contact, as shown in Figures 68(c-d), compared to the pure sand in Figures 68(a-b). These successive layers of calcium carbonate increase the roughness of the sand grains, enhancing the texture.

This increase in roughness, caused by the calcium carbonate precipitating on the surface of the sand grains, improves the mechanical behavior of the soil. Additional treatment cycles could further amplify this roughness, leading to a larger friction angle, which increases the

doi:10.6342/NTU202404421

resistance of the specimen during shearing or under cyclic loading. This enhanced surface friction strengthens the overall structure of the treated soil.

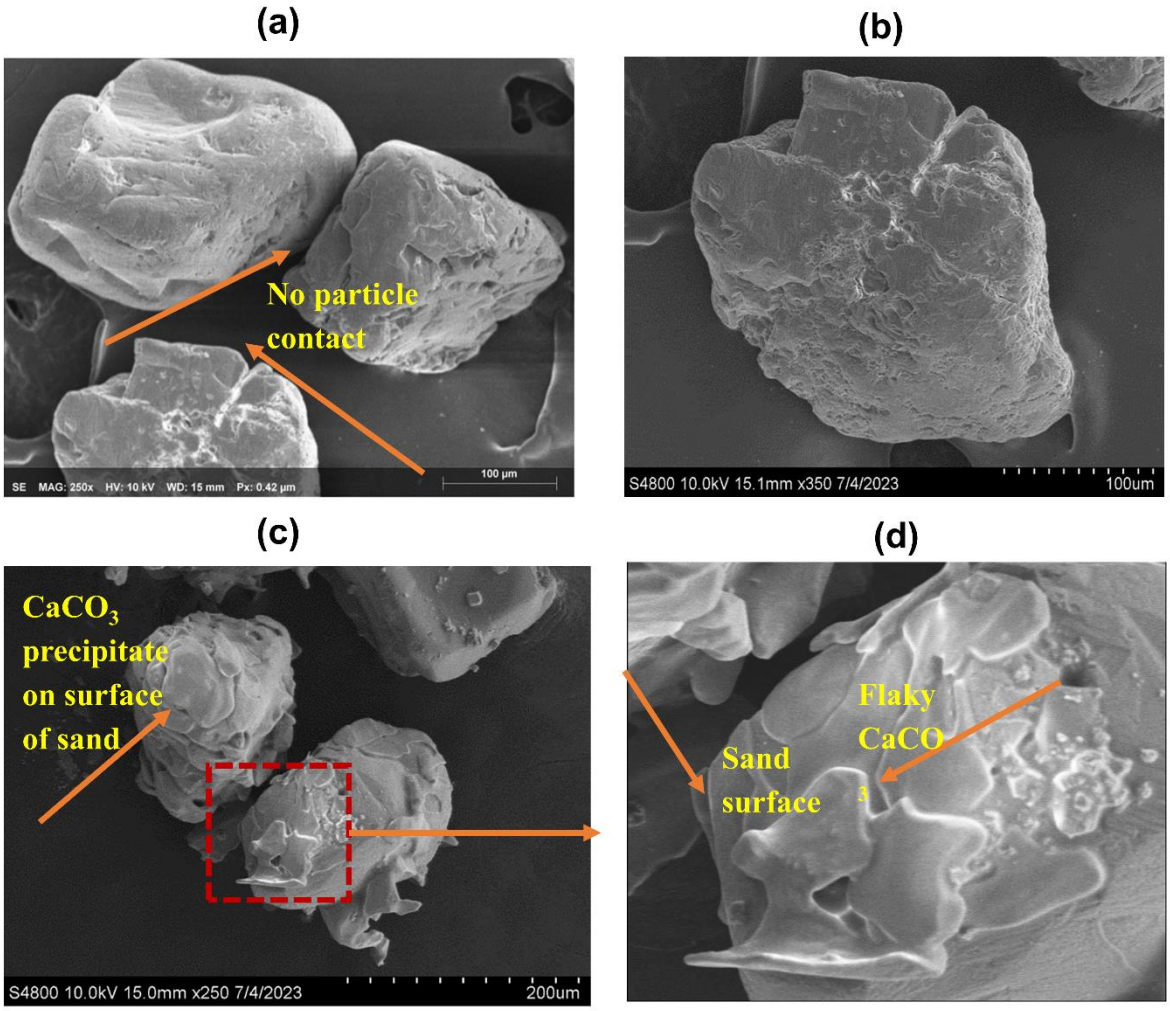

Figure 68: Particle to Calcite Precipitation (a-b) Pure sand (c-d) Sigma-treated samples

Similar to Sigma-treated samples, the CDH-treated sample at 14 days of curing showed particle to calcite precipitation on the surface and bridging of the soil grains. The size of the soil grain varied randomly all over the soil grains. EICP treatment influenced the material's roughness and binding, which influences the shear parameters and liquefaction resistance in the treated specimen.

doi:10.6342/NTU202404421

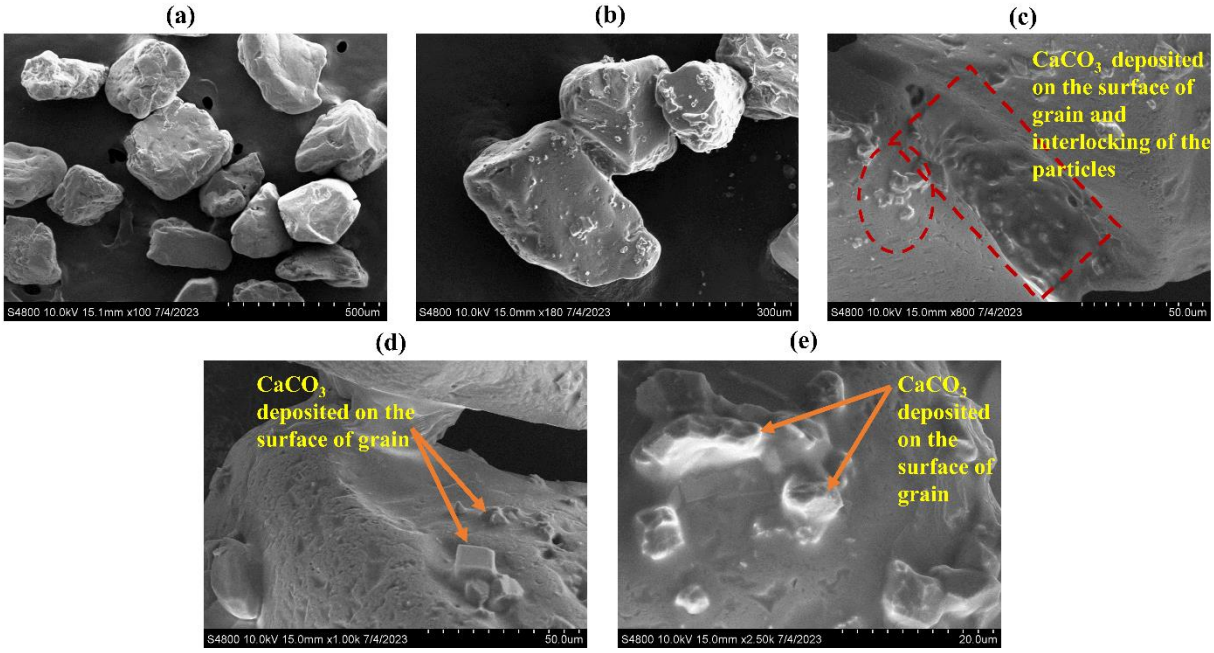

Figure 69: Particle to Calcite Precipitation (a-b) Pure sand (c-d) CDH-treated samples

4.6.1.3 Calcium Carbonate precipitate from Sigma Urease

The calcium carbonate precipitate obtained from the falcon tube test after 7 days of treatment was filtered and oven-dried at 110°C. A small portion of this precipitate was subjected to microscopic examination to analyze its shape and structure. The FE-SEM analysis and corresponding EDS elemental mapping of calcium minerals (represented as red dots) are shown in Figure 70c. The cementation solution used in this study was a mixture of calcium chloride and urea, with high concentrations (1M urea and 0.67M $CaCl_2$) were adopted in the study.

Al Qabany *et al.* (2012) and Qabany *et al.* (2013) reported that a lower cementation concentration of 0.25 M leads to a smaller-sized calcium carbonate crystal evenly distributed throughout the specimen. In field applications of EICP treatment, higher concentrations are often preferred to reduce treatment time and cycles, though achieving uniform calcium carbonate distribution remains a challenge.

doi:10.6342/NTU202404421

The size of calcium carbonate crystals formed during EICP treatment is influenced by the urease enzyme, which is about 12 nm in size and acts as a nucleation site. This leads to the formation of smaller crystals compared to those formed via MICP, resulting in more contact points between soil particles. Figure 70 illustrates agglomerated euhedral calcite crystals, where higher urease activity promotes their formation (Ahenkorah *et al.* 2021c). In some instances, rhombohedral-shaped calcite can be observed at lower magnification in Figure 70a.

The urease enzyme's size is approximately 12 nm, and when it acts as a nucleation site, the formed crystal is comparably more petite than the calcium carbonate crystal formed through MICP. This smaller crystal size in EICP offers an advantage as it creates more contact points compared to MICP treatment with similar carbonate content. Qabany and Soga (2013) reported that the crystal size at 1M cementation concentration was 35 µm.

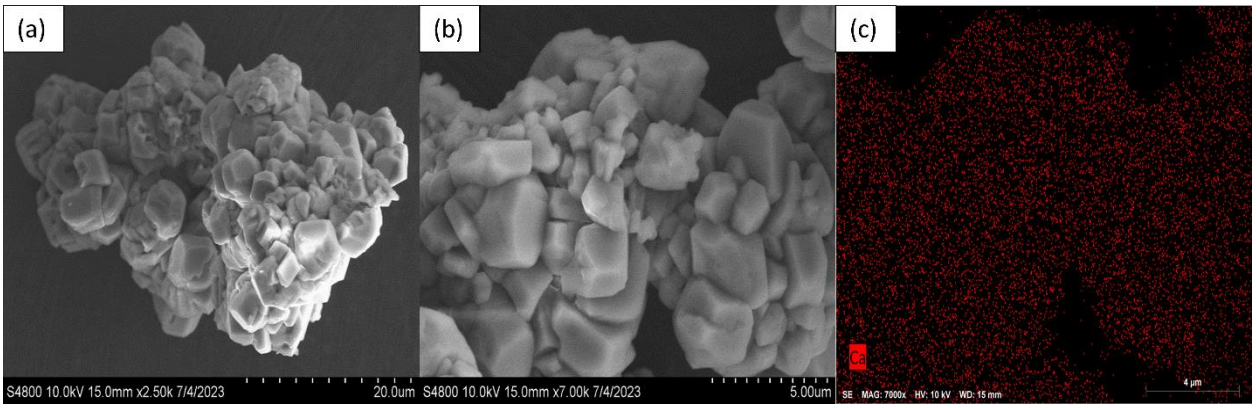

Figure 70: Microscopic analysis of Calcium Carbonate precipitate. (a and b) FE-SEM (c) EDS - Elemental mapping

4.6.1.4 Size of calcium carbonate crystal from Sigma Urease

The size of the calcium carbonate was measured using Image J software. In Figure 71a, 18 crystals were highlighted, while other crystals posed challenges due to the overlapping

doi:10.6342/NTU202404421

bedding patterns, making proper shape discernment difficult. In Figure 71b, the yellow dashed line box encompasses crystals 1 to 6, the violet solid line indicates crystals 7 to 12, and the brown dash double dotted lines enclose crystals 13 to 18. The size length is calculated in all highlighted crystals and depicted in a histogram plot. Figure 72 displays a substantial number of crystals with particle sizes ranging from 1.5 to 2 μm, while the second largest crystal size is observed between 3.5 to 4 μm. The precipitate exhibits a smooth texture without any discernible cleavage planes on the crystals.

doi:10.6342/NTU202404421

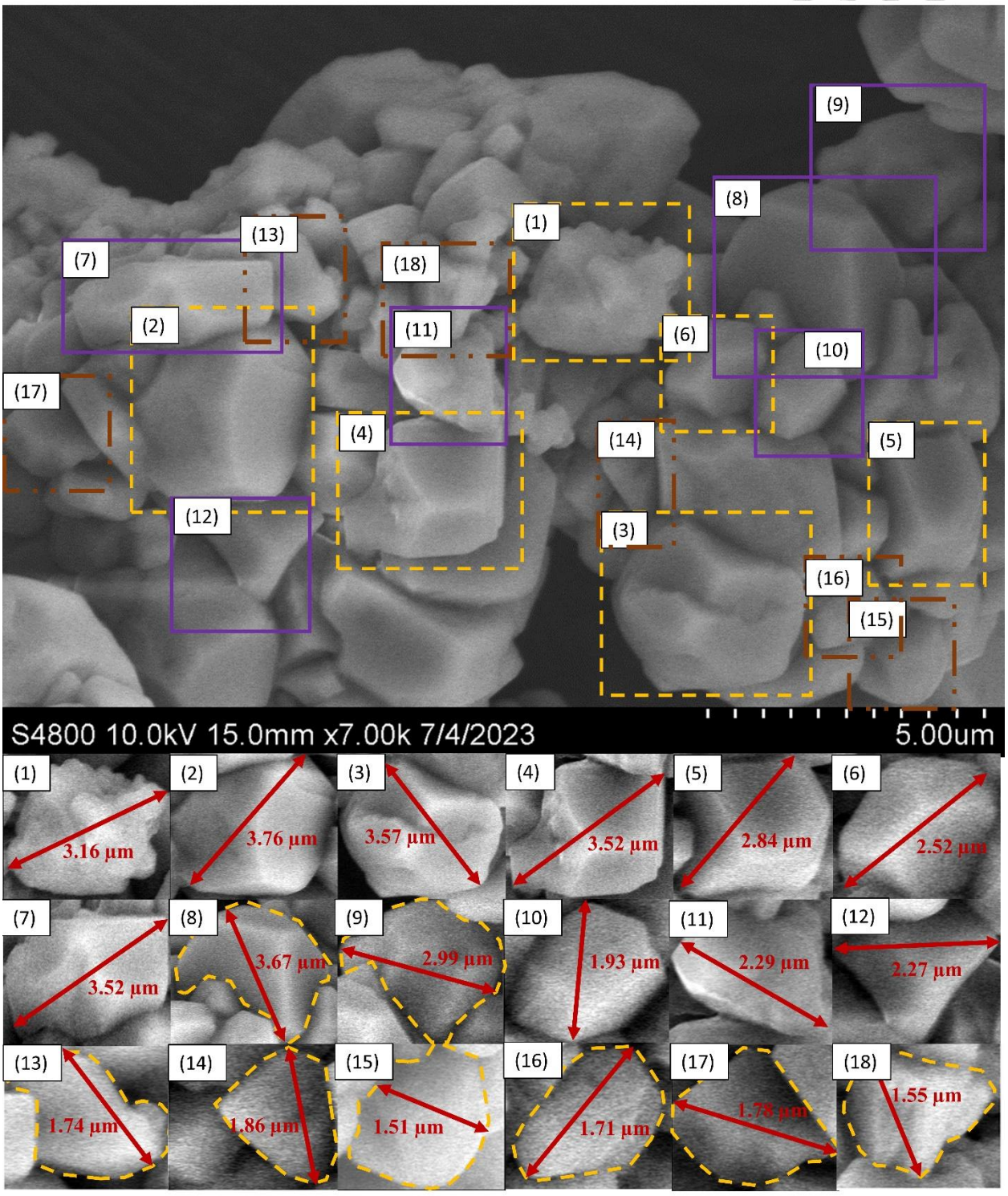

Figure 71: (a) FE-SEM image of Calcium carbonate precipitate (b) 18 selected crystals

doi:10.6342/NTU202404421

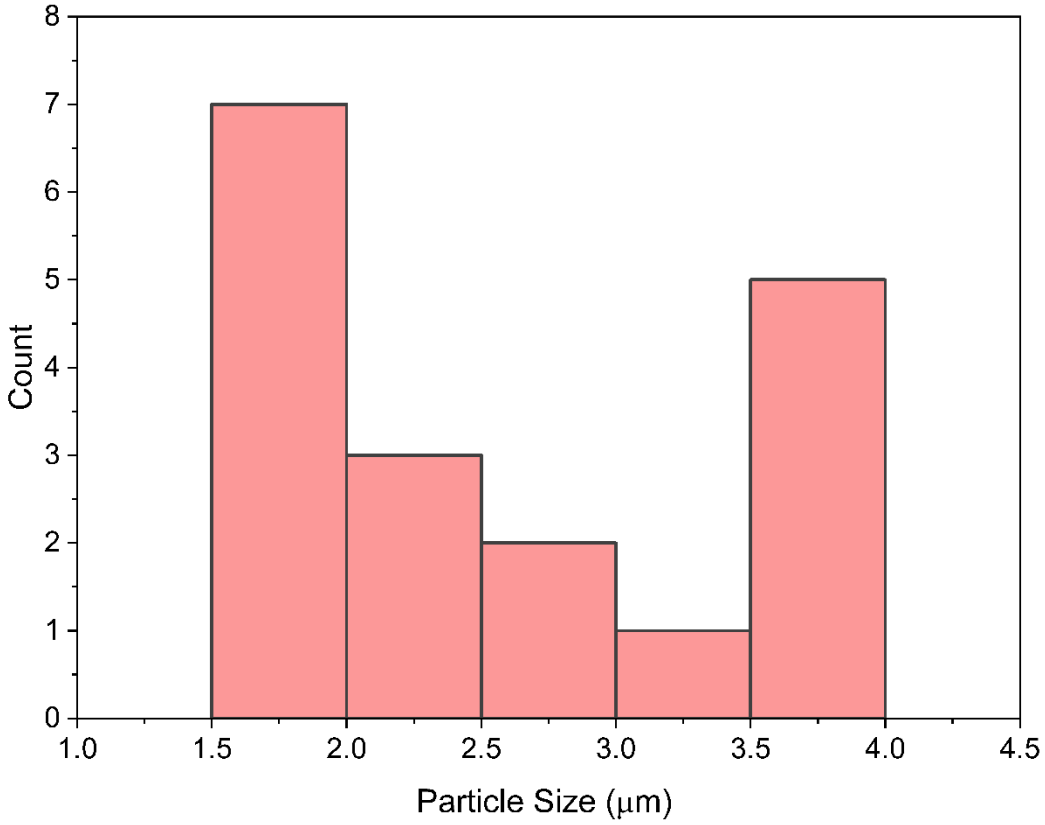

Figure 72: Histogram plot of the calcium carbonate crystal highlighted in figure 71a

4.6.1.5 3D imaging of Calcium Carbonate Precipitate

The 2-D FE-SEM image of the precipitate can be extended in 3-D imaging using Image J software. Figures 73 and 74 show the 3-D view of the precipitation with 7k and 2.5k magnification, respectively. As the precipitate crystals seemed to be entwined with each other and the crystals vary in different shapes, the height of the peak depicts the length of the crystal extended in the 3rd dimension.

doi:10.6342/NTU202404421

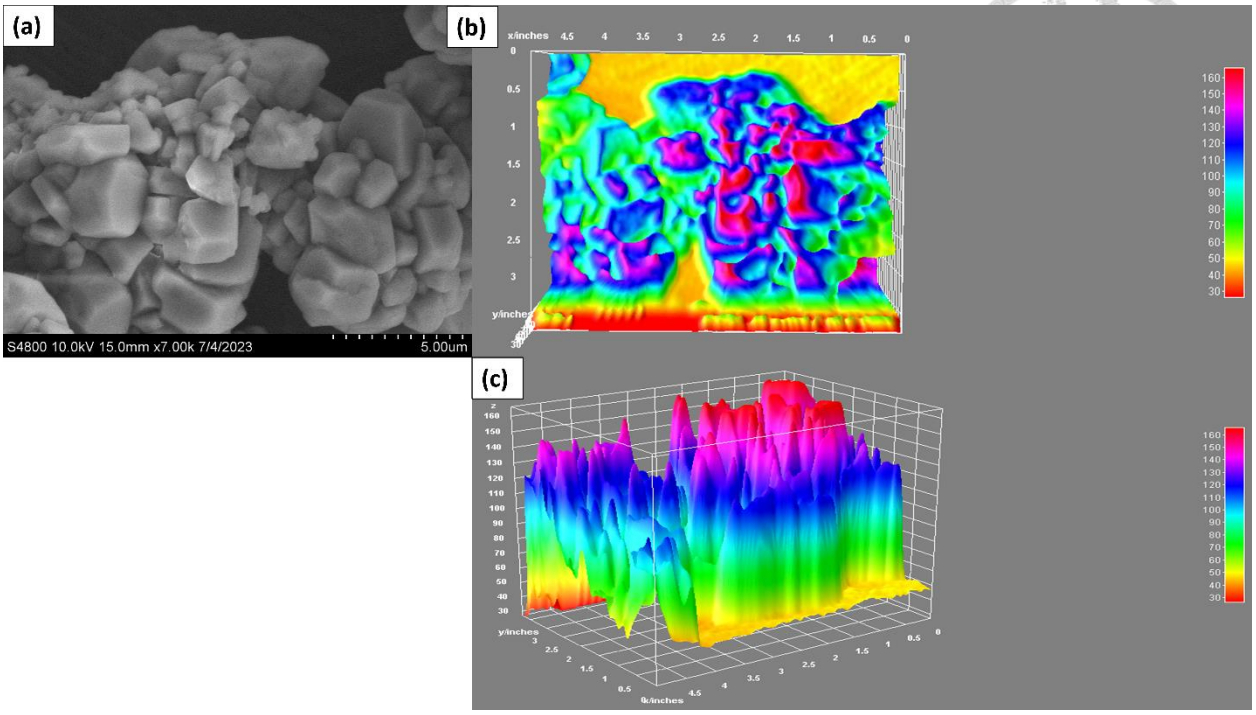

Figure 73: 3D imaging of $CaCO_3$ precipitate (7.5k magnification)

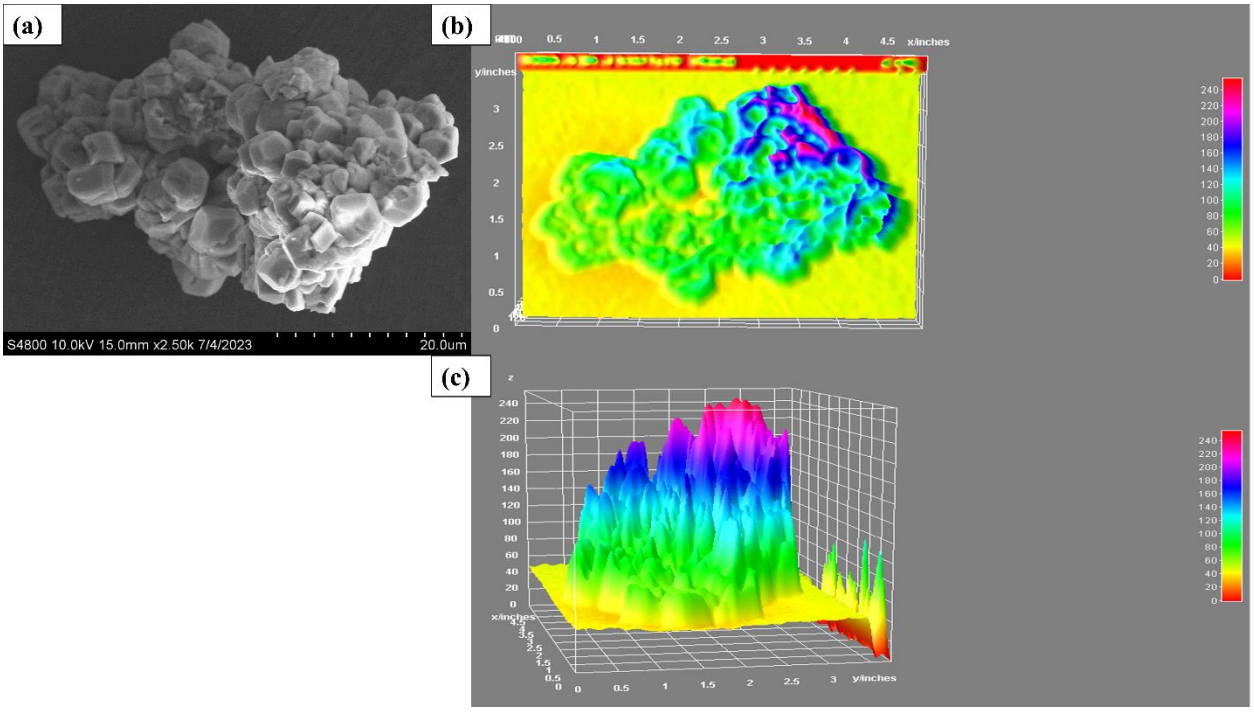

Figure 74: 3D imaging of $CaCO_3$ precipitate (2.5k magnification)

doi:10.6342/NTU202404421

4.6.1.6 Texture of Pure Sand

FE-SEM images of the pure sand exhibited a mixture of sub-angular and sub-rounded shapes coupled with varying textures, which were smooth in some areas and rough patches in others, which can be seen in Figure 75. Additionally, the sand grains display cleavage patterns. The texture and the structure of the soil grains significantly influence the improvement in the engineering properties and liquefaction resistance.

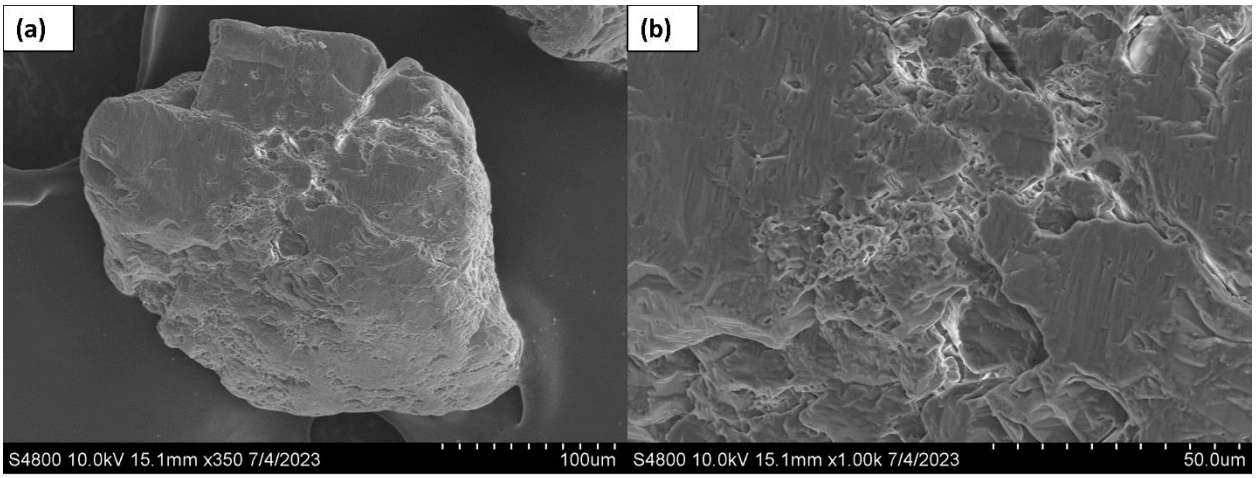

Figure 75: Texture of Pure Sand

4.6.2 Energy Dispersive Spectroscopy (EDS) Examination

4.6.2.1 Pure Sand

The primary mineral found in the pure sand was SiO_2. The spatial distribution of the Silica (Si) mineral was detected with green spots, as shown in Figure 76a. The intensity level of the Si mineral spiked in the pure sand, as shown in Figure 76b. Also, the pure sand (untreated) shows nil cementation with $CaCO_3$ precipitation.

doi:10.6342/NTU202404421

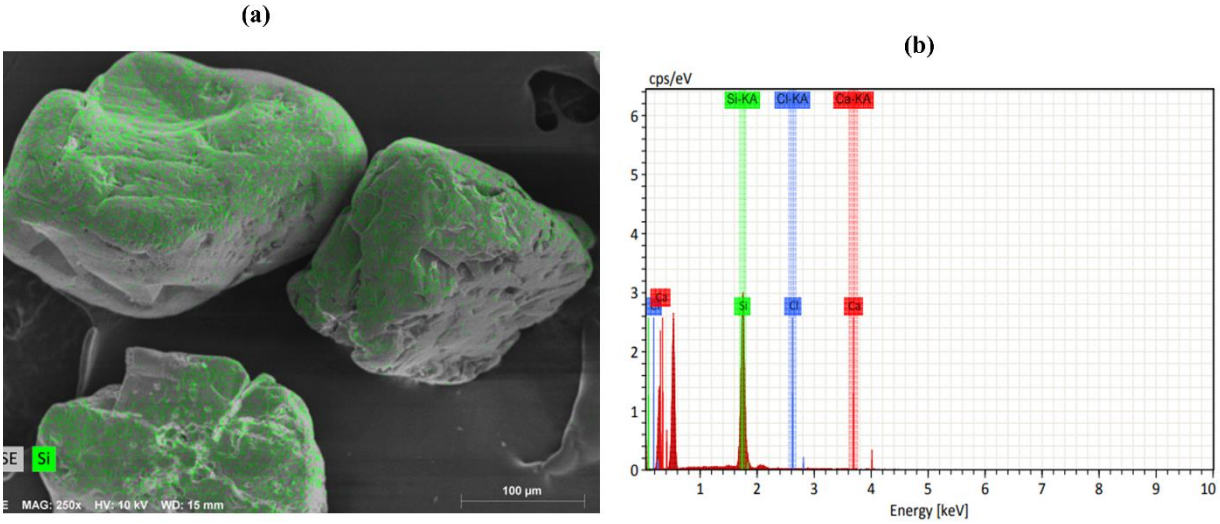

Figure 76: EDS mapping in Pure Sand

4.6.2.2 CDH-Treated Specimen at 7 days of curing

Figure 77 shows the CDH-treated specimen after 7 days of curing, illustrating the effect of EICP treatment at this stage. The treatment led to an increase in particle-to-particle contacts through calcium carbonate cementation. Calcium carbonate precipitation formed bridges between some inter-particle contacts, while leaving other parts of the sand particles uncoated. This uneven distribution could be due to the higher concentration of urea-calcium chloride, resulting in a more random deposition of calcium carbonate within the CDH-treated sand. In contrast, a lower concentration of urea-calcium chloride solution (0.25 mol/L) has been shown to produce similarly sized calcium carbonate crystals but with a more uniform spatial distribution (Al Qabany *et al.* 2012).

doi:10.6342/NTU202404421

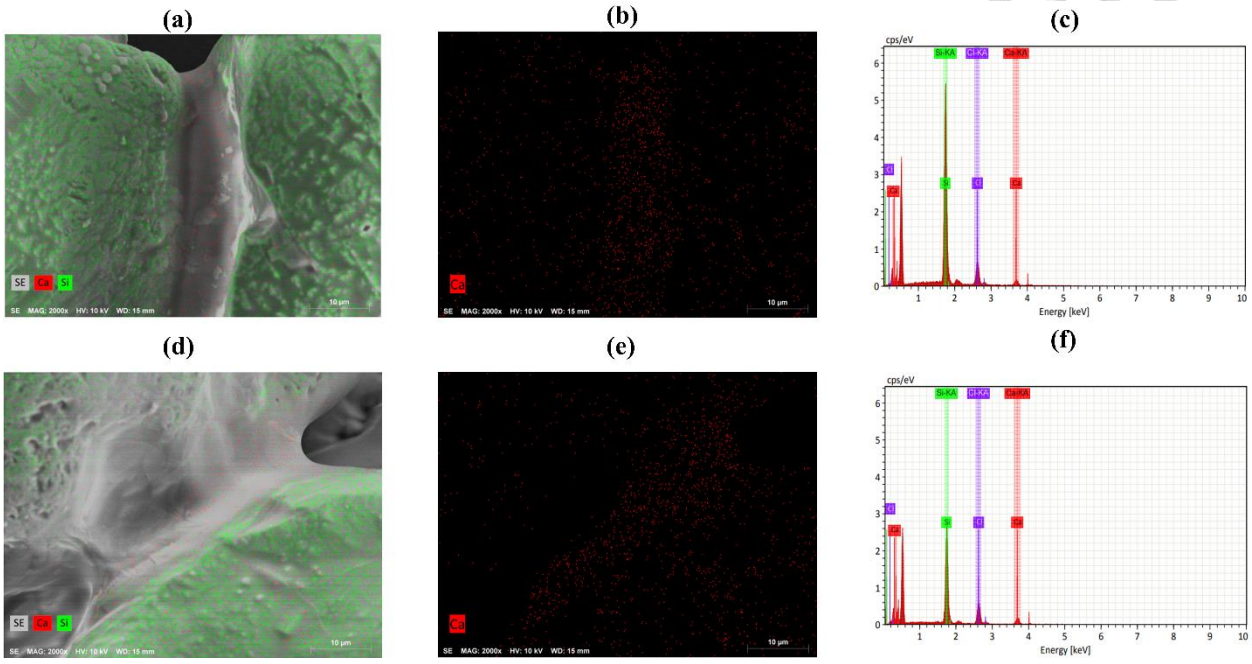

Figure 77: EDS mapping of CDH-treated samples (a-f) 7 days of curing

4.6.2.3 CDH-Treated Specimen at 14 days of curing

Figure 78 presents the CDH-treated specimen at 14 days of curing, where bio-cementation via EICP is seen to precipitate calcium carbonate both at the particle contacts and across the surface of the sand grains. This consistent deposition pattern aligns with observations by DeJong *et al.* (2010). In the elemental mapping, red and green dots represent calcium and silica minerals, respectively, providing valuable insights into the distribution of calcium carbonate within the treated sand.

At 14 days of curing, SEM images marked with red circles show both rhombohedral and anhedral crystal shapes in the CDH-treated soil, with the calcium carbonate distribution confirmed by EDS elemental mapping. Anhedral crystals were produced by low urease enzyme activity, while rhombohedral crystals resulted from higher urease activity

doi:10.6342/NTU202404421

(Ahenkorah *et al*. 2021d; Tirkolaei *et al*. 2020). This variation in crystal shape may be attributed to differences in enzyme purity and activity levels.

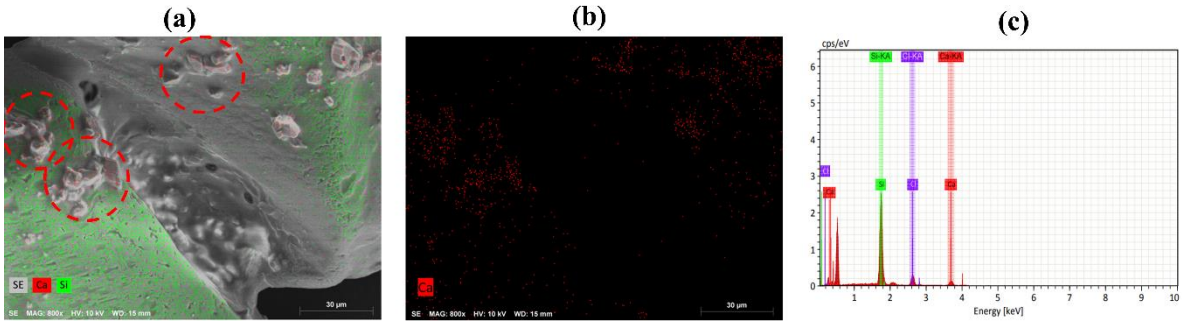

Figure 78: EDS mapping of CDH-treated samples (a-c) 14 days of curing

4.6.2.3 Sigma-Treated Specimen at 7 days of curing

The following Figure 79 shows the Sigma-treated specimen at 7 days of curing. The Sigma-treated sample revealed the presence of calcium carbonate precipitation at the bridging points of soil grains, where particle contacts occur, as well as on the surface of the sand grains, leading to an increase in surface roughness. The rise in cementation imparts stronger bonding, consequently enhancing the shear strength of the sand. Both red and green dots in the elemental mapping represent the calcium and silica minerals, respectively.

doi:10.6342/NTU202404421

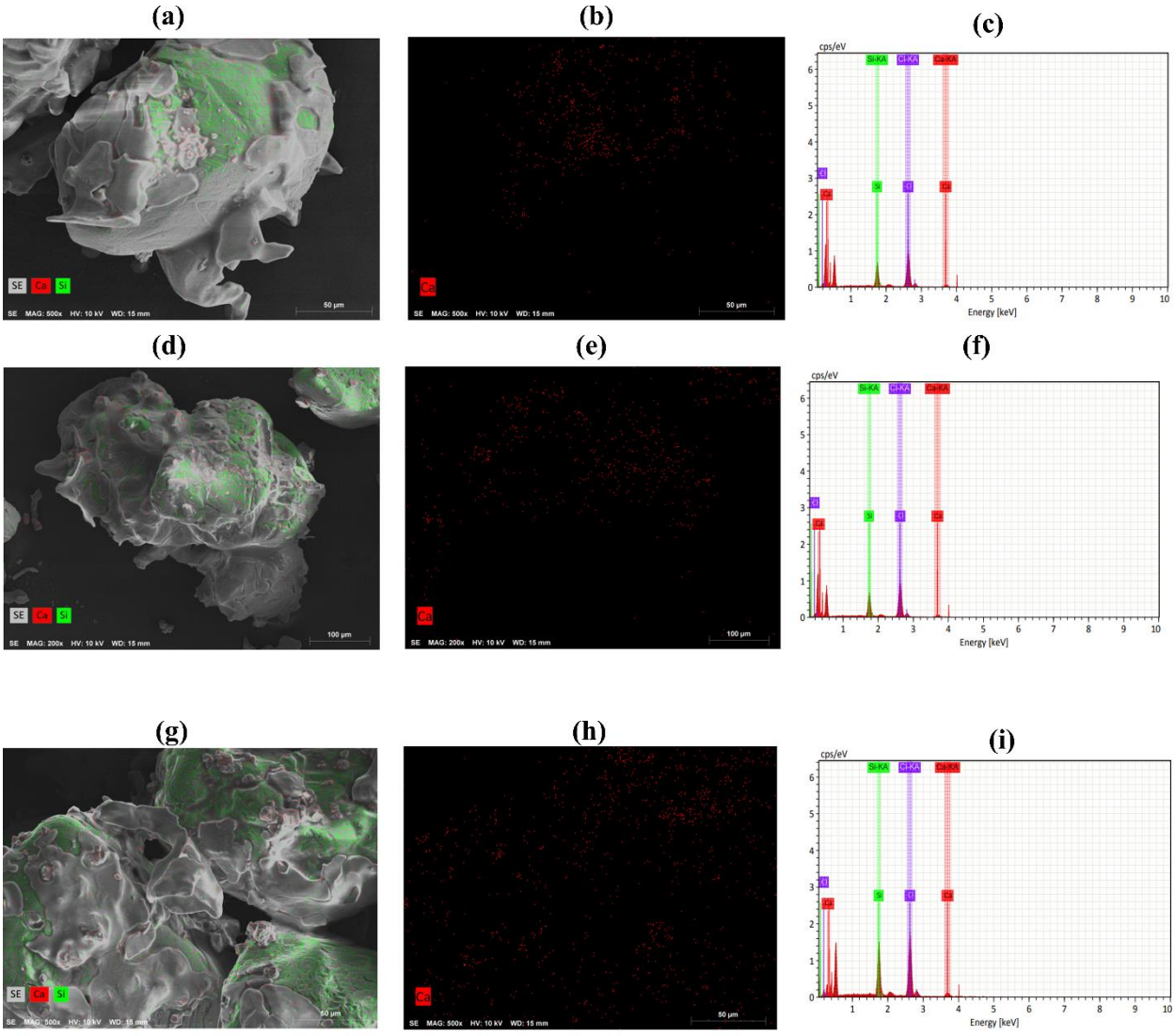

Figure 79: EDS mapping of Sigma-treated samples (a-i) 7 days of curing

4.6.3 X-ray Diffraction (XRD) analysis

4.6.3.1 CDH-Treated Specimen

XRD analysis is essential to identify the type of calcium carbonate crystals present in CDH-treated sand. Calcium carbonate exists in various crystalline polymorphs, including calcite, aragonite, and vaterite, with calcite being the most stable among them (Luo *et al.* 2022). Figure 80a-c illustrates the XRD patterns of pure sand and CDH-treated specimens at 7 and

doi:10.6342/NTU202404421

14 days of curing. The analysis confirms the formation of calcite crystals due to the EICP treatment.

Initially, calcite crystals form within the voids between soil grains and later deposit on the surface of the particles, increasing surface roughness. Small calcite peaks can be observed after 7 days of curing, while a more prominent calcite peak becomes visible after 14 days. In the pure sand, quartz is the dominant mineral, but after EICP treatment, calcite emerges as a new mineral, demonstrating the treatment's impact on the sand's mineral composition.

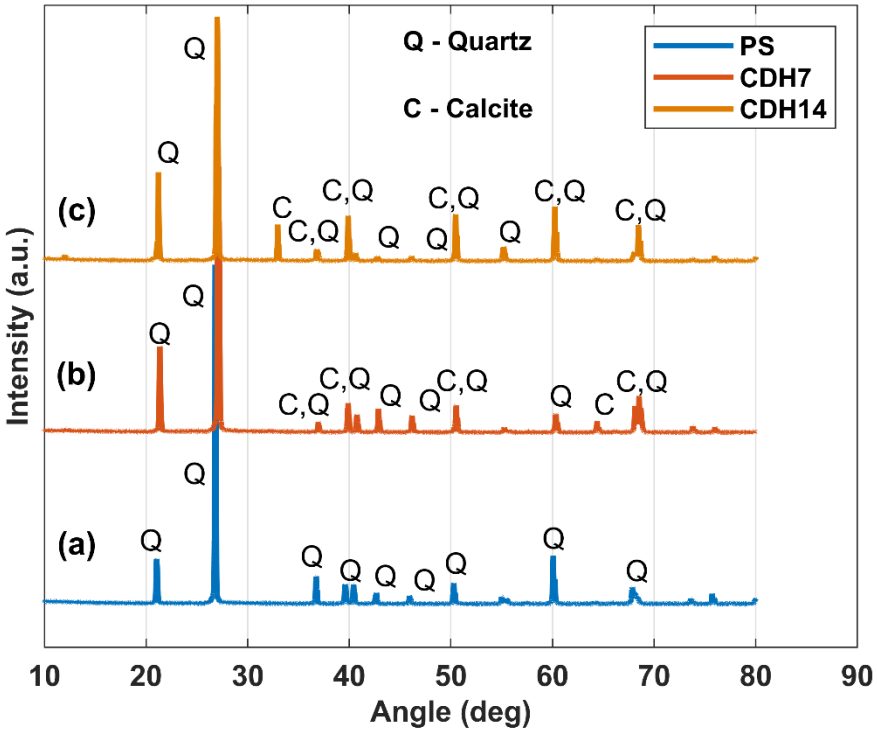

Figure 80: XRD results of (a) pure sand, (b) CDH-treated soil at 7 days of curing, (c) CDH-treated soil at 14 days of curing

doi:10.6342/NTU202404421

4.6.3.2 Sigma-Treated Specimen

Calcium carbonate crystals exist in five distinct crystal polymorphs: calcite, aragonite, vaterite, monohydracite, and ikaite. Among these, calcite is the most stable polymorph employed for ground improvement. According to Figure 81a, the XRD results of the calcium carbonate precipitate confirm the crystal type as calcite, as evidenced by the prominent diffraction angle of 29.79. Meanwhile, Figure 81b illustrates a significant quartz crystal peak at 26.79. EICP treatment using the urease enzyme resulted in the formation of calcite crystals in the calcium carbonate precipitate. Figure 81c depicts that few calcite peaks were observed in the Sigma-treated sand. The kind of crystal obtained from the research study aligns with previous research findings Wen *et al.* (2020). Their research delved into the impact of the initial concentration of urease and bacteria on precipitation kinetics and precipitation morphology. Microstructural analysis revealed that vaterite crystals formed from bacterial-induced treatment (MICP), while calcite crystals were produced from urease-induced treatment (EICP). This alignment with our study's results reinforces the consistency in identifying crystal polymorphs. Understanding these crystal characteristics is crucial for comprehending ground improvement methods' stability and potential performance.

doi:10.6342/NTU202404421

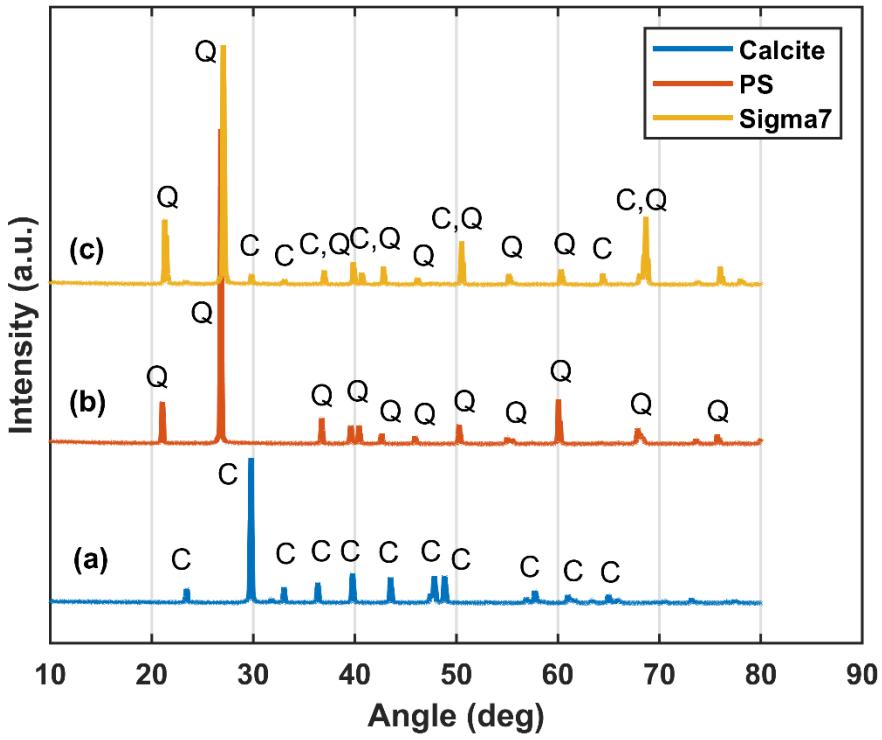

Figure 81: XRD results of (a) Calcite, (b) Pure Sand, (c) Sigma-treated soil at 7 days of curing

4.7 Acid Digestion for Triaxial Specimens

After performing the triaxial testing, the specimen was carefully removed. The specimen was divided into three samples: 'top,' 'middle,' and 'bottom'. Three samples were taken from each section and oven-dried. Similar to the previous acid digestion method, 10 grams of samples were taken from each specimen, and the same procedure was followed to calculate $CaCO_3$ remaining in the specimen. The results from acid digestion after performing the triaxial test give significant knowledge about the degradation of $CaCO_3$ and flushing off of $CaCO_3$. In both Figures 82 and 83, the CDH urease triaxial specimen and Sigma urease triaxial specimen showed the least $CaCO_3$ at the bottom of the specimen. Both types of saturation were done in the triaxial specimen, like manual saturation and back pressure

doi:10.6342/NTU202404421

saturation from the bottom to the top of the specimen. The flushing of $CaCO_3$ could happen during the saturation process if it is left with low precipitation. The durability of $CaCO_3$ via EICP is a significant factor that influences the efficiency of the treatment. Additionally, the cementation degradation or the breakage of $CaCO_3$ bonds under high confining pressure conditions in weak cementation could hamper the strength of the soil. Both triaxial testing using CDH urease and Sigma urease portray less $CaCO_3$ precipitation left in the soil under high confining pressure (200 kPa) than low confining pressure (50 kPa). Other researchers have observed similar remarks.

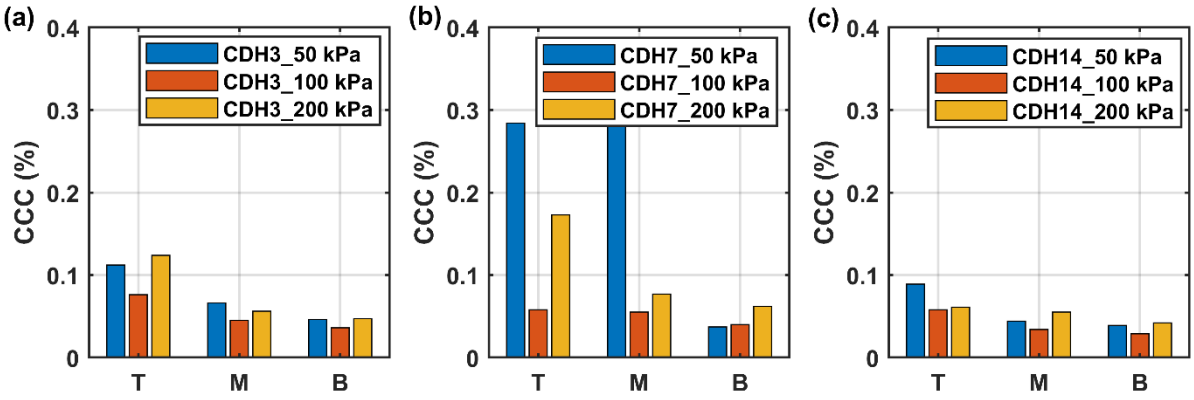

Figure 82: Acid Digestion Test results after static triaxial test (a) CDH-treated specimen at 3 days of curing (b) CDH-treated specimen at 7 days of curing (c) CDH-treated specimen at 14 days of curing

doi:10.6342/NTU202404421

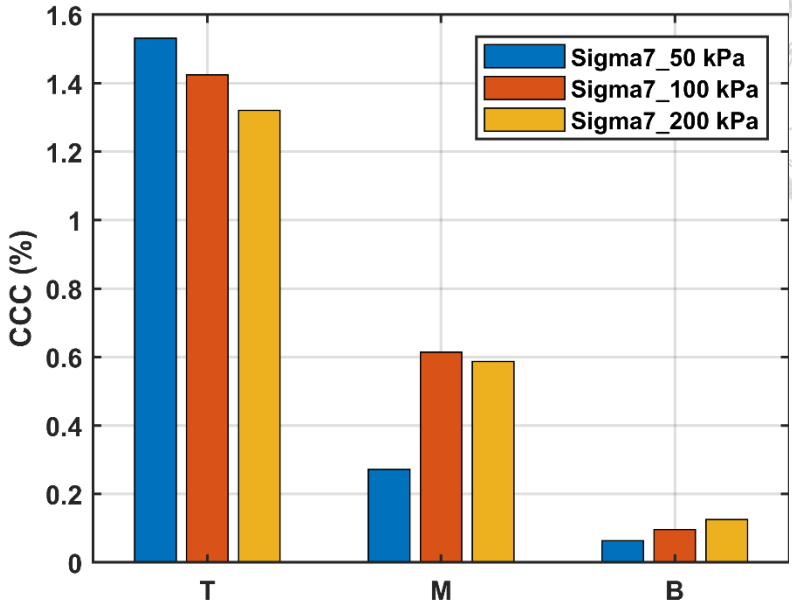

Figure 83: Acid Digestion Test results after static triaxial test (a) Sigma-treated specimen at 7 days of curing

Liu *et al.* (2019b) performed experimental testing to check the durability of the MICP-treated soil in three conditions: wet-dry, freeze-thaw, and acid rain. The MICP-treated soil lost almost 85% of strength after one cycle of wet-dry cycles, 58% reduction after 15 freeze-thaw cycles, and 83% reduction after 15 days of immersion in acid rain with a pH of 3.5. The unbonded/weak $CaCO_3$ tends to get washed away at wet-dry cycles, as shown in Figure 84. A small percentage of $CaCO_3$ acts to deposit at the interparticle contact, acts as a bridge between soil particles, and provides permeability retention in the treated soil (Cheng *et al.* 2012; Zhao *et al.* 2014). As mentioned in Figure 84, some amount of $CaCO_3$ was flushed off at the bottom of the specimen during saturation.

doi:10.6342/NTU202404421

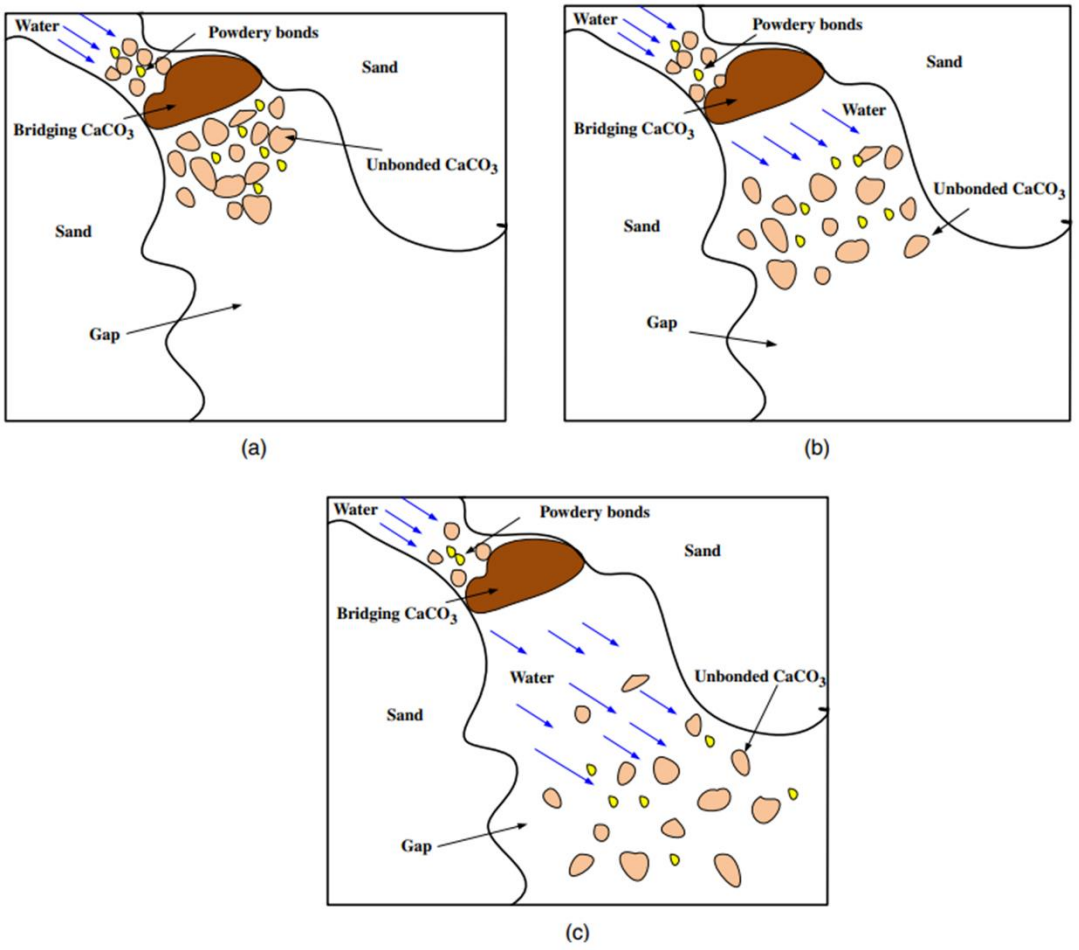

Figure 84: Schematic representation of flush off of weak $CaCO_3$ precipitate (Liu *et al.* 2019b).

As the sand used for the research study was fine silica sand with poorly graded, the precipitated $CaCO_3$ gets degraded during the consolidation and shearing of the triaxial specimen under increase of confining pressure (Feng and Montoya 2016; Lin *et al.* 2016; Montoya *et al.* 2013). Sasaki and Kuwano (2016) performed liquefaction resistance in non-plastic fines content in two different soils: toyoura sand and Urayasu sand. The cementation degradation was measured by monitoring the shear wave velocity during the consolidation of the specimen. The shear wave velocity results confirmed the degradation or break off of

doi:10.6342/NTU202404421

the weak cementation $CaCO_3$ because of the fines. This degradation could be reduced with higher cementation of $CaCO_3$ or multiple injections of the treatment solution to improve strength and liquefaction resistance in the soil. Nafisi *et al.* (2020) investigated the shear strength envelopes in three types of sand Ottawa 20-30, Ottawa 50-70, and Nevada sand by performing drained triaxial compression tests under three different confining pressures, 10,100 and 400 kPa in four levels of treatment (untreated, light, moderate and heavy). The shear wave velocity during the shearing of the triaxial testing was monitored as a measure of cementation degradation during the increase of axial strain. The following Figure 85 shows the shear wave velocity during shearing. The reduction in the shear velocity at light, moderate, and heavy cementation levels dropped approximately 3% of axial strain. Later, faster cementation degradation was observed during the increase in axial strain.

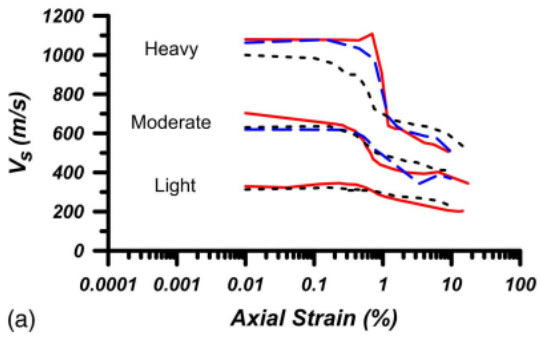

Figure 85: Variation of shear wave velocity during shearing

doi:10.6342/NTU202404421

Chapter 5 CONCLUSIONS

A comprehensive series of preliminary investigations, drained triaxial compression tests, and microscopic analyses were conducted on pure sand and EICP-treated specimens. The following conclusions can be drawn from the study:

1. The falcon tube test experiments discuss the influence of the urease enzyme on the chemical constituents (urea and calcium chloride solutions) in the calcium carbonate precipitation by EICP treatment. The optimal EICP formulation was determined as 1M Urea, 0.67 M Calcium Chloride, and 3 g/l urease enzyme was adopted for the soil treatment.
2. Analysis of penetration depth after two treatment cycles over 7 days revealed a significant reduction compared to measurements taken on days 3 and 7 during a single treatment cycle fall cone test. The potential for improved precipitation rates in the fall cone test, leading to resistance in penetration depth, was evident with successive treatment cycles. Notably, a substantial increase in % CCC was observed in the acid digestion results after one treatment cycle, suggesting the possibility of further enhancement with additional treatment cycles.
3. Lower concentrations of urea and $CaCl_2$ demonstrated a uniform distribution of calcium carbonate after a single treatment cycle at 3 days of curing. However, introducing two treatment cycles increased $CaCO_3$ concentration at the specimen's top surface, indicating a precipitation disparity. Combo 2 and 4 consistently exhibited the highest $CaCO_3$ and precipitation ratios across all curing times and treatment cycles: prolonged curing times and increased treatment cycles under drained conditions led to non-uniform $CaCO_3$ precipitation.

doi:10.6342/NTU202404421

4. The influence of pH and electrical conductivity in the urease activity and the formation of calcium carbonate precipitation were also studied. The EICP treatment solution's ionic activity reflected the electrical conductivity measurement. The high alkaline atmosphere creates a favorable condition for $CaCO_3$. The urease enzymes exhibited similar behavior in the pH and electrical conductivity variation versus time.
5. The uniformity of the calcium carbonate distribution along the specimen height affects the efficiency of the EICP treatment in the soil. Non-uniform calcium carbonate distribution could deform easily, providing small shear resistance in triaxial testing. One-phase of EICP treatment and undrained conditions produced a more uniform calcite distribution in the soil.
6. Under different confining conditions, One-phase EICP treatment exhibited increased peak deviatoric stress in the EICP-treated and pure sand specimens. The increased cementation in the treatment resulted in a more robust specimen, with significantly higher peak deviatoric stress observed under different curing conditions. The calcium carbonate content resulting from EICP treatment contributed to sustained shearing across all confining pressures compared to the pure sand, indicating improved mechanical behavior.
7. EICP-treated specimens exhibited more significant dilation compared to the pure sand. Calcium carbonate content improved dilatancy characteristics due to the particle grains' interlocking and the particle's roughness by precipitation. EICP-treated specimens improved in moving towards the dilation side compared to the pure sand. Initially, the cementation effects in the bio-cemented specimen led to higher

doi:10.6342/NTU202404421

contraction than the pure sand, but after some time, it shifted to the dilation side. Both CDH14_50 kPa and Sigma7_50 kPa showed higher dilation compared to pure sand.

8. The increase in bio-cementation through EICP was significantly associated with the rise in effective cohesion rather than the friction angle. Calcium carbonate content slightly affected the friction angle in peak and residual strength at different curing times. In both cases of EICP-treated soil, the effective cohesion increased from 0 kPa to 11.16 kPa at peak strength and to 8.84 kPa at residual strength after 14 days of curing (CDH-treated). Similarly, the effective cohesion increased from 0 kPa to 9.13 kPa at peak strength and to 4.83 kPa at residual strength after 14 days of curing (Sigma-treated).
9. The deformation response and pore pressure development in the EICP-treated specimen revealed the mechanical behavior of the treated specimen during cyclic loading. The compression strain at liquefaction time in EICP-treated specimens was lower than in pure sand. The decrease in compression strain in the CDH7_100 kPa sample ranged from approximately 5% to 36%, spanning CSR values from 0.31 to 0.212. Similar behavior observed in Sigma7_100 kPa ranged from approximately 45 to 65%, spanning CSR values from 0.31 to 0.25. Moreover, the dissipation of the pore water pressure during cyclic loading, leading to liquefaction, was prolonged in the EICP-treated specimens. Consequently, the number of cycles to liquefaction increased significantly compared to pure sand. The enhancement in liquefaction resistance in CDH7_100 kPa ranged from approximately 120% to 400%, covering CSR values from 0.31 to 0.212. Similar behavior observed in Sigma7_100 kPa ranged from approximately 170 to 220%, covering CSR values from 0.31 to 0.25. The

doi:10.6342/NTU202404421

liquefaction curves demonstrated that the one-phase EICP treatment with one treatment cycle at 7 days of curing showed a significant liquefaction resistance in the treated sand.

10. FE-SEM analysis showed two types of calcium carbonate precipitation in the EICP-treated sample: a) particle-to-particle contact precipitation and b) particle-to-calcite precipitation. Both kinds of precipitation contributed to the mechanical behavior of the soil improvement. FE-SEM images of the calcium carbonate precipitate revealed the agglomerated euhedral calcite crystal formed via EICP treatment. The size of the calcite crystal was measured and displayed a smooth texture devoid of cleavage planes on the crystal. EDS analysis coupled with elemental mapping was performed on corresponding FE-SEM images to identify the presence of calcium carbonate precipitation.
11. Finally, XRD analysis was conducted on the precipitate, pure sand, and EICP-treated sample, confirming the formation of calcite - a type of crystal for calcium carbonate, regarded as the most stable crystal structure. A few peaks of calcite crystals emerged in the EICP-treated sample, as seen from the XRD results.

This comprehensive study enhances our understanding of the intricate mechanisms and effects of EICP treatment on soil behavior, thereby contributing valuable insights to ground improvement techniques.

doi:10.6342/NTU202404421

RECOMMENDATIONS

1. Laboratory studies are needed to investigate the critical parameters of the long-term engineering performance of the EICP treatment in wet-dry cycles, freeze-thaw cycles, and acid rain conditions. EICP treatment under weak cementation is susceptible to washing off $CaCO_3$ and reduces the strength. Therefore, higher cementation with a high intact force is essential to increase the durability of the EICP treatment. The rainfall or other environmental factors on the EICP-treated ground could lead to the flushing off of $CaCO_3$, which reduces the strength and stiffness of the treated soil. It is vital to study the durability of the precipitation via EICP/MICP treatment in in-situ applications.
2. As the present research study focused on static and dynamic triaxial laboratory testing, the next step is to study the seismic performance of the EICP treatment. Large-scale laboratory tests with shaking table and centrifuge testing help evaluate EICP treatment's feasibility in field applications. The monitoring of shear wave velocity, pore water pressures, and vertical settlement in the untreated and treated soil. The treated soil improved the shear strength and reduced the surface settlement and excess pore water pressure ratio. It is also prone to a higher magnitude of surface acceleration than prone liquefaction resistance.
3. The present research study focused on one treatment cycle. In order to increase the amount of $CaCO_3$ precipitation, multiple treatment cycles are essential. The higher the precipitation, the higher the strength and stiffness of the soil. Various treatment cycles for 7 days of curing could be studied in the future, which is believed to provide higher shear strength parameters and liquefaction resistance

doi:10.6342/NTU202404421

4. The present research study assessed the liquefaction resistance at 100 kPa in three different CSR ratios the variation of liquefaction resistance with different confining pressure which could help in designing safe structures especially in seismic prone areas. The study sheds some light on predicting the liquefaction potential at different soil depth and under different loading conditions.
5. The ground temperature could influence the EICP treatment and the deposition of the calcium carbonate. Higher temperatures of the ground in deeper soil could affect the bridging/or interparticle contact of the $CaCO_3$ between the soil grains. Hence, it is crucial to study the thermal conductivity and the range of temperature for a higher efficiency of EICP treatment.

doi:10.6342/NTU202404421

REFERENCES

Ahenkorah, I., Rahman, M.M., Karim, M.R., and Beecham, S. (2021a): Enzyme induced calcium carbonate precipitation and its engineering application: A systematic review and meta-analysis, *Constr. Build. Mater.*, 308, 125000. https://doi.org/10.1016/j.conbuildmat.2021.125000

Ahenkorah, I., Rahman, M.M., Karim, M.R., and Beecham, S. (2021b): Optimisation of chemical constituents on enzyme-induced carbonate precipitation in test-tube and soil, *Geotechnical Research*, 8(3), 66-84. http://doi.org/10.1680/jgere.21.00006

Ahenkorah, I., Rahman, M.M., Karim, M.R., Beecham, S., and Saint, C. (2021c): A Review of Enzyme Induced Carbonate Precipitation (EICP): The Role of Enzyme Kinetics, *Sustainable Chemistry*, 2(1), 92-114. https://www.mdpi.com/2673-4079/2/1/7

Ahenkorah, I., Rahman, M.M., Karim, M.R., Beecham, S., and Saint, C. (2021d): A Review of Enzyme Induced Carbonate Precipitation (EICP): The Role of Enzyme Kinetics, *Sustain. Chem.*, 2(1), 92-114. http://doi.org/10.3390/suschem2010007

Al Qabany, A., Soga, K., and Santamarina, C. (2012): Factors Affecting Efficiency of Microbially Induced Calcite Precipitation, *J. Geotech. Geoenviron. Eng.*, 138(8), 992-1001. http://doi.org/10.1061/(asce)gt.1943-5606.0000666

Almajed, A. (2019): Enzyme induced cementation of biochar-intercalated soil: fabrication and characterization, *Arabian Journal of Geosciences*, 12(13). http://doi.org/10.1007/s12517-019-4557-z

Almajed, A., Khodadadi Tirkolaei, H., and Kavazanjian, E. (2018): Baseline Investigation on Enzyme-Induced Calcium Carbonate Precipitation, *J. Geotech. Geoenviron. Eng.*, 144(11). http://doi.org/10.1061/(asce)gt.1943-5606.0001973

doi:10.6342/NTU202404421

Almajed, A., Lateef, M.A., Moghal, A.A., and Lemboye, K. (2021a): State-of-the-Art Review of the Applicability and Challenges of Microbial-Induced Calcite Precipitation (MICP) and Enzyme-Induced Calcite Precipitation (EICP) Techniques for Geotechnical and Geoenvironmental Applications, *Crystals*, 11(4). http://doi.org/10.3390/cryst11040370

Almajed, A., Lateef, M.A., Moghal, A.A.B., and Lemboye, K. (2021b): State-of-the-Art Review of the Applicability and Challenges of Microbial-Induced Calcite Precipitation (MICP) and Enzyme-Induced Calcite Precipitation (EICP) Techniques for Geotechnical and Geoenvironmental Applications, *Crystals*, 11(4), 370. https://www.mdpi.com/2073-4352/11/4/370

Almajed, A., Tirkolaei, H.K., Kavazanjian, E., Jr., and Hamdan, N. (2019): Enzyme Induced Biocementated Sand with High Strength at Low Carbonate Content, *Sci. Rep.*, 9(1), 1135. http://doi.org/10.1038/s41598-018-38361-1

Amini, Y., and Hamidi, A. (2014): Triaxial shear behavior of a cement-treated sand–gravel mixture, *J. Rock Mech. Geotech. Eng.*, 6(5), 455-465. https://doi.org/10.1016/j.jrmge.2014.07.006

Arab, M.G., Alsodi, R., Almajed, A., Yasuhara, H., Zeiada, W., and Shahin, M.A. (2021a): State-of-the-Art Review of Enzyme-Induced Calcite Precipitation (EICP) for Ground Improvement: Applications and Prospects, *Geosciences*, 11(12). http://doi.org/10.3390/geosciences11120492

Arab, M.G., Omar, M., Almajed, A., Elbaz, Y., and Ahmed, A.H. (2021b): Hybrid technique to produce bio-bricks using enzyme-induced carbonate precipitation (EICP) and

doi:10.6342/NTU202404421

sodium alginate biopolymer, *Construction and Building Materials*, 284. http://doi.org/10.1016/j.conbuildmat.2021.122846

Arab, M.G., Rohy, H., Zeiada, W., Almajed, A., and Omar, M. (2021c): One-Phase EICP Biotreatment of Sand Exposed to Various Environmental Conditions, *Journal of Materials in Civil Engineering*, 33(3). http://doi.org/10.1061/(asce)mt.1943-5533.0003596

ASTM_D2487−17 (2018): Standard Practice for Classification of Soils for Engineering Purposes (Unified Soil Classification System). http://doi.org/10.1520/d2487-17

ASTM_D5311-11 (2012): Standard Test Method for Load Controlled Cyclic Triaxial Strength of Soil. http://doi.org/10.1520/d5311-11

ASTM_D7181-11. (2011). Standard Test Method for Consolidated Drained Triaxial Compression Test for Soils. In. United States: ASTM.

ASTM_D7181-20 (2020): Standard Test Method for Consolidated Drained Triaxial Compression Test for Soils. http://doi.org/10.1520/d7181-20

Blakeley, R.L., and Zerner, B. (1984): Jack bean urease: the first nickel enzyme, *Journal of Molecular Catalysis*, 23(2), 263-292. https://doi.org/10.1016/0304-5102(84)80014-0

Carmona, J.P.S.F., Oliveira, P.J.V., and Lemos, L.J.L. (2016): Biostabilization of a Sandy Soil Using Enzymatic Calcium Carbonate Precipitation, *Procedia Eng.*, 143, 1301-1308. http://doi.org/10.1016/j.proeng.2016.06.144

Chandra, A., and Ravi, K. (2020). Effect of Magnesium Incorporation in Enzyme-Induced Carbonate Precipitation (EICP) to Improve Shear Strength of Soil. In Advances in

doi:10.6342/NTU202404421

Computer Methods and Geomechanics (pp. 333-346). https://doi.org/10.1007/978-981-15-0890-5_28

Cheng, L., and Cord-Ruwisch, R. (2012): In situ soil cementation with ureolytic bacteria by surface percolation, *Ecological Engineering*, 42, 64-72. http://doi.org/10.1016/j.ecoleng.2012.01.013

Cheng, L., and Cord-Ruwisch, R. (2014): Upscaling Effects of Soil Improvement by Microbially Induced Calcite Precipitation by Surface Percolation, *Geomicrobiology Journal*, 31, 396-406. http://doi.org/10.1080/01490451.2013.836579

Cheng, L., Cord-Ruwisch, R., and Shahin, M.A. (2013): Cementation of sand soil by microbially induced calcite precipitation at various degrees of saturation, *Canadian Geotechnical Journal*, 50(1), 81-90. http://doi.org/10.1139/cgj-2012-0023

Cheng, L., Shahin, M.A., and Mujah, D. (2017): Influence of Key Environmental Conditions on Microbially Induced Cementation for Soil Stabilization, *Journal of Geotechnical and Geoenvironmental Engineering*, 143(1), 04016083. http://doi.org/10.1061/(ASCE)GT.1943-5606.0001586

Chiet, K.T.P., Kassim, K.A., Chen, K.B., Martula, U., Yah, C.S., and Arefnia, A. (2015). Effect of Reagents Concentration on Biocementation of Tropical Residual Soil *Soft Soil Engineering International Conference*,

Choi, S.-G., Hoang, T., and Park, S.-S. (2019): Undrained Behavior of Microbially Induced Calcite Precipitated Sand with Polyvinyl Alcohol Fiber, *Applied Sciences*, 9(6). http://doi.org/10.3390/app9061214

doi:10.6342/NTU202404421

Cui, Zheng Jun jie, and Han-jiang, L. (2016): Experimental study of effect of particle size on strength of bio-cemented sand, *Rock and Soil Mechanics*, 37(S2), 397-402. http://doi.org/10.16285/j.rsm.2016.S2.051

Cui, M.-J., Lai, H.-J., Hoang, T., and Chu, J. (2020): One-phase-low-pH enzyme induced carbonate precipitation (EICP) method for soil improvement, *Acta Geotechnica*, 16(2), 481-489. http://doi.org/10.1007/s11440-020-01043-2

Cui, M.-J., Lai, H.-J., Hoang, T., and Chu, J. (2021a): Modified one-phase-low-pH method for bacteria or enzyme-induced carbonate precipitation for soil improvement, *Acta Geotech.* http://doi.org/10.1007/s11440-021-01384-6

Cui, M.-J., Zheng, J.-J., Chu, J., Wu, C.-C., and Lai, H.-J. (2021b): Bio-mediated calcium carbonate precipitation and its effect on the shear behaviour of calcareous sand, *Acta Geotechnica*, 16(5), 1377-1389. http://doi.org/10.1007/s11440-020-01099-0

Cui, M.-J., Zheng, J.-J., Zhang, R.-J., Lai, H.-J., and Zhang, J. (2017): Influence of cementation level on the strength behavior of bio-cemented sand, *Acta Geotech.*, 12(5), 971-986. http://doi.org/10.1007/s11440-017-0574-9

DeJong, J.T., Mortensen, B.M., Martinez, B.C., and Nelson, D.C. (2010): Bio-mediated soil improvement, *Ecol. Eng.*, 36(2), 197-210. http://doi.org/10.1016/j.ecoleng.2008.12.029

Feng, K., and Montoya, B.M. (2016): Influence of Confinement and Cementation Level on the Behavior of Microbial-Induced Calcite Precipitated Sands under Monotonic Drained Loading, *J. Geotech. Geoenviron. Eng.*, 142(1). http://doi.org/10.1061/(asce)gt.1943-5606.0001379

doi:10.6342/NTU202404421

Follmer, C., Barcellos, G.B.S., Zingali, R.B., Machado, O.L.T., Alves, E.W., Barja-Fidalgo, C., Guimaraes, J.A., and Carlini, C.R. (2001): Canatoxin, a toxic protein from jack beans (Canavalia ensiformis), is a variant form of urease (EC 3.5.1.5): biological effects of urease independent of its ureolytic activity, *Biochemical Journal*, 360(1), 217-224. http://doi.org/10.1042/bj3600217

Fouladi, A.S., Arulrajah, A., Chu, J., and Horpibulsuk, S. (2023): Application of Microbially Induced Calcite Precipitation (MICP) technology in construction materials: A comprehensive review of waste stream contributions, *Construction and Building Materials*, 388. http://doi.org/10.1016/j.conbuildmat.2023.131546

Gao, Y., Hang, L., He, J., and Chu, J. (2018): Mechanical behaviour of biocemented sands at various treatment levels and relative densities, *Acta Geotechnica*, 14(3), 697-707. http://doi.org/10.1007/s11440-018-0729-3

Gao, Y., Hang, L., He, J., and Chu, J. (2019a): Mechanical behavior of biocemented sands at various treatment levels and relative densities, *Acta Geotech.*, 14(3), 697-707. http://doi.org/10.1007/s11440-018-0729-3

Gao, Y., He, J., Tang, X., and Chu, J. (2019b): Calcium carbonate precipitation catalyzed by soybean urease as an improvement method for fine-grained soil, *Soils and Found.*, 59(5), 1631-1637. https://doi.org/10.1016/j.sandf.2019.03.014

Gao, Y., Wang, L., He, J., Ren, J., and Gao, Y. (2022): Denitrification-based MICP for cementation of soil: treatment process and mechanical performance, *Acta Geotechnica*, 17(9), 3799-3815. http://doi.org/10.1007/s11440-022-01489-6

Ghionna, V.N., and Porcino, D. (2006): Liquefaction Resistance of Undisturbed and Reconstituted Samples of a Natural Coarse Sand from Undrained Cyclic Triaxial

doi:10.6342/NTU202404421

Tests, *J. Geotech. Geoenviron. Eng.*, 132(2), 194-202. http://doi.org/10.1061/(ASCE)1090-0241(2006)132:2(194)

Gitanjali, A., Jhuo, Y.-S., Yeh, F.-H., and Ge, L. (2024): Bio-cementation of sand using enzyme-induced calcite precipitation: Mechanical behavior and microstructural analysis, *Construction and Building Materials*, 417, 135360. http://doi.org/10.1016/j.conbuildmat.2024.135360

Gomez, M.G., Anderson, C.M., Graddy, C.M.R., DeJong, J.T., Nelson, D.C., and Ginn, T.R. (2017): Large-Scale Comparison of Bioaugmentation and Biostimulation Approaches for Biocementation of Sands, *Journal of Geotechnical and Geoenvironmental Engineering*, 143(5), 04016124. http://doi.org/10.1061/(ASCE)GT.1943-5606.0001640

Gomez, M.G., Graddy, C.M.R., DeJong, J.T., Nelson, D.C., and Tsesarsky, M. (2018): Stimulation of Native Microorganisms for Biocementation in Samples Recovered from Field-Scale Treatment Depths, *Journal of Geotechnical and Geoenvironmental Engineering*, 144(1), 04017098. http://doi.org/10.1061/(ASCE)GT.1943-5606.0001804

Gowthaman, S., Yamamoto, M., Chen, M., Nakashima, K., and Kawasaki, S. (2023): Baseline investigation on enzyme induced calcium phosphate precipitation for solidification of sand, *Frontiers in Built Environment*, 9. http://doi.org/10.3389/fbuil.2023.1307650

Hamdan, N., and Kavazanjian Jr, E. (2016): Enzyme-induced carbonate mineral precipitation for fugitive dust control, *Géotechnique*, 66(7), 546-555.

doi:10.6342/NTU202404421

Han-Long, L., Peng, X., Yang, X., Jian-Ping, W., Yu-Min, C., and Jian, C. (2018): Dynamic behaviors of MICP-treated calcareous sand in cyclic tests, *Chinese Journal of Geotechnical Engineering*, 40(1), 38-45.

Han, C., Li, D., Rao, Y., and Wang, J. (2020): Study on hysteretic deformation characteristics and energy dissipation of granite under cyclic loading, *China Rock 2020*, 570, 032024.

Han, Z., Cheng, X., and Ma, Q. (2016): An experimental study on dynamic response for MICP strengthening liquefiable sands, *Earthq. Eng. & Eng. Vib.*, 15(4), 673-679. http://doi.org/10.1007/s11803-016-0357-6

He, J., Fang, C., Mao, X., Qi, Y., Zhou, Y., Kou, H., and Xiao, L. (2022a): Enzyme-Induced Carbonate Precipitation for the Protection of Earthen Dikes and Embankments Under Surface Runoff: Laboratory Investigations, *Journal of Ocean University of China*, 21(2), 306-314. http://doi.org/10.1007/s11802-022-4821-9

He, J., Gao, Y., Gu, Z., Chu, J., and Wang, L. (2020): Characterization of Crude Bacterial Urease for CaCO3 Precipitation and Cementation of Silty Sand, *Journal of Materials in Civil Engineering*, 32(5), 04020071. http://doi.org/10.1061/(ASCE)MT.1943-5533.0003100

He, J., Mao, X., Zhou, Y., and Tang, Q. (2022b): Cementation of Sand With Enzyme-Induced Carbonate Precipitation (EICP) Using Concrete-Extracted Calcium, *Frontiers in Physics*, 9. http://doi.org/10.3389/fphy.2021.825356

He, J., Yang, F., Qi, Y.-S., Fang, C.-H., Yan, B.-Y., Zhang, Y., Hang, L., and Gao, Y.-F. (2021): Improvement in silty sand with enzyme-induced carbonate precipitation:

doi:10.6342/NTU202404421

laboratory model experiment, *Acta Geotechnica*. https://doi.org/10.1007/s11440-021-01361-z

He, J., Yang, F., Qi, Y.-S., Fang, C.-H., Yan, B.-Y., Zhang, Y., Hang, L., and Gao, Y.-F. (2022c): Improvement in silty sand with enzyme-induced carbonate precipitation: laboratory model experiment, *Acta Geotech.*, 17(7), 2895-2905. http://doi.org/10.1007/s11440-021-01361-z

Hu, W., Cheng, W.C., Wen, S., and Yuan, K. (2021): Revealing the Enhancement and Degradation Mechanisms Affecting the Performance of Carbonate Precipitation in EICP Process, *Front Bioeng Biotechnol*, 9, 750258. http://doi.org/10.3389/fbioe.2021.750258

Huang, Y., and Wang, L. (2017): Reply to the discussion by Ochoa-Cornejo et al. on "Laboratory investigation of liquefaction mitigation in silty sand using nanoparticles" [Eng.Geol.204:23–32], *Engineering Geology*, 221, 202. https://doi.org/10.1016/j.enggeo.2017.02.024

Iamchaturapatr, J., Piriyakul, K., and Petcherdchoo, A. (2022): Characteristics of sandy soil treated using EICP-based urease enzymatic acceleration method and natural hemp fibers, *Case Studies in Construction Materials*, 16, e00871. https://doi.org/10.1016/j.cscm.2022.e00871

Javadi, N., Khodadadi, H., Hamdan, N., and Kavazanjian, E. (2018). EICP Treatment of Soil by Using Urease Enzyme Extracted from Watermelon Seeds. *IFCEE*, Orlando, Florida.

doi:10.6342/NTU202404421

Jiang, M.J., Yan, H.B., Zhu, H.H., and Utili, S. (2011): Modeling shear behavior and strain localization in cemented sands by two-dimensional distinct element method analyses, *Computers and Geotechnics*, 38(1), 14-29. https://doi.org/10.1016/j.compgeo.2010.09.001

Jiang, N.-J., Yoshioka, H., Yamamoto, K., and Soga, K. (2016): Ureolytic activities of a urease-producing bacterium and purified urease enzyme in the anoxic condition: Implication for subseafloor sand production control by microbially induced carbonate precipitation (MICP), *Ecological Engineering*, 90, 96-104. https://doi.org/10.1016/j.ecoleng.2016.01.073

Karakan, E., Sezer, A., and Tanrinian, N. (2019a): Evaluation of effect of limited pore water pressure development on cyclic behavior of a nonplastic silt, *Soils and Foundations*, 59(5), 1302-1312. http://doi.org/10.1016/j.sandf.2019.05.009

Karakan, E., Tanrinian, N., and Sezer, A. (2019b): Cyclic undrained behavior and post liquefaction settlement of a nonplastic silt, *Soil Dynamics and Earthquake Engineering*, 120, 214-227. http://doi.org/10.1016/j.soildyn.2019.01.040

Kavazanjian, E., and Hamdan, N. (2015). Enzyme Induced Carbonate Precipitation (EICP) Columns for Ground Improvement *Ifcee 2015*,

Keykha, H.A., and Asadi, A. (2017): Solar Powered Electro-Bio-Stabilization of Soil with Ammonium Pollution Prevention System, *Advances in Civil Engineering Materials*, 6(1), 360-371. http://doi.org/10.1520/acem20170001

Lade, P.V., and Overton, D.D. (1989): Cementation Effects in Frictional Materials, *J. Geotech. Eng.*, 115(10), 1373-1387. http://doi.org/10.1061/(ASCE)0733-9410(1989)115:10(1373)

doi:10.6342/NTU202404421

Lee, M., Gomez, M.G., San Pablo, A.C.M., Kolbus, C.M., Graddy, C.M.R., DeJong, J.T., and Nelson, D.C. (2019): Investigating Ammonium By-product Removal for Ureolytic Bio-cementation Using Meter-scale Experiments, *Scientific Reports*, 9(1), 18313. http://doi.org/10.1038/s41598-019-54666-1

Li, Y., Guo, Z., Wang, L., Li, Y., and Liu, Z. (2020): Shear resistance of MICP cementing material at the interface between calcareous sand and steel, *Materials Letters*, 274. http://doi.org/10.1016/j.matlet.2020.128009

Likos, W.J., and Jaafar, R. (2014): Laboratory Fall Cone Testing of Unsaturated Sand, *Journal of Geotechnical and Geoenvironmental Engineering*, 140(8), 04014043. http://doi.org/10.1061/(ASCE)GT.1943-5606.0001143

Lin, H., O'Donnell, S.T., Suleiman, M.T., Kavazanjian, E., and Brown, D.G. (2021): Effects of Enzyme and Microbially Induced Carbonate Precipitation Treatments on the Response of Axially Loaded Pervious Concrete Piles, *J. Geotech. Geoenviron. Eng.*, 147(8). http://doi.org/10.1061/(asce)gt.1943-5606.0002565

Lin, H., Suleiman, M.T., Brown, D.G., and Kavazanjian, E. (2016): Mechanical Behavior of Sands Treated by Microbially Induced Carbonate Precipitation, *Journal of Geotechnical and Geoenvironmental Engineering*, 142(2). http://doi.org/10.1061/(asce)gt.1943-5606.0001383

Liu, B., Zhu, C., Tang, C.-S., Xie, Y.-H., Yin, L.-Y., Cheng, Q., and Shi, B. (2020): Bio-remediation of desiccation cracking in clayey soils through microbially induced calcite precipitation (MICP), *Engineering Geology*, 264. http://doi.org/10.1016/j.enggeo.2019.105389

doi:10.6342/NTU202404421

Liu, L., Liu, H., Stuedlein, A.W., Evans, T.M., and Xiao, Y. (2019a): Strength, stiffness, and microstructure characteristics of biocemented calcareous sand, *Can. Geotech. J*, 56(10), 1502-1513. http://doi.org/10.1139/cgj-2018-0007

Liu, S., Wen, K., Armwood, C., Bu, C., Li, C., Amini, F., and Li, L. (2019b): Enhancement of MICP-Treated Sandy Soils against Environmental Deterioration, *Journal of Materials in Civil Engineering*, 31(12). http://doi.org/10.1061/(asce)mt.1943-5533.0002959

Loh, C.-H., and Tsay, C.-Y. (2019): Responses of the Earthquake Engineering Research Community to the Chi-Chi (Taiwan) Earthquake, *Earthquake Spectra*, 17(4), 635-656. http://doi.org/10.1193/1.1430680

Luo, C., Yang, X., and Li, J. (2022): Mechanical Properties of Single-Crystal Calcite and Their Temperature and Strain-Rate Effects, *Materials*, 15, 4613. http://doi.org/10.3390/ma15134613

Marri, A., Wanatowski, D., and Yu, H. (2012): Drained behaviour of cemented sand in high pressure triaxial compression tests, *Geomechanics and Geoengineering*, 7(3), 159-174.

Martin, K., Tirkolaei, H.K., and Kavazanjian, E. (2021): Enhancing the strength of granular material with a modified enzyme-induced carbonate precipitation (EICP) treatment solution, *Constr. Build. Mater.*, 271, 121529. http://doi.org/10.1016/j.conbuildmat.2020.121529

Martin, K.K., Tirkolaei, H.K., and Kavazanjian, E. (2024): Field-Scale EICP Biocemented Columns for Ground Improvement, *Journal of Geotechnical and Geoenvironmental Engineering*, 150(8), 05024006. http://doi.org/10.1061/JGGEFK.GTENG-11635

doi:10.6342/NTU202404421

Marzadori, C., Miletti, S., Gessa, C., and Ciurli, S. (1998): Immobilization of jack bean urease on hydroxyapatite: urease immobilization in alkaline soils, *Soil Biology and Biochemistry*, 30(12), 1485-1490. https://doi.org/10.1016/S0038-0717(98)00051-0

Meng, H., Shu, S., Gao, Y., He, J., and Wan, Y. (2021a): Kitchen waste for Sporosarcina pasteurii cultivation and its application in wind erosion control of desert soil via microbially induced carbonate precipitation, *Acta Geotech.*, 16(12), 4045-4059. http://doi.org/10.1007/s11440-021-01334-2

Meng, H., Shu, S., Gao, Y., Yan, B., and He, J. (2021b): Multiple-phase enzyme-induced carbonate precipitation (EICP) method for soil improvement, *Eng. Geol.*, 294, 106374. https://doi.org/10.1016/j.enggeo.2021.106374

Miftah, A., Tirkolaei, H.K., and Bilsel, H. (2019). Strengthening Beach Sand By Enzyme Induced Calcium Carbonate Precipitation *8th Geotechnical Symposium*, TÜ Süleyman Demirel Kültür Merkezi,Istanbul.

Mitchell, and Santamarina (2005): Biological considerations in geotechnical engineering, *Journal of Geotechnical and Geoenvironmental Engineering*, 131(10), 1222-1233. http://doi.org/10.1061/(ASCE)1090-0241(2005)131:10(1222)

Montoya, B.M., and DeJong, J.T. (2015): Stress-Strain Behavior of Sands Cemented by Microbially Induced Calcite Precipitation, *J. Geotech. Geoenviron. Eng.*, 141(6), 04015019. http://doi.org/10.1061/(ASCE)GT.1943-5606.0001302

Montoya, B.M., Dejong, J.T., and Boulanger, R.W. (2013): Dynamic response of liquefiable sand improved by microbial-induced calcite precipitation, *Géotechnique*, 63(4), 302-312. http://doi.org/10.1680/geot.SIP13.P.019

doi:10.6342/NTU202404421

Mortensen, B.M. (2011): Effects of environmental factors on microbial induced calcium carbonate precipitation, *J. Appl. Microbiol.*, 111(2), 338-349. http://doi.org/10.1111/j.1365-2672.2011.05065.x

Muhammed, A.S., Kassim, K.A., Ahmad, K., Zango, M.U., Chong, C.S., and Makinda, J. (2021): Influence of multiple treatment cycles on the strength and microstructure of biocemented sandy soil, *International Journal of Environmental Science and Technology*, 18(11), 3427-3440. http://doi.org/10.1007/s13762-020-03073-5

Nafisi, A., Montoya, B.M., and Evans, T.M. (2020): Shear Strength Envelopes of Biocemented Sands with Varying Particle Size and Cementation Level, *J. Geotech. Geoenviron. Eng.*, 146(3), 04020002. http://doi.org/10.1061/(ASCE)GT.1943-5606.0002201

Nafisi, A., Safavizadeh, S., and Montoya, B.M. (2019): Influence of Microbe and Enzyme-Induced Treatments on Cemented Sand Shear Response, *J. Geotech. Geoenviron. Eng.*, 145(9), 06019008. http://doi.org/10.1061/(ASCE)GT.1943-5606.0002111

Neda Javadi, and Hamed Khodadadi, N.H., Edward Kavazanjian (2018). EICP Treatment of Soil by Using Urease Enzyme Extracted from Watermelon Seeds. *IFCEE*, Florida, United States.

Nemati, M., and Voordouw, G. (2003): Modification of porous media permeability, using calcium carbonate produced enzymatically in situ, *Enzyme and Microbial Technology*, 33(5), 635-642. http://doi.org/10.1016/s0141-0229(03)00191-1

Neupane, D., Yasuhara, H., Kinoshita, N., and Ando, Y. (2015): Distribution of mineralized carbonate and its quantification method in enzyme mediated calcite precipitation

doi:10.6342/NTU202404421

technique, *Soils and Foundations*, 55(2), 447-457. http://doi.org/10.1016/j.sandf.2015.02.018

Neupane, D., Yasuhara, H., Kinoshita, N., and Unno, T. (2013): Applicability of Enzymatic Calcium Carbonate Precipitation as a Soil-Strengthening Technique, *Journal of Geotechnical and Geoenvironmental Engineering*, 139(12), 2201-2211. http://doi.org/10.1061/(asce)gt.1943-5606.0000959

Ng, W.-S., Lee, M.-L., and Hii, S.-L. (2012): An overview of the factors affecting microbial induced calcite precipitation and its potential application in soil improvement, *International Journal of Civil and Environmental Engineering*, 6, 188-194.

Oliveira, P.J.V., Freitas, L.D., and Carmona, J.P.S.F. (2017): Effect of Soil Type on the Enzymatic Calcium Carbonate Precipitation Process Used for Soil Improvement, *Journal of Materials in Civil Engineering*, 29(4). http://doi.org/10.1061/(asce)mt.1943-5533.0001804

Paassen, L.A.v., Ghose, R., Linden, T.J.M.v.d., Star, W.R.L.v.d., and Loosdrecht, M.C.M.v. (2010): Quantifying Biomediated Ground Improvement by Ureolysis: Large-Scale Biogrout Experiment, *Journal of Geotechnical and Geoenvironmental Engineering*, 136(12), 1721-1728. http://doi.org/10.1061/(ASCE)GT.1943-5606.0000382

Pettit, N.M., Smith, A.R.J., Freedman, R.B., and Burns, R.G. (1976): Soil urease: Activity, stability and kinetic properties, *Soil Biology and Biochemistry*, 8(6), 479-484. https://doi.org/10.1016/0038-0717(76)90089-4

Piumetti, M., and Illanes, A. (2022). Enzymes and Their Function, Molecular Dynamics and Complexity in Catalysis and Biocatalysts. Springer.

doi:10.6342/NTU202404421

Putra, H., Yasuhara, H., Erizal, Sutoyo, and Fauzan, M. (2020): Review of Enzyme-Induced Calcite Precipitation as a Ground-Improvement Technique, *Infrastructures*, 5(8). http://doi.org/10.3390/infrastructures5080066

Putra, H., Yasuhara, H., Kinoshita, N., Erizal, and Sudibyo, T. (2018): Improving Shear Strength Parameters of Sandy Soil using Enzyme-Mediated Calcite Precipitation Technique, *Civil Engineering Dimension*, 20(2), 91-95. http://doi.org/10.9744/ced.20.2.91-95

Putra, H., Yasuhara, H., Kinoshita, N., and Hirata, A. (2017): Optimization of Enzyme-Mediated Calcite Precipitation as a Soil-Improvement Technique: The Effect of Aragonite and Gypsum on the Mechanical Properties of Treated Sand, *Crystals*, 7(2). http://doi.org/10.3390/cryst7020059

Putra, H., Yasuhara, H., Kinoshita, N., Neupane, D., and Lu, C.W. (2016): Effect of Magnesium as Substitute Material in Enzyme-Mediated Calcite Precipitation for Soil-Improvement Technique, *Front Bioeng Biotechnol*, 4, 37. http://doi.org/10.3389/fbioe.2016.00037

Qabany, A.A., and Soga, K. (2013): Effect of chemical treatment used in MICP on engineering properties of cemented soils, *Géotechnique*, 63(4), 331-339. http://doi.org/10.1680/geot.SIP13.P.022

Qian, Z., Wei-min, Y., Zhang-rong, L., Qiong, W., and Yong-gui, C. (2022): Advances in soil cementation by biologically induced calcium carbonate precipitation, *Rock and Soil Mechanics*, 43, 345-357. http://doi.org/10.16285/j.rsm.2021.6249

Rajasekar, A., Moy, C.K.S., Wilkinson, S., and Sekar, R. (2021): Microbially induced calcite precipitation performance of multiple landfill indigenous bacteria compared to a

doi:10.6342/NTU202404421

commercially available bacteria in porous media, *PLoS One*, 16(7), e0254676. http://doi.org/10.1371/journal.pone.0254676

Rui, W., Xiao-hua, P., Chao-sheng, T., Chao, L., Dian-long, W., Zhi-hao, D., and Bin, S. (2022): Dynamic behaviors of MICP and fiber-treated calcareous sand under dynamic triaxial testing, *Rock and Soil Mechanics*, 43, 2643-2654. http://doi.org/10.16285/j.rsm.2021.2027

Sahrawat (1984): Effects of temperature and moisture on urease activity in semi-arid tropical soils, *Plant and Soil*, 78, 401-408.

Saif, A., Cuccurullo, A., Gallipoli, D., Perlot, C., and Bruno, A.W. (2022): Advances in Enzyme Induced Carbonate Precipitation and Application to Soil Improvement: A Review, *Materials*, 15(3), 950. http://doi.org/10.3390/ma15030950

Sasaki, T., and Kuwano, R. (2016): Undrained cyclic triaxial testing on sand with non-plastic fines content cemented with microbially induced CaCO3, *Soils and Found.*, 56(3), 485-495. http://doi.org/10.1016/j.sandf.2016.04.014

Sherwood, P.T. (1993). Soil Stablization with Cement and lime.

Shu, S., Yan, B., Meng, H., and Bian, X. (2022): Comparative study of EICP treatment methods on the mechanical properties of sandy soil, *Soils and Found.*, 62(6), 101246. https://doi.org/10.1016/j.sandf.2022.101246

Simatupang, M. (2020, 2020/11/01). Liquefaction Resistance of Sand Improved with Enzymatically Induced Calcite Precipitation based on Laboratory Investigation. *IOP Conference Series: Earth and Environmental Science*,

doi:10.6342/NTU202404421

Simatupang, M., and Okamura, M. (2017): Liquefaction resistance of sand remediated with carbonate precipitation at different degrees of saturation during curing, *Soils and Found.*, 57(4), 619-631. http://doi.org/10.1016/j.sandf.2017.04.003

Simatupang, M., Okamura, M., Hayashi, K., and Yasuhara, H. (2018): Small-strain shear modulus and liquefaction resistance of sand with carbonate precipitation, *Soil Dyn. Earthquake Eng.*, 115, 710-718. http://doi.org/10.1016/j.soildyn.2018.09.027

Simatupang, M., Sukri, A.S., Nasrul, Sulha, and Putri, T.S. (2019, 2019/10/01). Effect of confining pressures on the shear modulus of sand treated with enzymatically induced calcite precipitation. *IOP Conference Series: Materials Science and Engineering*,

Singh, A., Paramkusam, B.R., and Maiti, P.R. (2021): Cyclic degradation and pore pressure dynamics of EICP treated hydrocarbon contaminated sands, *Soil Dyn. Earthquake Eng.*, 140. http://doi.org/10.1016/j.soildyn.2020.106369

Song, J.Y., Ha, S.J., Jang, J.W., and Yun, T.S. (2020a): Analysis of improved shear stiffness and strength for sandy soils treated by EICP, *Journal of the Korean Geotechnical Society*, 36(1), 17-28.

Song, J.Y., Sim, Y., Jang, J., Hong, W.-T., and Yun, T.S. (2020b): Near-surface soil stabilization by enzyme-induced carbonate precipitation for fugitive dust suppression, *Acta Geotechnica*, 15(7), 1967-1980. http://doi.org/10.1007/s11440-019-00881-z

Stocks-Fischer, S., Galinat, J.K., and Bang, S.S. (1999): Microbiological precipitation of CaCO3, *Soil Biology and Biochemistry*, 31(11), 1563-1571. https://doi.org/10.1016/S0038-0717(99)00082-6

doi:10.6342/NTU202404421

Sun, X., Miao, L., Chen, R., Wang, H., Wu, L., and Xia, J. (2021): Liquefaction Resistance of Biocemented Loess Soil, *J. Geotech. Geoenviron. Eng.*, 147(11), 04021117. http://doi.org/10.1061/(ASCE)GT.1943-5606.0002638

Terzis, D., and Laloui, L. (2019): Cell-free soil bio-cementation with strength, dilatancy and fabric characterization, *Acta Geotechnica*, 14(3), 639-656. http://doi.org/10.1007/s11440-019-00764-3

Tirkolaei, H.K., Javadi, N., Krishnan, V., Hamdan, N., and Kavazanjian, E. (2020): Crude Urease Extract for Biocementation, *J. Mater. Civ. Eng.*, 32(12), 04020374. http://doi.org/10.1061/(ASCE)MT.1943-5533.0003466

Tobler, D.J., Maclachlan, E., and Phoenix, V.R. (2012): Microbially mediated plugging of porous media and the impact of differing injection strategies, *Ecological Engineering*, 42, 270-278. http://doi.org/10.1016/j.ecoleng.2012.02.027

Torsten Wichtmann, and Theodor Triantafyllidis (2015): An experimental database for the development, calibration and verification of constitutive models for sand with focus to cyclic loading: part I—tests with monotonic loading and stress cycles, *Acta Geotech.*, 11, 739-761.

Tsuchida, H. (1970): Prediction and countermeasure against the liquefaction in sand deposits, *Abstract of the Seminar in the Port and Harbor Research Institute*, 31-333.

Tuttle, Hartleb, Wolf, and Mayne (2019): Paleoliquefaction Studies and the Evaluation of Seismic Hazard, *Geosciences*, 9(7). http://doi.org/10.3390/geosciences9070311

Wei-zhong, W. (2005): Evolution Law of Hysteresis Curve of Rock under Cyclic Loading, *Journal of Southwest Jiaotong University*.

doi:10.6342/NTU202404421

Wen, K., Li, Y., Amini, F., and Li, L. (2020): Impact of bacteria and urease concentration on precipitation kinetics and crystal morphology of calcium carbonate, *Acta Geotechnica*, 15(1), 17-27. http://doi.org/10.1007/s11440-019-00899-3

Whiffin, V.S. (2004). Microbial CaCO3 precipitation for the production of biocement *Murdoch University]*. Western Australia.

Whiffin, V.S., van Paassen, L.A., and Harkes, M.P. (2007): Microbial Carbonate Precipitation as a Soil Improvement Technique, *Geomicrobiology Journal*, 24(5), 417-423. http://doi.org/10.1080/01490450701436505

Wu, L., Miao, L., Kawasaki, S., and Wang, H. (2022): Effects of Reaction Conditions on EICP-Treated Desert Aeolian Sand, *KSCE J. Civ. Eng.*, 26(6), 2662-2674. http://doi.org/10.1007/s12205-022-1585-0

Wu, S., Li, B., and Chu, J. (2021a): Stress-Dilatancy Behavior of MICP-Treated Sand, *Int. J. Geomech.*, 21(3). http://doi.org/10.1061/(asce)gm.1943-5622.0001923

Wu, Y., Li, N., Wang, X., Cui, J., Chen, Y., Wu, Y., and Yamamoto, H. (2021b): Experimental investigation on mechanical behavior and particle crushing of calcareous sand retrieved from South China Sea, *Engineering Geology*, 280, 105932. https://doi.org/10.1016/j.enggeo.2020.105932

Xiang, J., Qiu, J., Wang, Y., and Gu, X. (2022): Calcium acetate as calcium source used to biocement for improving performance and reducing ammonia emission, *Journal of Cleaner Production*, 348, 131286. https://doi.org/10.1016/j.jclepro.2022.131286

Xiao, P., Liu, H., Stuedlein, A.W., Evans, T.M., and Xiao, Y. (2019a): Effect of relative density and biocementation on cyclic response of calcareous sand, *Canadian Geotechnical Journal*, 56(12), 1849-1862. http://doi.org/10.1139/cgj-2018-0573

doi:10.6342/NTU202404421

Xiao, P., Liu, H., Stuedlein, A.W., Evans, T.M., and Xiao, Y. (2019b): Effect of relative density and biocementation on cyclic response of calcareous sand, *Can. Geotech. J*, 56(12), 1849-1862. http://doi.org/10.1139/cgj-2018-0573

Xiao, P., Liu, H., Xiao, Y., Stuedlein, A., and Evans, T. (2018a): Liquefaction resistance of bio-cemented calcareous sand, *Soil Dyn. Earthquake Eng.*, 107, 9-19. http://doi.org/10.1016/j.soildyn.2018.01.008

Xiao, P., Liu, H., Xiao, Y., Stuedlein, A.W., and Evans, T.M. (2018b): Liquefaction resistance of bio-cemented calcareous sand, *Soil Dyn. Earthquake Eng.*, 107, 9-19. http://doi.org/10.1016/j.soildyn.2018.01.008

Xiao, Y., He, X., Evans, T.M., Stuedlein, A.W., and Liu, H. (2019c): Unconfined Compressive and Splitting Tensile Strength of Basalt Fiber–Reinforced Biocemented Sand, *Journal of Geotechnical and Geoenvironmental Engineering*, 145(9). http://doi.org/10.1061/(asce)gt.1943-5606.0002108

Xiao, Y., He, X., Stuedlein, A.W., Chu, J., Evans, T.M., and Paassen, L.A.v. (2022): Crystal Growth of MICP through Microfluidic Chip Tests, *Journal of Geotechnical and Geoenvironmental Engineering*, 148(5), 06022002. http://doi.org/10.1061/(ASCE)GT.1943-5606.0002756

Xiao, Y., Stuedlein, A.W., Ran, J., Evans, T.M., Cheng, L., Liu, H., Paassen, L.A.v., and Chu, J. (2019d): Effect of Particle Shape on Strength and Stiffness of Biocemented Glass Beads, *J. Geotech. Geoenviron. Eng.*, 145(11), 06019016. http://doi.org/10.1061/(ASCE)GT.1943-5606.0002165

Xie, D., Zhang, R., and Wang, J. (2023): The influence of environmental factors and precipitation precursors on enzyme-induced carbonate precipitation (EICP) process

doi:10.6342/NTU202404421

and its application on modification of recycled concrete aggregates, *Journal of Cleaner Production*, 395, 136444. https://doi.org/10.1016/j.jclepro.2023.136444

Yanli, W., and Yong, W. (2009): Experimental Study on Evolutionary Characteristics of Dynamic Pore water pressure of saturated sands, *Journal of Tongji University*, 37(12). http://doi.org/10.3969/j.issn.0253-374x.2009.12.008

Yasuhara, H., Neupane, D., Hayashi, K., and Okamura, M. (2012): Experiments and predictions of physical properties of sand cemented by enzymatically-induced carbonate precipitation, *Soils and Found.*, 52(3), 539-549. http://doi.org/10.1016/j.sandf.2012.05.011

Yong, W. (2009): Experimental Study on Evolutionary Characteristics of Dynamic Pore Water Pressure of Saturated Sands, *Journal of Tongji University*.

Yu, X., Chu, J., Yang, Y., and Qian, C. (2021): Reduction of ammonia production in the biocementation process for sand using a new biocement, *Journal of Cleaner Production*, 286. http://doi.org/10.1016/j.jclepro.2020.124928

Yuan, H., Hui Yang, S., Andrus, R.D., and Hsein Juang, C. (2004): Liquefaction-induced ground failure: a study of the Chi-Chi earthquake cases, *Engineering Geology*, 71(1-2), 141-155. http://doi.org/10.1016/s0013-7952(03)00130-3

Yuan, H., Ren, G., Liu, K., Zheng, W., and Zhao, Z. (2020): Experimental Study of EICP Combined with Organic Materials for Silt Improvement in the Yellow River Flood Area, *Applied Sciences*, 10(21). http://doi.org/10.3390/app10217678

Zeng, C., Van Paassen, L.A., Zheng, J.-j., Stallings Young, E.G., Hall, C.A., Veenis, Y., Van der Star, W.R.L., Konstantinou, M., and Kavazanjian, E. (2022): Soil stabilization with microbially induced desaturation and precipitation (MIDP) by denitrification: a

doi:10.6342/NTU202404421

field study, *Acta Geotechnica*, 17(12), 5359-5374. http://doi.org/10.1007/s11440-022-01721-3

Zhang, J., Wang, X., Shi, L., and Yin, Y. (2022a): Enzyme-induced carbonate precipitation (EICP) combined with lignin to solidify silt in the Yellow River flood area, *Construction and Building Materials*, 339, 127792. https://doi.org/10.1016/j.conbuildmat.2022.127792

Zhang, J., Yin, Y., Shi, L., Bian, H., and Shi, W. (2022b): Experimental investigation on mechanical behavior of sands treated by enzyme-induced calcium carbonate precipitation with assistance of sisal-fiber nucleation, *Front. Earth Sci.*, 10. http://doi.org/10.3389/feart.2022.992474

Zhang, J., Yin, Y., Shi, W., Bian, H., Shi, L., Wu, L., Han, Z., Zheng, J., and He, X. (2023): Strength and uniformity of EICP-treated sand under multi-factor coupling effects, *Biogeotechnics*, 1, 100007. http://doi.org/10.1016/j.bgtech.2023.100007

Zhang, Q., Ye, W., Su, W., Wang, Q., and Chen, Y. (2024): Mechanical behavior of EICP-treated calcareous sands under high confining pressures, *Journal of Rock Mechanics and Geotechnical Engineering*. http://doi.org/10.1016/j.jrmge.2024.04.017

Zhang, Y., Guo, H.X., and Cheng, X.H. (2014): Influences of calcium sources on microbially induced carbonate precipitation in porous media, *Materials Research Innovations*, 18(sup2), S2-79-S72-84. http://doi.org/10.1179/1432891714z.000000000384

Zhao, Q., Li, L., Li, C., Li, M., Amini, F., and Zhang, H. (2014): Factors Affecting Improvement of Engineering Properties of MICP-Treated Soil Catalyzed by Bacteria and Urease, *Journal of Materials in Civil Engineering*, 26(12), 04014094. http://doi.org/10.1061/(ASCE)MT.1943-5533.0001013

doi:10.6342/NTU202404421

doi:10.6342/NTU202404421